The Role of Unconformities in the Distribution of Clay and Porosity in North Sea Clastic Reservoirs

Abdulati A. Araibi

Submitted for the degree of Doctor of Philosophy

Heriot-Watt University

Institute of Petroleum Engineering

School of Energy Geoscience Infrastructure and Society

August 2018

ABSTRACT

The effect of an unconformity surface on the quality of underlying clastic reservoirs has long been a matter of considerable debate. Two opposing hypotheses have been proposed. One supports a relationship between the presence of an unconformity surface and the quality of the underlying reservoir, either by enhancement or reduction of porosity (e.g. Ketzer et al., 2009 and Shanmugam, 1990). By contrast, the opposing hypothesis argues that there is no evidence for the existence of such a relationship (e.g. Ehrenberg and Jakobsen, 2001 and Bjorkum et al., 1990).

In this study, both hypotheses were examined by evaluating the role of the unconformity surfaces on the quality of selected North Sea clastic reservoirs. In particular, the study focussed on the Late Triassic Skagerrak Formation in Kittiwake Field, Central North Sea, which underlies the Mid-Cimmerian unconformity, and the Middle Jurassic Brent Group sandstones in the Tampen Spur area, Northern North Sea, which underlie the Base-Cretaceous Unconformity. This thesis presents the results of detailed sedimentological and petrographic analysis of over 200 core samples, including their lithology, texture, mineralogy and diagenetic characteristics, in order to investigate the existence of any diagenetic changes that may have affected the reservoir quality, and to consider any possible relationship with the overlying unconformity surfaces.

Thin-section petrography and SEM analysis shows that there are several lines of evidence for the existence of post-depositional diagenetic changes within the studied sandstones, which included the generation of secondary porosity and the formation of authigenic kaolinite. These diagenetic changes are mainly due to the dissolution of detrital framework grains (particularly feldspar) and intergranular cement (particularly calcite), and the local precipitation of authigenic clay. Both of these diagenetic processes have had a significant effect on the reservoir properties. The distribution of the secondary porosity and authigenic kaolinite clearly indicate late stage diagenetic processes, which clearly post-date the majority of mechanical compaction, and therefore also post-date the origin of the unconformity surfaces.

The study demonstrates that there is no relationship between the studied unconformity surfaces and the observed diagenetic changes (i.e., secondary porosity and authigenic kaolinite) within the selected reservoirs. Therefore, any such relationship reported elsewhere is most likely to be a localised phenomenon, and should not be extended as a general rule to all unconformities.

Acknowledgment

All praise is to Allah for his generosity and blessings which allowed me to complete this work.

This work wouldn't be possible without the great support that I have received from my parents. I would like to express my sincere gratitude to them and ask Allah to bless them and forgive them.

A special gratitude to my supervisors Dr. Helen Lever and Prof. Dorrik Stow who provided a great support and invaluable help during the period of my PhD study.

A big thank you prof. Andrew Aplin and Dr. Jim Buckman for agreeing to be my examiners and spending time in reading my thesis.

I would like to express my sincere appreciation to my friend Dr. Eltazy Khalid for his continuous support during my study.

Many thanks to Dr. Zeinab Smillie, all IPE and BGS staff who helped with the laboratory work.

Special thanks to: ESEM Facility Manager who is responsible for running the Scanning Electron Microscope facility within the Institute of Petroleum Engineering. I extend my thanks to Hin On Martin Chu from the Institute of Thin Films, Sensors and Imaging (University of the West of Scotland).

I am also thankful to:

- My brothers for supporting from a distance.
- Misfer Almari, Shereef Bankole, Mohamad Alhamadi and all my friends and colleagues at HWU. Without your company my PhD would have been difficult to endure.

My Final and deepest gratitude is to my wife and kids for their support and patience during my study which have played a major role in my success.

ACADEMIC REGISTRY

Research Thesis Submission

Name:			
School:			
Version: *(i.e. First, Resubmission, Final)*		Degree Sought:	

Declaration

In accordance with the appropriate regulations I hereby submit my thesis and I declare that:

1) the thesis embodies the results of my own work and has been composed by myself
2) where appropriate, I have made acknowledgement of the work of others and have made reference to work carried out in collaboration with other persons
3) the thesis is the correct version of the thesis for submission and is the same version as any electronic versions submitted*.
4) my thesis for the award referred to, deposited in the Heriot-Watt University Library, should be made available for loan or photocopying and be available via the Institutional Repository, subject to such conditions as the Librarian may require
5) I understand that as a student of the University I am required to abide by the Regulations of the University and to conform to its discipline.
6) I confirm that the thesis has been verified against plagiarism via an approved plagiarism detection application e.g. Turnitin.

* *Please note that it is the responsibility of the candidate to ensure that the correct version of the thesis is submitted.*

Signature of Candidate:		Date:	

Submission

Submitted By *(name in capitals):*	
Signature of Individual Submitting:	
Date Submitted:	

For Completion in the Student Service Centre (SSC)

Received in the SSC by *(name in capitals):*			
1.1 Method of Submission *(Handed in to SSC; posted through internal/external mail):*			
1.2 E-thesis Submitted (**mandatory for final theses)**			
Signature:		Date:	

TABLE OF CONTENT

LIST OF FIGURES xi

Chapter 1 Introduction 1

1.1 Importance of unconformities to the hydrocarbon industry 1

1.1.1 Unconformities and Porosity Enhancement 3

1.1.2 Unconformities and cemented zones 5

1.1.3 Unconformities and Hydrocarbon Migration 6

1.2 Aims of the thesis 8

1.3 Research methods 9

1.3.1 Sedimentological analysis 9

1.3.2 Petrographic analysis 10

1.4 Thesis structure 12

Chapter 2 Review 14

2.1 Unconformities - Background 14

2.1.1 Identifying unconformities-stratigraphic relationship 16

2.1.2 Recognition of unconformities 22

2.2 Origin, Development and Evolution of the North Sea 28

2.2.1 Introduction 28

2.2.2 Main Structural events which controlled the North Sea 28

2.3 Stratigraphy of North Sea 32

2.3.1 Devonian Period 32

2.3.2 Carboniferous period 32

2.3.3 Permian Period 33

2.3.4 Triassic Period 34

2.3.5 Jurassic Period 34

2.3.6 Cretaceous Period 37

2.3.7 Cenozoic Era 37

2.4 Clay Mineralogy and Sandstone Diagenesis in the North Sea 39

2.4.1 Early (shallow) diagenesis 39

2.4.2 Burial diagenesis 40

Chapter 3 North Sea Jurassic Unconformities: A Statistical and Sedimentological Overview 42

3.1 Introduction 42

3.2 Data Screening 42

3.3 Statistical analysis 44

3.4 Core description 49

3.4.1 Sediment facies 49

3.4.2 Unconformity characteristics 50

Chapter 4 Case Study 1: The role of Mid-Cimmerian Unconformity on the distribution of porosity and kaolinite in the Skagerrak Formation of the Kittiwake Field, Central Viking Graben 53

4.1 The Mid-Cimmerian Unconformity (MCU) 53

4.2 The Central Viking Graben Kittiwake Field 54

4.2.1 Introduction 54

4.2.2 Field stratigraphy 54

4.2.3 Geological History 57

4.2.4 Reservoirs 58

4.3 Sedimentological Analysis 60

4.3.1 Sedimentological analysis results 61

4.4 Petrographic Analysis 66

4.4.1 Lithological Texture 66

4.4.2 Sandstone Classification 67

4.4.3 Quantitative analysis 68

4.5 Spatial distribution of minerals and porosity and their relationship to the Mid-Cimmerian Unconformity 80

4.5.1 Feldspar 80

4.5.2 Kaolinite 82

4.5.3 Mica 85

4.5.4 Porosity 88

4.6 Discussion of results 93

4.6.1 Potential mechanisms for the production of secondary porosity and precipitation of kaolinite 93

4.6.2 Origin and timing of dissolution and production of secondary porosity ..99

4.6.3 Origin and timing of kaolinization 112

4.7 Conclusion 114

Chapter 5 Case Study 2: The role of the Base-Cretaceous Unconformity in the distribution of porosity and kaolinite in Brent Group sandstones of the Tampen Spur area, Northern North Sea 116

5.1 The Base-Cretaceous Unconformity 116

5.2 Introduction to the Tampen Spur area 117

5.3 Stratigraphy of the Brent Group in Tampen Spur area 119

5.3.1 Broom Formation 120

5.3.2 Rannoch Formation 120

5.3.3 Etive Formation 122

5.3.4 Ness Formation 122

5.3.5 Tarbert Formation 122

5.4 Sedimentological analysis 123

5.4.1 Sedimentological analysis results 123

5.5 Petrographic Analysis 133

5.5.1 Lithological Texture 134

5.5.2 Sandstone Classification 135

5.5.3 Quantitative analysis 136

5.6 Spatial distribution of minerals and porosity in Brent Group below the Base-Cretaceous Unconformity 148

5.6.1 Rannoch Formation 148

5.6.2 Etive Formation 161

5.6.3 Tarbert Formation 168

5.7 Discussion of results 174

5.7.1 Potential mechanisms for the dissolution of minerals and precipitation of others in the Brent Group 174

5.7.2 Origin and timing of dissolution and production of secondary porosity 175

5.7.3 Origin and timing of kaolinization 187

5.8 Conclusion 190

Chapter 6 Results from other North Sea wells 192

6.1 Identified unconformities 192

6.1.1 Base Humber Group Unconformity (BHU) 192

6.1.2 Base Kimmeridgian Unconformity (BKU) 192

6.2 Introduction to the studied wells 192

6.3 Well 2/5-17 in Heather Field 193

6.3.1 Sedimentological analysis 193

6.3.2 Petrographic analysis 196

6.3.3 Spatial distribution of minerals and porosity below the Base Humber Unconformity 199

6.3.4 Conclusion 206

6.4 Well 15/17-B2 in Piper Field 208

6.4.1 Sedimentological analysis 209

6.4.2 Petrographic analysis 209

6.4.3 Spatial distribution of feldspar and porosity below the Base Kimmeridgian Unconformity 214

6.4.4 Discussion and Conclusion 218

Chapter 7 Summary and Conclusion 222

7.1 Principal findings 222

7.2 Suggestions for future study 228

LIST OF FIGURES

Figure 1-1. An example of the association of stratigraphic traps with unconformities. . . 3

Figure 1-2. Graphical representation showing increase of average core porosity in Zone 4 of Ivishak Formation with increasing proximity to the unconformity. 5

Figure 1-3. Division of the vertical structures of an unconformity. 7

Figure 2-1. Unconformity at Siccar Point 14

Figure 2-2. Chronostratigraphic diagram showing the six North America Phanerozok depositional sequences and their bounding unconformities. 15

Figure 2-3 Types of unconformities 16

Figure 2-4. An overview for the underlying great unconformity of the Grand Canyon of Arizona with the overlying Tapeats Sandstone of Cambrian age formed about 175 million years ago 17

Figure 2-5. Display part of disconformity in Capitol Reef National Park, Utah. 18

Figure 2-6. The Marshall Paraconformity represented by the contact between the Ototara Limestone and Gee Greensand visible on the beach north of Kakanui. The contact is the Marshall Paraconformity 19

Figure 2-7. An example showing part of the nonconformity in the Wind River gorge of Wyoming. 19

Figure 2-8. Relationship between an unconformities' surface and subcrop (A) or supracrop (B) 21

Figure 2-9. Strata geometry within an unconformity bounded depositional sequence ... 22

Figure 2-10. North Sea area geographical map 29

Figure 2-11. Diagrams depicting the major tectonic events which controlled and formed the North Sea basin during Proterozoic and Phanerozoic in Scotland and England 30

Figure 3-1. Detailed stratigraphic chart for the whole North Sea area (Northern, Central and Southern North Sea).. 43

Figure 3-2. An example of how data were plotted by depth for each well 47

Figure 3-3. An example of how each well was divided into groups by textural facies. .48

Figure 3-4. An example of the statistical analysis carried out for each facies above and below the unconformity surface in Well 14/19-3.. 48

Figure 3-5. Showing sediment core logging for Well 21/18-2A and the presence of the unconformity surface at depth 10017 ft. 51

Figure 3-6. Showing an example of calibrating Mid-Cimmerian Unconformity from cores of Well 21/18-2A to wireline log's character and core logging.....52

Figure 4-1. Location of the Kittiwake Field in the Central North Sea, ...55

Figure 4-2. 2-D line through the discovery Well 21/18-2A of Kittiwake Field. 56

Figure 4-3. Stratigraphic column of the Kittiwake area.....56

Figure 4-4. General stratigraphy and lithostratigraphy of Western Platform in the Central North Sea.....57

Figure 4-5. Wireline log character of Well 21/18-2A and facies description of the Kittiwake Field.....60

Figure 4-6. Sedimentological core description of Well 21/18-6 in the Kittiwake Field. 62

Figure 4-7. Sedimentological core descriptions of Well 21/18-2A in the Kittiwake Field.. 63

Figure 4-8. Sedimentological core descriptions of Well 21/18-3 in the Kittiwake Field... 64

Figure 4-9. Sedimentological core descriptions of Well 21/18-4 in the Kittiwake Field.. 65

Figure 4-10. Sandstone classification diagrams.....68

Figure 4-11. Thin-section photomicrographs showing different petrographic features..72

Figure 4-12. Thin-section photomicrographs of some authigenic and accessory minerals. 75

Figure 4-13. Thin-section photomicrographs and backscattered electron images. 78

Figure 4-14. Thin-section photomicrographs and backscattered electron images. 79

Figure 4-15. BSE images showing evidence for the alteration and dissolution of feldspar grains within Skagerrak Sandstone.. 81

Figure 4-16. The vertical distribution patterns of feldspars below the Mid-Cimmerian Unconformity in the studied wells.. 82

Figure 4-17. BSE images showing the various types and distribution of kaolinite below the unconformity surface in Skagerrak Sandstone. 84

Figure 4-18. The vertical distribution patterns of clay below the Mid-Cimmerian Unconformity in the studied wells.. 85

Figure 4-19. A correlation between clay and feldspar below the unconformity surface in Kittiwake field. 86

Figure 4-20. The vertical distribution patterns of mica below the Mid-Cimmerian Unconformity in the studied wells.. 87

Figure 4-21. A correlation between measured core porosity (He porosity) and a visible point counted modal porosity for the four studied wells. 89

Figure 4-22. The distribution of porosity and feldspar below the unconformity surface in the four studied wells.. 91

Figure 4-23. Scatter plots showing lack of correlation between porosity content and feldspar, except in Well 21/18-6. 92

Figure 4-24. Hypothetical diagram showing the mechanisms of how meteoric waters may be distributed and extend underneath the unconformity surface 95

Figure 4-25. Oil degradation at an OWC; after Head et al. (2003). 98

Figure 4-26. Backscattered electron images. 101

Figure 4-27. Backscattered electron images 105

Figure 4-28. Backscattered electron images 107

Figure 5-1. Seismic reflection data for the Base-Cretaceous Unconformity (blue) in the top of rotated fault block of Snorre Field. 117

Figure 5-2 Location map of the Tampen Spur area in the North Sea 118

Figure 5-3 Giant fields in the Tampen Spur area. 119

Figure 5-4. The stratigraphy of the Brent Group as represented by Well 34/10-8 in the Gullfaks Field. (C = coal beds).. 121

Figure 5-5. Sedimentological core descriptions of the Tarbert, Ness, Etive and Rannoch Formations in Well 34/10-1 in the Gullfaks Field.. 125

Figure 5-6. Sedimentological core descriptions of the Rannoch Formation in Well 34/10-4 in the Gullfaks Field.. 126

Figure 5-7. Sedimentological core descriptions of the Tarbert Formation in Well 34/10-8 in the Gullfaks Field.. 127

Figure 5-8. Sedimentological core descriptions of the Tarbert Formation in well 34/10-34 in the Gullfaks Vest Field.. 128

Figure 5-9. Sedimentological core descriptions of the Rannoch Formation in well 33/9-13S in the Statfjord Nord Field.. 129

Figure 5-10. Sedimentological core descriptions of the Etive Formation in well 34/7-16 in the Vigdis Field. 130

Figure 5-11. Sedimentological core descriptions of the Tarbert Formation in well 34/7-19 in the Vigdis Field.. 131

Figure 5-12. Sedimentological core descriptions of the Tarbert Formation in well 34/7-20 in the Snorre Field. 132

Figure 5-13. Sedimentological core descriptions of the Tarbert Formation in well 30/6-10 A in the Oseberg Field.. 133

Figure 5-14. Sandstone classification diagrams, all the samples fall in the arkose and lithic arkose fields. 136

Figure 5-15. Photomicrographs showing different petrographic features observed in the studied sandstones.. 141

Figure 5-16. Optical micrographs showing..... 144

Figure 5-17. Optical micrographs images showing. 147

Figure 5-18. Thin-section photomicrographs and backscattered electron images from the three studied wells for the Rannoch Formation. 150

Figure 5-19. The volume and distribution of feldspar in the Rannoch Formation for the three studied wells.. 151

Figure 5-20. Vertical distribution of plagioclase within the Brent Group in Wells 34/10-1 and 34/10-4. 152

Figure 5-21. Thin-section photomicrographs and backscattered electron images. 153

Figure 5-22. Distribution patterns of clay minerals (includes kaolinite) toward the Base-Cretaceous Unconformity in the Rannoch sandstones. 155

Figure 5-23. Optical micrograph images for the Rannoch sandstones. 157

Figure 5-24. The distribution of carbonate cement under the Base-Cretaceous Unconformity in the three studied wells. 157

Figure 5-25. Positive correlation between measured core porosity and the point counted porosity for two of the studied wells. 159

Figure 5-26. Degrees of dissolution of feldspar grains and/or carbonate cement and the formation of secondary porosity within the Rannoch Formation in the Brent Group.. 159

Figure 5-27. A negative correlation between porosity and carbonate cement in the Rannoch Formation. 160

Figure 5-28. The distribution of porosity below the unconformity surface in the three studied wells. 160

Figure 5-29. **A** and **B**. Showing dissolution of feldspar grains and enhancement of porosity in Wells 34/10-1, 1840.20 m and 34/7-16, 2393.80 m, respectively. **C**. BSE showing euhedral booklet of kaolinite formed in situ in Well 34/7-16, 2416.70 m. **D**. BSE showing early diagenetic or detrital kaolinite squeezed between grains in Etive Formation of Well 34/7-16, 2416.70 m. 162

Figure 5-30. The distribution of feldspar grains within Etive Formation below the BCU in the two studied wells for Etive Formation. 163

Figure 5-31. Distribution of clay minerals (includes kaolinite) toward the Base-Cretaceous Unconformity for the Etive sandstones in both wells. 165

Figure 5-32 Distribution patterns of carbonate cement toward the Base-Cretaceous Unconformity for the Etive sandstones in both wells. 166

Figure 5-33. The distribution of total porosity in the Etive Formation below the Base-Cretaceous Unconformity. 168

Figure 5-34. Feldspar contents below the Base-Cretaceous Unconformity. 169

Figure 5-35. The distribution of clay (particularly kaolinite) below the Base-Cretaceous Unconformity in the Tarbert Formation within four of the six studied wells. 171

Figure 5-36. Carbonate cement distribution (commonly calcite) below the Base-Cretaceous Unconformity in four of the six studied wells. 172

Figure 5-37. Distribution of porosity below the Base-Cretaceous Unconformity. 174

Figure 5-38. Thin-section photomicrographs and backscattered electron images.. 181

Figure 5-39. Locations of wells in the Gullfaks Field.. 186

Figure 6-1. Sedimentological core descriptions of the Tarbert Formation in Well 2/5-17 in the Heather Field.. 195

Figure 6-2. Thin-section photomicrographs Showing: **A**. corroded and fractured quartz grains 198

Figure 6-3. Distribution of feldspar grains below the Base Humber Unconformity. ...199

Figure 6-4. A correlation between the content of kaolinite and porosity in the Tarbert Formation below the unconformity surface. 201

Figure 6-5. A correlation between the content of kaolinite and feldspar within the Tarbert Formation below the unconformity surface. 201

Figure 6-6. Distribution of kaolinite below the Base Humber Unconformity in the studied well. 202

Figure 6-7. Distribution of calcite cement below the Base Humber Unconformity in the studied well. 203

Figure 6-8. Vertical variation in the content of porosity toward the unconformity surface. 205

Figure 6-9. Stratigraphic relationships for the formation of the Upper Jurassic sediments in the Piper Field. 208

Figure 6-10. Lithological stratigraphy and core descriptions of the Piper Formation in Well 15/17-B2 in the Piper Field.. 210

Figure 6-11. Thin-section photomicrographs. 213

Figure 6-12. Distribution of feldspar grains below the Base Kimmeridgian Unconformity in the studied well. 215

Figure 6-13. Lack of correlation between the porosity and the feldspar content below the Base Kimmeridgian Unconformity in the Piper Formation. 217

Figure 6-14. Lack of correlation between the porosity and clay content below the Base Kimmeridgian Unconformity in the Piper Formation 217

Figure 6-15. Distribution of porosity below the Base Kimmeridgian Unconformity in the studied well. 218

Figure 6-16. Schematic diagram showing a possible migration path for the acidic fluids and hydrocarbon from the graben to margin crestal structure. 221

LIST OF TABLES

Table 1-1. Examples of unconformity traps.....2

Table 2-1 A list of criteria which can be used for recognizing and identifying unconformities and the processes that occurred to create these unconformities as well as their expected effect on the reservoir characteristics. 27

Table 2-2. Major tectonic events which affected the geology of the North Sea. 31

Table 3-1. An example of the investigation carried out for each of the selected wells in the area of interest.. 43

Table 3-2. An example of the investigation carried out for each of the selected wells in the area of interest in terms of its core characteristics (e.g. porosity and permeability) and description.. 46

Table 3-3. An example from three of the studied wells showing the evaluation that was carried out for each well.....47

Table 4-1. A summary of lithological textures of facies. 67

Table 4-2. Petrographic Analysis Data for Well 21/18-6. 69

Table 4-3. Petrographic Analysis Data for Well 21/18-2A.....69

Table 4-4. Petrographic Analysis Data for Well 21/18-3 70

Table 4-5. Petrographic Analysis Data for Well 21/18-4 70

Table 4-6. Petrographic analysis data of porosity content below the unconformity surface in wells 21/18-6, 21/18-2A, 21/18-3 and 21/18-4. 77

Table 4-7. Petrographic analysis data of feldspar content below the unconformity surface in Wells 21/18-6, 21/18-2A, 21/18-3 and 21/18-4. 81

Table 4-8. Petrographic analysis data of mica content below the unconformity surface in wells 21/18-6, 21/18-2A, 21/18-3 and 21/18-4. 87

Table 5-1. Summary of lithological textures of Brent Group sandstones. 135

Table 5-2. Petrographic analysis data for Well 33/9-13 137

Table 5-3. Petrographic analysis data for Well 34/7-20 137

Table 5-4. Petrographic analysis data for Well 34/7-19 137

Table 5-5. Petrographic analysis data for Well 34/7-16. 138

Table 5-6. Petrographic analysis data for Well 34/10-8 138

Table 5-7. Petrographic analysis data for Well 34/10-34 138

Table 5-8. Petrographic analysis data for Well 34/10-4 139

Table 5-9. Petrographic analysis data for Well 34/10-1 139

Table 5-10. Petrographic analysis data for Well 30/6-10A..... 139

Table 5-11. Petrographic analysis data of porosity volume below the unconformity surface in the studied wells. 146

Table 5-12. Petrographic analysis data of feldspar content below the Base-Cretaceous Unconformity in Wells 34/10-1, 34/10-4 and 33/9-13..... 149

Table 5-13. Petrographic analysis data of clay content below the Base-Cretaceous Unconformity in Wells 34/10-1, 34/10-4 and 33/9-13..... 154

Table 5-14. Volume and distribution of carbonate cements below the Base-Cretaceous Unconformity in Wells 34/10-1, 34/10-4 and 33/9-13..... 156

Table 5-15. Value and distribution of porosities in the Rannoch Formation below the BCU. 158

Table 5-16. Petrographic analysis data of feldspar content below the Base-Cretaceous Unconformity in Wells 34/10-1 and 34/7-16. 161

Table 5-17. Petrographic analysis data of clay content (includes kaolinite) below the Base-Cretaceous Unconformity in Wells 34/10-1 and 34/7-16. 164

Table 5-18. Petrographic analysis data of carbonate cement content below the Base-Cretaceous Unconformity in Wells 34/10-1 and 34/7-16. 166

Table 5-19. Petrographic analysis data of porosities volume below the Base-Cretaceous Unconformity in wells 34/10-1 and 34/7-16. 167

Table 5-20. Petrographic analysis data of feldspar content below the Base-Cretaceous Unconformity in six studied wells. 169

Table 5-21. Petrographic analysis data of clay (commonly kaolinite) content below the Base-Cretaceous Unconformity in the Tarbert Formation. 170

Table 5-22. Petrographic analysis data of carbonate cement (commonly calcite) content below the Base-Cretaceous Unconformity in four of the six studied wells. 172

Table 5-23. Petrographic analysis data of the porosities volume below the Base-Cretaceous Unconformity in six studied wells. 173

Table 6-1. Showing the lithological texture of the two studied formations in Well 2/5-17. 196

Table 6-2. Petrographic analysis data for Well 2/5-17 196

Table 6-3. Showing the lithological texture of the studied piper formation in Well 15/17-B2.. 211

Table 6-4. Petrographic analysis data for well 15/17-B2 211

Chapter 1 **Introduction**

1.1 Importance of unconformities to the hydrocarbon industry

The effect of unconformities on reservoir quality has long been a matter of controversy. Several studies have been published suggesting a profound relationship exists between the presence of unconformity surfaces and reservoir quality. By contrast, others have indicated that no such relationship exists. The existence and nature of any such relationship is significant for exploration geologists who might wish to target a potential hydrocarbon play beneath an unconformity surface. It is also important for reservoir sedimentologists in their assessment of reservoir quality above or below unconformities that occur within a known reservoir succession.

Authors who support the existence of such a relationship claim that many unconformities associated with stratigraphic traps have been found around the world, and there is a relationship between the producing reservoir formations and these unconformities (Shanmugam, 1988). They suggest that unconformities are not just a representation of sea level change events or global tectonic events but also can cause diagenetic changes in the older sediments and control the distribution of the reservoir in different ways by different geological processes. The diagenetic processes associated with the creation of the unconformities may either enhance porosity and permeability or enhance cementation, therefore creating either a high or low permeability zone, respectively, near the unconformity surface. Which of these processes occurs will therefore have a significant effect on reservoir quality (Rittenhouse, 1972).

Furthermore, it has been proposed that the structure and characteristics of these unconformities may also play a significant role in the processes of hydrocarbon migration and accumulation. They may work as a seal zone or traps in the areas of hydrocarbon accumulation where they are highly cemented, or they may act as pathways for fluid flow when they are associated with high permeability layers (Wu et al., 2012). There are also some examples (Table 1-1) of hydrocarbon reservoirs that are overlain or truncated by unconformities and this arrangement is known as an unconformity traps (Shanmugam, 1988). These stratigraphic traps may be located either beneath the unconformities (called

truncation traps or sub-unconformity traps) or above the unconformities (called supra-unconformity traps) (Figure 1-1), (Biddle and Wielchowsky, 1994). Unconformity traps generally work by the unconformity being overlain by impermeable sealing rocks; however, if the unconformity surface is cemented it may act as sealing layer itself.

Table 1-1. Examples of unconformity traps

Field	Trap
Antelope Hills (California)	Above Miocene unconformity
Gippsland Australia	Below Oligocene unconformity
Cutbank Montana	Above lower cretaceous unconformity
Statfjord Norwegian North Sea	Below Base Cretaceous unconformity

In contrast, other authors argue against the existence of such a relationship saying that there is no marked evidence for such a relationship and that any such effects could be a localised phenomenon (e.g. (Bjorkum et al., 1990). Those authors suggest that, even if erosion took place over a million to a few millions of years, the erosion rate would be expected to be a few tens to hundreds of metres and the rate of erosion would be greater than the rate of propagation of dissolution. Therefore, the sedimentary rocks below the unconformity surfaces would not be expected to preserve a distinct diagenetic change related to the creation of the unconformity. Furthermore, the absence of a systematic increase in the dissolution of feldspar grains towards the Cimmerian unconformity has previously been recognised within the Middle Jurassic Brent Group by (Ehrenberg and Jakobsen, 2001). Those authors documented that the dissolution of feldspar grains within the Brent Group sandstones in Gullfaks Field is most likely to be related to the biodegradation of oil and not related to the influx of meteoric water through the unconformity surface.

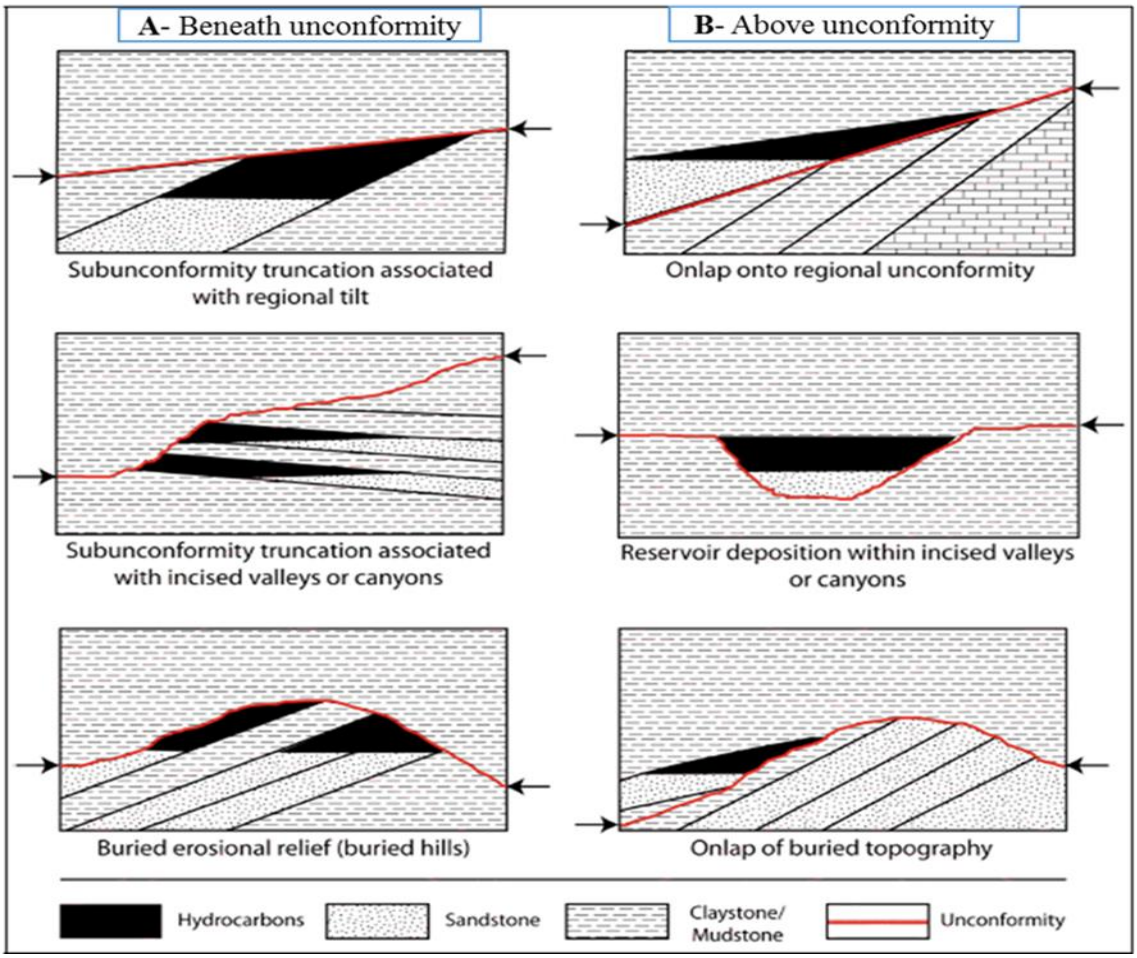

Figure 1-1. An example of the association of stratigraphic traps with unconformities. (A) Traps beneath an unconformity. (B) Traps above an unconformity. After Biddle and Wielchowsky (1994).

1.1.1 Unconformities and Porosity Enhancement

In sedimentary rocks, the generation of secondary porosity is interpreted to be a post-depositional product formed as a result of partial to complete dissolution of the framework minerals and/or authigenic cements (Bloch, 1994). Evidence for the dissolution of unstable minerals and cements in clastic rocks and enhancement of reservoir porosity is well documented in many studies (Wilkinson et al., 2014).

The processes that create unconformities can enhance porosity of reservoirs which occur beneath these unconformities (Shanmugam, 1988). During erosion and uplift of the sequence, framework grains and unstable cements (e.g. calcite) are likely to be dissolved by acidic meteoric waters. Leaching of minerals by meteoric water may lead to enhanced

porosity and create a large volume of secondary porosity (Giles and Marshall, 1986). According to (Jian-Ping et al., 2000) the porosity and permeability had been improved and hydrocarbons were accumulated near the unconformity surface at the bottom of the Paleogene in the Junggar Basin, Northwest China. Moreover, according to (Shanmugam, 1988) many hydrocarbon reservoirs display enhancement of porosity beneath the unconformities (e.g. Statfjord Field in the North Sea and Prudhoe Bay Field, Alaska). The Middle Jurassic sandstone in the Statfjord Field occurs beneath the Cimmerian Unconformity, and in this succession the feldspar and other framework grains are interpreted as having been dissolved by percolated meteoric water forming widespread dissolution porosity and solution channels, which may enhance the permeability as well. In the case of Prudhoe Bay Field, where the Ivishak Formation has been truncated by the Neocomian Unconformity, percolation of acidic meteoric water along the unconformity is interpreted as having dissolved the chert leading to enhanced porosity. According to Shanmugam and Higgins, (1988) porosity has been increased both laterally and vertically with respect to the unconformity surface, laterally and vertically from 15 % at the point of 30 km (and 550 m depth) from the unconformity to about 30% near the unconformity (Figure 1-2). In the same succession, permeability also increased from 50 md to 800 md near the unconformity. The authors used this example as a significant indication of the effect of unconformities on porosity enhancement.

However, other published studies indicate that the ability of acidic meteoric water percolating along the unconformity to leach and dissolve minerals is most likely to be limited and decrease with increasing distance along the flow path, as meteoric water when it starts to penetrate will usually be undersaturated, and with interaction between these waters and some minerals it will become saturated. Therefore the dissolution of a large amount of minerals and formation of secondary porosity by meteoric water, if it exists, is most likely to be restricted to the upper part of the flow system (Giles and Marshall, 1986). Any dissolution of grains and/or cements is most likely to be balanced by the generation and precipitation of a similar volume of diagenetic minerals, which will form as product of the dissolved minerals (Bjorlykke, 1984).

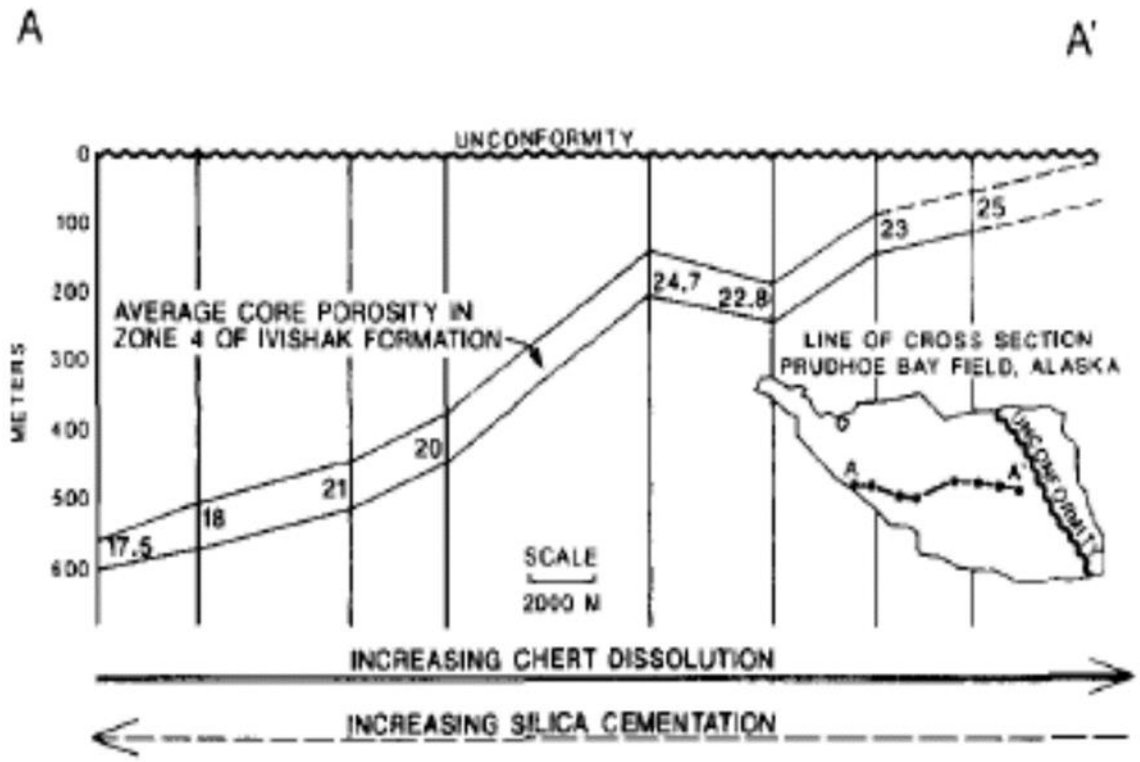

Figure 1-2. Graphical representation showing increase of average core porosity in Zone 4 of Ivishak Formation with increasing proximity to the unconformity. Prudhoe Bay Field Alaska. (From (Shanmugam and Higgins, 1988)).

Furthermore, uplifted and exposed sedimentary rocks that are subjected to meteoric waters are usually prone to erosion as well; the rate of this erosion is dependent on many factors, for example properties of the exposed material, the topography and climate of the area. Therefore any expected effect of meteoric water on the exposed sedimentary rocks will be only preserved if the rate of erosion was less than the rate of meteoric water penetration and alteration; otherwise the diagenetic effect of these waters (e.g., dissolution or kaolinitization of minerals) on sedimentary rock will be eroded and is unlikely to be seen (Bjorkum et al., 1990).

1.1.2 Unconformities and cemented zones

Some of the studies that have proposed the existence of a relationship between the presence of unconformity surfaces and enhanced reservoir quality have further suggested a region of increased cementation beneath the unconformity. They suggest that wide cementation zones may also develop beneath unconformities. These cemented zones cause low permeability zones, leading to poorer reservoir quality; these zones may act as

a diagenetic trap for hydrocarbons. An example of cementation beneath the unconformity is the Parkman Field in the Williston basin, Saskatchewan (Miller, 1972). According to (Wu et al., 2012), if the unconformity surface is highly cemented or if the porosity below the unconformity has decreased due to weathering, then the unconformity surface may act as a seal or a barrier preventing migration of hydrocarbons. However, this is not widely accepted, as other studies have illustrated that sedimentary rocks below the unconformity surfaces would not be expected to preserve a distinct diagenetic change related to the creation of the unconformity (Bjorkum et al., 1990). Bjorkum et al. (1990) studied the possible diagenetic effect of the Late Cimmerian Unconformity on the sandstones of the Rannoch Formation in Gullfaks Field, and concluded that "the significance of unconformities for kaolinitization in sandstones needs to be re-evaluated".

1.1.3 Unconformities and Hydrocarbon Migration

Hydrocarbon migration pathways are one of the important factors for the accumulation of hydrocarbons, because they control the hydrocarbon migration direction, providing a bridge between the source rock and traps and can give an indication of the location of the hydrocarbon accumulation as well. From the 1990s, many researchers started to study the different types of migration pathways for fluids, focusing on fault structures and sandstones in terms of lithological characteristics and their controlling factors (Gao et al., 2013a). They found that some unconformity surfaces may play a significant role in hydrocarbon migration and accumulation. According to Gao et al. (2013), in basins associated with unconformities, the unconformities can act either as a pathway or a barrier to migration of hydrocarbons. Hydrocarbons can be prevented from migrating and can be trapped by unconformities when the unconformity surface is highly cemented and fluids will not be able to flow. However, they may also act as avenues for hydrocarbons migration (Wu et al., 2012); if they are associated with coarse sediments they then will be able to form pathways for fluid to flow. An example of hydrocarbon migration along an unconformity surface is the Maracaibo Basin in Venezuela, where oil was found to be seeping within the sediments associated with pre-Miocene unconformity for hundreds of metres (Talukdar, 1985).

Furthermore, (Wu et al., 2012) suggest that an unconformity is not a surface but can be a complex structural body; they further documented that the pre-Paleogene unconformity

surface of the Sikeshu Sag, Junggar basin in China is divided into three layers: the upper part is close to the unconformity surface and lies at the bottom of the overlying rocks. This layer represents the transgressive sand and basal conglomerate developed during the transgressive period; the middle layer is a weathered clay layer, which may have formed due to physical, chemical and biologic weathering and, finally, the lower layer is a leached zone formed just below the unconformity surface (Figure 1-3). The upper layer basal conglomerate has good physical properties; therefore, it will be the best layer for hydrocarbon transport, because with the increasing porosity and permeability of the layer, its ability for hydrocarbon transportation will increase. In contrast, the weathered mid-layer, which has fine grains formed by the different weathering processes and compacted by overlying sediment, may act as a cap rock for the hydrocarbons. The lower layer of this unconformity structure body, which is called the leached layer, has good secondary porosity and permeability due to the dissolution of some grains; this dissolution has improved the properties of the layer, thus forming a good reservoir (Gao et al., 2013b).

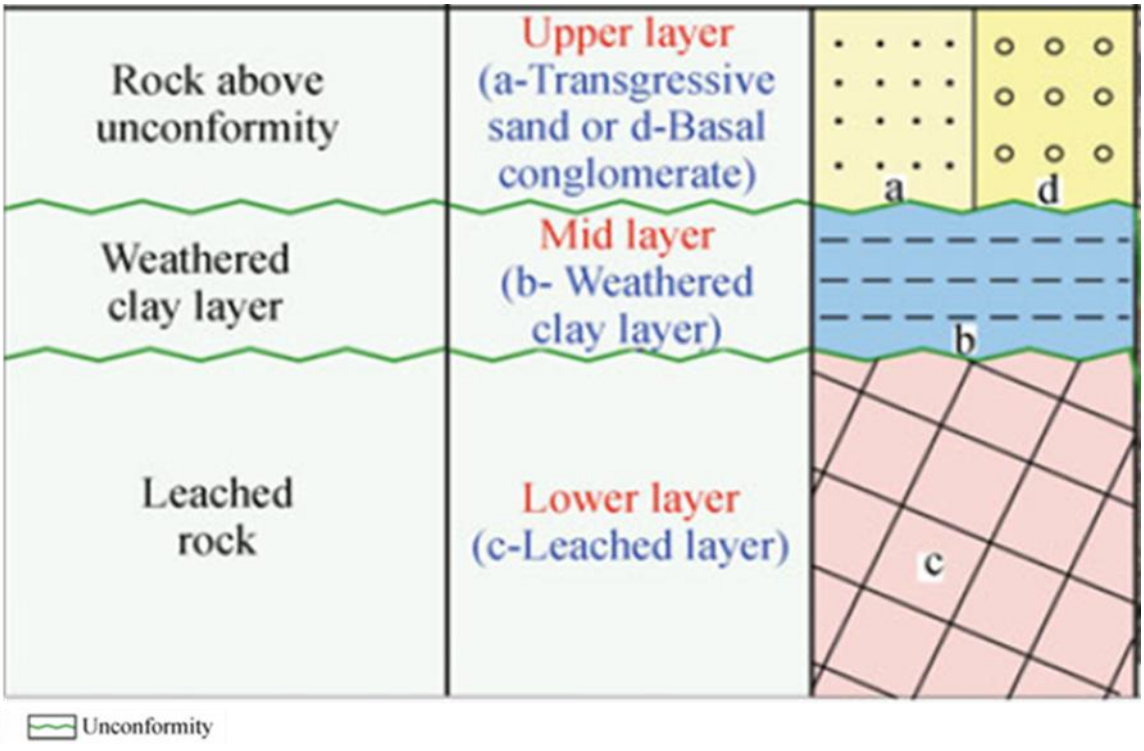

Figure 1-3. Division of the vertical structures of an unconformity. (After (Wu et al., 2012))

1.2 Aims of the thesis

Two opposing hypotheses have been developed in relation to the effect of an unconformity surface on the quality of clastic reservoirs. One poses that there is a marked change in sandstone porosity (either a reduction or enhancement) related to the unconformity; the other poses that there is no significant effect. This study aims to examine both hypotheses by investigating selected major unconformities that occur within or overlying North Sea Clastic reservoirs. The two principal case studies used investigate the effects of: (a) the Mid-Cimmerian Unconformity on reservoir sandstones of the Late Triassic Skagerrak Formation in Kittiwake Field, Central North Sea; and (b) the Base-Cretaceous Unconformity on reservoir sandstones of the Middle Jurassic Brent Group in the Tampen Spur area, Northern North Sea. Other case examples are examined more briefly.

The study specifically aims to:

1. Investigate the existence of any diagenetic changes in the selected sandstones that may have affected their reservoir quality by (either by enhancement or reduction of porosity).
2. Investigate any possible relationship of such diagenetic changes, where they exist, with the unconformity surfaces located at the top of these reservoirs.

In order to achieve the stated aims, it was necessary to:

1. Identify a number of regional and/or local unconformities in the North Sea area of study, in order to select those sections best suited for detailed study.
2. Identify the processes that have acted to create these unconformities and link these to the properties currently displayed by the unconformities.
3. Study how these unconformities may affect the reservoir quality.
4. Examine in detail the texture of sandstones in order to identify the different facies of sandstones and the distribution of their porosity.
5. Examine in detail the mineralogy of sandstones in order to identify any change in the primary composition.
6. Identify and quantify the presence of any authigenic minerals and highlight the diagenetic processes that may act to create these minerals.

7. Identify and quantify the presence of secondary pores within the studied sandstones and highlight the diagenetic processes that may act to create these pores.
8. Identify the potential mechanisms for the production of secondary porosity and authigenic minerals.
9. Identify and describe the nature and timing of any generated secondary porosity and/or authigenic minerals in the studied sandstones in order to investigate if it is related to the unconformity surface or not.

1.3 Research methods

In this study, sedimentological and petrographic analyses are the main approach that has been applied in order to understand the role of unconformities in the distribution of clay and porosity in selected North Sea clastic reservoirs.

1.3.1 Sedimentological analysis

The sedimentological core logging was carried out for all the selected wells following the procedure described in Appendix A.1. Description started with determination of grainsize by visual comparison of small sandstone samples using Wentworth size classification scale, followed by the description of lithology and sedimentary structures of each well. All field logs were then converted to graphic logs using Easycore software.

The main targets of these descriptions are as follows:

1. To confirm the presence and depth of unconformity surface and to match it with the composite log data.
2. To obtain useful information about the sandstone textural features.
3. To examine the depositional features in the studied interval where samples have been taken.
4. To differentiate between facies by describing the sedimentary structures presented and grain size, so that a series of discrete facies can be identified and changes in the sediments characteristics within the same facies can be investigated.

5. To interpret the depositional environment of each facies, so that the relation between the change of characteristics and the depositional environment can be studied.

1.3.2 Petrographic analysis

The petrographic analysis has been performed mainly by optical microscopy and scanning electron microscopy (SEM), supported by limited X-ray diffraction (XRD) results from previous studies, where appropriate.

1.3.2.1 Optical microscopy

All the samples chosen for petrographic study have been taken from wells that intersect with unconformity surfaces, starting from the point closest to the unconformity surface and below, so that a vertical comparison analysis could be made in order to study the effect of the unconformity surfaces on the physical properties of the sediments underneath. All the samples were taken from the logged cores, so that each sample was assigned to its facies based on core observations. Samples were taken from the logged cores both above and below the identified unconformities with more focus on the core sections underneath the unconformities. Several wells has been studied at each reservoir location contributing to same facies (detail of the screening criteria provided in section 3.2). In order to obtain representative samples and robust results one sample was collected at half foot frequency below the unconformity surfaces allowing thorough analysis close to each unconformity surface.

A total of 297 samples were collected from 21 wells in the UK Central and Northern North Sea and 98 samples from 11 wells in the Norwegian North Sea. All the selected samples were then sent to a specialist laboratory for thin-section preparation. In total, 212 thin-sections were prepared for detailed petrographic analysis. All the prepared thin-sections were impregnated with blue epoxy resin in order to identify the pore space easily. More details for the preparation of samples and analysis procedure of each sample are presented in Appendix A.2.

Using an optical microscope, each thin-section was then described in detail in order to:

1. Ensure that samples are representative of the main targeted sedimentological facies.
2. Describe and identify the texture of each sample at microscope scale to be able to analyse and identify the different facies of the sandstone and the distribution of its porosity.
3. Identify and quantify the different types of porosity and their distribution, destruction and/ or enhancement with depth underneath the unconformity surface.
4. To identify and quantify the different types of sandstone framework minerals in order to quantify any change in the primary composition.
5. To identify and quantify the presence of any authigenic mineralogy and highlight the diagenetic processes that may have occurred.
6. To identify and describe the nature of authigenic minerals and diagenetic processes in order to establish if they are related to the unconformity surface or not.

1.3.2.2 Point counting

Each thin-section sample was point-counted with 300 point per thin-section to maintain consistency and quantify the main sandstones texture and composition. The point counting result of each sample was then reported in a table as percentages of bulk volume, and transferred to excel sheet in order to be used for sandstone classification diagram and to generate porosity and minerals distribution diagrams. More details for the point counting procedure and the results of each thin-section sample are presented in Appendix A.2 and B.

1.3.2.3 Scanning Electron Microscopy

19 polished thin-section samples were also prepared and investigated using scanning electron microscopy method (SEM), which provides much higher resolution technique. This technique allowing clearer observation of porosity, diagenesis and mineralogical distribution in sandstones (Buckman, 2014). It was particularly useful in recognising the authigenic clay minerals (particularly kaolinite) from the detrital clay minerals, as well as any possible diagenetic processes. Details for the preparation of samples and analysis procedure are presented in Appendix A.3. The main objectives of this analysis were to:

1. Observe in greater detail the previously identified sandstone textures from the optical microscopy analysis
2. Make high resolution observations of minerals and porosity distribution in the studied sandstone samples.
3. Allow highly detailed observation of the porosity textural and their relationships to the minerals.
4. Allow accurate identification for any possible diagenetic processes.
5. Recognise the authigenic clay minerals (particularly kaolinite) from the detrital clay minerals.

1.4 Thesis structure

This chapter (Chapter 1) outlines the scientific rationale and aims of the study, highlighting the importance of unconformities to the hydrocarbon industry and the controversy that exists surrounding their influence on reservoir quality. It then briefly presents the methodology used.

Chapter 2 provides the background to this study with a review of (a) the types, origin, recognition and importance of unconformities, and (b) the origin, development and stratigraphy of the North Sea. This section highlights the stratigraphic distribution of the principal unconformities.

Chapters 3 provides a more detailed overview of the North Sea Jurassic unconformities, providing some statistical and sedimentological data on the nature of these surfaces, and the variation in facies and reservoir properties associated with them. From this overview, the specific examples to be used as case studies are selected.

Chapter 4 presents the first case study. Using sedimentological and petrographic analysis, this chapter evaluates the role of Mid-Cimmerian Unconformity on the distribution of porosity and kaolinite in the Skagerrak Formation of the Kittiwake Field in the Central Viking Graben. The chapter contains a brief summary about the geology of the studied area, results of the analysis performed, as well as a discussion of these results.

Chapter 5 presents the second case study. Using sedimentological and petrographic analysis, this chapter evaluates the role of the Base-Cretaceous Unconformity on the distribution of porosity and kaolinite in the Brent Group sandstones of the Tampen Spur area, Northern North Sea. The chapter contains a brief summary about the geology of the studied area, results of the analysis performed, as well as a discussion of these results.

Chapter 6: Using sedimentological and petrographic analysis, this chapter presents the results of the analysis performed for other North Sea wells, discussion of the obtained results and a brief conclusion.

Chapter 7: The main discussion of results is given in each of the case study chapters (Chapters 4, 5 and 6). This chapter, therefore, summarizes the principal findings and discussion from the whole thesis, draws the main conclusions, and suggests further work on the topic.

Chapter 2 **Review**

2.1 Unconformities - Background

The first unconformity recognized in 18th century was the base Devonian unconformity at Siccar Point in the south east of Scotland, where James Hutton observed the relationship between the deposition of the Upper Devonian Old Red Sandstone and Lower Silurian grey slate (Figure 2-1). From that time, unconformities were recognised as features of considerable significance to geological history. These unconformities, which were caused by either absence of deposition or erosion over a long period of time represent a large gap in the geological record. They have been often used as suitable surfaces to subdivide stratigraphic sequences in sedimentary basins (Wu et al., 2012).

Figure 2-1. Unconformity at Siccar Point

Unconformities are defined by (Bates and Jackson, 1970) as a structural relationship between rock layers in terms of contact, characterized by a period of non-deposition or insufficiency in the deposition rate of sediments, or by weathering or erosion prior to the deposition of new younger strata, the erosion being either subaqueous or subaerial (Liu et al., 1997). Therefore, unconformities are recognized as a basic tool

which divides the stratigraphic column into different depositional sequences or unconformity bounded units. An example of unconformities which have acted as stratigraphic sequence boundaries are the unconformities in the North America Cratonic Interior; in this case, six major unconformities have been identified which divide the stratigraphic column of cratonic deposits into six separate sequences of stratigraphic units (Figure 2-2). These identified sequences were identified as having a higher rank than a megagroup, by (Sloss, 1963). This particular type of bounding unconformities were formed due to the large scale relative change in sea-level over a long period of time and very high amplitudes (Burgess et al., 1997).

Generally, Geologists have distinguished four types of unconformities: angular unconformities, disconformities, non-conformities and paraconformities. Each type of unconformity is created by different processes in various environments. These processes involve periods of non-deposition or periods of erosion, which removes some of the deposited sediments, followed by resumption of deposition (Catuneanu, 2006).

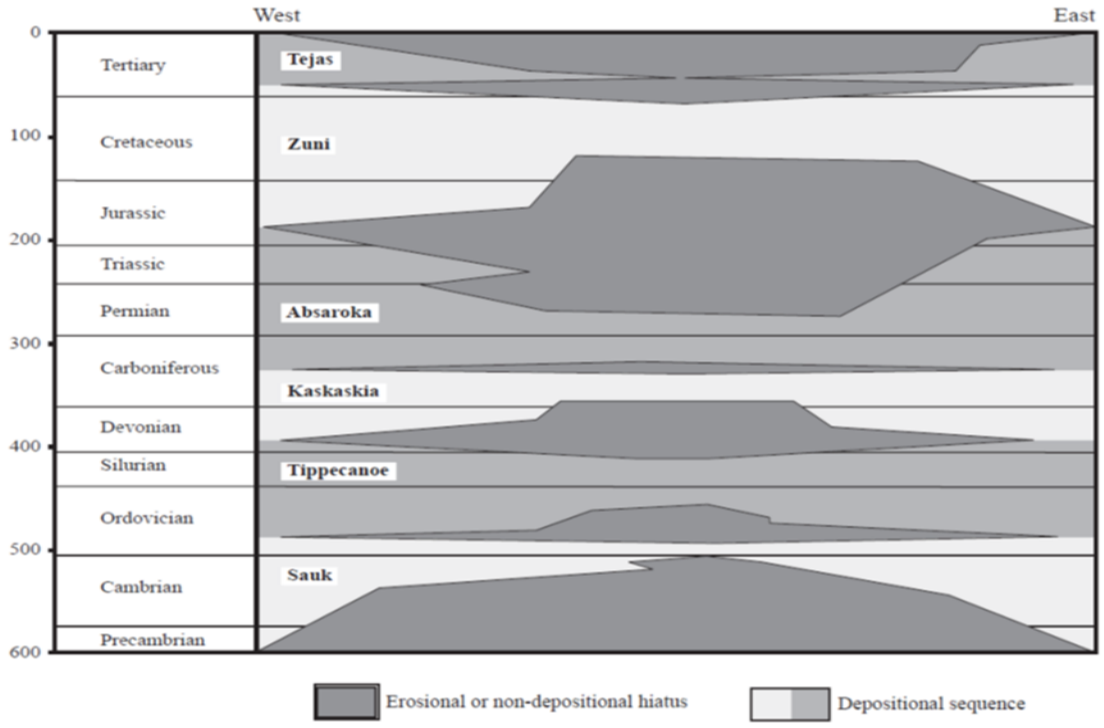

Figure 2-2. Chronostratigraphic diagram showing the six North America Phanerozok depositional sequences and their bounding unconformities, (from Sloss (1963).

2.1.1 Identifying unconformities-stratigraphic relationship

Angular unconformity: This type is formed if the older sediments have been tilted and truncated by erosion, then younger sediments were deposited on this erosion surface. The old sediments were accommodated in an area and then, due to the deformation the sediments, rocks were uplifted and tilted or folded, after which erosion removed part of the uplifted sediments; finally new subsidence occurred and new deposition of sediments took place on the top of the previous sediments, (Figure 2-3 a). This type of unconformity usually occurs in regions with high tectonic activity and is usually easy to recognise. Examples of angular unconformities include the base Devonian unconformity at Siccar Point, Scotland and the great unconformity in the Grand Canyon of Arizona, separating rocks of Precambrian age (Figure 2-4).

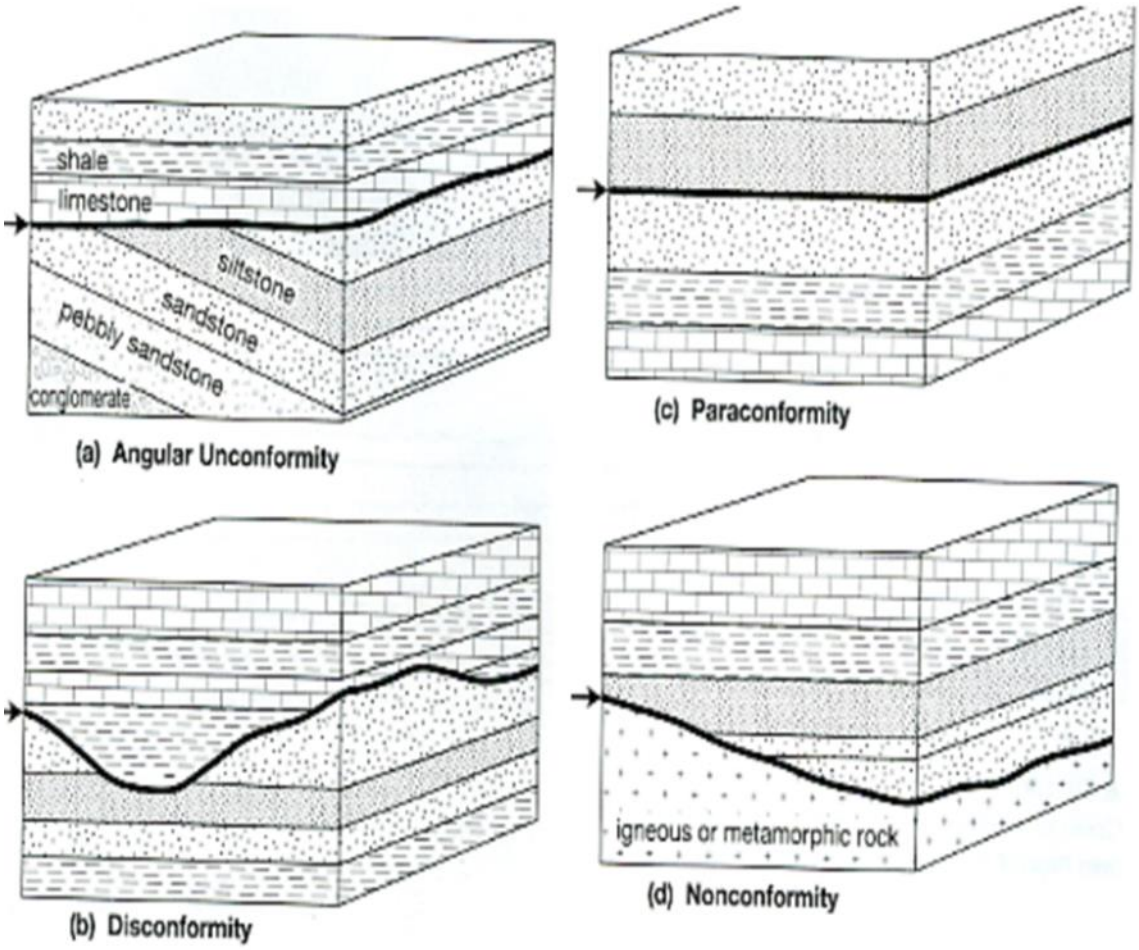

Figure 2-3 Types of unconformities

Figure 2-4. An overview for the underlying great unconformity of the Grand Canyon of Arizona with the overlying Tapeats Sandstone of Cambrian age formed about 175 million years ago (after, Swierczek, 2012)

Disconformity: this is an erosion surface between two bodies of sediments without the lower body being tilted before the deposition of the upper sediments' body. In this case, the first sequence will be deposited during subsidence, then uplift and erosion will occur, then new subsidence and deposition will occur (Figure 2-3 b). An example of this kind of unconformity is the Triassic disconformity in the Capitol Reef National Park, Utah (Figure 2-5).

Figure 2-5. Display part of disconformity in Capitol Reef National Park, Utah, where the Triassic Chinle Formation in the central part of the picture has a sharp contact (black line) with the overlying upper Triassic Wingate Sandstone (after, Swierczek, 2012).

Paraconformity: This is a type of unconformity that forms due to a period of non-deposition followed by a resumption of sedimentation and usually with no clear evidence of erosion (Figure 2-3 c), although early cementation nodules may occur along the paraconformity surface; an example of a paraconformity is the Oligocene Marshall paraconformity, New Zealand (Figure 2-6).

Nonconformity: This type of unconformity separates crystalline metamorphic or igneous rocks from the overlying sedimentary rocks. They usually indicate that a long period of erosion has occurred before the deposition of the younger sediments (Figure 2-3d). An example of this unconformity is the nonconformity in the Wind River Gorge of Wyoming (Figure 2-7).

Figure 2-6. The Marshall Paraconformity represented by the contact between the Ototara Limestone and Gee Greensand visible on the beach north of Kakanui. The contact is the Marshall Paraconformity. http://www.mikepole.com/.

Figure 2-7. An example showing part of the nonconformity in the Wind River gorge of Wyoming where the red line indicates the irregular contact between Precambrian granitic rocks and younger sediments (Swierczek, 2012).

In addition, sequence stratigraphy was also used to identify unconformities, unconformities have been divided into two main categories in terms of the environment in which they form: subaerial and submarine. A subaerial unconformity is an erosion or non-deposition surface formed largely in non-marine conditions, when there is high amplitude fall in the sea level. The subaerial unconformity is recognized as an important stratigraphic contact type because the most important breaks in the rocks' record are of this type (Catuneanu, 2006) , whereas the submarine unconformity (submarine erosion) is formed by marine erosion, either as a result of rapid rise of sea level or by a slow fall in the sea level. Unconformities can, however, also extend between non-marine and marine conditions, so that the same surface as sequence boundary can be created by subaerial erosion onshore and by submarine erosion offshore and may extend into correlative conformity deeper in the basin (Vail et al., 1977).

The relationship between the strata within a sequence and the unconformities forming the boundaries of depositional sequences can be either concordant or discordant: either parallel or non-parallel. If the strata are discordant, either below or above the unconformity surface, this gives us physical evidence of the presence of an unconformity. However, if the strata are concordant below and above the surface (parallel to it), that means there is no physical evidence of an unconformity along that surface. Discordance is the main physical standard which has been used to determine the presence of sequence boundaries, the particular type of discordant relationship will allow the identification of the type of unconformity, which may result from either non-deposition or erosion.

Truncation is the termination of strata which are cut off from their original depositional boundary by erosion; this is can be either erosional truncation, where the stratum terminates against the boundary above due to erosion (Figure 2-8 a-1) or structural truncation, which may form due to different structure events. Lapout is the lateral termination of strata against a physical boundary at the time of original deposition and it has been divided into two types:

Toplap: is a strata termination against the upper surface and it laps out at the top boundary of the depositional sequence. This horizon is initially inclined and forms mainly due to non-deposition and it usually occurs in shallow marine deposits and sometimes may occur in deep marine deposits (Figure 2-8 a-2).

Baselap: (either onlap or downlap) forms at the lower boundary of the depositional sequences. Onlap is baselap in which an initially horizontal stratum terminates against an inclined surface, or in which an initially inclined strata terminate in an updip against a surface of greater inclination (Figure 2-8 b-1). Downlap is baselap in which initially inclined strata terminate in a downdip against a horizontal or inclined surface (Figure 2-8 b-2) (Mitchum Jr et al., 1977). Both downlap and onlap indicate non-depositional hiatuses rather than erosional hiatuses (Woodcock and Strachan, 2000). In the case where there is no strata termination against the upper and lower boundary this will form top and base concordance (Figure 2-8 a and b-3).

The unconformities which bound depositional sequences are usually characterized by offlap at the top and strata onlap at the base, in coastal, marine and non-marine settings (Figure 2-9), (Christie-Blick, 1991). Strata which may terminate by either offlap or onlap in one direction can be terminated by downlap in the other direction (Mitchum Jr et al., 1977). Therefore, the downlap surface may be present both at the base and within the depositional sequences. In some cases, if the underlying unconformity is characterized by significant topographic relief, for example in basins controlled by faults (e.g. grabens) the strata may terminate by offlap, onlap and downlap in the same sequence (Christie-Blick, 1991).

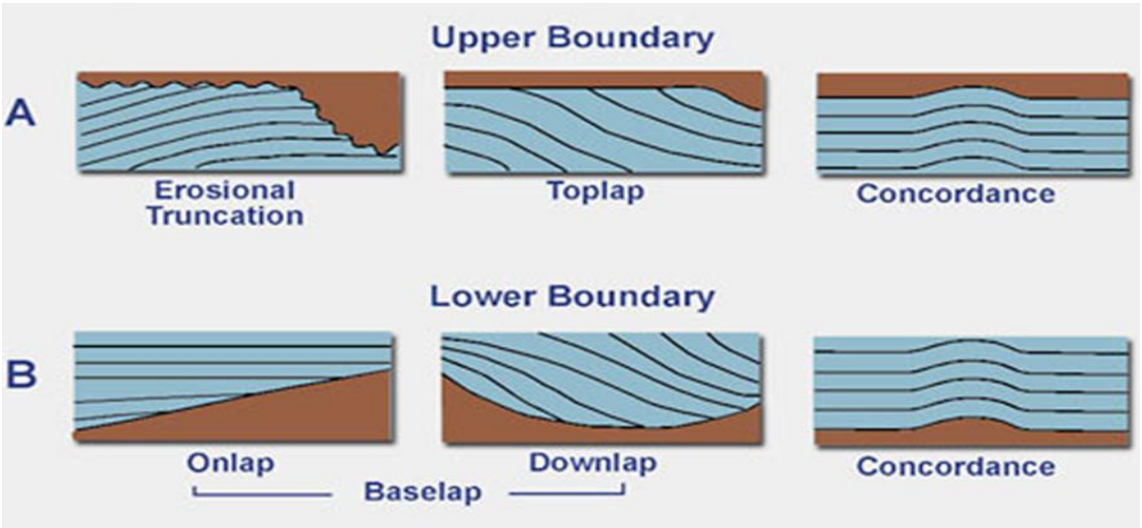

Figure 2-8. Relationship between an unconformities' surface and subcrop (A) or supracrop (B) (Vail et al., 1977).

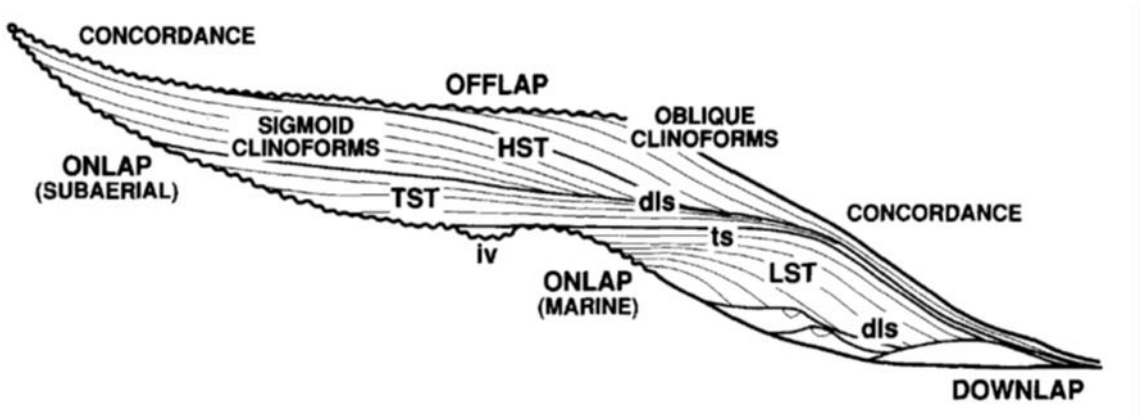

Figure 2-9. Strata geometry within an unconformity bounded depositional sequence (Christie-Blick, 1991).

2.1.2 Recognition of unconformities

According to (Shanmugam, 1988) a list of criteria can be used for recognizing and identifying unconformities, these criteria are classified into three types based on whether they are sedimentary, paleontological or structural. Observation of a single criterion may not indicate unconformity; however the association of many criteria will increase the likelihood that an unconformity is present (Krumbein, 1942). The following are the main criteria that can be used for recognising unconformities.

2.1.2.1 Structural criteria

The following are the most principle structural criteria:

1. Discordance of Dip

One of the most important structural criteria is the discordance of dip above and below the unconformity surface, where an angular relationship occurs between the strata below and above the surface as a result of erosion of old tilted strata followed by deposition of new younger strata. One of the best examples of this angular unconformity type is the unconformity at Siccar Point in Scotland (Figure 2-1). Outcrops and seismic profiles are the best places for recognising the discordance of dip. Truncated unconformities that may be formed as a result of eustatic sea level fall usually show low structural discordance compared with those formed as a result of

tectonic uplift (Shanmugam, 1988). According to Shanmugam, 1988, if there is no tectonic uplift the truncated unconformity formed during a period of low sea level is usually greatest at the shelf edge and progresses up-shelf by headward erosion and down-cutting of a river valley.

2. Erosional Surface

The undulant contact which cut the underlying sediment unit as a result of erosion or subaerial exposure of this unit usually called the erosional surface. This surface can usually be clearly observed in surface outcrops, whereas in subsurface data undulatory surfaces may be difficult to identify, unless associated with solution features such as karst topography in carbonate sequences or vugs, caves, leached fossils and sink holes. An example of a disconformity marked by an erosional surface is that on the buried karst topography under the lower Pennsylvanian rocks in South-eastern Kansas, developed on the Middle Mississippian limestone (Krumbein, 1942).

2.1.2.2 Sedimentary Criteria

The following are the most principle sedimentary criteria:

1. Degree of Deformation

The change in the degree of deformation between two units indicates that the lower unit has been deformed and eroded before the deposition of the upper unit. This is one of the criteria that indicate erosional unconformities. However, it should be noted that a similar kind of change can be observed just due to the different lithology types of the two units.

2. Basal Conglomerate

The conglomerate unit which contains some pebbles from the underlying unit is called a basal conglomerate; this unit contains weathered rounded and angular pebbles and usually occurs above an erosional unconformity. An example of a basal conglomerate unit is the Pennsylvanian detrital chert that occurs directly above the Pennsylvanian unconformity in the Texas Permian Basin (Shanmugam, 1988).

3. Weathered Chert

Weathered chert is usually porous and chalky white in colour, whereas fresh chert is usually dense and dark in colour. This weathered chert is good indicator for subaerial erosional unconformities, where it may exist below and above the unconformity surface. However, it is important to distinguish between beds with in-situ weathered chert and beds with transported chert.

4. Enhanced Porosity Zones

If carbonate sequences are subaerially exposed to meteoric water, karst topography and cavernous porosity will be developed as a result of dissolution. Similarly, if silica clastic units are exposed to acidic meteoric water, dissolution of some grains and cement will take place, leading to development of porosity and permeability beneath the unconformity surface. However, caution must be exercised because high porosity and permeability can also be formed and developed where there is no unconformity surface.

5. Sharp Change in Lithology

Sharp lithological changes may indicate a significant stratigraphic breaks or subaerial exposure, for example when beds of fluvial origin are overlain by marine deposits.

6. Duricrust

The term duricrust has been used to describe a hard crust that may occur on the surface in a semiarid climate. The main types of duricrust are calcrete, silcrete and ferricrete. Calcrete, which is composed of calcium carbonate crusts, sand, gravel and clay usually develops in semiarid or arid regions at or near the surface. Silcrete usually represent hard crusts of silicified sand that may developed during the subaerial weathering. Ferricrete represents a hard mass of surficial sand and gravel which are cemented by iron oxide that may have developed due to oxidation during weathering of red bed units, which may reach a hundred metres in thickness (Shanmugam, 1988).

7. Submarine Canyons and Channels

The submarine channels which are commonly filled with turbidite sandstones, debris flow, slumps and mudstone can be used as indicators of submarine erosion.

8. Kaolinite

Kaolinite is the most common mineral at unconformities, The association of diagenetic kaolinite with subaerially exposed surfaces was studied by (Al-Gailani, 1981). However, caution must be exercised, because kaolinite may also develop during burial diagenesis not just with subaerial exposure.

9. Glauconitic Minerals

Authigenic marine minerals rang in composition from glauconitic mica to glauconitic smectite. Glauconitic minerals are usually formed in open marine environment in water depths of 50 to 500 m. However, occasionally they may develop directly above major hiatus as a result to a contours currents at water depth ranged from 1600 – 2500 m (Odin, 1985). An example of that is the existence of the glauconitic zone in the break between Ellenburger limestone and the lower Brend in north central Texas. The occurrence of glauconitic minerals in deep marine zones may indicate erosion, whereas the occurrence in shallow marine zones can be indicator of a slow deposit period. On the other hand, glauconitic minerals may also form in conformable facies; therefore glauconite is a doubtful criterion in recognising an unconformity's surface and should be supported with other evidence' for example, glauconite usually appears coarser and deeper in colour if it is associated with an unconformity (Shanmugam, 1988).

10. Phosphatic Pellets

Phosphatic nodules or pellets can be used as an indicator of submarine unconformities, as it has been reported by several writers that occurrences of phosphatic pellets and nodules are associated with unconformities (Krumbein, 1942). In the subsurface the phosphatic pellets and nodules can be recognised by their appearance in well cutting or by phosphate chemical tests.

11. Manganese Nodules

Manganese Nodules are usually associated with erosional surfaces formed by strong bottom currents in deep water, therefore, manganese nodules found in the rock record may be used as indicator for a submarine erosional surface.

2.1.2.3 Palaeontological Criteria

The following are the most principle palaeontological criteria:

1. Abrupt faunal change

The major breaks along unconformities are mainly recognised by the use of fossils to date the rocks below and above the unconformity; if the fossils are considerably different in age, this means there is a major temporal break. Abrupt faunal change without an age difference may be produced as a result of environmental change. In the subsurface, the evidence for unconformities can be recognised from microfossils in the rock cuttings.

2. Land plants or animals in situ

The occurrence of land animals and land plants in situ are commonly used as indication of a gap between adjacent units.

Other features that may be associated with unconformities can be used with the previous criteria for recognising unconformities. However, many of these features may occur in conformable sequence; therefore caution must be always exercised when using one of these criteria in recognising unconformities and one should try to look for associations of numbers of criteria to increase the chances that an unconformity is present.

Each of the previous types of criteria used for recognizing and identifying unconformities is usually associated with a different unconformity type in terms of its origin, either subaerial origin, submarine origin or both. Table 2-1 shows a breakdown of these criteria and their association with different unconformity types and the processes that occurred to

create these unconformities, as well as their expected effect on the reservoir characteristics.

Table 2-1 A list of criteria which can be used for recognizing and identifying unconformities and the processes that occurred to create these unconformities as well as their expected effect on the reservoir characteristics (Shanmugam, 1988).

Unconformity type	Formation Processes	Expected Effects	Evidence for
Submarine Erosion	created by either transgression, mass movement, turbidity currents, thermohaline currents, carbonate dissolution, storms and clastic influx	➢ Removal of material ➢ No change in properties	➢ Submarine canyons and channels ➢ Glauconitic minerals in deep marine ➢ Manganese Nodules ➢ Abrupt faunal break ➢ Seismic Reflection Profiles
Subaerial Erosion	created by either tectonic uplifts or eustatic sea level fall	➢ Removal of material ➢ Erosional can enhance porosity in the underlying siliciclastic, carbonate and even igneous rocks	➢ Discordance of dip ➢ Erosional surface ➢ Regional truncation ➢ Change in degree of deformation ➢ Fluvial Valleys ➢ Basal Conglomerate ➢ Weathered chert ➢ Zones of enhanced porosity ➢ Abrupt faunal break ➢ Seismic Reflection patterns ➢ Log patterns ➢ Stable isotopes ➢ Oil Seeps
Submarine Exposure		➢ Cementation ➢ Phosphatization in some cases	➢ Glauconitic minerals in shallow marine ➢ Abrupt faunal break
Subaerial Exposure		➢ Dissolution: porosity may increases below most erosional unconformities due to dissolution of unstable cements (e.g., calcite) and framework grains (e.g., feldspar) which are subject to dissolution by acidic meteoric waters. ➢ Cementation: in exemption cases subaerial exposure may cause cementation with porosity reduction	➢ buried soil horizons ➢ silcrete, calcrete and ferricrete ➢ abrupt change in lithology ➢ tidal flat facies ➢ volcanic ash (in some cases) ➢ kaolinite (in some cases)

2.2 Origin, Development and Evolution of the North Sea

2.2.1 Introduction

The North Sea is located northwest of central Europe and is touches the shores of Great Britain, Denmark, Norway, the Netherlands, Belgium, Germany and the northern tip of France (Figure 2-10). The North Sea formed as a separate geological region following the Caledonian orogeny between 510 and 390 million years ago. Subsequently, the region has undergone a number of significant geological events and changes in plate tectonic settings, which are summarized in the following sections, tables and figures.

2.2.2 Main Structural events which controlled the North Sea

The main events which controlled the geological structure of the North Sea from the Palaeozoic to Cenozoic can be described briefly in eight main events. Three of these events are related to the changing organization of the major plate-margins (for example subduction-accretion processes and ocean-creation); the other five events are related to intraplate deformation (Glennie, 1998). Figure 2-11 shows an overview of these different tectonic phases.

2.2.2.1 Precambrian events

2.2.2.2 The Caledonian plate cycle (510- 390 million years ago)

The Caledonian Mountains formed as a result of the collision between Baltica, Laurentia and Avalonia. They were formed during Late Cambrian to Late Silurian times by a combination of the Athollian and Caledonian Orogenies. Before these events, the North Sea area comprised widely separated continental fragments and different parts of the Early Palaeozoic Iapetus Ocean and Tornquist Sea (Figure 2-11 C).

2.2.2.3 The Variscan plate cycle (380- 270 million years ago)

This cycle lasted from the Devonian to the Late Carboniferous (Table 2-2), during which time adjustments in plate motions caused rifting between the margins of the Scandinavian

cratons and Laurentia. The extension can be clearly identified in Devonian reactivation of Caledonian features and by the structural relief present during the Early Carboniferous.

The Late Carboniferous Variscan Orogeny marked the southern Proto-Tethys Ocean closure and creation of the supercontinent Pangaea (Figure 2-11 E). This tectonic event is an important event for the North Sea's hydrocarbon potential, because it marks the beginning of the sedimentary infill of the basins located under the current North Sea. From the Permian period onwards the North Sea has lain in an intraplate setting; however, this region did not remain quiet, as another five significant tectonic events were identified. The deformation styles created by all these events have been influenced by the pre-Permian geological and structural arrangement inherited from the Caledonian and Variscan orogenies and the original Precambrian blocks.

Figure 2-10. North Sea area geographical map

2.2.2.4 Permo-Triassic rifting and thermal subsidence

In the late Permian, subsidence was occurring in the Moray Firth region and in the east-west trending Southern and Northern Permian basins. This subsidence may coincide with the beginning of subsidence in the regions which would later become the Viking Graben and the Central Graben (Figure 2-11 F). The subsidence continued through the Triassic to the early Jurassic, when it was terminated by the Middle Jurassic thermal doming.

2.2.2.5 Middle Jurassic domal uplift

Due to the development of a strong but transient mantle plume below the central North Sea area, uplift, rifting and widespread erosion developed throughout the central North Sea region, as well as volcanism and the triple junction rift system.

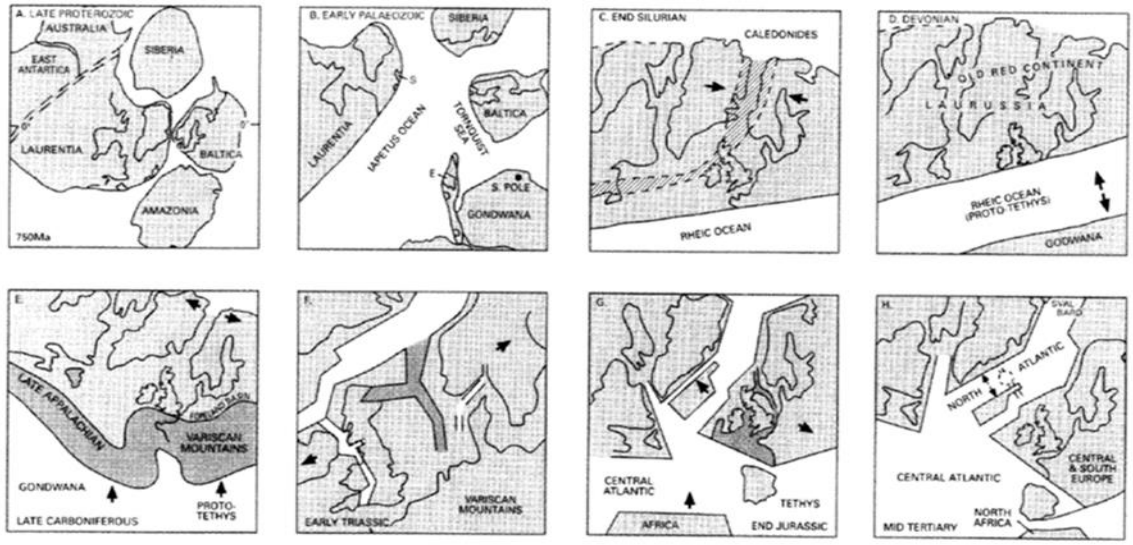

Figure 2-11. Diagrams depicting the major tectonic events which controlled and formed the North Sea basin during Proterozoic and Phanerozoic in Scotland and England (after (Glennie and Underhill, 2009).

2.2.2.6 The Late Jurassic to earliest Cretaceous extensional tectonics

Extensional tectonics and rifting during the Late Jurassic and Early Cretaceous are significantly important to understand the hydrocarbon system in the North Sea. The extensional tectonics related to rifting led to rotations of fault blocks which formed major structural traps within the Viking and Central Grabens, whereas in the west of the

Shetland areas the development of an extensional basin was followed by post-rift thermal subsidence in the North Sea in the period of the late Cretaceous and Cenozoic.

2.2.2.7 Development of the Iceland hot spot and North Atlantic rifting

In the western parts of the UK, the far-field tectonic influence of the North Sea rifting was replaced during the Cretaceous by more local extension linked to the sea floor spreading associated with the initiation of the North Atlantic Ocean (Table 2-2). At first, this rifting was concentrated along the Rockall-Faroes Trough (Figure 2-11 G), but by the Mid Tertiary it had been changed to the present axis (Figure 2-11 H). The Iceland hot spot development and the opening of the Atlantic Ocean were the main factors controlling Cenozoic uplift in the British Isles. The western rift arm in the North Sea and the Inner Moray Firth have been affected by the resultant regional eastwards tilt (Hillis et al., 1994, Thomson and Underhill, 1993).

Table 2-2. Major tectonic events which affected the geology of the North Sea (after Glennie and Underhill (2009)).

Age	Period		Events in the North Sea	Southern North Sea
Cenozoic	Miocene	INTRAPLATE SETTING	REGIONAL SUBSIDENCE CENTRED OVER GRABEN SYSTEM	↑ Zechstein diapirism
	Oligocene		Doming of West Shetlands; Uplift of Moray Firth & Scottish Highlands	Inversion of NW-SE trending sub-basin (SNS)
	Eocene		↑	↑
	Palaeocene		↑	↑
Cretaceous	Late		↑	↑
	Early		↑	↑ Zechstein diapirism
Jurassic	Late		Rapid subsidence of inner Moray Firth;	Erosion
	Middle			Rapid Sole Pit subsidence
	Early		Volcanic activity in East Moray Firth	RIFT & WRENCH TECTONICS
Triassic			Earliest Zechstein diapirism	
				4000 m Triassic in Polish Trough
			DEVELOPMENT OF NW EUROPEAN BASIN/GRABEN SYSTEM	
				ZECHSTEIN FLOODING OF SUB-SEA-LEVEL BASINS
Permian	Late		SUBSIDENCE OF MORAY FIRTH, NORTHERN & SOUTHERN PERMIAN BASINS	
	Early	VARISCAN PLATE CYCLE	E –W Scottish dyke swarms volcanics	Extrusion of L. Rotliegend volcanics
Carboniferous	Stephanian			Inversion of Sole Pit Basin
	Westphalian		RIFTING IN NORTH BRITISH ISLES	2500 m Upper Carboniferous (SNS)
	Namurian		↓	VARISCAN FOREDEEP
	Dinantian			↑
			Renewed uplift of Scottish Highlands	↑
Devonian	Late			BAC – ARC–RIFTING
	Middle		Volcanics in Orcadian Basin	↓
	Early			↓ OLD RED SANDSTONE
				↓
			Granites in Scottish Highlands and Lake District; Subsidence in Orcadian Basin; Volcanics in S. Scotland	
Silurian		CALEDONIAN PLATE CYCLE	Collision of the Norwegian Caledonides with the Scotland Northern highlands Caledonides and Greenland Closure of the Iapetus Ocean	
Ordovician	Upper		Closure of the Tornquist Sea	
	Middle		Andesitic volcanism south of Lake District	
	Lower		Uplift - > source for conglomerates and turbidite fans in the Southern Uplands	
Cambrian			Carbonate-platform deposition	

2.2.2.8 Tectonic inversion of the Mesozoic basins

During the Late Cretaceous and Tertiary, the former sedimentary basins across north-west Europe, including the southern North Sea, were involved in tectonic inversion due to the intraplate compression caused by the Atlantic Ocean spreading and the collision of Africa and Europe.

2.3 Stratigraphy of North Sea

This section presents a brief summary of the stratigraphy of the main geological period of the whole North Sea area, the Northern, Central and Southern parts of the North Sea.

2.3.1 Devonian Period

During the Devonian Period (410 Ma- 360 Ma) the newly formed Caledonian mountains were eroded and in low-lying areas widespread red bed sedimentation was formed. Most of the Southern North Sea remained an upland area, with high erosion rates, while in lower lying areas to the north deposits formed from this erosion are referred to as the Old Red Sandstones (Downie, 1998). The Old Red Sandstone mainly comprises deltaic and fluvial sediments, spread over a large area and may reach up to 11 km of thickness. In the Mid-Devonian, around 375 million years ago, extension and rifting began in the southern Central North Sea, marked by marine limestone deposits.

Unconformities: The Devonian-Carboniferous boundary is marked by a major unconformity which developed as a response to the north-south compressive events related to the final phases of the Caledonian continental collision (Glennie, 2009).

2.3.2 Carboniferous period

During the Carboniferous period, most of the North Sea area was a flat low-lying coastal plain formed by the erosion of the Caledonian Mountain range. In the Early Carboniferous, around 360 million years ago, extension and rifting began in the Southern North Sea Basin, followed by deposition of deltaic sediments close to the low-lying land mass or deep water sediments within the graben areas (Cameron et al. 1992). The main thickness of North Sea Carboniferous deposition accumulated in the Southern North Sea

(Leckie, 1982). Sediments of shallow marine and fluvio-deltaic and locally volcanic origin have accumulated in most parts of the central North Sea in areas where there was regional crustal extension. In the Northern North Sea, Lower Carboniferous stratigraphy is characterised by volcanic activity. Therefore, it is possible to find some plugs, sills, basaltic lavas, tuffs and dykes in this part of the succession (Ziegler, 1977). The Carboniferous period is an important period for the North Sea petroleum geology due to its great thicknesses of coal and carbonaceous shale, which has been determined to be the main source rock for the gas accumulation in Carboniferous and younger Permian reservoirs in the Southern North Sea; furthermore, it has some important sandstone bodies which act as hydrocarbon reservoirs (Glennie, 2009).

Unconformities: Approximately 300 million years ago, during the Late Carboniferous Variscan Orogeny, the Carboniferous rocks in the North Sea were gently faulted, folded, uplifted and eroded, creating an angular unconformity between Carboniferous and younger strata across the North Sea. In the Southern North Sea more than 1500m of the Carboniferous strata has been eroded due to the regional uplift (Besly, 1998).

2.3.3 Permian Period

After the Variscan Orogeny and between 280-210 million years ago, in the Permian to Triassic Periods, more than 2700 m of strata were deposited, including red bed facies and evaporite successions (Glennie and Underhill, 2009). During the Permian, two basins were formed, the South Permian Basin and the North Permian Basin. These two basins are separated by a high which is located between central Denmark and the Mid North Sea-Ringkøbing-Fyn (Taylor, 1990). The Permian Rotliegend Group (red beds) which have been accumulated in the post-Variscan basin and extended from eastern England to the Russo-Polish border is known as Southern Permian Basin. The other smaller accumulation of red beds, which occurred between the Mid North Sea Ringkøbing-Fyn High and the Egersund and the Shetland platforms is known as the Northern Permian Basin. Another area where the Rotliegend Group occurred is within the Moray Firth Basin. A Late Permian marine transgression led to deposition of cyclical evaporitic successions (Zechstein Formation) in the Southern and Northern Permian basins. The thickness of this formation reaches up to 1000 m (Cameron, 1992).

Unconformities: On the eastern side of the South Permian Basin the Rotliegend sedimentary succession can be divided into two units, Upper and Lower units. The Lower Rotliegend unit is characterised by the presence of acidic volcanic rocks and is separated from the Upper Rotliegend unit by the Saalian Unconformity, which was formed as a result of the uplift and erosion associated with the development of the Variscan Orogeny (Glennie, 2009). The rare volcanic rocks of the Upper Rotliegend are basaltic.

2.3.4 Triassic Period

The North Sea Triassic sediments reflect the tectonic changes that accompanied the closing of the Palaeozoic Era. During the Triassic, a complete succession of sediments (up to 2 km) were deposited in the Southern North Sea basin (Leckie, 1982). The Southern North Sea Basin is dominated by fine, with some coarse-grained clastics sandstones, shale and evaporates. In the Central North Sea, only the Bunter Shale Formation is present. This is most likely related to the period of erosion during the Middle Jurassic, which may have eroded any other sediments. In the North of the Southern North Sea Basin a several grabens were formed during Triassic. Very thick sequences of clastic sediments were filled into the Triassic Grabens, ranging from claystone to conglomerates (Leckie, 1982).

Unconformities: In the Late Triassic, minor rifting occurred and the Viking Graben developed in the area of the Northern North Sea. Regional uplift and tilting of Triassic sediment occurred due to the mantle plume, which developed at this time beneath the North Sea region. Although the tectonic activity during this time was low, some tectonic phases and minor unconformities were developed. Reactivation of the Variscan basement faults in the Late Triassic and Early Jurassic enhanced the subsidence in the Sole Pit Basin and triggered the earliest mid-Triassic halokinesis (Glennie and Boegner, 1981).

2.3.5 Jurassic Period

The major phase of rifting in the North Sea was in the Jurassic period. The rifting started in the late Triassic in the north and then spread southwards. This rifting event created and/or extended the Viking Graben in the North during the Middle Jurassic (Underhill and Partington, 1993). Many isolated basins have been formed due to this rifting, each basin has a unique sedimentary succession. Faults along the rift edges encouraged and concentrated Zechstein salt tectonism and differential loading. Many alluvial fans and

deltas were deposited within the rift valley successions due to the erosion of exhumed ridges on the footwall side of normal faults. The Statfjord Sand of the Viking Graben is one of the reservoir formations formed through this process.

The Lower Jurassic marine layers are widespread over the Southern North Sea and adjacent areas, whereas they are absent in the eastern parts of the Southern Viking Graben, Moray Firth and the Central Graben. The absence of Lower Jurassic strata in these areas is probably due to the erosion caused by post-depositional uplift of the Southern Viking Graben and the Central Graben (Glennie, 1998).

In the northern North Sea Basin, Jurassic strata comprise of many formations, the Statfjord Formation and Dunlin Formation are two of these. The Statfjord Formation deposition passes upwards from a continental alluvial environment to a marginal marine environment. The Dunlin Formation deposition is mainly prodeltaic mudstones; the main source of these sediments was the active fault margins (Leckie, 1982). These layers of the Early Jurassic are described as important hydrocarbon reservoirs, especially in the Inner Moray Firth, where they form the lower reservoirs of the Beatrice Field, and in the North Viking Graben, where they are often potential reservoir layers below the Brent Group succession of the Middle Jurassic (Glennie, 2009).

The boundary between the lower and Middle Jurassic sediments is marked by a widespread stratigraphic break called the Mid-Cimmerian Unconformity, extending from the North Viking Graben to the Southern North Sea and from the Moray Firth to Danish Central Graben. (Glennie and Underhill, 2009). The development of this unconformity was associated with a relative fall in sea level, marked by the start of non-marine deposition.

The sediments laid down above the unconformity to form the Brent Group, involved a deltaic succession, including reservoir, seal and source rocks in the North Viking Graben, and the Fladen Group of the Central Graben and Moray Firth (Underhill, 1998). The Brent Group lower section comprises of the Etive and Rannoch Formations, which are upward coarsening, micaceous sandstones. The Brent Group middle section comprises the Ness Formation: this Formation represents a fluvial-deltaic facies with channel, lagoon, and

coal deposits. The upper section, the Tarbert Formation, comprises fine to medium sandstones with mudstone and subordinate siltstone representing a marine transgression.

During the Middle Jurassic paralic sediments were accumulated when a significant subaerial thermal dome formed within the Central North Sea. This was due to the development of a widespread, hot and transient mantle-plume head (Underhill and Partington, 1993). Widespread domal uplift occurred in the centre of the Central North Sea and led to the development of an erosional unconformity: for example, during this period more than 1000 m of the Jurassic and Triassic strata was eroded from the Cleaver Bank High (Glennie, 1986).

Late Jurassic was a time of significant extensional faulting. In the beginning, the rift was very strong in the extremities of the present graben system and with time it propagated back towards the dome centre (Fraser, 1993). The onset of this significant rift perhaps started to occur around 155 million years ago, in the middle Oxfordian to early Kimmeridgian (Underhill, 1991). According to (Johnson et al., 2005), seismic sections show that the sedimentary succession of the upper Jurassic were thicker toward the syndepositional faults. There is a variation in the style of the rift between the Central and Northern North Sea. This variation was likely to have been controlled by two main factors: 1- The variation of tectonic grain and basement composition between the Central and Northern North Sea, which can affect the structural development (Erratt et al., 1999). 2- The absence of the Upper Permian salt deposits in the Northern North Sea (Helgeson, 1999).

During the Jurassic period many types of potential reservoirs were formed, including, for example, the Middle Jurassic Brent Group (deltaic, shallow marine and coastal sandstone reservoirs), Brae-Miller Formations (deep marine sandstones) in the Late Jurassic. The Humber Group in the Late Jurassic, are dominated by shale and mudstone and divided into the Heather formation and Kimmeridge Clay Formation, considered as the main hydrocarbon source rock in the Northern North Sea (Graham et al., 2003).

Unconformities: As outlined above, the active tectonics and associated sea-level rise and fall, led to a series of important unconformities within the Jurassic succession. These include the following regionally significant unconformities: (a) the Mid-Cimmerian

Unconformity (MCU); (b) the Base Humber Group Unconformity (BHU); (c) the Base Kimmeridgian Unconformity (BKU); and (d) the Base-Cretaceous Unconformity (BCU).

2.3.6 Cretaceous Period

The Cretaceous System period can be separated into two significant sequences: the early Cretaceous Cromer Knoll Group, which is mainly composed of siliciclastic facies unconformably overlying the Late Jurassic Humber Group. This transfer from the Humber Group to the Cromer Knoll Group marks the end of rift activity and the start of the thermally controlled subsidence in the Northern North Sea. Most of the North Sea was covered by shallow warm sea during the Late Cretaceous and thick deposits of chalk have accumulated, the dominant marine conditions during the Late Cretaceous led to the deposition of a thick succession of chalky limestone over the Southern and Central North Sea. Late Cretaceous deposits are more argillaceous in the North, where they are assigned to the Shetland Group (Oakman and Partington, 1998). The transition from the Chalk Group in the southern and Central area of the North Sea to argillaceous in the deeper waters of the northern of North Sea may be due to a higher rate of subsidence in the northern areas, which dropped the seabed below the local carbonate compensation depth (Leckie, 1982).

Unconformities: For the northern and central North Sea, the Cretaceous saw a period of relatively continuous sedimentation with none or few minor unconformities developed. The southern North Sea, however, experienced more significant uplift in some regions and hence the development of pronounced unconformities.

2.3.7 Cenozoic Era

In the early part of the Tertiary Period, rapid subsidence was occurring in the Viking and Central Graben, during the Laramide Orogenic phase (from Late Cretaceous to Middle Eocene). As a result of the rifting and associated palaeogeographic changes, the rift flanks were eroded. At the same time, uplift of the Shetland platform, which probably formed due to the increase of mantle activity below this area, caused erosion and exhumation to take place (Ziegler, 1994). The material which was eroded was transported toward the east and accumulated in the outer Moray Firth. The succession deposited during the Palaeocene to early Eocene Epochs can be divided into two sedimentary successions. The

first succession of deposition was dominated mainly by submarine fans, the second depositional succession was mainly dominated by shelf and coastal deposition (Glennie and Underhill, 2009). During the Sub-Hercynian and the Laramide Orogenies, inversion related tectonic activity occurred in some basins, such as the Broad Fourteenth, Southern Central Graben and West Netherland basin, which caused erosion, removing most of the Cretaceous deposits in these basins. This inversion also formed different structures and important traps (Ziegler, 1977).

During the rest of the Tertiary Period, subsidence continued and basins were filled by a succession of sands and muds (Bowman, 2009). In the Southern North Sea, during the Oligocene to Miocene Epochs, a number of the basement faults were reactivated by dextral strike-slip motion (Glennie, 1986), leading to a reactivation of salt tectonics. In the early Quaternary period, the rapid subsidence became more widespread and led to the preservation of more than 600 m of Pleistocene progradational delta deposits and glacigenic deposits (Kent, 1967). During the Cenozoic, thermal maturation of the organic material and migration of the generated hydrocarbon occurred. Therefore the Tertiary subsidence history in the North Sea is of economic interest (Nielsen et al., 1986).

Unconformities: The main unconformities of the Cenozoic succession in the North Sea are associated with the early tectonic activity and therefore occur within the Paleocene and Eocene successions.

2.4 Clay Mineralogy and Sandstone Diagenesis in the North Sea

The most common clay minerals are kaolinite ($Al_2Si_2O_5(OH)_4$), illite ($KAl_3Si_3O_{10}(OH)_2$), chlorite ($(Fe\text{-}Mg)5Al_2Si_3O_{10}(OH)_8$) and smectite $(Na, Ca)0,3(Al, Mg)_2Si_4O_{10}(OH)_2.n(H_2O)$. All types of clay may occur as detrital components or due to diagenetic reactions. In general most of the observed clay minerals in North Sea reservoirs are authigenic and the distribution of these minerals depends mainly on the diagenetic processes.

The main driving mechanisms for diagenetic reactions are changes in existing pore-fluid chemistry, temperature and pressure. This reactions needs a thermodynamic drive so that the precipitated minerals are more stable than the dissolved minerals.

At shallow depth some clay minerals such as kaolinite and smectite may form due to early diagenetic processes during meteoric water flow or as a result of weathering. This early diagenetic processes can be considered a continuation of the weathering process. For example:

Rock (feldspar, mica) + water = clay + cations.

With greater burial depth and higher temperatures these minerals become unstable:

Clay (kaolinite, smectite) + cations (K +) = aluminosilicate (illite) + quartz + water.

Modified from Bjørlykke, K. (1998).

2.4.1 Early (shallow) diagenesis

Kaolinite, smectites, and chlorite may occurs as early diagenetic (eogenetic) cements depends on the rate of weathering and composition of the detrital minerals, climate and composition of pore water.

The kaolin family of aluminosilicates and kaolinite needs low ionic, low pH waters and therefore they are common in fluvial and deltaic environments.

When fluvial and deltaic sediments flushed by meteoric water shortly after deposition the changing of the water geochemistry may lead to diagenetic reactions. For example if

feldspathic sandstones is flushed with meteoric water this will lead to dissolution of unstable minerals (e.g. feldspar and mica) and precipitation of kaolinite:

$2K\ (Na)\ A1Si_3O_8 + 2H + 9H_2O = A1_2SiO_5\ (OH)_4 + 2H_4SiO_4 + 2K(Na +)$

This reaction only occurs in open system as it requires the supply of protons and the removal of cations such as Na + and K + and silica by fluid flow. Furthermore ground waters are often in the stability field of kaolinite .(Bjørlykke, 1998). Plagioclase and albite can also dissolve in similar way and the reaction will be controlled by the Na +/H+ ratio.

Smectites and related minerals usually form in Na–K-rich, alkaline brines with existing of oxidizing conditions (Jeans, 1978). Chlorite develops in marine waters and glauconite usually occurs in Fe-rich, oxidized shallow marine environments (Odin & Matter, 1981).

The existing shape of these clays varies from one to other based on their mineralogy and chemistry (Wilson & Pittman, 1979). Kaolinite tend to occur as euhedral hexagonal crystals or pore-filling aggregates. Smectites usually replace grains that contain Mg and Fe and occurs as very small crystals lining intergranular pores.

2.4.2 Burial diagenesis

During burial diagenesis kaolinite, illite and chlorite may occur as burial diagenetic (Mesogenetic) cements. Kaolinite may occurs as vermiform masses which fill and occupy pores. It can also form as a replacement of altered feldspar minerals. (Ehrenberg et al., 1993). At deeper burial and high temperatures that exceed 70°C the remaining K-feldspar and kaolinite may react leading to formation of illite, which occurs as a fibrous pore-filling mineral that strongly reduces the reservoir quality. However if the K-feldspar in sandstones were completely leached in shallow burial by flushing of meteoric water kaolinite may remain stable and do not react to illite even with burial depth and high temperatures because there will be no K-feldspar to supply the required potassium to form illite. If the released silica during the feldspar dissolution allowed to build up in the pore water, smectite rather than kaolinite may become the stable clay minerals. Chlorite may also occur as burial diagenetic (Mesogenetic) cements as radial detrital grain coatings composed of euhedral plates which usually shield detrital grains from further diagenetic processes

In addition, many studies documented that dissolution of feldspar and precipitation of kaolinite can occur at deeper burial as a result of the generation of acids from source rocks or due to the biodegradation of oil in the reservoirs (Burley, 1986). Even if small amount of acid were generated kaolinite may form without removing the potassium if k-feldspar is present.

Other studies also suggested that the kaolinite may form due to aqueous transportation of dissolved aluminium in the surrounding shales into the sandstone body.(Ehrenberg, 1991).

In general, the dissolution of unstable minerals (e.g. feldspar) and the precipitation of other minerals (e.g. kaolinite) is well documented in the North Sea. Each basin has a different depositional history and clay diagenesis is influenced by many different factors such as the primary clastic composition of sedimentary rocks, a source of a high amount of aggressive fluid, available mineral species, depositional environment and diagenetic history. All these factors may cause changes in geochemistry of the pore fluids and diagenetic reactions will take place.

In summary Most of the North Sea diagenetic clays rich zones are interpreted to be generated due to the intense alteration of detrital aluminosilicates (particularly feldspar) as a result of early (shallow) diagenesis processes (e.g. subaerial weathering of the top of the sandstone) or burial diagenesis processes that may formed due to the presence of high acidic fluids generated as a result of thermal maturation of organic matter in the surrounding shales.

Chapter 3 North Sea Jurassic Unconformities: A Statistical and Sedimentological Overview

3.1 Introduction

Having reviewed North Sea stratigraphy (Chapter 2, Section 2.2) and having considered the areas of particular interest to the hydrocarbon industry, it is evident that there are several stratigraphic periods and associated unconformities suitable for more detailed study for this research. These include: (a) the Paleogene period and unconformities associated with North Atlantic opening, which affect Paleocene/Eocene reservoirs; (b) the Jurassic period and unconformities linked to an active phase of rifting and extensional tectonics, which affect a range of Upper and Middle Jurassic reservoirs; and (c) the Permian-Carboniferous periods and unconformities linked to the Variscan orogenic episode, which affect late Carboniferous and Permian reservoirs. Using adobe illustrator a summary of the whole of the North Sea stratigraphy was drawn (Figure 3-1).

Further consideration of the available data within the British Geological Survey (BGS) data base, and the Common Data Access (CDA) data base (also known as UKOilandGasData), led to specific focus on the Jurassic period. A total of 130 wells that penetrated through all or parts of the Jurassic succession were selected for further screening.

3.2 Data Screening

The data available for each of these 130 wells includes: core description reports, composite logs, biostratigraphy reports and full geological reports. These were interrogated for each well in order to compile a database for this study, including well name, well intent, current owner, field name, block, location, reservoir name, and most importantly whether the well has been cored or not. Table 3-1 provides an example of this data, and a detailed database is given in Appendix A.5.

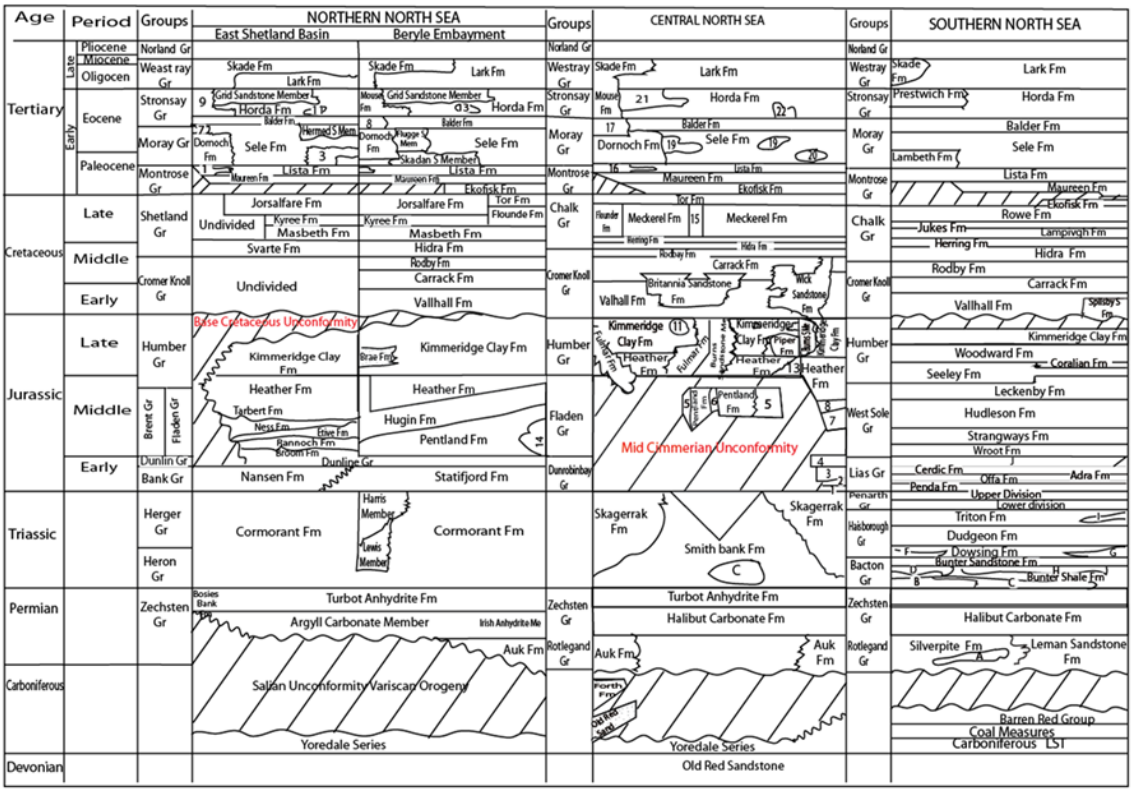

Figure 3-1. Detailed stratigraphic chart for the whole North Sea area (Northern, Central and Southern North Sea). Legend of this figure is explained in appendix A.4.

Table 3-1. An example of the investigation carried out for each of the selected wells in the area of interest. The detailed database is provided in Appendix A.5.

Well Name	Field Name	Block	Cored	Location	Reservoir Name	Reservoir Age	Cored Intervals	Unc Name
21/18-2A	Kittiwake	18	Y	west of the Central Graben	Fulmar and Skagerrak Fm	Upper Triassic and Upper Jurassic sandstones	10244-10517	MCU
21/18-6	Kittiwake	18	Y	west of the Central Graben.	Fulmar and Skagerrak Fm	Upper Triassic and Upper Jurassic sandstones	9881-10100	MCU
14/19-3	Claymore	19	Y	South margin of Witch Ground Graben	Sandstones of Middle and Upper Jurassic	Middle and Upper Jurassic	8014-8425	BHU

All cored wells were then selected to investigate further whether they intersect an unconformity surface or not. Using the list of criteria presented in section 2.1.2 (Chapter 2), as well as the available well data (i.e. composite logs, biostratigraphy reports), a total of 32 (cored) wells were found to be crossed by at least one unconformity surface.

Finally, after extensive investigation in order to identify the unconformity surfaces from the available data, sedimentological core logging was carried out on the 32 selected wells in order to verify and confirm the presence of the detected unconformity surface/s. The studied core intervals were held at the British Geological Survey core store, Keyworth, UK and at the Norwegian Petroleum Directorate's core store, Stavanger, Norway.

The principal unconformity surfaces identified within the studied wells include:

1. The Mid-Cimmerian Unconformity (MCU)
2. The Base-Cretaceous Unconformity (BCU)
3. Base Humber Group Unconformity (BHU)
4. Base Kimmeridgian Unconformity (BKU)

3.3 Statistical analysis

The wells that were found to cross an unconformity surface were then listed in a spreadsheet and studied carefully in terms of their core characteristics and description (Table 3-2) and for each well an evaluation was made of whether there were any changes in the physical properties (e.g. porosity and permeability) across the unconformity, which might be related to that unconformity surface (Table 3-3).

Particular note was made of wells that show similar lithologies above and below the unconformity surface. This group enables a better assessment of whether any contrast in properties across the unconformity is due mainly to the presence of the unconformity surface, rather than to other factors, such as marked lithological change (see below).

For further investigation and to be able to select the best wells that can achieve the purpose of this study, the data have been plotted by depth for each well (Figure 3-2). Simple statistical analysis has been performed for each selected well to compare the

characteristics of the sediments lying above and below the unconformity surfaces. This included: mean, median and mode as measures of central tendency; standard deviation, range, and minimum/maximum values, as measures of the data distribution and variance; and sample sufficiency to examine whether or not there are enough samples to provide meaningful statistics (population distribution).

However, as noted above, changes in the sediment characteristics can be controlled by a number of different factors (e.g. lithology, composition, grain size, sediment architecture, and depositional environment). Thus, in order to narrow the range of variables that might affect such changes in sediments lying above or below the unconformity surfaces, it was decided to focus on examples with closely comparable facies across the unconformity. The sedimentary successions within each well were characterised into facies based on mean grain size (Figure 3-3). Statistical analysis was carried out for each facies above and below the unconformity, where there was sufficient data (Figure 3-4).

The outcome of this analysis was very mixed. Amongst the 32 wells examined with core data across an unconformity surface, there is no uniformly systematic response in reservoir quality (i.e. porosity and permeability change) directly linked with the unconformity, although the following trends are observed:

- 10 wells show a marked decrease in reservoir quality across the unconformity surface, with a 50-95% decrease in horizontal permeability (kh) and a 15-25% decrease in porosity. Of these, the change is very localised to at or near the unconformity in only 3 wells, whereas it represents a more general trend related to a marked facies difference in the other 7 wells.

- 11 wells show a marked increase in reservoir quality across the unconformity surface, with a 10-200 times increase in horizontal permeability (kh) and a 20-85% increase in porosity. Of these, the change is localised to a zone of around 1-2 m below (or straddling) the unconformity surface in 7 wells, whereas it represents a more general trend in the other 4 wells.

- 8 wells show no clear change at or near the unconformity surface.

- 3 wells have relatively few or incomplete data (i.e. data from below but not above the unconformity surface).

These results show that about 30% of the wells examined (i.e. 10 out of 32) appear to demonstrate some marked change in reservoir quality, either positive or negative, close to the unconformity surface. However, it is also noted that all these observations are within the context of a small-scale variability in porosity values and a much larger-scale variability in permeability values throughout the well sections examined. This variability is considered most closely related to facies changes, as well as to localised cementation (concretion zones) in some cases.

Table 3-2. An example of the investigation carried out for each of the selected wells in the area of interest in terms of its core characteristics (e.g. porosity and permeability) and description. The table shows some of the core data obtained above and below the Mid-Cimmerian Unconformity (which was recognised at a depth 10332 ft) for Well 21/18-3 in the Kittiwake Field. The full dataset for all wells is given in Appendix A.5.

Depth	Permeability%	Porosity%	Grain Density	Lithology
10314	0.01	4.5	2.74	SS,GY,FGR,VWCMT,MIC,PYR,DOL
10315	0.02	5.4	2.73	AA
10316	0.02	6.1	2.72	AA
10317	0.05	11.6	2.7	SS,GY,FGR,WCMT,MIC,PYR
10318	0.07	12.3	2.7	AA
10319	0.12	12.7	2.7	AA
10320	0.09	12.2	2.7	AA
10321	0.1	11.7	2.69	AA
10322	0.09	12.9	2.73	AA
10323	0.01	5.5	2.76	SS,GY,FGR,VWCMT,MIC,PYR,DOL
10324	0.07	12.7	2.71	SS,GY,FGR,WCMT,MIC,PYR
10325	0.07	12.9	2.7	AA
10326	0.06	13	2.72	AA
10327	0.09	12.9	2.68	AA
10328	0.06	13.3	2.7	AA
10329	0.09	13.4	2.68	AA
10330	0.07	11.9	2.69	AA
10331	0.07	11.5	2.71	AA
10332	0.22	10.8	3.01	SS,GY,FGR,WCMT,ABNDT,PYR
10333	0.3	16.7	2.64	SS,GY,FGR,WCMT,MIC
10334	0.47	12.5	2.66	AA
10335		12.4	2.68	SS,GY,FGR,WCMT,MIC,PYR,(NPP)
10336		14.8	2.66	AA(NPP)
10337	0.61	17.4	2.67	AA
10338	5.9	18.5	2.71	SS,GY,FGR,WCMT,MIC,PYR,W.SH FRAGS
10339	0.49	18.1	2.65	SS,GY,FGR,WCMT,MIC
10340	0.01	3.8	2.78	SS,GY,FGR,VWCMT,MIC,PYR,DOL
10341		15.1	2.67	SS,GY,FGR,WCMT,MIC,PYR,(NPP)
10342		17.6	2.66	SS,GY,FGR,WCMT,MIC,PYR,(NPP)
10343		16.1	2.69	AA (NPP)
10344		16.7	2.71	SS,GY,FGR,WCMT,MIC,PYR,(NPP)
10345		17.6	2.69	AA (NPP)
10346	0.87	16.4	2.7	AA
10347	0.44	16.2	2.64	SS,GY,FGR,WCMT,MIC
10348	0.41	13.9	2.65	AA
10349	0.52	14.4	2.65	AA
10350		14	2.68	SS,GY,FGR,WCMT,MIC,PYR,(NPP)
10351		13.3	2.66	AA (NPP)
10352				NO PLUG POSSIBLE
10353	0.18	11.9	2.66	SS,GY,FGR,WCMT,MIC,PYR
10354	0.38	12.4	2.67	AA

Table 3-3. An example from three of the studied wells showing the evaluation that was carried out for each well to see whether there were any measurable changes in the physical properties of the studied cores (e.g. porosity and permeability) above and below the unconformity surface. A detailed dataset is given in Appendix A.5.

Well Name	Field Name	Location	Uncon	Observed changes in core plug data	Observed changes in wireline logs	Processes that may created Unc	Unco type
21/18- 3	Kittiwake	West of the Central Graben	MCU	Permeability and Porosity are higher under the UNC than above it	GR is lower under the UNC surface and small increase in the resistivity below the UNC	The central North Sea area was subjected to mid Jurassic regional uplift and erosion followed by Late Jurassic subsidence	Subaerial erosion
2/05-17	Heather	Northern North Sea	BHU	Possibly small change in the physical properties of sediments underneath the UNC	GR log is much lower underneath the UNC surface than above.	Possibly as a result of faulting followed by erosion across the field crest	Subaerial erosional
3/03-N14	Ninian	East Shetland Basin	BHU	Not enough data available	Not enough data available	Due to Kimmerdgian tectonic activity. This resulted in periods of erosion and marine transgression.	Submarine erosion

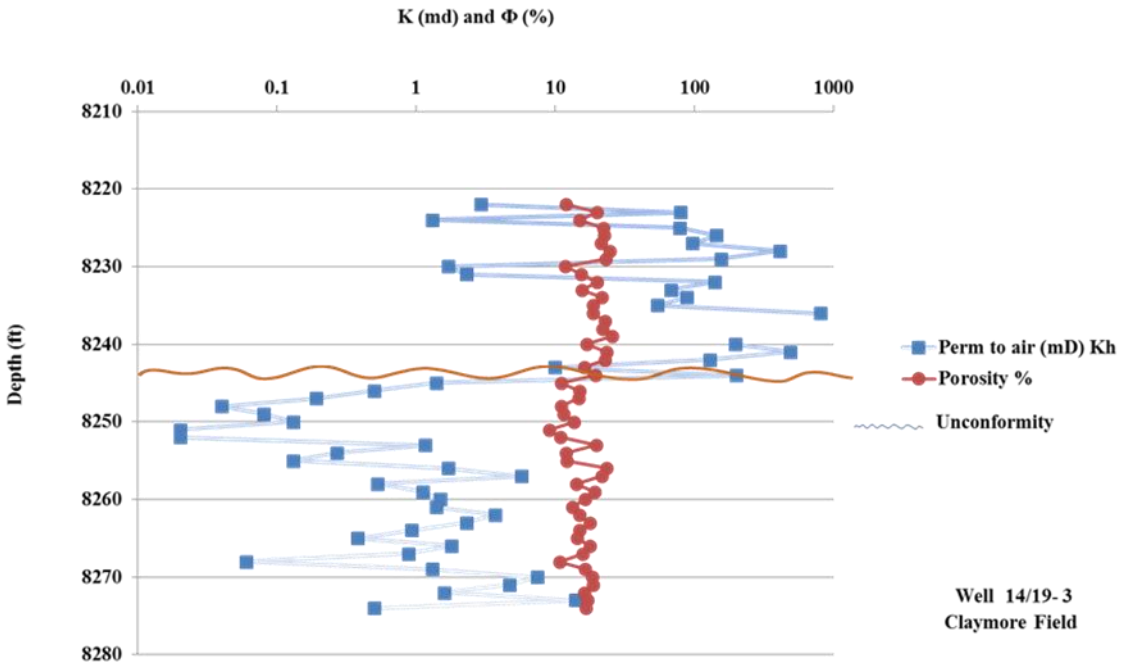

Figure 3-2. An example of how data were plotted by depth for each well; this figure represents the characteristics of porosity and permeability in Well 14/19-3 above and below the unconformity surface. More details are given in Appendix A.5.

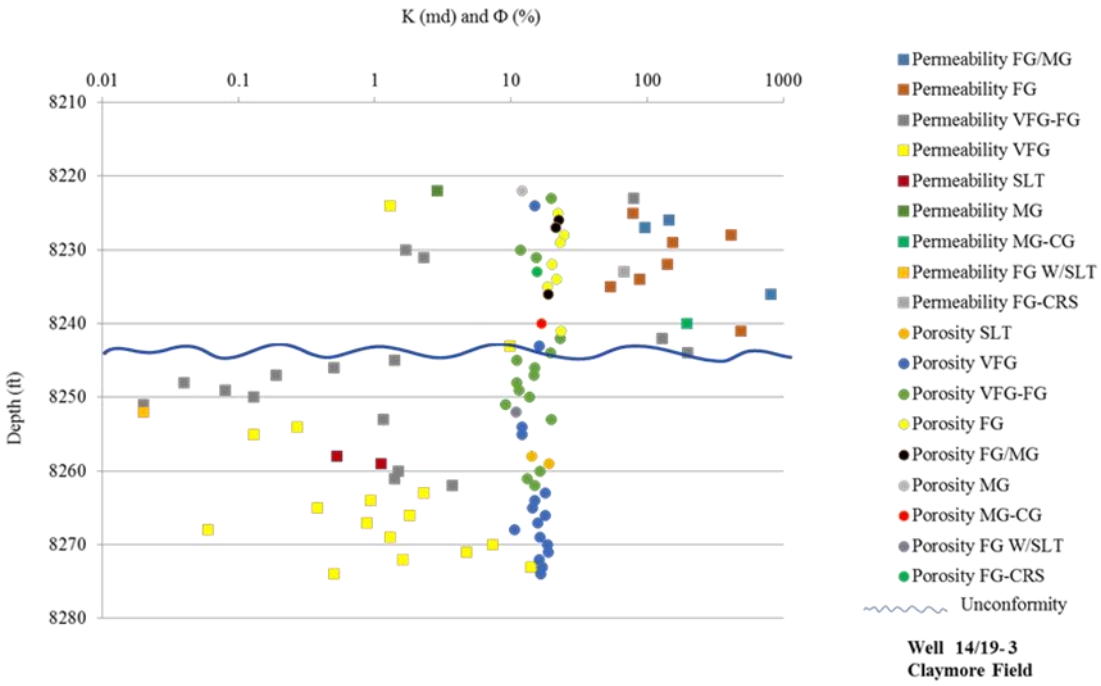

Figure 3-3. An example of how each well was divided into groups by textural facies. The data were then plotted by depth for each facies; this figure represents the characteristics of porosity and permeability of each observed facies in Well 14/19-3 above and below the unconformity surface. (Siltstone (SLT), Very fine-grained sandstone (VFG), Very fine to fine-grained sandstone (VFG-FG), Fine-grained sandstone (FG), Fine to medium-grained sandstone (FG-MG), Medium-grained sandstone (MG), Medium to coarse-grained sandstone (MG-CG), Coarse-grained sandstone (CG)). Further details are given in Appendix A.5.

Statistics above the unconformity

Permeability		Porosity	
VFG-FG		VFG-FG	
Mean	53.25	Mean	17.5
Median	41.15	Median	17.65
Standard Deviation	62.5	Standard Deviation	4.9
Minimum	1.7	Minimum	11.8
Maximum	129	Maximum	22.9
Count	4	Count	4

Statistics below the unconformity

Permeability		Porosity	
VFG-FG		VFG-FG	
Mean	17.4	Mean	14.1
Median	0.83	Median	14.2
Standard Deviation	57.19	Standard Deviation	3.2
Minimum	0.02	Minimum	9.1
Maximum	199	Maximum	19.8
Count	12	Count	12

Figure 3-4. An example of the statistical analysis carried out for each facies above and below the unconformity surface in Well 14/19-3. See also Appendix A.5.

3.4 Core description

Sediment description was carried out on cores from the 32 selected wells. Description started with determination of grain size by visual comparison of small sandstone samples using the Wentworth size classification scale, followed by the description of the lithology and sedimentary structures of each well (see Appendix A.1). Special attention was paid to confirming the location of the unconformity surface and in noting any marked facies or other changes across the boundary. The principal results of this study are given below for the 32 wells studied here. More detailed observations are given for each of the case study wells in Chapters 5, 6 and 7.

3.4.1 Sediment facies

The sediment characteristics observed reflect the range of depositional environments in which they were originally deposited. These include fluvial 'red-beds' from a continental environment, through a range of coastal, deltaic and open marine environments. These interpretations have been made by previous studies and are available from the well reports held in the BGS Database. The present study was able to confirm these interpretations.

For the purposes of this study, and to focus on potential reservoir characteristics, it was decided to identify sediment facies mainly on the basis of textural properties. However, the facies identified do take into account differences in sedimentary structures, the nature of bioturbation, or inferred depositional environments. These textural facies types are:

- Siltstone (SLT)
- Very fine-grained sandstone (VFG)
- Very fine to fine-grained sandstone (VFG-FG)
- Fine-grained sandstone (FG)
- Fine to medium-grained sandstone (FG-MG)
- Medium-grained sandstone (MG)
- Medium to coarse-grained sandstone (MG-CG)
- Coarse-grained sandstone (CG)

3.4.2 Unconformity characteristics

The presence and depth of the unconformity surfaces are noted in each well (Figure *3-5*) and matched with the composite log data. For instance, Figure *3-6* shows an example of calibrating the observed unconformity surface from cores of Well 21/18-2A to the composite log. In Well 21/18-2A the unconformity surface was observed at a depth of 10017 ft, separating the Upper Triassic Skagerrak Formation from the Upper Jurassic Fulmar Formation.

In most of the wells examined, the unconformity surfaces encountered are clearly evident from a marked change in the overall sedimentary characteristics, which generally reflects a significant change in depositional environment. This is perhaps unsurprising, since the Base-Cretaceous Unconformity represents a time gap of up to 100 Ma, and the Mid-Cimmerian Unconformity represents a time gap of up to 50 Ma. The other Jurassic unconformities encountered are more localised and represent mess time gaps.

Because the unconformities mostly separate formations from different depositional environments, it is very difficult to find two closely comparable facies above and below an unconformity surface in any of the studied wells. Even in the wells where there are two similar facies in terms of their grain size, there are significant differences in sedimentary structures, bioturbation, cementation or other features. Therefore, instead of carrying out a detailed comparative analysis between facies above and below the unconformity surfaces, for the individual case studies selected, it was decided to perform sedimentological and petrographic analysis only on the sediments lying beneath the unconformity surfaces. Starting from a point closest to the unconformity surface and working deeper in the succession, this should reveal any systematic trends, if they exist, in reservoir characteristics linked to that surface.

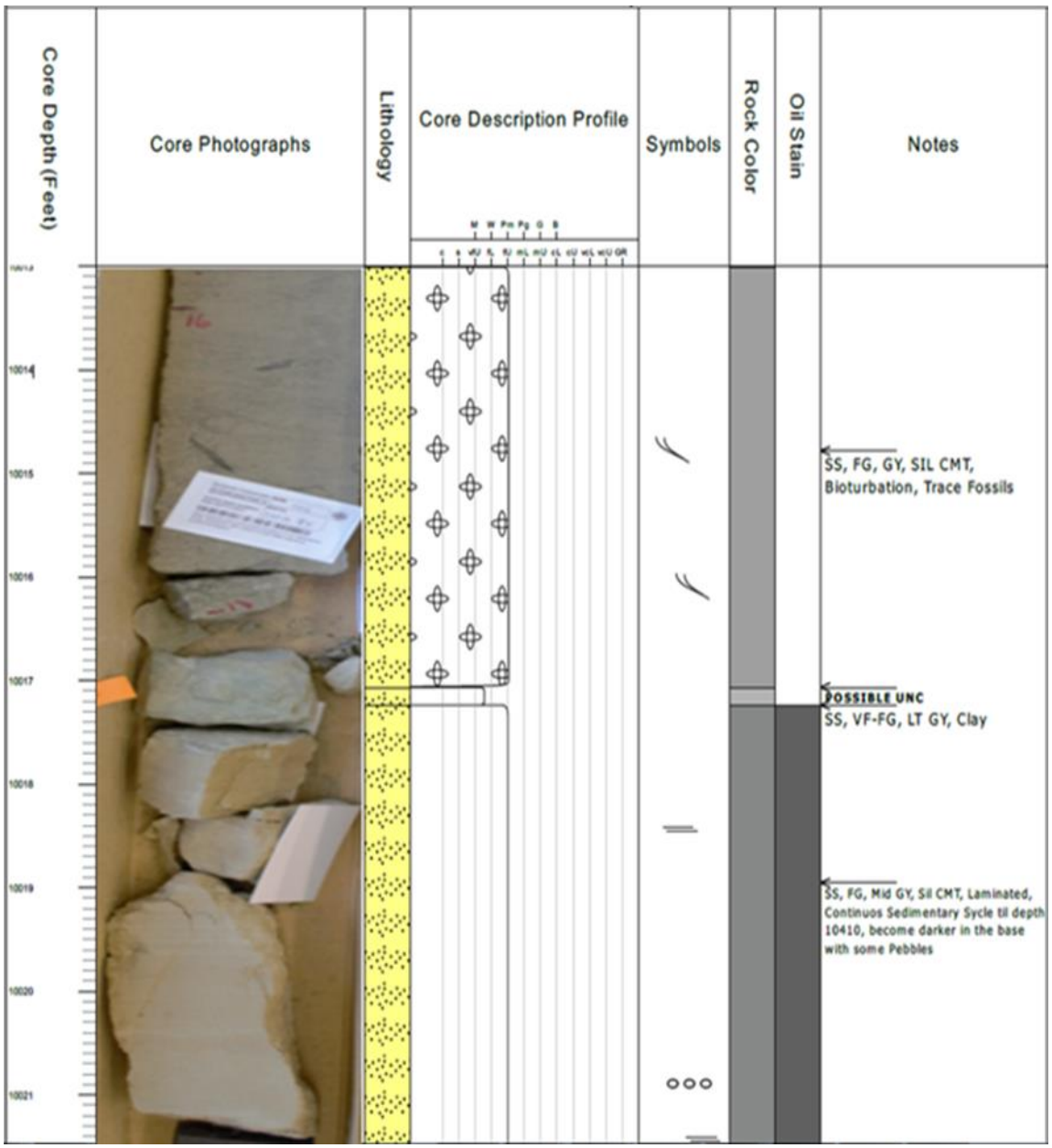

Figure 3-5. Showing sediment core logging for Well 21/18-2A and the presence of the unconformity surface at depth 10017 ft. Detailed core logs for each of the case study wells are provided in Chapters 4, 5 and 6, respectively. Detailed legend is given in appendix A.1.2.

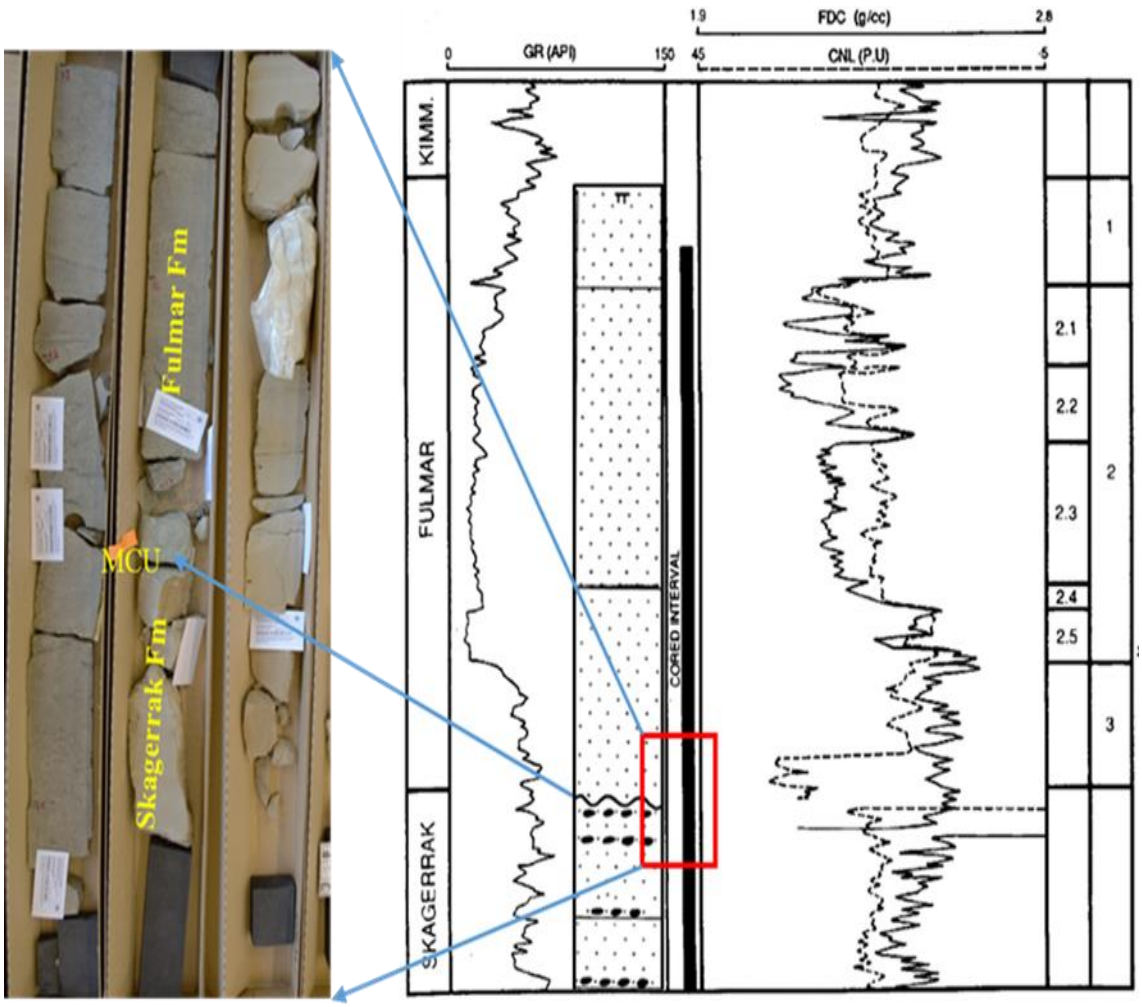

Figure 3-6. Showing an example of calibrating Mid-Cimmerian Unconformity from cores of Well 21/18-2A to wireline log's character and core logging; modified from (Glennie and Armstrong, 1991).

Chapter 4 Case Study 1: The role of Mid-Cimmerian Unconformity on the distribution of porosity and kaolinite in the Skagerrak Formation of the Kittiwake Field, Central Viking Graben

4.1 The Mid-Cimmerian Unconformity (MCU)

The Mid-Cimmerian unconformity is a regional unconformity developed within the succession of Lower and Middle Jurassic sediments in NW Europe and beyond. Much of the Lower Jurassic succession and parts of the Middle Jurassic have been eroded and/or were never deposited. Some deposits of this age are preserved in localised accommodation space. Therefore, the unconformity is generally represented by Middle and Upper Jurassic sediments directly overlying Triassic sediments, and representing a time gap of up to 50 Ma. The unconformity has been recognized over the North Sea and much of Europe, and the causal mechanism and stratigraphic relations of this unconformity have been discussed by many authors.

Mapping of stratigraphic relationships below and above the Mid-Cimmerian Unconformity has been used by (Underhill and Partington, 1993) to understand the nature of the mechanism that led to the formation of this unconformity. Their mapping of the youngest stratigraphy preserved beneath the unconformity indicated that erosion led to progressive truncation of beds across the North Sea region. The maps show a series of concentric to elliptical subcrop patterns existing within the Triassic and older beds, sub-cropping below the unconformity in the central region, close to the triple junction. A further map for the post-unconformity units shows how the overlying units onlap onto the unconformity and indicates that the point of marine flooding migrates toward the central area and is sealed by the youngest strata. Underhill and Partington (1993, 1994), who identified this unconformity as the intra-Aalenian unconformity, used a sequence stratigraphic approach to confirm the presence and the causal mechanism of the Mid-Cimmerian Unconformity. They interpreted the erosion to be caused by uplift related to increased heat rising from a presumed hot-spot during the Middle Jurassic, and before the Middle and Late Jurassic rifting of the North Sea (Davies et al., 1999).

In the studied Kittiwake Field, the deposition of the Upper Triassic Skagerrak sandstones is separated from the Upper Jurassic Fulmar marine sandstones by the Mid-Cimmerian Unconformity.

4.2 The Central Viking Graben Kittiwake Field

4.2.1 Introduction

The Kittiwake field is located approximately 100 miles ENE of Aberdeen in the western platform area of the Central North Sea (Figure 4-1). The Kittiwake field lies within Block 21/18, awarded to the Shell/Esso partnership in December 1980. The field was discovered in 1981 by Well 21/18-2a. The reservoir occurs at a depth of about 10 000 ft TVDSS and the exploration well encountered an approximately 200 ft oil column in the Upper Jurassic Fulmar Formation sandstone. This field, which involves both stratigraphic and structural trapping, forms an east-west-trending elongated dome-shaped feature (

Figure 4-2) (Glennie, 1998). The Fulmar Formation in this field unconformably overlies the Triassic Skagerrak Formation; both formations are separated by the Mid-Cimmerian Unconformity (MCU). In this study the main target will be the Skagerrak Formation, which lies directly below the Mid-Cimmerian Unconformity. Therefore, any possible diagenetic effects related to this unconformity would be expected to be observed in this formation.

4.2.2 Field stratigraphy

The main reservoir formations in the Kittiwake Field are the Fulmar and Skagerrak Formations; both formations occur at a depth of about 10000 ft TVSS. The Skagerrak Formation is underlain by the Upper Permian Zechstein halite, and the Fulmar Formation is overlain by Late Jurassic Kimmeridge Clay and Cretaceous sediments (Figure 4-3). The deposition of the Skagerrak Formation, preservation of the Fulmar Formation and the creation of the structural aspects of the Kittiwake trap are controlled mainly by the diapiric movement of the underlying Zechstein halite (Glennie and Armstrong, 1991).

Although dating of the Late Triassic continental Skagerrak Formation is difficult, it is likely that, in the Kittiwake field, the Skagerrak Formation is entirely pre-Rhaetian in age,

older than 201.3-208.5 Ma. The Skagerrak Formation is unconformably overlain by the shallow-marine sandstones of the Upper Jurassic Fulmar Formation. The Fulmar Formation grades up into the deep marine Kimmeridge Clay Formation. The Base-Cretaceous Unconformity separates the Kimmeridge Clay Formation from the Lower Cretaceous Valhall Formation.

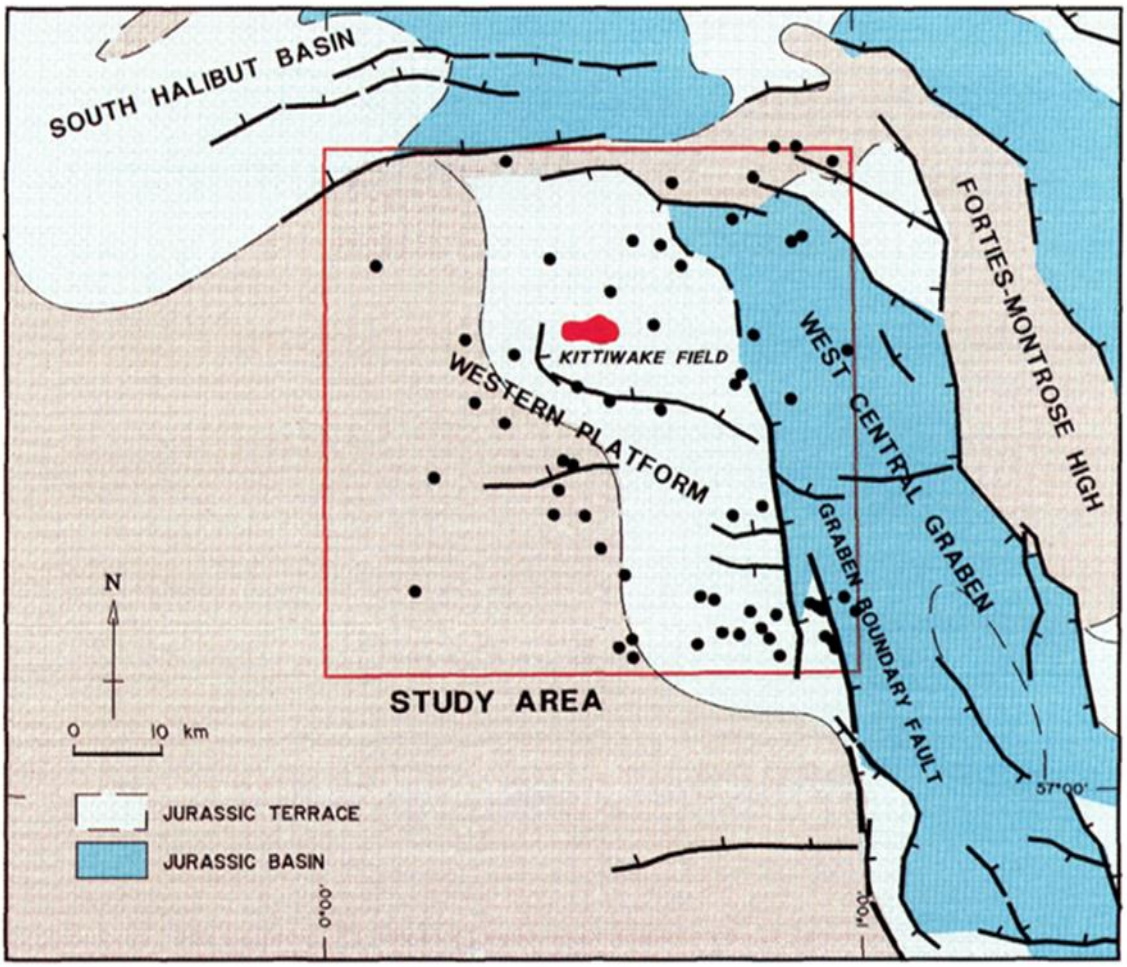

Figure 4-1. Location of the Kittiwake Field in the Central North Sea, after (Wakefield et al., 1993).

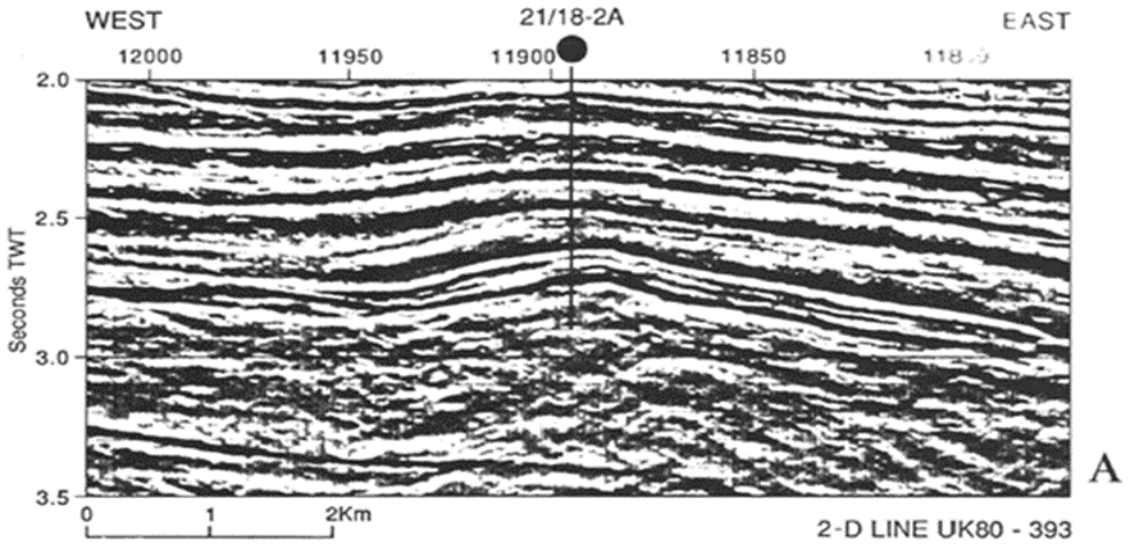

Figure 4-2. 2-D line through the discovery Well 21/18-2A of Kittiwake Field; from (Glennie and Armstrong, 1991).

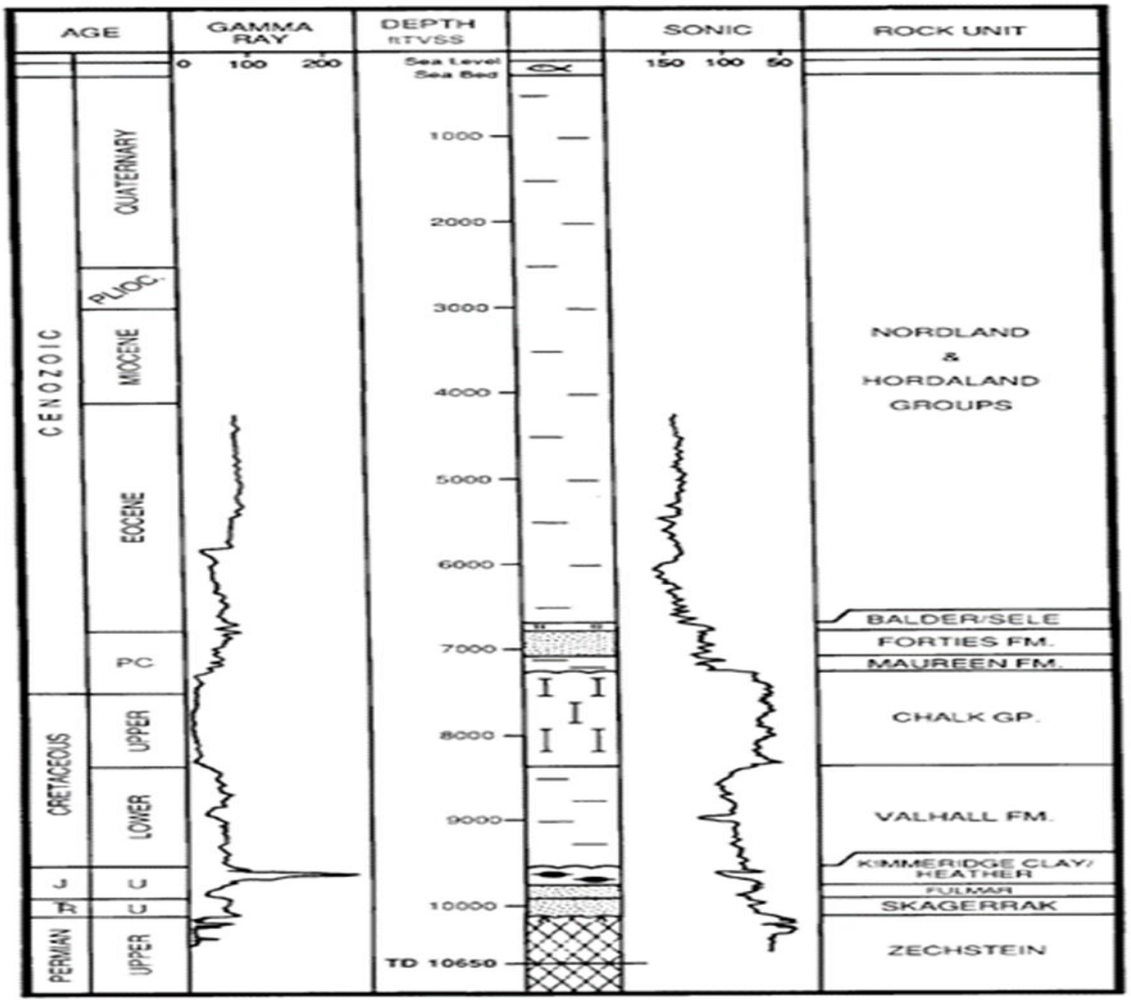

Figure 4-3. Stratigraphic column of the Kittiwake area; from (Glennie and Armstrong, 1991).

4.2.3 Geological History

The diapiric movement of Zechstein halite in the Triassic has played a significant role in controlling deposition and preservation of reservoir sediments and in structural trap formation. After deposition of the Early Triassic Zechstein evaporite sequence, in the semi-arid environment, the lacustrine mudstones of the Triassic Smith Bank Formation were deposited. This formation is not present in the Kittiwake field, where the Late Triassic Skagerrak Formation lies directly above the Zechstein halite group. The movements of salt which were triggered by reactivation of faults and different processes in the pre-Zechstein basement across the Central Graben created diapers (salt highs) separated by thick sequences (pods) of Smith Bank Mudstone (Glennie, 2009). It is suspected that dissolution of these salt highs at the crest of the diapirs helped to form the topographic lows where fluvial channel and sheet flood sands of the Skagerrak Formation were preferentially deposited. Therefore, the Upper Triassic Skagerrak Formation was deposited directly over the Zechstein salt, although it is younger than the Smith Bank Formation (Figure 4-4).

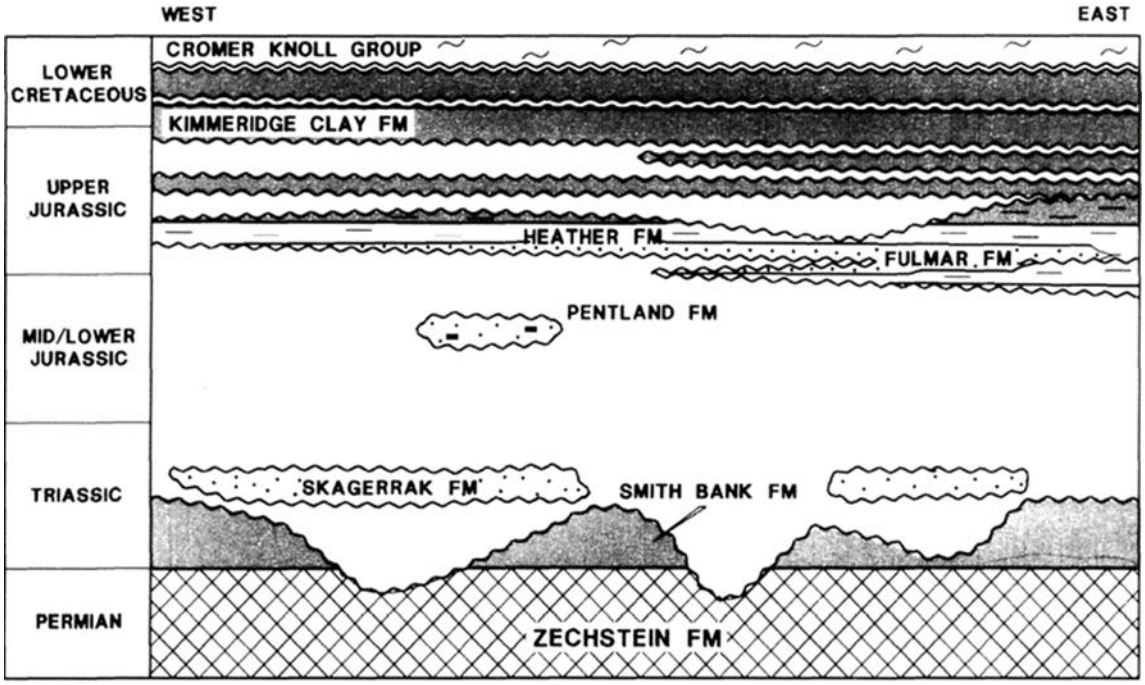

Figure 4-4. General stratigraphy and lithostratigraphy of Western Platform in the Central North Sea, after (Wakefield et al., 1993). The Triassic Skagerrak Formation lies below the Mid-Cimmerian Unconformity and directly on Zechstein salt domes, although it is interpreted to be younger than the Smith Bank Formation.

Uplift and erosion of the Western Platform in the Central North Sea during the Lower to Middle Jurassic resulted in erosion and removal of the sands on the top of the Smith Bank pods. Subsequently, Late Jurassic subsidence resulted in a return to a marine condition, where marine transgression flooded the topographic lows and led to deposition of the shoreline and shallow marine sands of the Fulmar Formation. Further transgression resulted in gradual transition from Fulmar Formation Sandstone into the deeper marine shales of the Heather Formation, overlain by Kimmeridge Clay Formation, which covered the whole of the Central North Sea.

According to (Lane, 1991), seismic evidence indicates that during the Early Cretaceous another subsidence started. Mild diapiric uplift of the Kittiwake structure and gentle subsidence to the adjacent area continued until the Mid-Eocene, resulting in the modern Kittiwake structure.

4.2.4 Reservoirs

The field contains two oil bearing reservoirs, the Fulmar and Skagerrak Formations. However, only the Middle Fulmar sandstones are classified as good oil reservoirs. The log character and the lithology of the Kittiwake field have been summarized from Well 21/18-2A in Figure 4-3. This study will focus mainly on the Skagerrak Formation, as it lies directly underneath the Mid-Cimmerian Unconformity.

4.2.4.1 Skagerrak Formation

The term Skagerrak was introduced by (Deegan and Scull, 1977) to describe the Triassic red, brown and grey fine-grained sandstone and shale sediments. The sandstones are generally moderately or poorly sorted. The formation can be divided into three facies associations: overbank red sandstones, claystones and siltstones, alluvial sheet-flood sandstones with interbedded mudstone intraclasts, and well-sorted cross-bedded fluvial-channel sandstones. The main compositions of Skagerrak Formation are arkosic to lithic-arkosic arenites (Nguyen et al., 2013). The widespread Skagerrak Formation in the North Sea has been sub-divided into six main members, ranging from sand dominated to mud dominated, each with a thickness of hundreds of metres. These members are named: Joshua Mudstone, Josephine Sandstone, Jonathan Mudstone, Joanne Sandstone, Julius Mudstone and Judy Sandstone members. However, in the present study area of the West

Central Graben Kittiwake Field, only thin sandstone is extended over the salt diapirs and adjacent salt wall crests. The Skagerrak Formation is variable in colour, and this variable degree of reddening may indicate deep oxidation in the Upper Triassic sediments during the erosion of the Mid-Cimmerian Unconformity or due to exposure during the discontinuous sedimentation (Goldsmith et al., 1995). In the Kittiwake Field, sheet-flood and overbank sediments are the main facies of the Skagerrak Formation. The Skagerrak Formation is overlain unconformably by the Upper Jurassic Fulmar Formation and underlain by the Upper Permian Zechstein halite (Glennie, 2009).

4.2.4.2 Fulmar Formation

The term Fulmar was introduced by Shell to describe the shallow marine sandstones in the western Central Graben in 1970s. The Fulmar Formation is Callovian to Late Ryazanian in age (145–166.1 Ma) and comprises mainly very fine- to medium-grained, generally argillaceous or carbonate cemented, bioturbated sandstone (Cordey et al., 1993). It was deposited in shallow, low to moderately high-energy, storm-influenced marine environments. In the Kittiwake field, the Fulmar Formation can be divided into three reservoir units: Units 1 and 3 are very poor reservoir quality, whereas unit 2, which has been subdivided into five subunits, represents the best reservoir properties in the Kittiwake Field. Units 2.1, 2.4 and 2.5 have moderate reservoir properties because of very fine grain size with abundance of clay, and the units 2.2 and 2.3 have the best reservoir quality (Figure 4-5). The thickness of unit 2 decreases from the central area toward both west and east, whereas the thickness of unit 3 decreases only from the east to west (Lane, 1991).

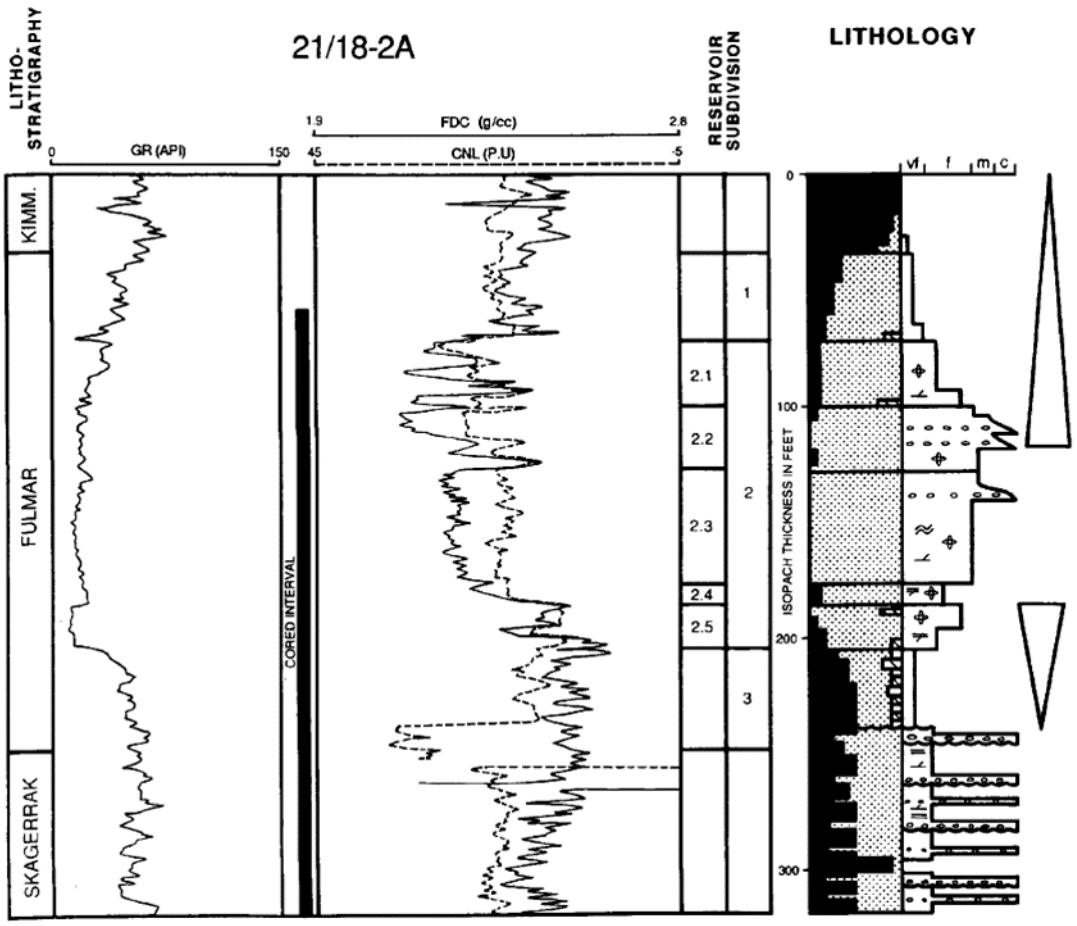

Figure 4-5. Wireline log character of Well 21/18-2A and facies description of the Kittiwake Field; from (Lane, 1991).

4.3 Sedimentological Analysis

This section will present the results of sedimentological descriptions that have been conducted for the available cores on the four wells located in the Kittiwake field in the Central Graben of the North Sea, allowing the observation of sediment details and interpretation of facies.

Sedimentological description (core logging) was performed for more than 70 feet of core of each well from the Wells 21/18-2A, 21/18-3, 21/18-4 and 21/18-6. Description started with determination of grainsize by visual comparison of small sandstone samples, using the Wentworth size classification scale. After the determination of grain sizes, the lithology and sedimentary structures have been described for each well. The total described core length was approximately 372 feet.

4.3.1 Sedimentological analysis results

Figure 4-6, Figure 4-7, Figure 4-8 and Figure 4-9 illustrate the stratigraphic core descriptions of the four wells located in the Kittiwake Field in Block 21. From the core descriptions it was clear that the four wells have similar sandstone types and are divided into two different formations in terms of their sedimentary structure and the depositional environment. These formations are separated by an erosional unconformity.

The upper sandstone facies, which represent the shore line to shallow marine sandstone of Fulmar Formation, are a good reservoir formation, consisting of very fine to fine-grained sand, generally argillaceous or carbonate cemented, bioturbated sandstone. It was deposited in shallow, low to moderately high-energy, storm-influenced marine environments. It is poor to moderately sorted and varies from light to dark grey and brownish grey in colour.

The lower sandstone formation, which represents the Upper Triassic Skagerrak Formation consists mainly of very fine to fine-grained sandstone; the sandstones are generally laminated, moderately or poorly sorted and vary from light to medium grey in colour and become more red coloured with depth. The formation can be divided into the two facies associations identified in the Kittiwake Field, which are sheet-flood and overbank sediments.

As the Skagerrak Formation is the main target of this study, because it lies directly underneath the Mid-Cimmerian Unconformity, most samples have been taken from this formation for deeper investigation and petrographic analysis to study the mineralogical composition and diagenetic process in this formation; more details are presented in the following section.

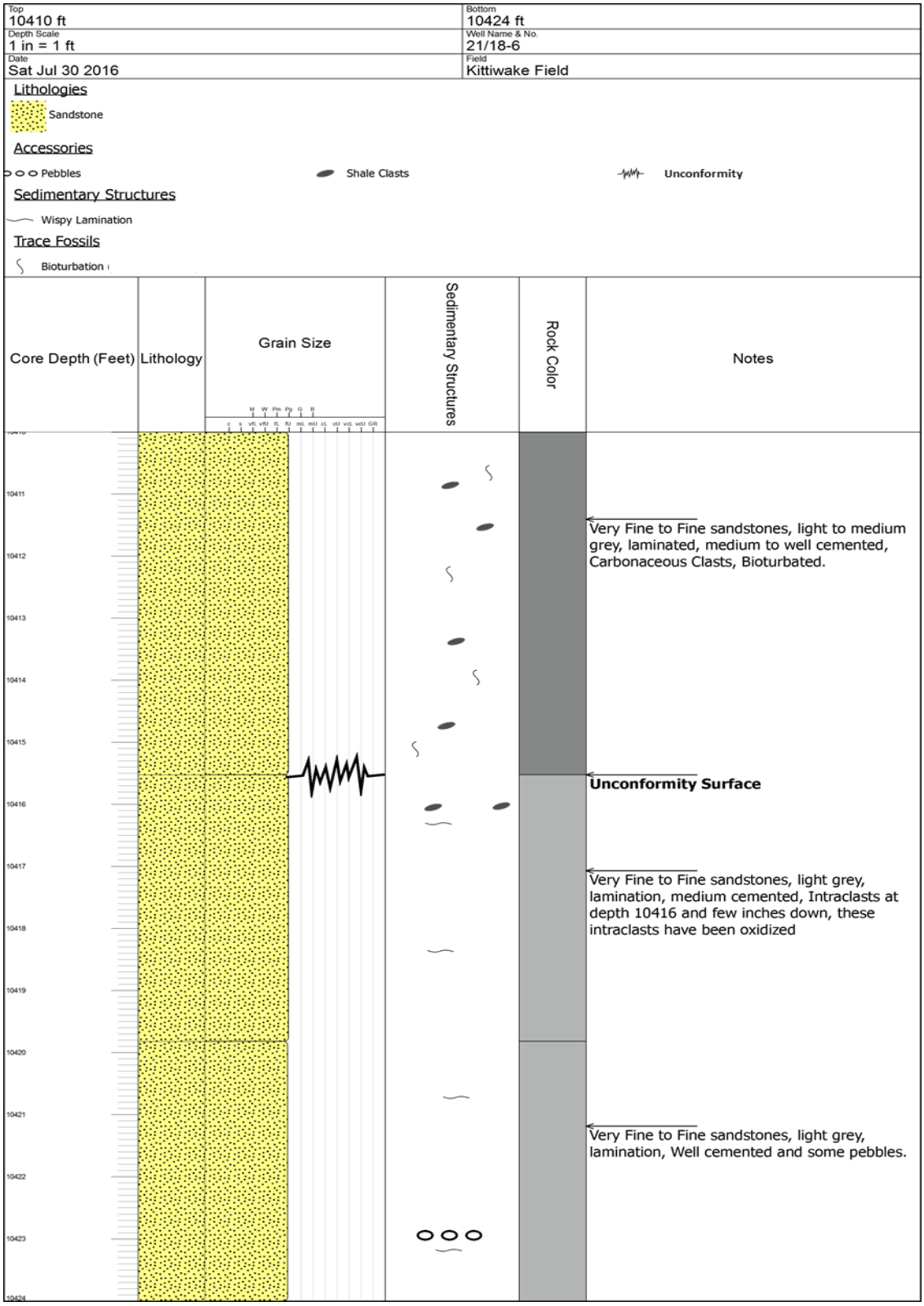

Figure 4-6. Sedimentological core description of Well 21/18-6 in the Kittiwake Field. The figure illustrates the sedimentological core descriptions and location of the Mid-Cimmerian Unconformity at depth 10415.5 ft, which separates the Triassic Skagerrak Formation from the Upper Jurassic Fulmar Formation.

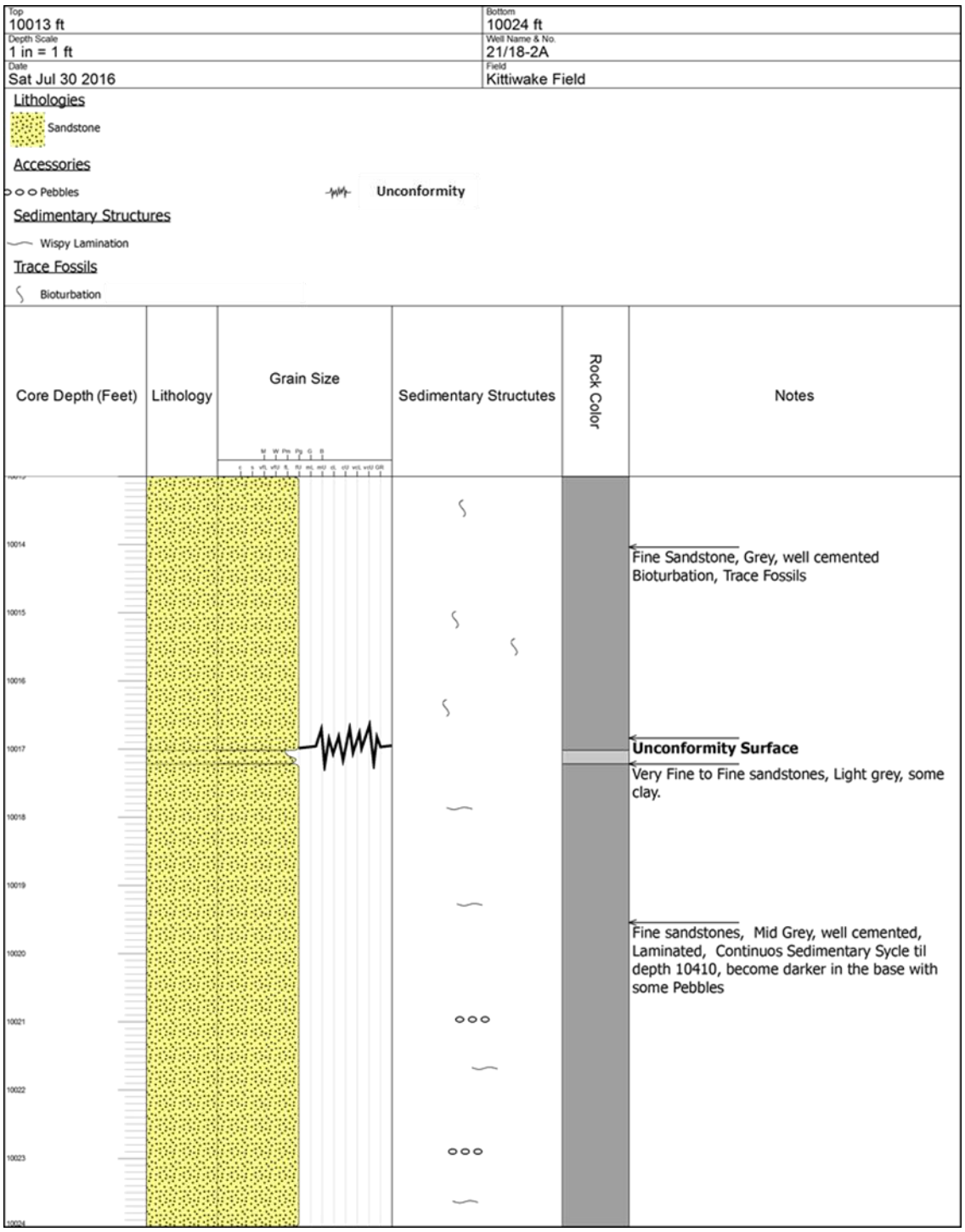

Figure 4-7. Sedimentological core descriptions of Well 21/18-2A in the Kittiwake Field. The figure illustrates the sedimentological core descriptions and location of the Mid-Cimmerian Unconformity at depth 10017 ft, which separates the Triassic Skagerrak Formation from the Upper Jurassic Fulmar Formation.

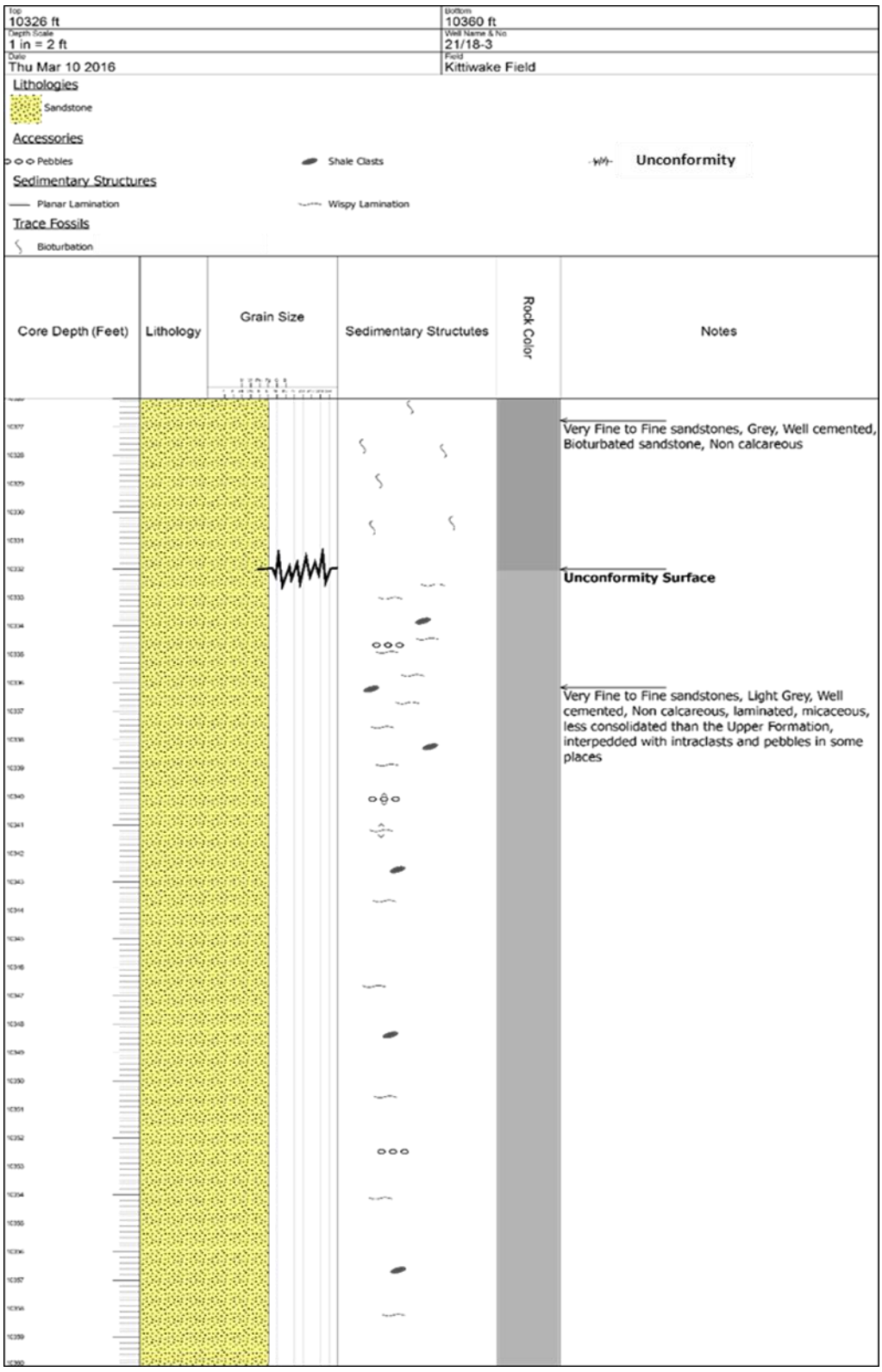

Figure 4-8. Sedimentological core descriptions of Well 21/18-3 in the Kittiwake Field. The figure illustrates the sedimentological core descriptions and location of the Mid-Cimmerian Unconformity at depth 10332 ft, which separates the Triassic Skagerrak Formation from the Upper Jurassic Fulmar Formation.

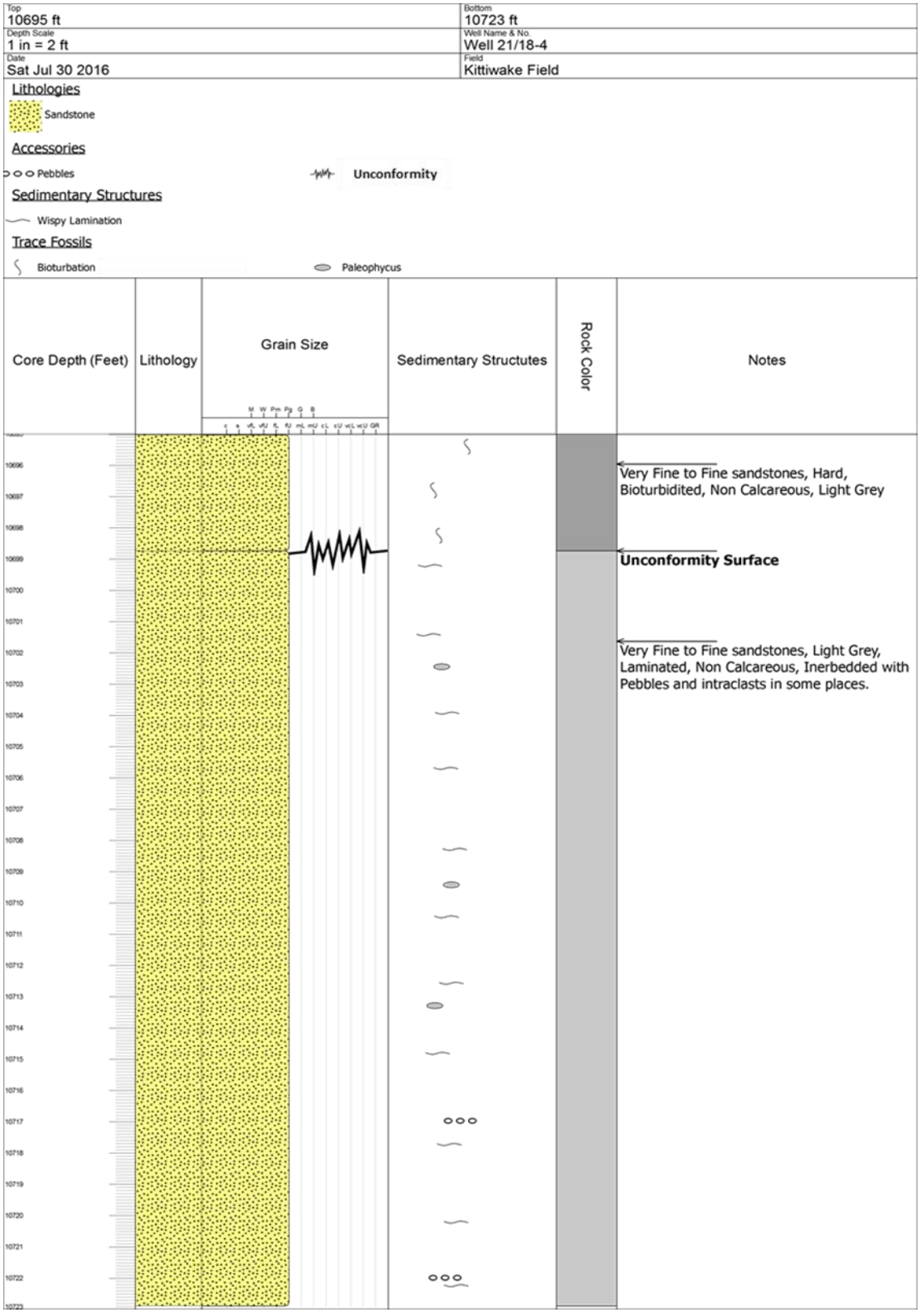

Figure 4-9. Sedimentological core descriptions of Well 21/18-4 in the Kittiwake Field. The figure illustrates the sedimentological core descriptions and location of the Mid-Cimmerian Unconformity at depth 10698.75 ft, which separate the Triassic Skagerrak Formation from the Upper Jurassic Fulmar Formation.

4.4 Petrographic Analysis

Thin-section petrographic analysis is a very useful tool in identifying the lithological texture, mineralogy, porosity and classification of sandstones. The petrographic analysis has been carried out by optical microscopy and scanning electron microscope (SEM). A petrographic study of 41 thin-section samples for the 4 wells from the Kittiwake Field is included in this chapter.

4.4.1 Lithological Texture

In general, the studies of the four wells of the Skagerrak Formation in the Kittiwake Field show that, based on the grain size, there are three sandstone facies in the Skagerrak Formation. Variability of grain-size across all facies is limited: most of the facies sandstones are in the range of very fine to fine sand grain size. Therefore, each sample was allocated a facies code based on the grain size (e.g. 1, 2 or 3), this will allow easy identification and comparison to the samples with similar characteristics. Table 4-1 showing the textures, grain size and sorting characteristics of each of these sandstone facies.

Facies 1 sandstone is very fine grained and poorly to moderately sorted. Detrital grains are usually sub-angular to sub-rounded, the grain contact shapes indicate a limited amount of compaction. This is supported by the presence of some lithic clasts and contorted flakes of mica. This facies is mainly represented in Well 21/18-3.

Facies 2 has similar textural characteristics, except that it has very fine to fine sand grain size and represents the majority of Wells 21/18-6 and 21/18-4 and some sandstones of Well 21/18-3.

Facies 3 also exhibits similar textural characteristics to facies 1 and 2, however, with coarser grain size (commonly fine sand) and mostly occurs in Well 21/18-2A.

Table 4-1. A summary of lithological textures of facies. VFS = very fine sand, VF-FS= very fine to fine sand, FS= fine sand. P-M = poor to medium sorting, SA-SR= sub-angular to sub-rounded sand.

Facies Code	Grain Size	Sorting	Roundness
1	VFS	P-M	SA-SR
2	VF-FS	P-M	SA-SR
3	FS	P-M	SA-SR

4.4.2 Sandstone Classification

Most of the thin-section samples that have been taken for this study are sandstones. The range of sandstone types identified from the 41 thin-sections is shown in Figure 4-10. Petrographic analysis data for the detrital components of each well (Table 4-2, Table 4-3, Table 4-3 and Table 4-5), shows that the main framework grains were quartz, feldspar and rock fragments, the most common accessory mineral was found to be mica. Using the Pettijohn's, 1975 classification scheme (where polycrystalline quartz is counted as rock fragments, see Appendix B.2), most of the Skagerrak Formation sandstones were classified as arkosic to subarkosic sandstone, where they consisted mainly of quartz, feldspar and granitic rock fragments. A small number of sandstone samples were lithicarkose to lithicsubarkose, as a result of higher rock fragment content, and one sandstone sample falls into the feldspar litharenite category due to its high rock fragment content (24%, Well 21/18-4, depth 10698.5 ft). Most of the very fine to fine sandstone facies were distributed between arkose to subarkose, whereas the coarser sandstone facies were mainly lithicarkose to lithicsubarkose. The trend of increasing rock fragments and polycrystalline quartz with increasing grain size is typical for terrigenous sediments, according to (Pettijohn et al., 1972).

The different facies which have been classified here are more likely to be due to variation in the depositional process and not related to the differences in the sediments source area.

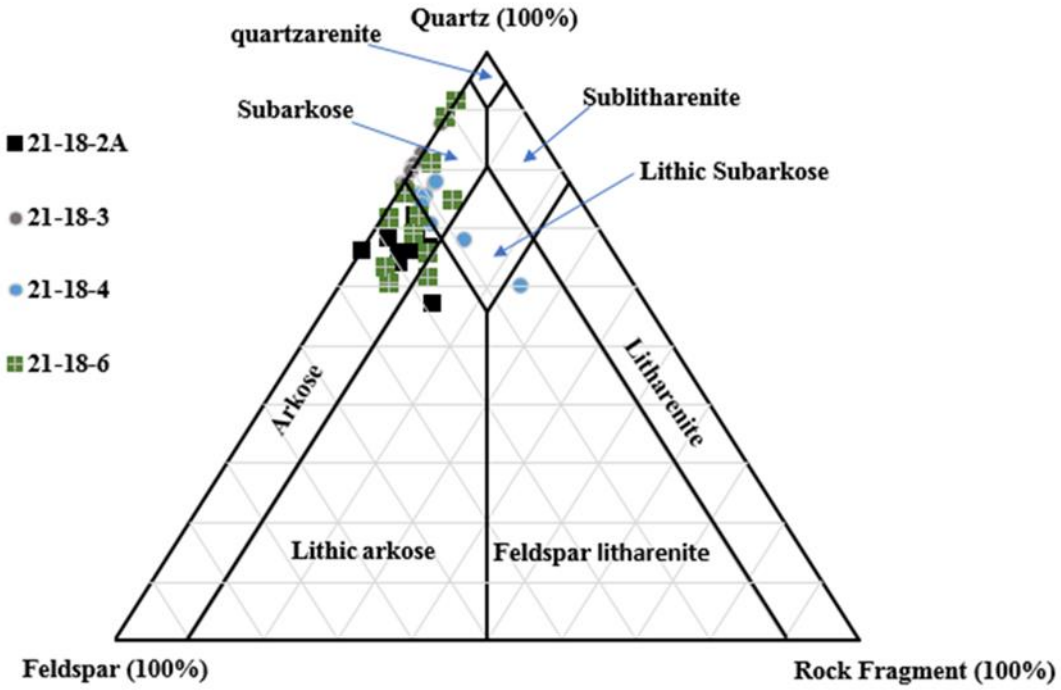

Figure 4-10. Sandstone classification diagrams (modified from Pettijohn et al. (1972)).

4.4.3 Quantitative analysis

Quantitative analysis of sandstones was carried out to quantify and determine the percentage of framework grains, cements and the porosity observed in each studied sample. The quantitative analysis of the studied samples are summarized in four tables, each table represents the petrographic results of several samples from particular well within the Kittiwake Field (Table 4-2, Table 4-3, Table 4-3 and Table 4-5).

Table 4-2. Petrographic Analysis Data for Well 21/18-6.

Sample no	Core Depth (ft)	Facies	CONSTITUENT (%)									Total (%)
			Porosity %	Framework Minerals			Accessory Minerals		Cement		Others	
				Quartz	Feldspar	Rock Fragment	Mica	Opaque Minerals	Calcite	Clay	Iron Oxide	
24	10414.7	1	10	55	5	0	2	0	0	20	8	100
25	10415.7	1	14.9	44.7	9.3	1	2.8	0	0	24.3	3	100
26	10415.8	1	13.3	50	6.3	0	2.3	0	0	23.4	4.7	100
27	10417	1	13.6	44.7	10.3	4.7	5	0	0	19.3	2.4	100
28	10418.75	1	11.6	41.7	13.3	2.7	2	0	5	21	2.7	100
29	10420.2	1	8.4	41	15.5	0.5	2.1	0	0	29.9	2.6	100
30	10424	1	9	45.1	13.6	0.5	1.6	0	1.6	25.6	3	100
1-B1	10431.2	1	9.1	37.5	20.3	4.1	1	0	5.6	13.6	8.8	100
2/B2	10437.3	2	2.3	36.3	13.3	3	16.7	0	4	20.6	3.8	100
3/B2	10449.4	1	7.7	45.4	17.3	6.3	2.1	0.1	5.2	11.7	4.2	100
4/B2	10459.5	1	6	40	17.7	7.3	2.3	0.1	6.2	16.4	4	100
5/B2	10468	1	4.6	41	20.7	3	1	0	9	18	2.7	100

Table 4-3. Petrographic Analysis Data for Well 21/18-2A

Sample no	Core Depth (ft)	Facies	CONSTITUENT%								Total %
			Porosity %	Framework Minerals			Accessory Minerals	Cement		Others	
				Quartz	Feldspar	Rock Fragment	Mica	Calcite	Clay	Iron Oxide	
50	10014.8	1	5	52	10	0	5	0	25	3	100
51	10016.8	1	10	45	17	0	0	0	25	3	100
53	10017.1	2	1.3	17	8.6	0	12	0	57.5	3.6	100
54	10017.5	1	4	38	16.6	3	5.6	0	28.3	4.5	100
55	10021	1	6.3	30	15	7.4	6	0	30.3	5	100
56	10023	1	7.8	38.1	16.3	1.4	8.9	0	25.4	2.1	100
23/B2	10026.5	2	3.4	40	13	2.3	13	0	23.3	5	100
24/B2	10033.8	2	2.3	36.4	13.3	4.7	16	0	23.3	4	100
25/B2	10053.9	1	1.3	38.3	13.4	3	4.3	18	19.2	2.5	100
26/B2	10076.9	2	6	35.3	16.3	3.3	8	3	25.6	2.5	100
27/B2	10111	1	7	33.9	13.6	3.6	3.3	3	29.3	6.3	100

Table 4-4. Petrographic Analysis Data for Well 21/18-3

Sample no	Core Depth (ft)	Facies	CONSTITUENT%								Total %
			Porosity %	Framework Minerals			Accessory Minerals	Cement		Others	
				Quartz	Feldspar	Rock Fragment	Mica	Calcite	Clay	Iron Oxide	
6/B2	10332	1	5	38.7	9.1	2.1	8.1	11.4	19.8	5.8	100
7/B2	10332.5	1	2	42.3	12.3	0	7.8	0	32.3	3.3	100
8/B2	10333.5	2	2.3	36.3	7.7	0	24	0	25	4.7	100
9/B2	10336.5	1	1.3	43.9	12.5	0.2	10.4	0	28.4	3.3	100
10/B2	10343.8	2	1	36	8.7	0	17	0	33.3	4	100
11/B2	10352.8	2	1	36	5	0	15	4	37	2	100
12/B2	10361	2	3.8	40	9.5	0	12	0	26.3	8.4	100
13/B2	10377.8	2	6.7	38	9.7	0	13.3	4.3	26.7	1.3	100

Table 4-5. Petrographic Analysis Data for Well 21/18-4

Sample no	Core Depth (ft)	Facies	CONSTITUENT (%)								Total (%)
			Porosity %	Framework Minerals			Accessory Minerals	Cement		Others	
				Quartz	Feldspar	Rock Fragment	Mica	Calcite	Clay	Iron Oxide	
14/B2	10698.5	1	4	39	10	16	3	0	23	5	100
15/B2	10698.75	2	2.7	40.7	9.3	2.3	8.3	0	33	3.7	100
16/B2	10700.5	3	4.3	28	8	1.3	24.7	7.3	21.4	5	100
17/B2	10701.8	2	5	35.5	10	1.3	6	12.3	27.3	2.6	100
18/B2	10708.5	3	1.7	27	7.8	1	24.4	11.4	24.4	2.3	100
19/B2	10714.5	2	1.3	38.3	12	4	3.7	11	25	4.7	100
20/B2	10724.5	2	7	36.7	10	2	8	4.3	24	8	100
21/B2	10734.15	2	3.8	38.7	11.3	2.3	5.3	7.3	27.3	4	100
22/B2	10746.5	2	7	38.3	10.7	7.3	3	5	25.4	3.3	100

4.4.3.1 Mineralogy

This section will describe in detail the main composition of the studied Skagerrak sandstones, based on the point counted results of the 41 studied samples.

4.4.3.1.1 Framework minerals

1. Quartz

The principal framework grain in all the studied sandstone samples was monocrystalline quartz. The quartz content in the studied samples ranged from 17 – 55%. Some quartz grains contain abundant mineral inclusions, and others show cracked and corroded quartz grains with precipitation (inclusion) of mica in some cases (Figure 4-11 A). Sutured boundaries between quartz grains were observed in some samples, which may indicate compaction processes (Figure 4-11 B).

2. Feldspar

Identifying feldspars definitely without staining is difficult, but it is likely that the majority were potassium feldspar, although plagioclase and microcline feldspars are present as well. The percentage of feldspar content in the studied samples ranged from 5 – 20%. Most of the observed feldspar grains exhibited variable degrees of alteration, replacement and in many cases partial or complete dissolution. Some feldspar grains, presumably originally calcium plagioclase, had been replaced partially or completely by authigenic calcite (Figure 4-11 C). Other feldspar grains were partially dissolved and re-filled with authigenic clay (Figure 4-11 D). In addition, in some cases, and within the same field of view, there were intact feldspar grains, partially dissolved grains and completely dissolved grains which increased the secondary porosity; some of these dissolved grains had been followed or replaced by precipitation of kaolinite, which creates microporosity (Figure 4-11 E).

3. Rock Fragments

As mentioned above polycrystalline quartz grains were considered as rock fragments and were the most common rock fragments found in most facies within the Skagerrak Formation. However other lithic clasts, shale fragments and clay intraclasts or pebbles of

clay were observed in some of the facies (Figure 4-11 F). Some of these fragments had been altered and oxidized. These fragments indicate that the provenance of these sediments is sedimentary, except that the polycrystalline quartz, if not caused by compaction processes, indicates a metamorphic provenance.

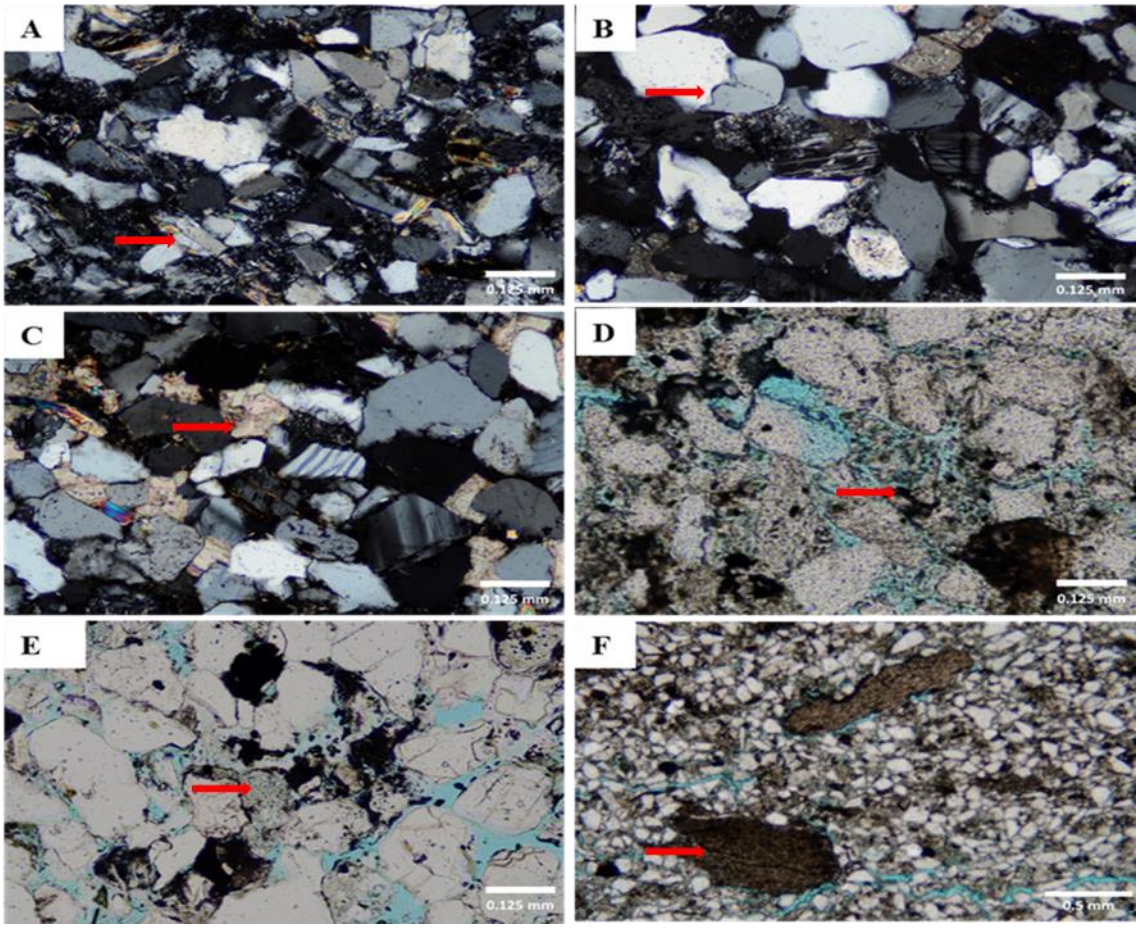

Figure 4-11. Thin-section photomicrographs showing different petrographic features. **A.** Typical view of very fine to fine-grained sandstone facies showing corroded quartz grains with precipitation (inclusion) of mica in some cases. 21/18-4, 10698.75. **B.** Typical view of very fine to fine-grained sandstone facies showing signs of compaction represented by the sutured boundaries between quartz grains. 21/18-6, 10449.4ft. **C**. Detailed view showing partial and complete dissolution of calcareous feldspar grain to be replaced by authigenic calcite. 21/18-2A, 10053.9 ft. **D**. Typical view of feldspar grains with inclusion – filled with clay. 21/18-6, 10424 ft. **E**. Detailed view of polished thin-section showing some dissolved feldspar grains which have been followed or replaced by precipitation of kaolinite and formation of microporosity. 21/18-6,10417ft. **F**. Typical view of fine grained sandstone facies showing shale fragments and clay intraclasts or pebbles of clay 21/18-2A, 10021 ft.

4.4.3.1.2 Accessory minerals

1. Mica

Micas, both muscovite and biotite are a common component in most sandstone sediments. The most common detrital mica in sedimentary rocks is muscovite, as it is chemically stable. Both types may form distinctive flakes that will usually occur parallel to the beds and lamination planes and with burial can be deformed and compacted between detrital grains (Figure 4-12 A). Muscovite is usually colourless in plane polarized light and bright blue to yellow under cross polarized light in thin-section; it was the most common mica observed in the Skagerrak Formation. However, biotite which is commonly strongly coloured brown or green and in some cases very pleochroic, was observed in many samples as well. From the selected sandstone samples, it was clear that there was significant variation in the distribution and content volume of mica between facies in the area of study, where some samples were particularly micaceous and other contained less than 2% mica. This variation in mica content appears to be proportional to grain size which can be related to the depositional process rather than to the provenance: the finer the grain size the more abundant the mica.

2. Iron oxide and pyrite

This widely separated cement was observed in all the studied samples, ranging in percentage from 2 - 5% and in some samples reaching 8%. Pyrite is opaque and appears black under plane polarized light. It was observed as clusters of black cubic shapes within pores or in association with other clay (Figure 4-12 B) and as dense nodules, framboids, or in amorphous form in some other samples. Alteration of pyrite to iron oxide may occur during uplift and exposure and appear as a red coloration along the edge of the pyrite (Figure 4-12 C).

4.4.3.1.3 Authigenic mineralogy

1. Calcite cement

Samples contained authigenic calcite cement ranging in percentage from 1% to 12%, with exception of one sample in well 21/18-2A, which contained about 18% calcite cement. The calcite may form in different ways, intergranular, euhedral and as replacement of

some feldspar grains with calcite cement (Figure 4-12 D). Figure 4-12 E shows poikilotopic calcite which has filled the pore space after a partial or complete grain dissolution as it squeezed between grains; this example shows the high birefringence and relief of calcite compared to the quartz grains. Figure 4-12 F shows partly dissolved plagioclase filled by calcite. Another type of calcite was observed as well; this calcite seems to have been precipitated in a late stage and may have formed mainly due to the replacement of feldspar grains.

Two different types of calcite were identified in the studied sandstones, these types of calcite suggest two phases of precipitation:

a. Early calcite cement: poikilotopic and intergranular calcite cement can be interpreted as exhibiting an early diagenetic process which may support the other detrital framework grains and prevent later diagenesis processes (Figure 4-12 E).
b. Late calcite cement: calcite which has been formed by alteration and replacement of feldspar grains or that has filled dissolution pores indicates that this cementation was formed later and post-dates the dissolution process (Figure 4-12 F).

The above characteristics may suggest that the sandstone has gone through early and late diagenesis processes and, therefore, the calcite in this sandstone represents two different phases of precipitation.

2. Kaolinite

In general, kaolinite is one of the clay minerals that commonly forms in patches filling the pore spaces; it is usually found in association with feldspar alteration and intermixed with other clay minerals (e.g. smectite and illite). It may form as cloudy white masses vermicular clusters or as blocky crystals. Kaolinite was one of the main authigenic clay minerals found in Skagerrak sandstones. It was observed in two distinct forms: irregular crystals in association with altered detrital mica flakes and usually poorly developed (Figure 4-13 A) and in more regular crystals or pseudohexagonal plates stacked in "booklets" (Figure 4-13 B). The latter are more common and may found occupying intergranular porosity or within secondary porosity that may have been formed by dissolution of feldspar grains.

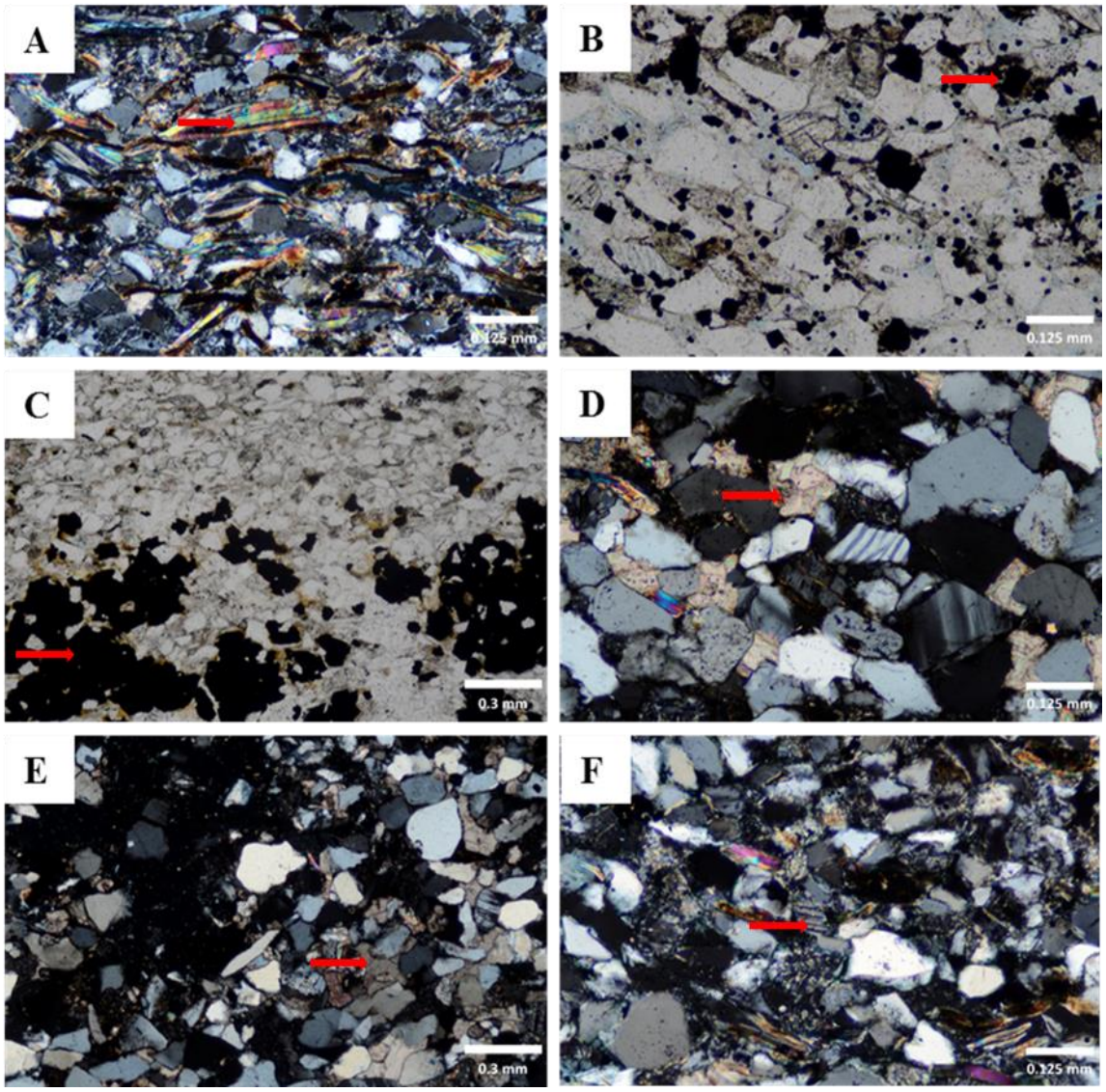

Figure 4-12. Thin-section photomicrographs of some authigenic and accessory minerals. **A**. showing distinctive flakes of mica compacted and deformed between detrital grains. 21/18-4, 10700.5ft. **B**. showing clusters of black cubic pyrite within pores or in association with other clay. 21/18- 4, 10724.5 ft. **C**. Typical view showing alteration of pyrite to iron oxide appearing as a red coloration along the edge of pyrite. 21/18-3, 10361 ft. **D**. Detailed view showing partial and complete dissolution of calcareous feldspar grain to be replaced by authigenic calcite. 21/18-2A, 10053.9 ft. **E**. View of poikilotopic calcite which has occupied the pore space. 21/18-6, 10468 ft. **F**. Detailed view showing late precipitation of calcite due to the replacement of feldspar grains. 21/18-2A, 10053.9 ft.

3. Chlorite Cements

Petrographic analysis showed that chlorite is a common clay grain coating for many of the studied samples in this area. The structural pattern of the observed chlorite grain coating was complex and in some cases seems to be associated with other clay types (e.g. illite or smectite). Chlorite grain coats may have been formed during early to medium diagenesis phases as a result of replacement of other clay minerals such as smectite and kaolinite or due to dissolution and re-precipitation of syn-depositional chlorite. The presence of such authigenic cements in Skagerrak sandstones may have played a significant role in limiting other types of cementation (e.g. quartz cementation) (Stricker and Jones, 2016). In many cases, partly or completely dissolved feldspar grains were observed coated by chlorite grain coats of cement, preserving the original shape of the feldspar grains from any further diagenesis effects. This clearly indicates that the chlorite grain coating was most likely to have occurred prior the dissolution of feldspar grains.

4.4.3.2 Porosity

Three main types of porosity, intergranular porosity, grain dissolution porosity (intragranular porosity) and microporosity, were identified within the studied Skagerrak sandstone. The visible point counted porosity in Skagerrak sandstone was relatively low, ranging between 1% up to about 8% in most samples, with the exception of the top part of the Skagerrak sandstone in Well 21/18-6, where it reached about 15% maximum (Table 4-6). The observed point counted porosity volume here included both primary and secondary porosity.

Table 4-6. Petrographic analysis data of porosity content below the unconformity surface in wells 21/18-6, 21/18-2A, 21/18-3 and 21/18-4.

Well 21/18-6		**Well 21/18-2A**		**Well 21/18-3**		**Well 21/18-4**	
MCU at (10415.5 ft)		MCU at (10017 ft)		MCU at (10332 ft)		MCU at (10698.75 ft)	
Depth (ft)	Porosity%	Depth (ft)	Porosity%	Depth (ft)	Porosity%	Depth (ft)	Porosity%
10415.7	14.9	10017.1	1.3	10332	5	10698.75	2.7
10415.8	13.3	10017.5	4	10332.5	2	10700.5	4.3
10417	13.6	10021	6.3	10333.5	2.3	10701.8	5
10418.75	11.6	10023	7.8	10336.5	1.3	10708.5	1.7
10420.2	8.4	10026.5	3.4	10343.8	1	10714.5	1.3
10424	9	10033.8	2.3	10352.8	1	10724.5	7
10431.2	9.1	10053.9	1.3	10361	3.8	10734.15	3.8
10437.3	2.3	10076.9	6	10377.8	6.7	10746.5	7
10449.4	7.7	10111	7				
10459.5	6						
10468	4.6						

1. Macroporosity

Two main types of macroporosity were observed: intergranular pores and grain dissolution pores. Only low percentages of intergranular porosity, which exists as pores between detrital grains were observed in the area of study, where total porosity did not exceed 15% and only some of this percentage was intergranular (Figure 4-13 C); the remaining percentage that contributed to the total porosity was mainly grain dissolution pores. This porosity has been interpreted as a secondary porosity formed due to the partial or complete dissolution of detrital grains (commonly feldspar), as their grain shape and outlines were still represented (Figure 4-13 D). However, some of these created pores were refilled by precipitation of clay or calcite (Figure 4-13 E). In addition to these main types of pores, elongated fractures and circumgranular porosity (developed around grains) were also observed from the thin-section samples in the area of study (Figure 4-13

F). This may have been formed as a result of pressure solution or due to load release during uplift. However, pores like this may also form as a result of poor sample preparation.

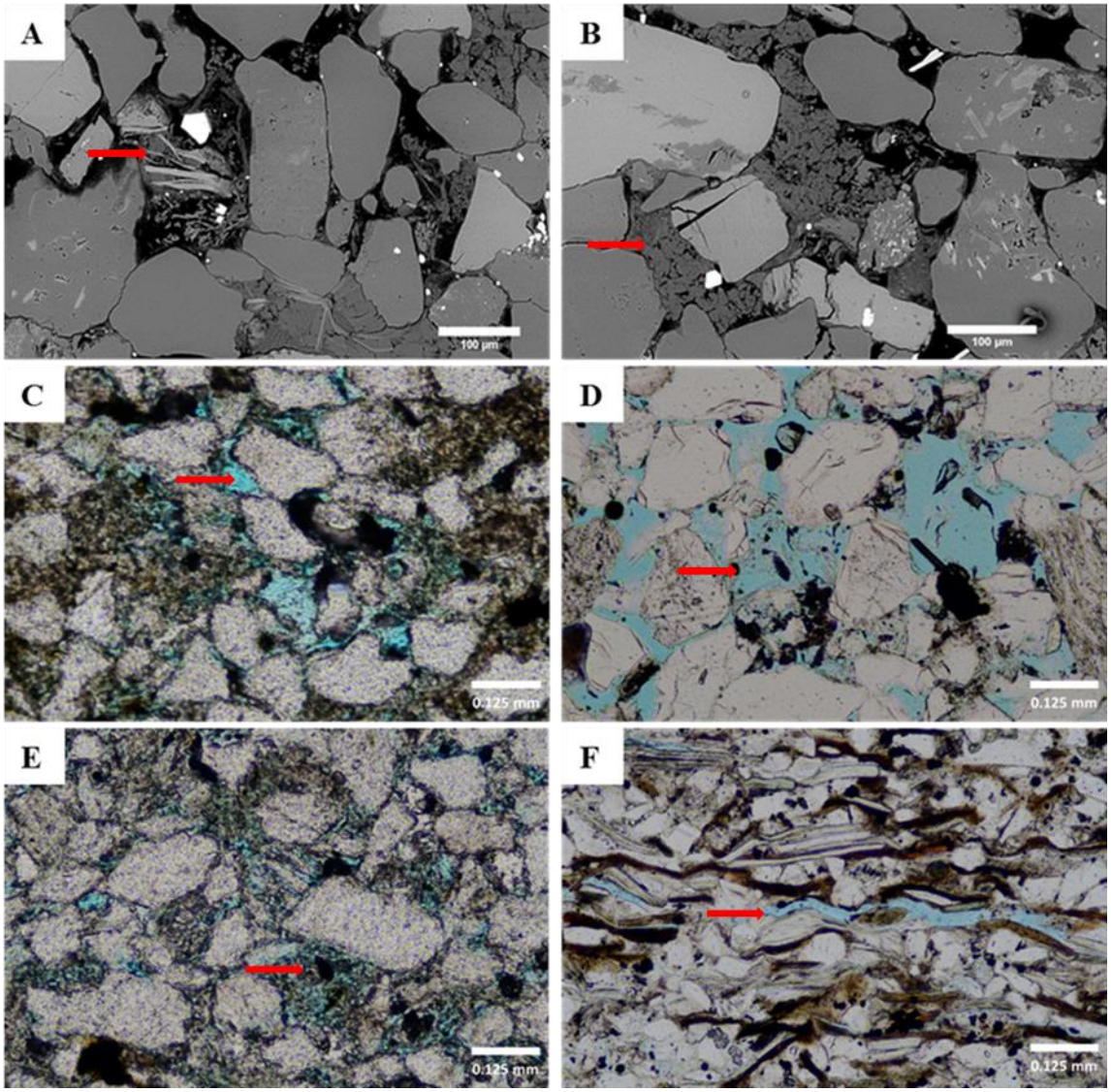

Figure 4-13. Thin-section photomicrographs and backscattered electron images showing: **A**. Kaolinite in association with altered detrital mica flakes. 21/18-6, 10417 ft **B**. SEM image showing kaolinite in regular crystals or pseudohexagonal plates stacked in "booklets". **C**. Intergranular porosity which exists as pores between framework detrital grains 21/18-2A, 54, 10017.5. **D**. Partial or complete dissolution of feldspar grain (the grain shape and outlines still represented), 21/18-6, 10417 ft. **E**. Secondary created pores refilled by precipitation of clay, 21/18-6, 10415.7 ft. **F**. Elongated fracture porosity, 21/18-4, 10700.5 ft.

2. Microporosity

This is defined as small pores that are usually associated with altered detrital grains and/or authigenic clays (Ulmer-Scholle et al., 2014). In the area of study, these micropores were recognised from the analysed samples under the microscope by the presence of blue impregnating resin within the very small pores or from the SEM (scan electronic microscope) images that were studied. Two main types of micropores were observed in Skagerrak sandstone. One was within the altered or leached detrital grains and most commonly within partially dissolved feldspar grains (Figure 4-14 A) and/or in between the expanded flakes of mica, in some cases (Figure 4-14 B). The second observed type of microporosity was the micropores associated with the authigenic clays, mainly within kaolinite crystals (Figure 4-14 C and D).

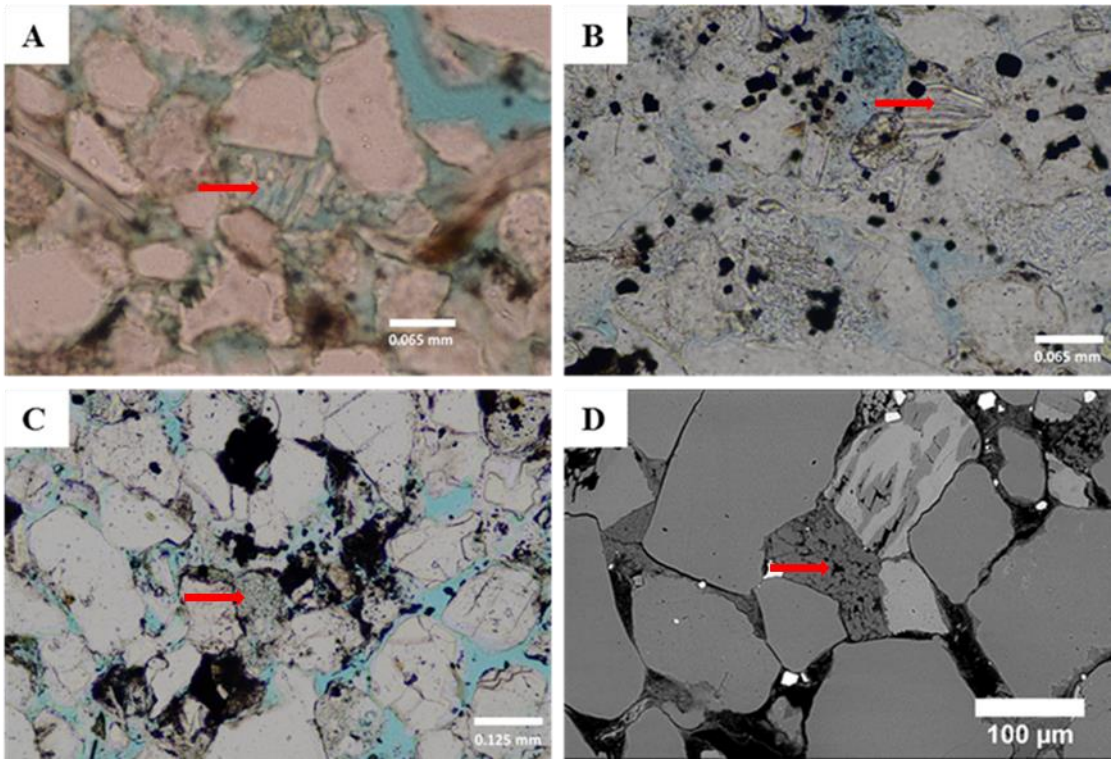

Figure 4-14. Thin-section photomicrographs and backscattered electron images showing: A. Typical view of micropores within partially dissolved reservoir grains. Well 21/18-2A, 10023 ft. **B**. Presence of micropores between the expanded flakes of mica. Well 21/18-4, 10724.5 ft. **C**. Detailed view showing micropores associated with the authigenic clays. Well 21/18-6, 27, 10417 ft. **D**. BSE image showing a microporous within mass of blocky kaolinite that was most likely to have been formed as result of feldspar alteration. Well 21/18-6. 10449.4 ft.

4.5 Spatial distribution of minerals and porosity and their relationship to the Mid-Cimmerian Unconformity

Most of the previous studies which suggest that unconformities have a direct effect on the underlying sediments attribute this to the leaching of certain minerals due to the influx of meteoric water during uplift and erosion. To be able to test this hypothesis, it was necessary to study the pattern of vertical distribution of unstable minerals and the reservoir properties under the unconformity surface in the studied wells.

4.5.1 Feldspar

There was no significant systematic vertical variation (vertical trend) in the volume and distribution of observed feldspar grains within the presented sandstones facies in the four studied wells in the Skagerrak Formation, except in one well, where systematic vertical variation of the feldspar volume was recognised. A fairly systematic decrease in feldspar volume toward the unconformity surface was recognised only in Well 21/18-6, in which the Skagerrak Formation was cut by the unconformity surface (Table 4-7). In Well 21/18-6, within the first 15 feet lying directly underneath the unconformity surface, the feldspar volume ranged from 6 – 15%, but reached 20% with increasing depth. This reduction of the amount of feldspar toward the unconformity surface is most likely to be due to the dissolution of the unstable feldspar grains; this can be either partial or complete dissolution. Evidence for this alteration and dissolution of feldspar was observed in the four studied wells within the Skagerrak Formation (Figure 4-15 A, B, C and D). In relationship to the unconformity surface, systematic variation in the feldspar content toward the unconformity surface was only evident in first 15 feet of Well 21/18-6, whereas in the other three wells, the feldspar content did not change systematically (Figure 4-16).

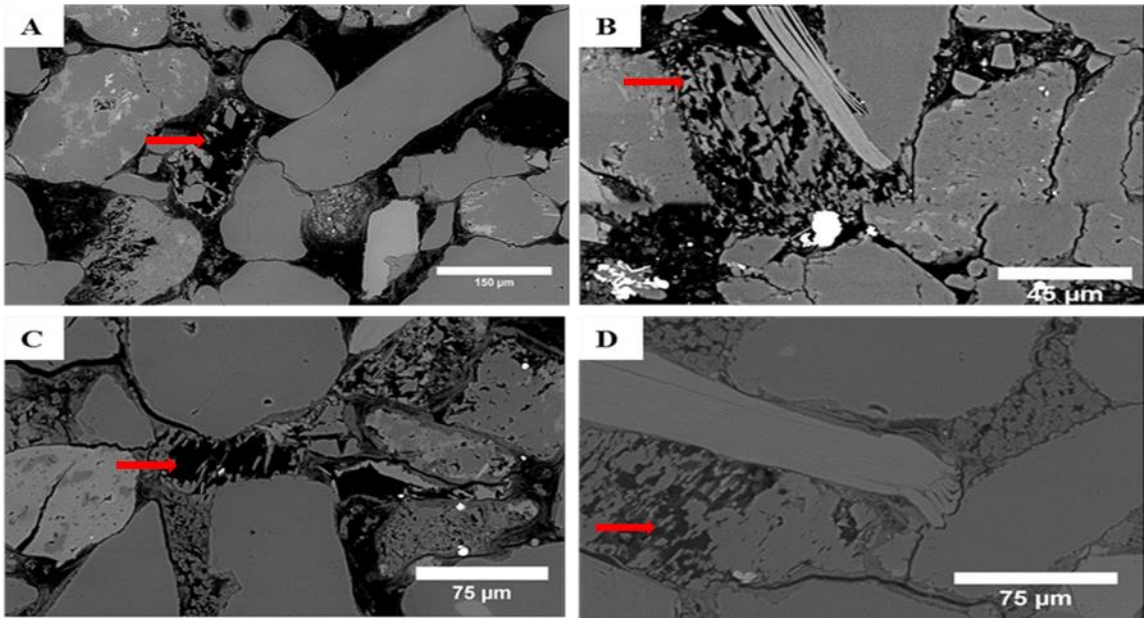

Figure 4-15. BSE images showing evidence for the alteration and dissolution of feldspar grains within Skagerrak Sandstone. **A**. BSE image showing complete dissolution of feldspar grains located about 34 ft below the unconformity surface in well 21/18-6, Depth: 10449.4 ft. **B**. BSE image showing partial dissolution of feldspar grains located just below the unconformity surface in Well 21/18-3, Depth: 10332 ft. **C**. BSE image showing partial dissolution of feldspar grains located about 0.5 ft below the unconformity surface in well 21/18-2A, Depth: 10017.5 ft. **D**. BSE image showing dissolution of feldspar grains located about 15 ft below the unconformity surface in well 21/18-4, Depth: 10714.5ft.

Table 4-7. Petrographic analysis data of feldspar content below the unconformity surface in Wells 21/18-6, 21/18-2A, 21/18-3 and 21/18-4.

Well 21/18-6		Well 21/18-2A		Well 21/18-3		Well 21/18-4	
MCU at (10415.5 ft)		MCU at (10017 ft)		MCU at (10332 ft)		MCU at (10698.75 ft)	
Depth (ft)	Feldspar%	Depth (ft)	Feldspar%	Depth (ft)	Feldspar%	Depth (ft)	Feldspar%
10415.7	9.3	10017.1	8.6	10332	9.1	10698.75	9.3
10415.8	6.3	10017.5	16.6	10332.5	12.3	10700.5	8
10417	10.3	10021	15	10333.5	7.7	10701.8	10
10418.75	13.3	10023	16.3	10336.5	12.5	10708.5	7.8
10420.2	15.5	10026.5	13	10343.8	8.7	10714.5	12
10424	13.6	10033.8	13.3	10352.8	5	10724.5	10
10431.2	20.3	10053.9	13.4	10361	9.5	10734.15	11.3
10437.3	13.3	10076.9	16.3	10377.8	9.7	10746.5	10.7
10449.4	17.3	10111	13.6				
10459.5	17.7						
10468	20.7						

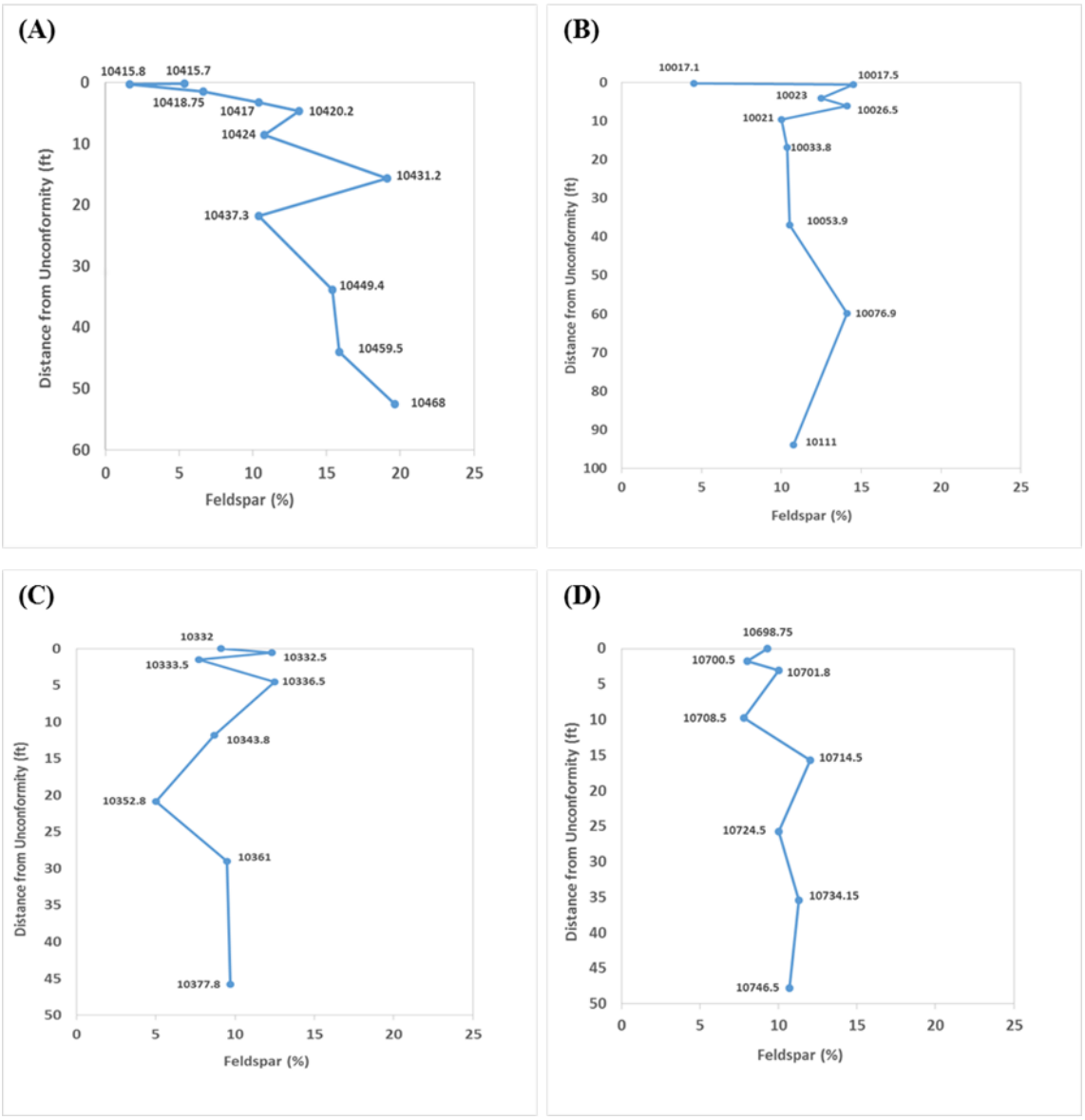

Figure 4-16. The vertical distribution patterns of feldspars below the Mid-Cimmerian Unconformity in the studied wells. **A**. Showing systematic decrease in the Feldspar amount toward the unconformity surface in Well 21/18-6. **B**, **C** and **D** show absence of vertical systematic distribution patterns of feldspars toward the unconformity surface in the Wells 21/18-2A, 21/18-3 and 21/18-4 respectively.

4.5.2 Kaolinite

Petrographic analysis identified that kaolinite is the most common clay mineral for all the studied wells in Skagerrak sandstones. In most samples kaolinite was observed in association with feldspar alteration and dissolution filling pore spaces (Figure 4-14 C and D) and in some other cases intermixed with other clay minerals (e.g. smectite and illite). As mentioned above, kaolinite was observed in two forms:

Firstly, as irregular crystals in association with altered detrital mica flakes and usually poorly developed (Figure 4-13 A) or intermixed with other clay minerals filling pore spaces, which could be either detrital or early diagenetic kaolinite, as it is very difficult to differentiate between the detrital and early authigenic kaolinite, especially within fine sandstones (Figure 4-17 A).

Secondly, it was observed in more regular crystals (well-crystallized) stacked in "booklets" or a vermicular habit which usually reflects a late diagenetic product formed in situ due to alteration and replacement of feldspar (Figure 4-17 B and C). The latter, which is commonly recognised as a microporous mass of blocky kaolinite within pore space, is most likely to have been formed as result of feldspar alteration and dissolution and usually appeared within a hint of the grain outline (Figure 4-17 D). Although the evidence indicates that most of the observed kaolinite was formed in situ and related to later diagenetic processes (including euhedral booklets and high microporosity within kaolinite masses), other types of kaolinite were observed as well. Therefore, the variations of kaolinite distribution below the Mid-Cimmerian Unconformity appear to be more complex than a direct relationship to feldspar mineral dissolution.

It was very difficult to quantitatively evaluate the volume or distribution trend of kaolinite within each well. This is because of the difficulty of highlighting and calculating the quantity of the kaolinite from the other clay types and to distinguish the authigenic (in situ) kaolinite from the detrital kaolinite within the total clay. One of the possible ways to ascertain the volume of kaolinite within the samples was to perform quantitative X-ray Diffraction Analysis (XRD). However, this method does not differentiate between the detrital and authigenic kaolinite, whereas the target was to determine in situ late diagenetic origin kaolinite that may have been formed later as a result of post deposition diagenetic processes and in relationship to the unconformity surface. Two other attempts to distinguish and establish the distribution and calculate the amount of kaolinite below the unconformity surface were attempted using the Raman Spectrometer and QEMSCAN analysis (Quantitative Evaluation of Minerals by scanning electron microscopy). Unfortunately, these attempts were not successful and suggested for future study (more details in Appendix A.6).

Therefore, because kaolinite is the main constituent of the clay mineral in the studied samples, the point counted clay mineral percentage has been used to approximate the

vertical distribution patterns of kaolinite below the Mid-Cimmerian Unconformity in the studied wells (Figure 4-18).

Excluding Well 21/18-6, no obvious vertical distribution trend of clay (including kaolinite) content toward the unconformity surface was observed. In addition to that and because precipitation of kaolinite is usually associated with feldspar alteration and dissolution, a positive correlation between feldspar and kaolinite is expected within the affected rocks. However, this correlation was only observed in Well 21/18-6, with a lack of correlation in the other three wells (Figure 4-19).

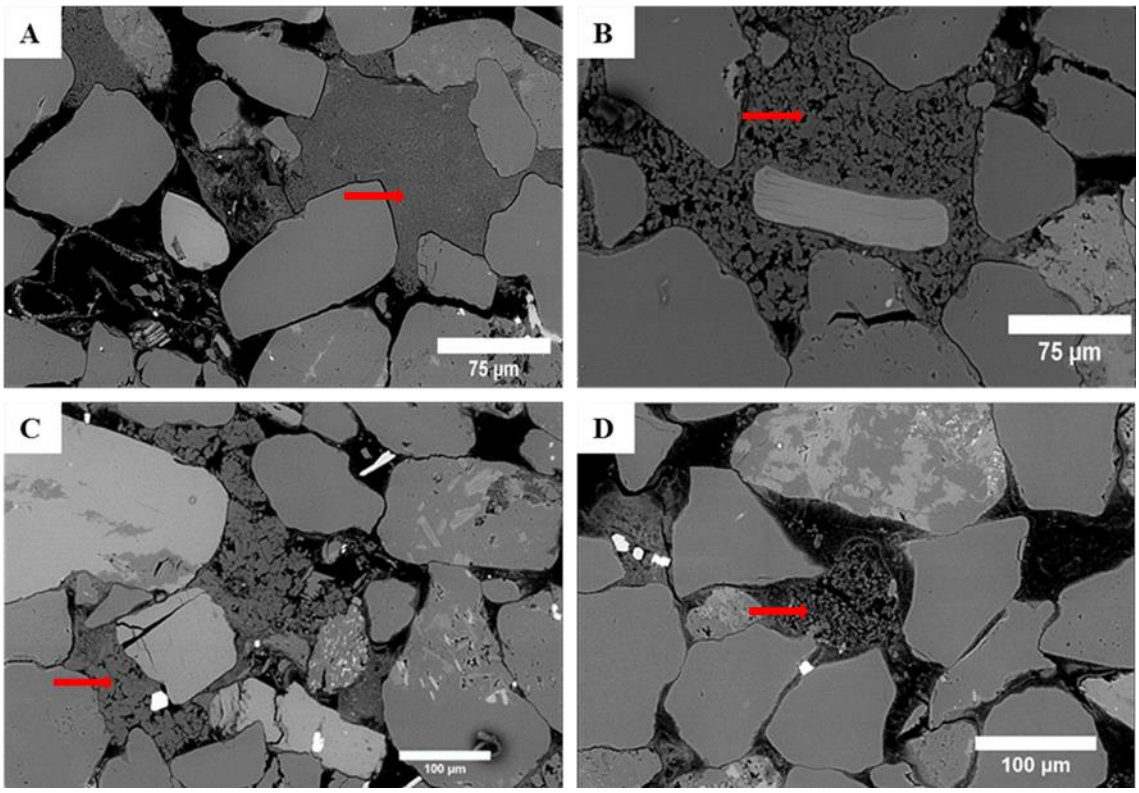

Figure 4-17. BSE images showing the various types and distribution of kaolinite below the unconformity surface in Skagerrak Sandstone. **A**. Showing intermixed clay (mainly kaolinite) squeezed between grains filling pore spaces which can be either detrital or early diagenetic kaolinite. Well 21/18-6, depth, 10417 ft. **B**. and **C**. BSE images showing regular crystals of kaolinite stacked in "booklets" or vermicular habit, reflecting a late diagenetic product formed in situ due to alteration and replacement of feldspar. Samples are from Wells 21/18-2A, depth 10017.5 ft and Well 21/18-6, depth 10417 ft. **D**. BSE showing kaolinite within pore space formed as result of feldspar alteration and dissolution and appearing with a hint of the grain outline. Well 21/18-6, depth 10449.4 ft.

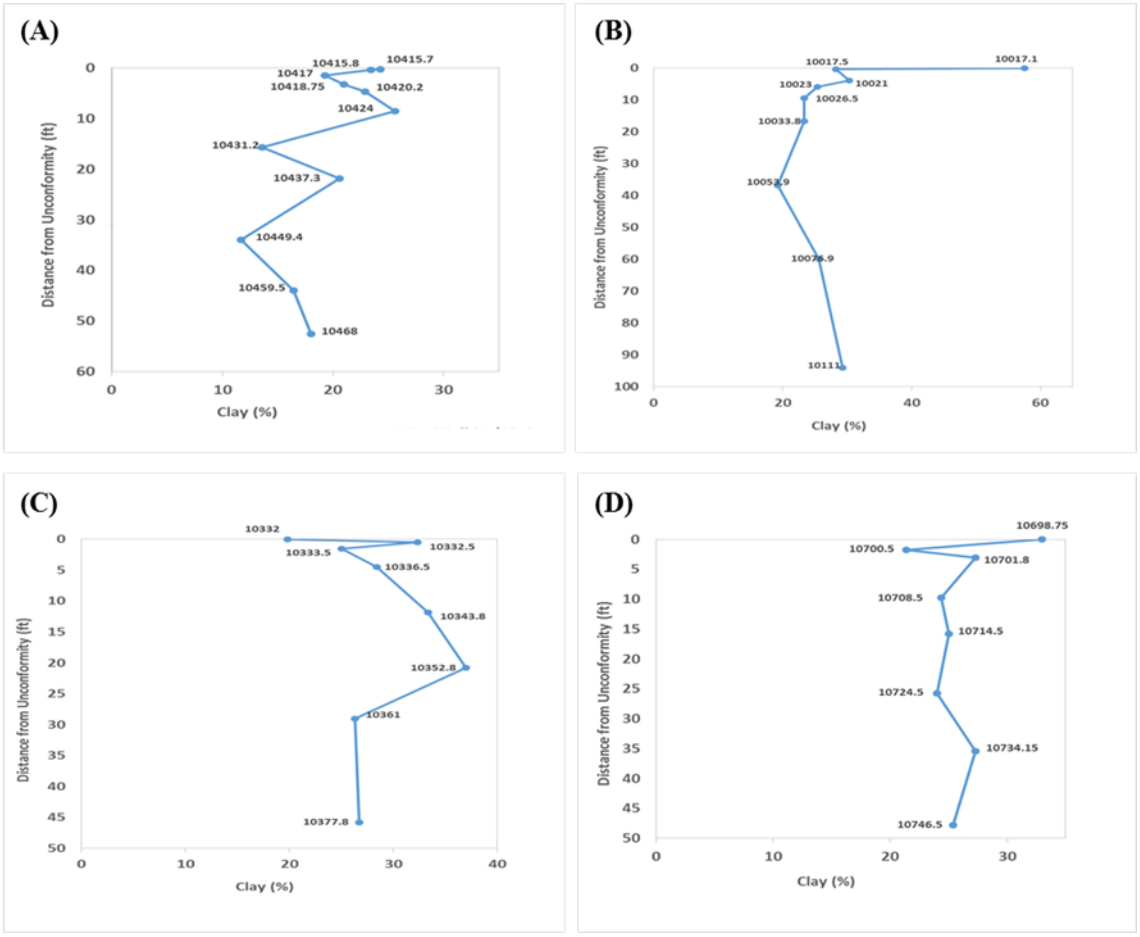

Figure 4-18. The vertical distribution patterns of clay below the Mid-Cimmerian Unconformity in the studied wells. (**A)**, (**B)**, (**C)** and (**D)** show absence of vertical systematic distribution patterns of clay toward the unconformity surface in the four studied Wells 21/18-6, 21/18-2A, 21/18-3 and 21/18-4 respectively.

4.5.3 Mica

Petrographic analysis data of the mica content in the four studied wells showed that mica is common component in most of the sandstone samples. It was observed in various colours throughout the sandstone samples, and sometimes with brown pleochroism, which suggests altered biotite. The burial mica was deformed and compacted between detrital grains, filling pore spaces and formed in distinctive flakes and parallel to the beds and lamination planes (Figure 4-12A). Petrographic analysis and the point counted data result showed that there was significant variation in the distribution and volume of mica between the different sandstone facies below the unconformity surface (Table 4-8). Some samples were particularly micaceous with more than 24% of mica content and others

contained less than 2% of mica. However, no vertical systematic distribution patterns of mica content toward the unconformity surface were observed in the four studied wells (Figure 4-20). Therefore, this variation in mica content is most likely to be proportional to grain size, which can be related to the depositional process rather than to the sediments' source or diagenesis process; in general the observation is that the finer the grain size the more abundant the mica.

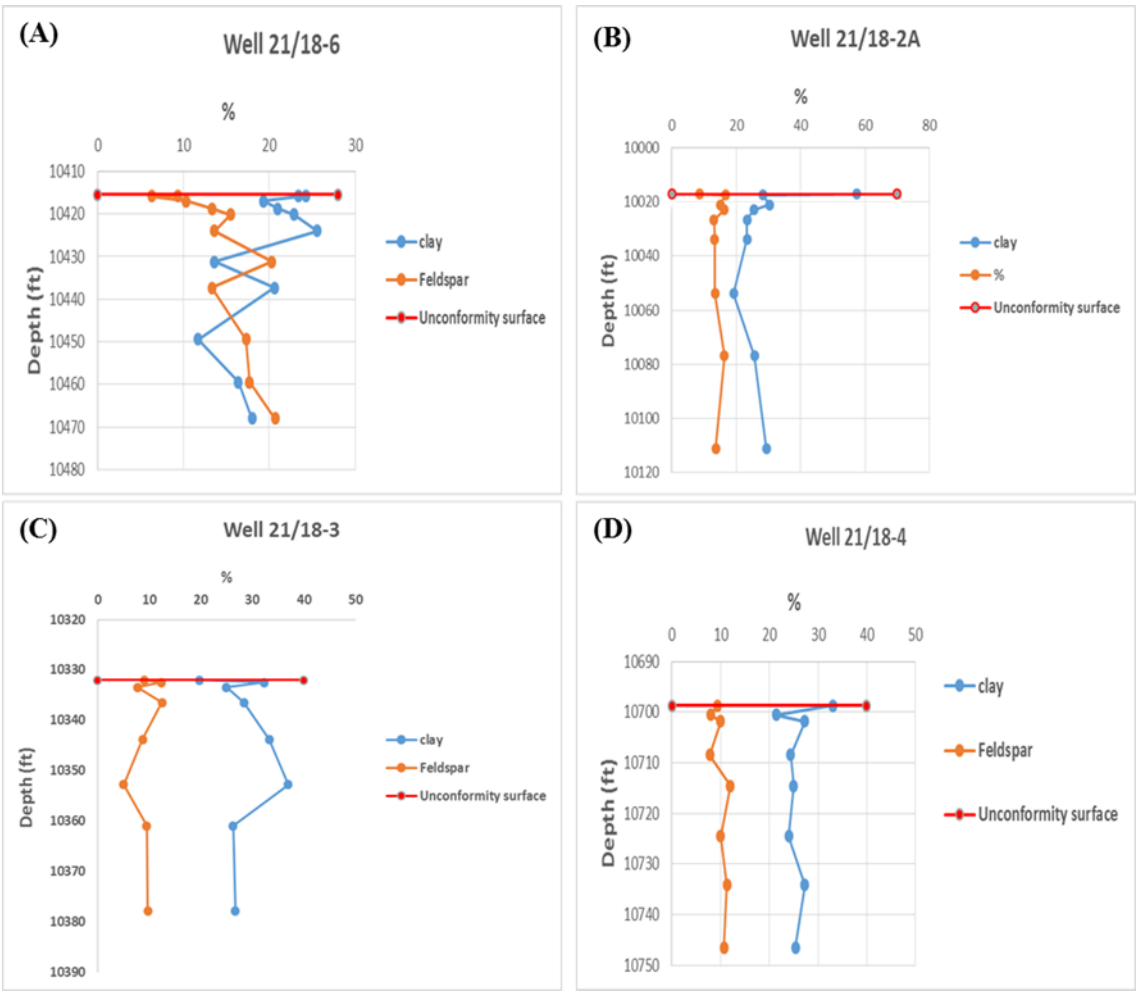

Figure 4-19. A correlation between clay and feldspar below the unconformity surface in Kittiwake field. Figures (**A)**, **(B)**, **(C)** and **(D)** shows lack of correlation, except in Well 21/18-6, which shows some positive correlation between clay and feldspar below the unconformity surface.

Table 4-8. Petrographic analysis data of mica content below the unconformity surface in wells 21/18-6, 21/18-2A, 21/18-3 and 21/18-4.

Well 21/18-6		Well 21/18-2A		Well 21/18-3		Well 21/18-4	
MCU at (10415.5 ft)		MCU at (10017 ft)		MCU at (10332 ft)		MCU at (10698.75 ft)	
Depth (ft)	Mica %	Depth (ft)	Mica %	Depth (ft)	Mica %	Depth (ft)	Mica %
10415.7	2.8	10017.1	12	10332	8.1	10698.75	8.3
10415.8	2.3	10017.5	5.6	10332.5	7.8	10700.5	24.7
10417	5	10021	6	10333.5	24	10701.8	6
10418.75	2	10023	8.9	10336.5	10.4	10708.5	24.2
10420.2	2.1	10026.5	13	10343.8	17	10714.5	3.7
10424	1.6	10033.8	16	10352.8	15	10724.5	8
10431.2	1	10053.9	4.3	10361	12	10734.15	5.3
10437.3	16.7	10076.9	8	10377.8	13.3	10746.5	3
10449.4	2.1	10111	3.3				
10459.5	2.3						
10468	1						

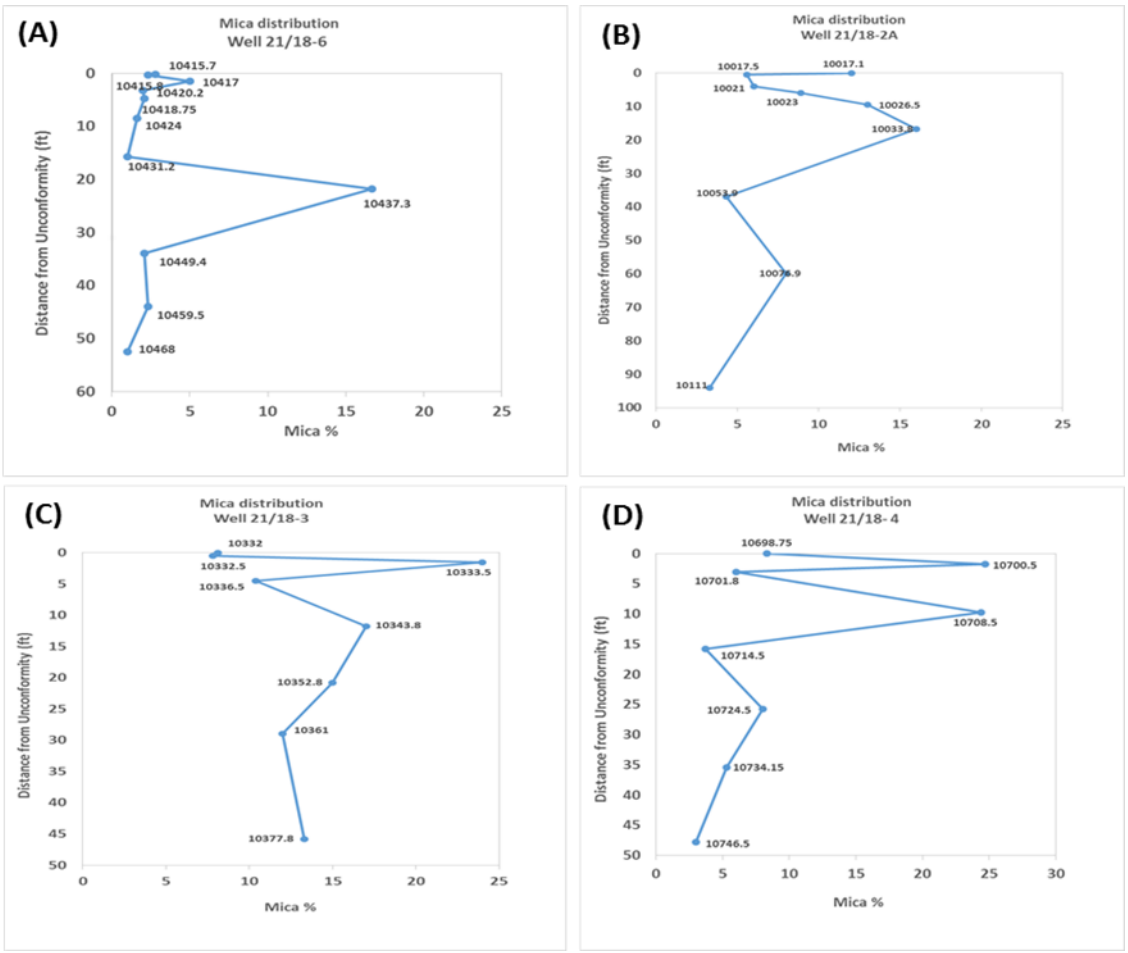

Figure 4-20. The vertical distribution patterns of mica below the Mid-Cimmerian Unconformity in the studied wells. (**A**), (**B**), (**C**) and (**D**) show absence of vertical systematic distribution patterns of mica toward the unconformity surface in the four studied wells.

4.5.4 Porosity

As mentioned in section 4.4.3.2, three main types of porosity, intergranular porosity, grain dissolution porosity and microporosity, were identified within the studied Skagerrak Sandstone. Although measured core porosity in the four studied wells ranged from 3 – 21%, visible point counted modal porosity was at a lower percentage and ranged from 1% up to about 8% in most of the analysed samples and the maximum obtained volume of porosity was about 15%, in Well 21/18-6; this included both the primary and secondary observed porosity types.

This difference between the value of measured core analysis porosity and the visible point counted modal porosity of thin-section samples is common, as measured core porosity values are commonly higher than visible point counted modal porosity, due to the difficulty of counting very small pore spaces and micropores, especially with the samples dominated by very fine to fine sandstone grains. Moreover, the depth of the samples taken for this study was not exactly the same as the depth for the samples of which have been previously used for measuring porosity; this is because the objective of this research was to collect samples in vertical depth with relationship to the unconformity surface. However, the correlation between measured core porosity (He porosity) and a visible point counted modal porosity for the four studied wells indicates that both porosity values are related (Figure 4-21).

4.5.4.1 Intergranular porosity

This primary porosity which exists as pores between framework grains was very low in the four studied wells. This is could be related to many factors, for example, grain size, sorting and the diagenesis process, as in many cases these pores were seen to be occupied and filled partially or completely by digenetic carbonate and clay cement (mentioned above in section 4.4.3, Figure 4-12 D and Figure 4-13 C and E) and/or by compacted flakes of mica (Figure 4-12 A). As the total volume of the porosity observed under the microscope was low, ranging between 1% - 8% in most cases with exception of Well 21/18-6, which reached 15%, it was somewhat difficult to point count each type of porosity separately. However, no visible systematic variation in the amount and vertical distribution of the total porosity, including the intergranular porosity, was recognised toward the unconformity surface.

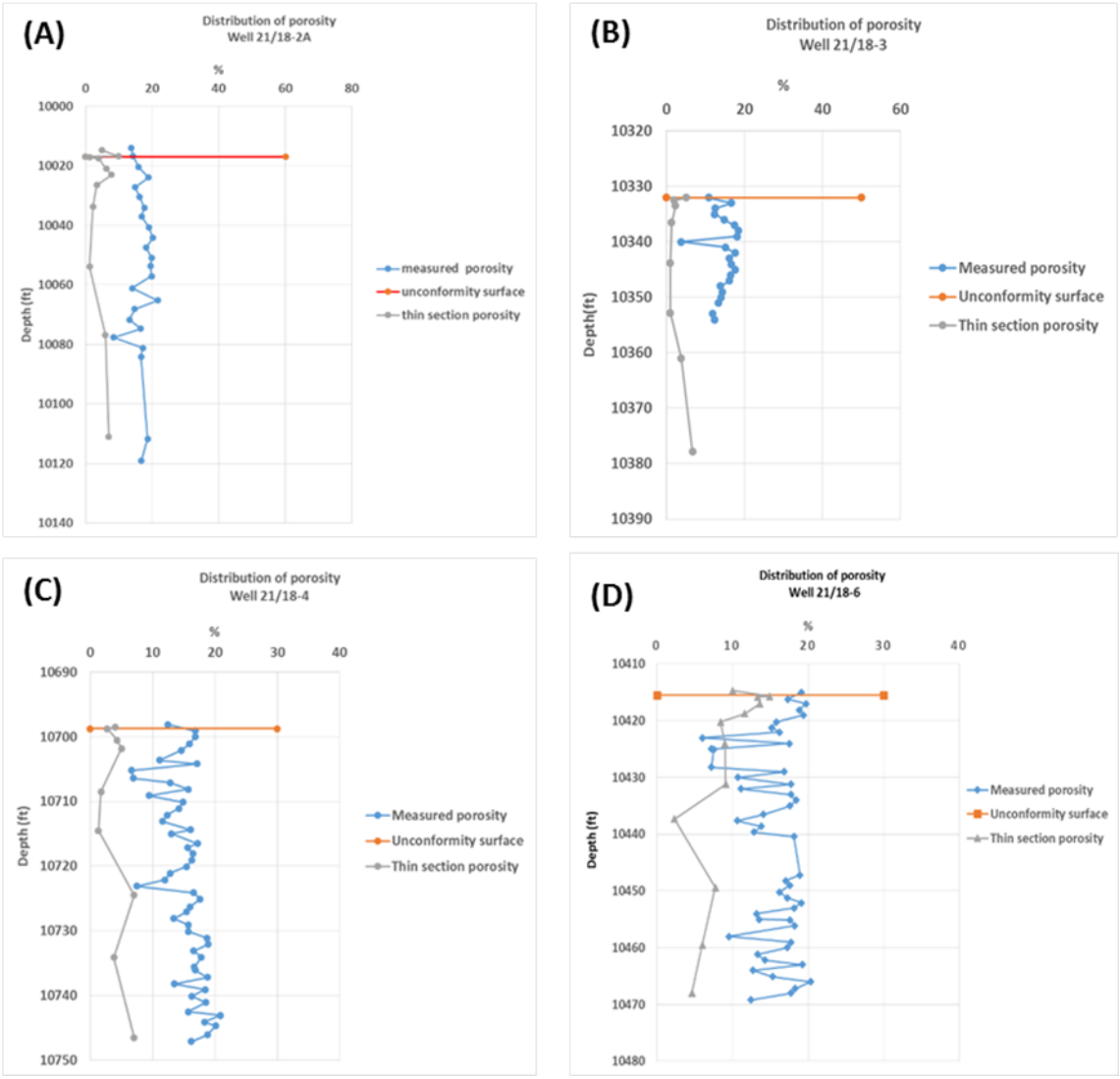

Figure 4-21. A correlation between measured core porosity (He porosity) and a visible point counted modal porosity for the four studied wells, (**A**), (**B**), (**C**) and (**D**), indicating that both porosity values are related.

4.5.4.2 Dissolution porosity

This porosity, which is interpreted as a secondary porosity, has been formed mainly due to the partial or complete dissolution of detrital grains (commonly feldspar). This type of porosity was found to be common in the four studied wells and was easily identified, especially in SEM images, as partial and complete dissolution of feldspar grains were obtained. In many samples the grain shape and outlines were still represented (Figure 4-15 A and C). This dissolution enhanced the volume of porosity within the Skagerrak

formation and contributed to the total measured and modal porosity. However, dissolution of feldspar is usually associated with the formation of other clay minerals (mainly kaolinite) (Figure 4-14 C and Figure 4-17 D) and this will reduce the potential volume of the enhanced secondary porosity.

The results of petrographic analysis for the four studied wells indicated that there was no significant systematic vertical variation (vertical trend) in the volume and distribution of the total porosity toward the unconformity surface, except in Well 21/18-6, where a fairly systematic increase in the porosity volume toward the unconformity surface was observed. Within the first 15 feet lying directly underneath the unconformity surface, the average total porosity volume decreased from about 15% to 4% or less at greater depth (Table 4-6). The increase of porosity toward the unconformity surface in Well 21/18-6 was compatible with the reduction of feldspar amount in the same area, as described in section 4.5.1 (Figure 4-22). It is most likely that there is relationship between this increase of secondary porosity and the decrease in the amount of feldspar grains. This leads to the assumption that dissolution of feldspar is the main source of enhanced secondary porosity in Well 21/18-6 in particular and in the other wells in general. However, although this enhanced porosity (dissolution porosity) was seen in most of the analysed samples from the four studied wells, a systematic correlation between porosity content and feldspar was only obtained in the top part of Well 21/18-6. This is possibly because the increase of porosity volume due to mineral dissolution will be balanced by the generation and precipitation of a similar volume of diagenetic minerals that have been formed as product of the dissolved minerals (Figure 4-23).

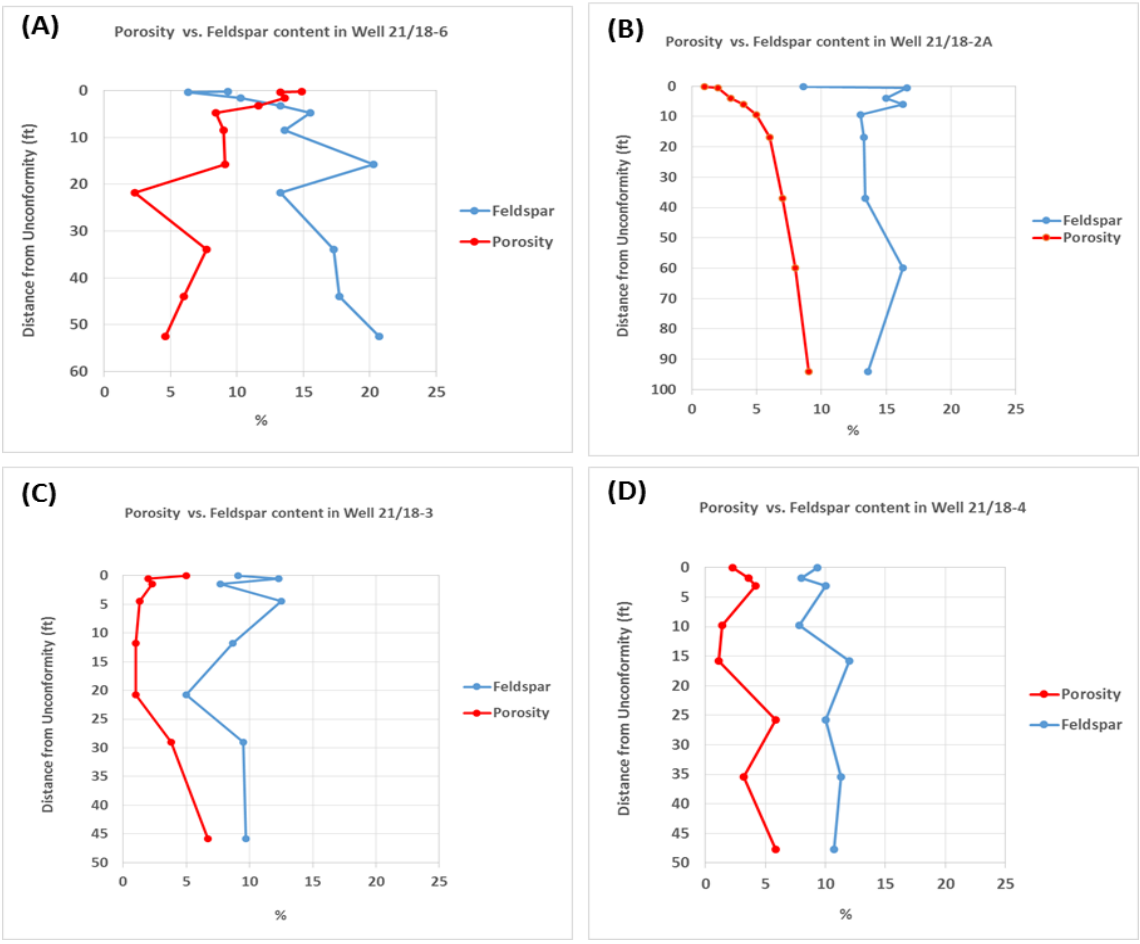

Figure 4-22. The distribution of porosity and feldspar below the unconformity surface in the four studied wells. (**A**) Shows possible correlation between porosity and feldspar until depth 10429 ft. (**B**), (**C**) and (**D**) do not indicate clear correlation between the distribution of porosity and feldspar 21/18-6, 21/18-2A, 21/18-3 and 21/18-4.

4.5.4.3 Microporosity

As described in section 4.4.3, this type of porosity is usually associated with altered detrital grains (mainly feldspar) and/or authigenic clays (commonly kaolinite). SEM studies (scanning electronic microscope) were particularly useful for identifying these pores, which are usually associated with the authigenic clays, mainly kaolinite, and are sometimes very difficult to recognise under the optical microscope. The SEM images confirmed that most of the observed micropores were associated with the authigenic clays (mainly within a mass of kaolinite crystals) and within the partially dissolved feldspar grains (Figure 4-14 and Figure 4-15). This type of porosity enhanced the total volume of

porosity within the area of study and contributed to the total measured and petrographic porosity (Table 4-6 in section 4.4.3).

Although this type of secondary porosity was recognised in most analysed samples, the distribution of these micropores within the four studied wells in the Skagerrak Formation was not very consistent, as it is associated with formation and distribution of grain dissolution and clay formation in most cases. However, it was somewhat similar to the distribution of the second type of porosity (grain dissolution porosity), where systematic vertical variation of porosity volume was identified only in the first 15 feet underneath the unconformity surface within Well 21/18-6.

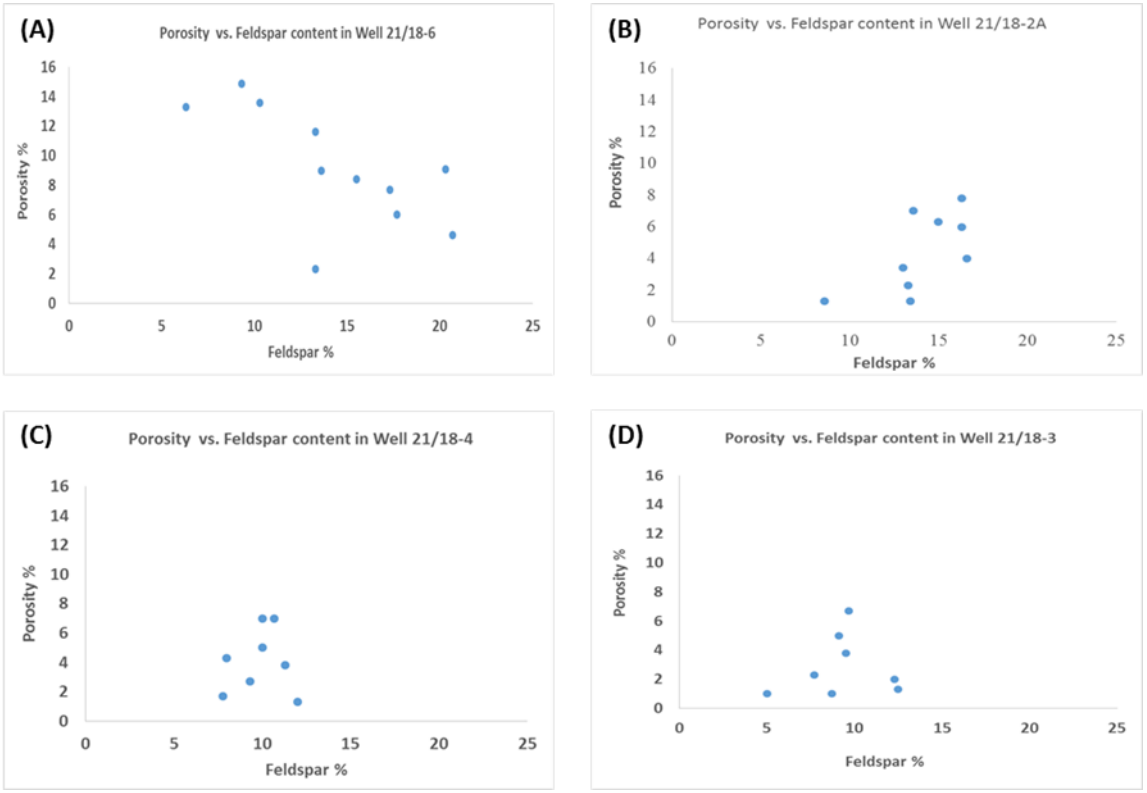

Figure 4-23. Scatter plots showing lack of correlation between porosity content and feldspar, except in Well 21/18-6.

4.6 Discussion of results

This section will discuss the various hypotheses that may responsible for the production of secondary porosity and precipitation of kaolinite in the Kittiwake field.

4.6.1 Potential mechanisms for the production of secondary porosity and precipitation of kaolinite

Partial or complete post-depositional dissolution of detrital grains or authigenic cements (or both) are the main source of secondary porosity in clastic rocks (Bloch, 1994). However, secondary porosity does not always enhance the rock's total porosity: the volume of secondary porosity formed by the dissolution of minerals may be counterbalanced by a similar decrease of porosity volume due the precipitation of diagenetic minerals that are formed as a response to the dissolution process (Bjorlykke, 1984). For a significant volume of secondary porosity to be formed in any potential reservoir, a number of prerequisites have to be met. Some of these prerequisites, which have been discussed by (Giles and Marshall, 1986) are:

1. A source of a high amount of aggressive fluid
2. A method for the movement of the leaching fluid from its source toward the sediments.
3. The ability of this fluid to affect the sediments before it becomes saturated
4. The presence of unstable minerals within the sediments to be leached.
5. The dissolution of minerals should not be accompanied by precipitation of a mineral product.

According to (Ehrenberg and Jakobsen, 2001), four common mechanisms may explain and can be considered for the nature and timing of post-depositional dissolution of framework grains and cements in sandstone sediments:

1. Influx of meteoric water shortly after the deposition of sediments;
2. Influx of meteoric water during erosion or Cimmerian uplift;
3. Influx of acidic component produced by thermal maturation of organic matter or by addition of CO_2 that may form as a result of thermal maturation of organic matter.
4. Release of organic acid and CO_2 that may form as a result of oil biodegradation.

These mechanisms are explained in detail below.

1. Influx of meteoric water shortly after the deposition of sediments

Meteoric water may affect the rocks shortly after their deposition and burial or after uplift and erosion (e.g., underneath unconformities formed as a result of uplift and erosion). In sedimentary basins, meteoric water may penetrate to significant depths, e.g. meteoric water penetrated up to depths of 2000 m in the Great Artesian Basin of Australia (Habermehl, 2006). However, the ability of this water to leach and dissolve minerals is most likely to be limited and to decrease with the increasing length of the flow path, as meteoric water, when starting to penetrate, will usually be undersaturated and with interaction between these waters and certain minerals it will become saturated. Therefore, the dissolution of a large amount of minerals and formation of secondary porosity by meteoric water is most likely to be restricted to the upper part of the flow system (Giles and Marshall, 1986). Evidence for dissolution of minerals by meteoric water has been documented by many authors. However, the process of how these waters interact with minerals and the effectiveness of the processes at depth are very complex.

The dissolution rate of minerals depends mainly on the pH of the meteoric water and the particular surface area of minerals (Bjorkum et al., 1990), as less pH, meaning more acidic water, leads to more leaching and dissolving capability to interacted minerals. Moreover, the reaction of this meteoric water during its penetration through the sediments may play a role in the leaching and dissolving capability of minerals: slow penetration of meteoric water through the sediment may cause quick saturation of the penetrated water and lead to less leaching power and thus decrease the thickness of the layer affected (Giles and Marshall, 1986).

2. Influx of meteoric water during erosion or Cimmerian uplift

The second mechanism that may explain the nature and timing of post-depositional framework grain and cement dissolution in sandstone sediments is the influx of meteoric water during erosion or Cimmerian uplift of sedimentary rocks, which is the main hypothesis addressed in this study. If the sedimentary rocks that have been buried and undergone early diagenetic processes are uplifted and exposed, they will be subjected to the effect of meteoric waters. According to (Morad et al., 2000), many factors may control

the distribution and the extent of meteoric waters below the unconformities surfaces. Some of these factors are**:** duration of sediment exposure, climate, hydraulic head, the porosity and permeability of the sediments, the composition of the sediment minerals, the presence of impermeable layers that may prevent the penetration of meteoric water and, finally, the presence of faults that may act as flow pathways for the meteoric water (Figure 4-24).

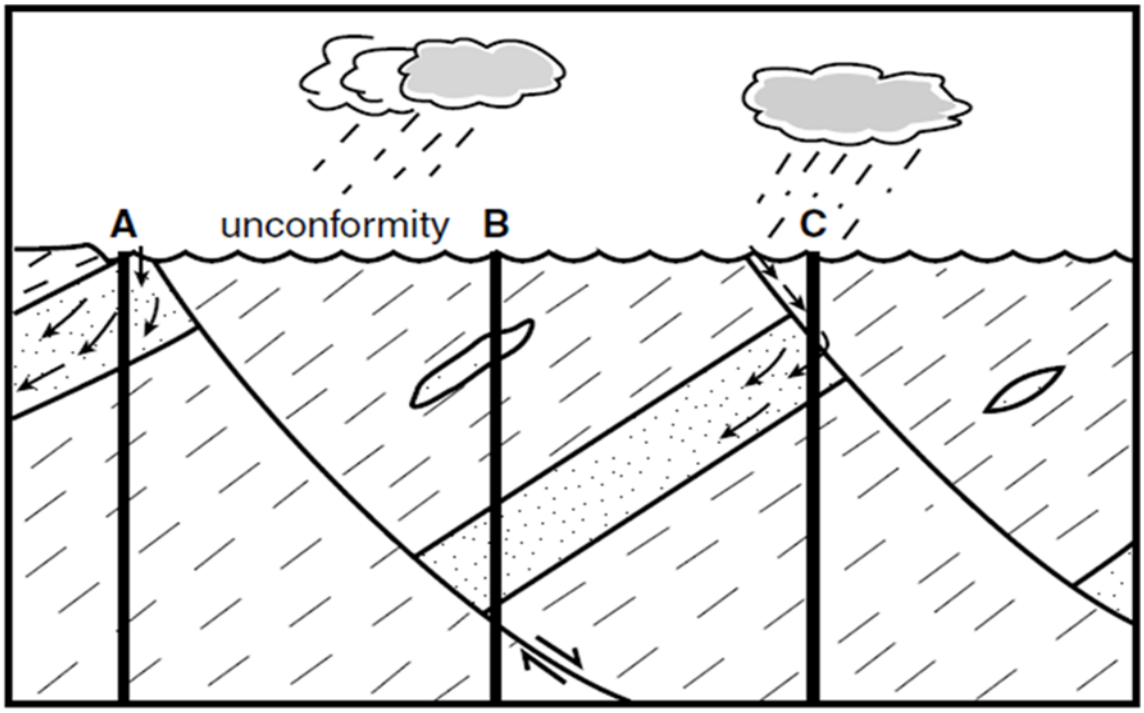

Figure 4-24. Hypothetical diagram showing the mechanisms of how meteoric waters may be distributed and extend underneath the unconformity surface, each well showing a different mechanism of how meteoric water may penetrate and causing alteration to the rocks below unconformity surface. Any alteration in Well A will be systematically related to the unconformity surface. In Well B, presence of the thick mud rock layer is most likely to halt penetration of meteoric water to the sandstone. In Well C, the fault may act as a conduit to the meteoric water; diagram modified from (Morad et al., 2000).

Although penetration of meteoric waters has been documented as reaching a depth of more than 2000 m in sedimentary rocks (e.g. in the Great Artesian Basin of Australia), the maximum suggested and registered diagenetic effect of these waters below unconformities' surfaces is not more than hundreds of metres and is expected to increase systematically toward the unconformity surface (Emery et al., 1990, Shanmugam, 1990) (see chapter 1 for more details of this effect).

Uplifted and exposed sedimentary rocks that are subjected to meteoric waters are usually prone to erosion as well; the rate of this erosion is dependent on many factors, for example, properties of the exposed material, topography and climate of the area. Therefore, it is important to know that the expected effect of meteoric water on the exposed sedimentary rocks will be only preserved if the rate of erosion was less than the rate of meteoric water penetration and alteration; otherwise the diagenetic effect of these waters (e.g., dissolution or kaolinitization of minerals) on sedimentary rock will be eroded and is unlikely to be seen (Bjorkum et al., 1990).

3. Influx of acidic component produced by thermal maturation of organic matter or by addition of CO_2 that may form as a result of thermal maturation of organic matter

Carbon dioxide that may form as a result of thermal maturation of source rock layers and is expelled during compaction of these layers is considered to be one of the important factors that may cause post-depositional dissolution of framework grains and cements in sedimentary rocks (Ehrenberg, 1991, Bloch, 1994). However, this process is relatively slow and can only be effective if there is a considerable thickness of organic matter to produce a high amount of the required CO_2 that can cause leaching and dissolution of framework grains and cements in sedimentary rocks (Ehrenberg, 1991).

Another type of acidic fluid thought to be responsible for generation of secondary porosity in deep burial sandstones is the organic acids (carboxylic) that commonly form directly before, during and after the generation of hydrocarbons. These organic acids are believed to cause dissolution of the aluminosilicate minerals in sandstones (Surdam et al., 1989). These acidic fluids are expected to be at their most acidic in the shale layer. When these fluids escape from the source rocks and flow toward the reservoirs or the surrounded sedimentary rocks, dissolution of some grains and carbonate cements may occur, therefore generating secondary porosity (Bloch, 1994). However, some doubts about this hypothesis have also been raised:

1. Mass balance calculations show that the generated amount of the organic acids is insufficient to cause the observed leaching and dissolution of framework grains and cements in sedimentary rocks (Giles and Marshall, 1986).

2. The ability of this acidic fluid to be transported from its source rock to the reservoir rocks, as the source rocks and surrounding shale usually contain some carbonate and feldspar grains that may react with the generated acidic fluids; therefore, the generated acid fluids may be neutralized and lose their corrosive power within or in the migration path before reaching the potential reservoir rocks (Lundegard et al., 1984, Bjorlykke, 1984).

4. Release of organic acid and CO_2 that may form as a result of oil biodegradation

Organic acids and CO_2 which may cause alteration and dissolution of some framework grains and carbonate cement in the sedimentary rocks may form in both source rocks (as mentioned above) and reservoir rocks. Within the reservoir rocks, these acidic fluids may form due to various alteration process of hydrocarbons. Biodegradation of hydrocarbons in reservoirs is considered to be one of the most important alteration processes (Larter et al., 2003) . Oil biodegradation occurs as a result of crude oil alteration caused by living microorganisms (commonly bacteria); this will lead to generation of organic acids and CO_2 and, therefore, more acidic oil (Taylor et al., 2001).

For the occurrence of oil biodegradation in subsurface reservoirs, many prerequisites are required, which include: the presence of living microorganisms and their ability to get into the oil column, the existence of water, the presence of sufficient electron acceptors (such as sulphates, oxygen and ferric iron) and inorganic nutrients (Peters et al., 2005). In subsurface reservoirs most oil biodegradation process occur within the transition zone of oil and water, which is called oil-water contact OWC, as within this area living organisms will be able to get access to the overlying oil, by diffusion, and to the inorganic nutrients that may be generated as a result of mineral dissolution in the water zone (Figure 4-25) (Head et al., 2003).

Many factors may control the degree of oil biodegradation, one of the most important of which is reservoir temperature. Oil biodegradation is usually found in shallow reservoirs with temperature less than 80°C and rarely found in deep reservoirs with higher temperatures (Head et al., 2003). This is possibly due to the difficulty for the organisms to live in reservoirs where temperature is more than 80°C. However it is not necessarily the case that all low temperature oil reservoirs will be biodegraded; this because it

possible for this non-biodegraded oil to be recently charged or because the reservoir has been paleopasteurized before the charge of oil (Wilhelms et al., 2001).

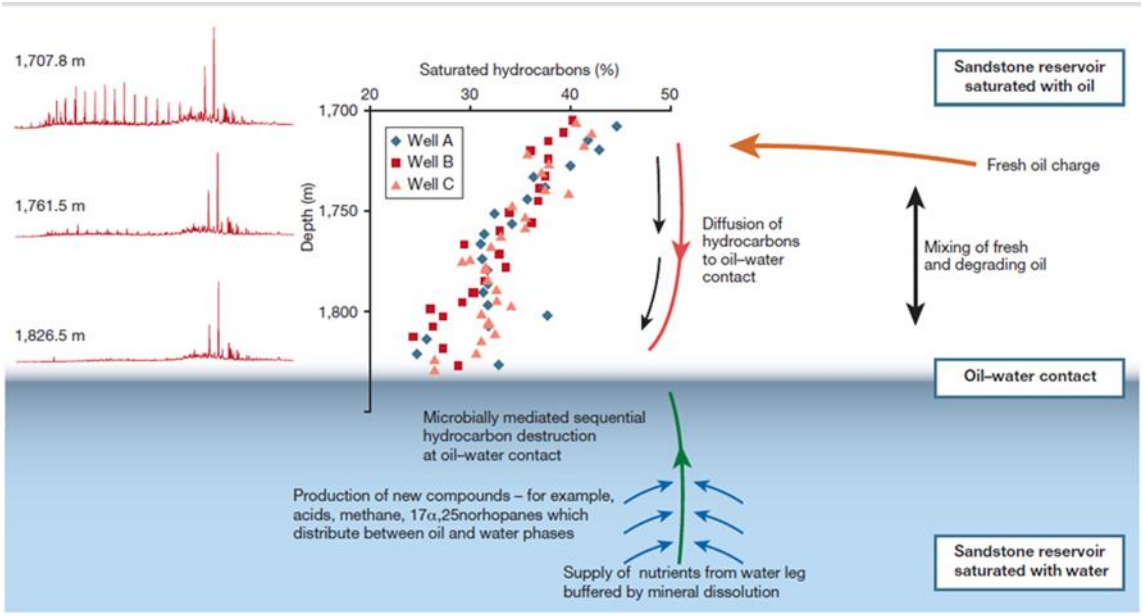

Figure 4-25. Oil degradation at an OWC; after Head et al. (2003).

Oil emplacement is assumed to be one of the factors that may inhibit the diagenesis process in subsurface reservoirs. However, the effect of oil charge on the diagenesis process is based mainly on the wettability of reservoir rocks (Saigal et al., 1992). In water wet reservoirs oil emplacement may cause significant effects on the diageneses process, as, after emplacement of oil, a thin film of water commonly forms on the minerals' surface. However, in oil wet reservoirs, where there is no water film coating, filling of oil may halt any diagenesis processes (Surdam et al., 1989). Furthermore, degradation of oil that occurs after the oil emplacement may cause an alteration of the reservoir's rocks and lead to formation of minerals (e.g. calcite and pyrite) (Wolicka and Borkowski, 2012). An example of the effect of oil degradation on reservoir rocks is the dissolution of plagioclase and formation of kaolinite in the Gullfaks Field (Ehrenberg and Jakobsen, 2001). Another example is the formation of carbonate cement in the Forth and Balmoral Fields, which is assumed to be related to the oil degradation process at OWC (Watson et al., 1995).

4.6.2 Origin and timing of dissolution and production of secondary porosity

Secondary porosity in sedimentary rocks is a post-depositional product that may be formed as a result of partial to complete dissolution of framework minerals or authigenic cements or both of them (Bloch, 1994). Dissolution of unstable framework grains (for example, feldspar, rock fragments and mica) are well documented in many studies (Wilkinson et al., 2014). Although it has been widely believed that dissolution of unstable minerals and cements in clastic rocks will enhance the potential reservoir porosity, other published studies (e.g. (Bjorlykke, 1984)) indicate that the presence of secondary porosity within the reservoir does not necessary mean that the total reservoir porosity will be enhanced, as the increased volume of pores due to mineral dissolution will be balanced by the generation and precipitation of a similar volume of diagenetic minerals that have been formed as products of the dissolved minerals.

In the area of study there were several lines of evidence for the creation of secondary porosity, this porosity was formed mainly due to the partial or complete dissolution of feldspar grains within the Skagerrak Formation. Significant amounts of feldspar grains have been dissolved from the Skagerrak Formation; this dissolution has been recognised in most analysed samples within the area of study and was the main reason for the creation of secondary porosity. As mentioned above this post-depositional dissolution of feldspar grains may occur by several mechanisms, and this study will try to detect which of the mentioned mechanism/s may be the main cause for grain dissolution and porosity enhancement in Skagerrak sandstone formation. Four different scenarios are possible:

4.6.2.1 First scenario: The influx of meteoric water shortly after the deposition of sediments

This scenario attributes the dissolution of feldspar grains to the influx of meteoric water shortly after the deposition of the Skagerrak sandstone sediments. Acidic meteoric water may have affected the rocks shortly after their deposition and burial, leading to dissolution of unstable minerals and enhancement of porosity. However, the ability of this water to leach and dissolve minerals was most likely to be limited and to decrease with depth, because meteoric water when starting to penetrate is usually undersaturated, and with interaction between this water and some minerals it will become saturated (Bjorlykke and Aagaard, 1992).

In the area of study, there is some evidence indicating that the influx of meteoric water shortly after the deposition was not the cause of the observed feldspar dissolution and formation of secondary porosity. **First**, the alteration and dissolution of feldspar grains were observed in almost all the collected samples from the Skagerrak Formation (Figure 4-17 D), whereas, during the deposition of late Triassic the climate was semi-arid, which means no abundance of meteoric waters would be expected (Ketzer et al., 2009).

Secondly, if the dissolution occurred directly after deposition, secondary pores formed by the dissolution of feldspar grains would most likely to be destroyed due to the compaction process, whereas oversized pores which were almost the same size as the other surrounding framework grains were observed within the analysed samples of the Skagerrak formation. These oversized pores have not been affected by compaction, despite the modern depth of burial, which is in excess of 3000 m, and the presence of some compaction signs, indicating that this dissolution is most likely to be late dissolution and post-date the compaction process (Figure 4-26 A and B).

Thirdly, in most of the studied samples some of the dissolved feldspar grains had been replaced by kaolinite. The generated kaolinite was within the secondary pore space and associated with microporosity, indicating no signs of compaction, despite the depth of sandstone burial, which currently exceeds of 3000 m (Figure 4-26 C and D).

All these types of evidence disprove the possibility that the dissolution of feldspar grains and creation of secondary porosity in the Skagerrak formation could be due to the influx of meteoric water shortly after the deposition of the Skagerrak sandstone sediments.

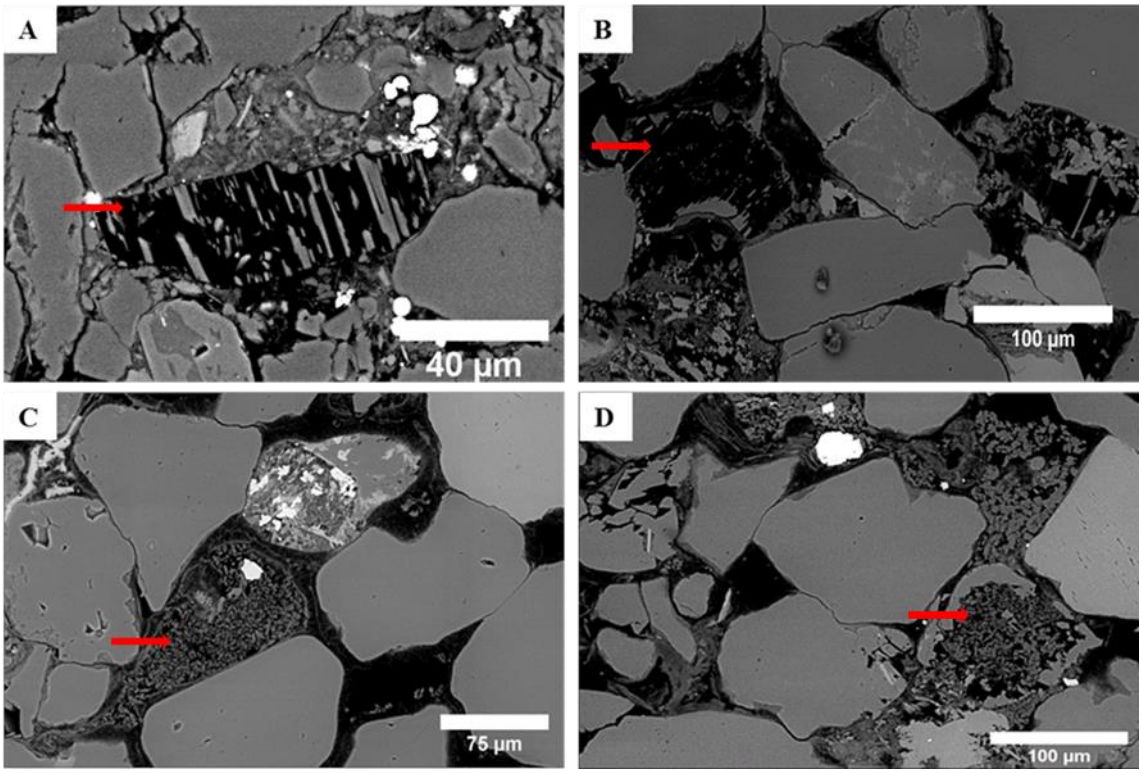

Figure 4-26. Backscattered electron images: **A** and **B** show that dissolution of feldspar grains produced oversized pores almost the same size as the other surrounding framework grains, with no signs of compaction, despite the depth of more than 3300 m, Well 21/18-3, 10332 ft and Well 21/18-2A, 10017.5 ft respectively. **C** and **D**: indicate formation of kaolinite within the pore space and associated with microporosity and indicating no signs of compaction, despite the depth of sandstone burial which is in excess of 3000 m, Wells 21/18-6, 10449.4 ft 10417 ft respectively.

4.6.2.2 The second scenario: The influx of meteoric water during erosion or Cimmerian uplift

This scenario attributes the dissolution of unstable minerals (mainly feldspars) to the influx of meteoric water during erosion or uplift of sedimentary rocks, which is the main hypothesis on which this study is based. Late diagenetic changes are expected to occur when sedimentary rocks which have undergone early and mid-diagenetic process are uplifted or eroded and subjected to the effect of meteoric water. As mentioned previously, the extent and distribution of meteoric waters beneath the unconformity's surface are controlled by many factors (Figure 4-24 in section 4.6.1). However, although penetration of meteoric waters has been observed reaching a depth of more than 2000 m in

sedimentary rocks, the thickness of pervasive late diagenetic influence of these waters below unconformities' surfaces usually varies between ten to hundreds of metres and is expected to increase systematically toward the unconformity surface (Emery et al., 1990, Shanmugam, 1990).

In the area of study, uplift and erosion of the Western Platform in the Central North Sea during the Lower to Middle Jurassic resulted in erosion and removal of the Early and Mid-Jurassic sandstones and the creation of the Mid-Cimmerian Unconformity or (Intra-Aalenian Unconformity) which lies directly above the Skagerrak Formation in the area of interest. To test the hypothesis of dissolution of unstable minerals (mainly feldspars) due to the influx of meteoric waters through the uplifted and eroded Skagerrak Sandstones on which this study was based, all the analysed samples from the four studied wells of Skagerrak formation were taken at regular intervals with depths starting directly below the unconformity surface and going deeper. Therefore, and because the Skagerrak sandstones were exposed at this unconformity surface, any possible late diagenetic change in relation to the formation of this unconformity surface will be expected to be seen in vertical trends, which means that any observed changes are expected to increase with proximity to this unconformity surface. However, this was not the case in any of the studied wells, except in Well 21/18-6, where systematic variation in the feldspar content toward the unconformity surface was only recognised in first 15 feet below the unconformity surface (Figure 4-16). This can be interpreted to be because the rate of erosion of the Skagerrak sandstones in this well is less than that in the other three wells, so exposed longer, and therefore any possible effect due to this exposure will be higher in this well than the others.

Petrographic analysis has shown much evidence for the late dissolution of feldspar grains and the creation of secondary pores in most of the analysed samples: the alteration and dissolution of feldspar grains was observed in almost all the collected samples from the Skagerrak Formation, despite depths of more than 3300 m. In many cases, the original shape of the partly or completely dissolved feldspar grains was clear and had been preserved by a remnant of chlorite grain coating, which indicates that the dissolution of feldspar grains is most likely to have occurred in a late diagenesis stage, after the chlorite grain coating was precipitated. These authigenic chlorite grain coats may have been formed during early to medium diagenesis phases as a result of replacement of other clay

minerals such as smectite and kaolinite, or due to dissolution and re-precipitation of syn-depositional chlorite (Stricker and Jones, 2016). This late dissolution of feldspar grains led to the creation of secondary pores and therefore enhanced the total porosity of Skagerrak Formation. However, in many cases the dissolution of feldspar grain was associated with the precipitation of pore filling kaolinite and/or illite (fibrous pore-lining diagenetic illite) which would lead to a relative decrease in the total porosity of Skagerrak sandstone.

As most of petrographic evidence demonstrates the late dissolution of feldspar grains, it seems to be that most of the created and enhanced secondary porosity was related to the dissolution of these feldspar grains. However, after the detailed analysis of the collected samples, several lines of evidence suggested that the dissolution and creation of secondary porosity was not related to the unconformity surface. These lines of evidence include the following points:

Firstly, the absence of a systematic decrease of feldspar volume toward the unconformity surface. As mentioned above, the thickness of pervasive late diagenetic influence of meteoric waters below unconformities' surfaces usually varies between ten to hundreds of metres and are expected to increase systematically toward the unconformity surface (Emery et al., 1990, Shanmugam, 1990). Therefore, according to this mechanism, it would be expected that the influx of meteoric waters and degree of dissolution of feldspar grains would increase toward the presented unconformity surface. Petrographic analysis results from the four studied wells indicated that there was no significant systematic vertical variation (vertical trend) in the volume and distribution of the dissolved feldspar grains or the total porosity, including secondary pores, toward the unconformity surface, except in Well 21/18-6, where a fairly systematic increase in the porosity volume toward the unconformity surface was recognised in the first 15 ft below the unconformity surface (mentioned in section 4.5.4, Figure 4-22 above). Within the first 15 feet lying directly beneath the unconformity surface, the average total porosity volume decreased from about 15% to 4% or even less, at greater depth. The increase of porosity toward the unconformity surface in Well 21/18-6 is compatible with the reduction of feldspar amount in the same area, as described in section 4.5.1 (Figure 4-23), which means that the dissolution of feldspar was the main cause of the created and enhanced secondary porosity. However, this systematic change was observed in only one well and only within

the first 15 ft below the unconformity surface. This may suggest an alternative cause for the dissolution of feldspar grains (such as biodegradation of oil), especially with the presence of oil water contact in the Kittiwake Field at a depth of 10430 ft, which almost the same depth where this dissolution takes place (more detail about this hypothesis will be discussed later).

Secondly, if the observed dissolution of feldspar was related to the influx of meteoric waters during the creation of the unconformity's surface, the generated secondary pores most likely to be partly destroyed, due to the compaction process at this depth of burial. Instead, the shapes of the partly and completely dissolved feldspar grains were clear in most samples and did not show any compaction signs; these dissolved remnants of feldspar grains are usually delicate structures and, therefore, if the dissolution of these grain was related to the influx of waters from the Mid-Cimmerian Unconformity during the Early to Mid-Jurassic period, it is very difficult to explain how these remnant delicate structures of feldspar grains resisted the expected major mechanical compaction process that may have formed due to the burial of depth which exceeds 3000m (Figure 4-26 A and B and Figure 4-27 A and B). It is also worth mentioning that some patches of albite were observed within or replacing the altered and dissolved feldspar grains in the studied sandstones; in most samples, these albites, which were formed as part or complete replacement of feldspar still maintained the original shape of the grain. As albite commonly dissolves faster than feldspar grains (Bjorkum et al., 1990), this indicates that these patches of albite were most likely to be formed post-dating the feldspar dissolution and the dissolution of feldspar grains must have taken place in deep burial, post-dating compaction (Figure 4-27 C and D).

Thirdly, the absence of any systematic increase of kaolinite volume toward the unconformity surface indicates that most of the observed kaolinite was formed in situ and related to late diagenetic processes. This is supported by the observed delicate euhedral booklets in most samples and the high microporosity within the kaolinite crystals. No obvious vertical distribution trend of clay (kaolinite) content toward the unconformity surface was observed (as mentioned in section 4.5.2 Figure 4-18), whereas, if the creation of these kaolinites was related to an influx of meteoric waters through the Mid-Cimmerian unconformity, systematic vertical change toward the unconformity surface would be expected.

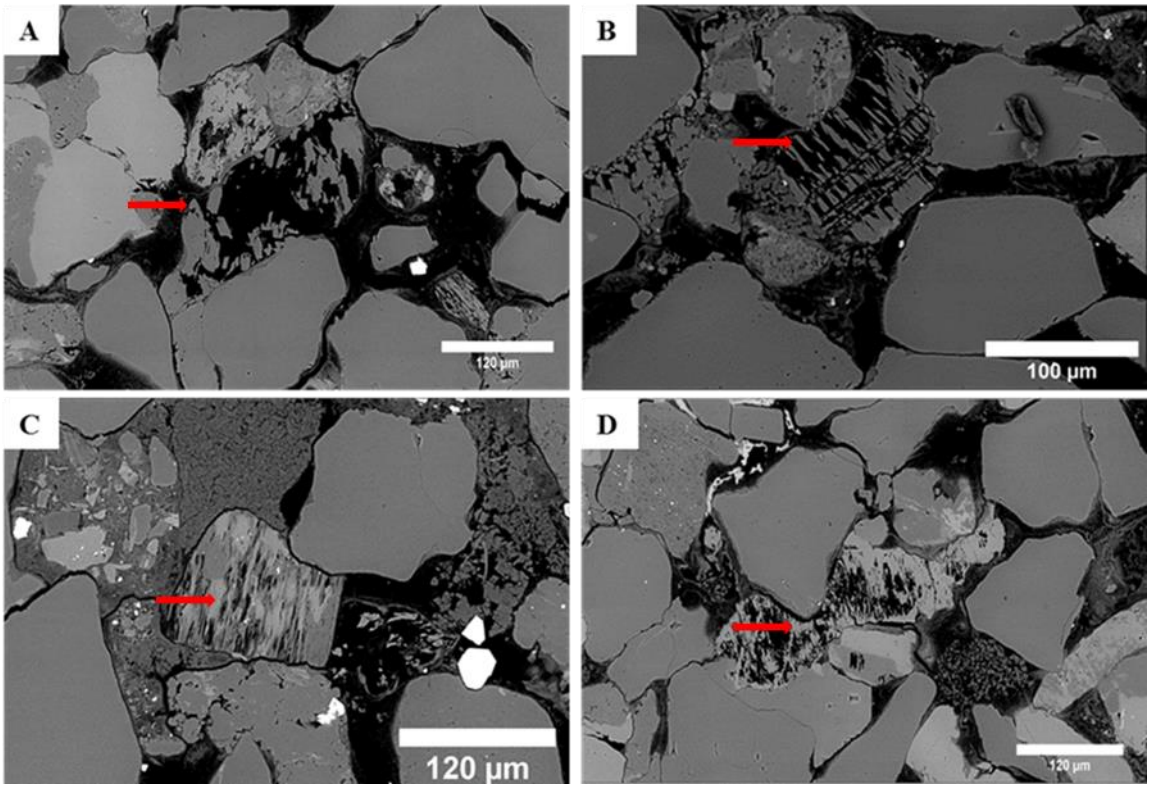

Figure 4-27. Backscattered electron images: **A** and **B**: Showing partial to complete dissolution of feldspar grains with the preservation of the shape of the feldspar grains with no compaction signs, despite the depth of more than 3300 m: Well 21/18-6, 10449.4 ft and Well 21/18-2A, 10017.5 ft respectively. **C** and **D**: Indicating authigenic albite in corroded feldspar grain associated with microporosity and indicating no signs of compaction, despite the depth of sandstone burial, which exceeds 3000 m: Well 21/18-6, 10449.4 ft.

Finally, the second and third items of evidence clearly indicate that the dissolution of feldspar grains in Kittiwake Field post-dates most of the mechanical compaction. Although characteristics of the compaction state (such as bending of mica grains, squeezed clay cement between grains, grain contact dissolution with sutured contacts and grain fracturing) were observed in many samples, SEM images and thin-section samples of the Skagerrak Formation sandstones revealed the presence of oversized secondary pores, which are associated with in situ diagenetic kaolinite. These secondary pores, which were approximately the same size as the surrounding framework grains and generated as a result of feldspar dissolution did not show any signs of compaction, despite the great depth of burial. The presence of characteristics of the compaction state and uncompacted pores and highly microporous kaolinite within the same field of view within

one sample (Figure 4-28) indicates that the dissolution of feldspar grains and the formation of kaolinite were most likely to have occurred in the late stages, after the end of most of the mechanical compaction, and, therefore, it was not related to the creation of the Mid-Cimmerian Unconformity in the top of the Skagerrak sandstones.

It could, of course, be argued that the observed compaction signs may have been formed as a result of a compaction process that may have occurred before the creation of the unconformity surface. This hypothesis can be disproved by the knowledge that the maximum thickness of deposition above the Skagerrak Formation, which was deposited in the Early and Mid-Jurassic period and eroded later on by the Mid-Cimmerian Unconformity, does not exceed a hundred metres in the best cases. This thickness of the sediments would not cause the observed signs of compaction and, possibly, only the initial phase of compaction would take place.

On the other hand, it is possible that the abundance of quartz cement may cause compaction resistance, therefore preserving the partial and completely dissolved feldspar grains that may have formed the oversized secondary pores. However, an abundance of quartz cement rarely forms in a depth range of 1.5 - 2 km (Dillon et al., 2004). This was supported by many studies which suggested that quartz cementation commonly precipitates in deep burial and in temperatures above 70–80° C, (e.g. (Aplin et al., 1993) and (Harwood et al., 2013).

In the area of study, this could not be the case, if the feldspar grains were dissolved during the creation of the unconformity surface, which was at a much shallower depth. In addition to that no abundant of quartz overgrowths have been observed in the studied well. Another possibility is that fluid overpressure may cause compaction resistance, downhole pressure data (from the repeat formation tester (RFT)) for the four studied wells which shows the pressure gradients in both formations within the Kittiwake Field are available from the CDA released by UK Government.

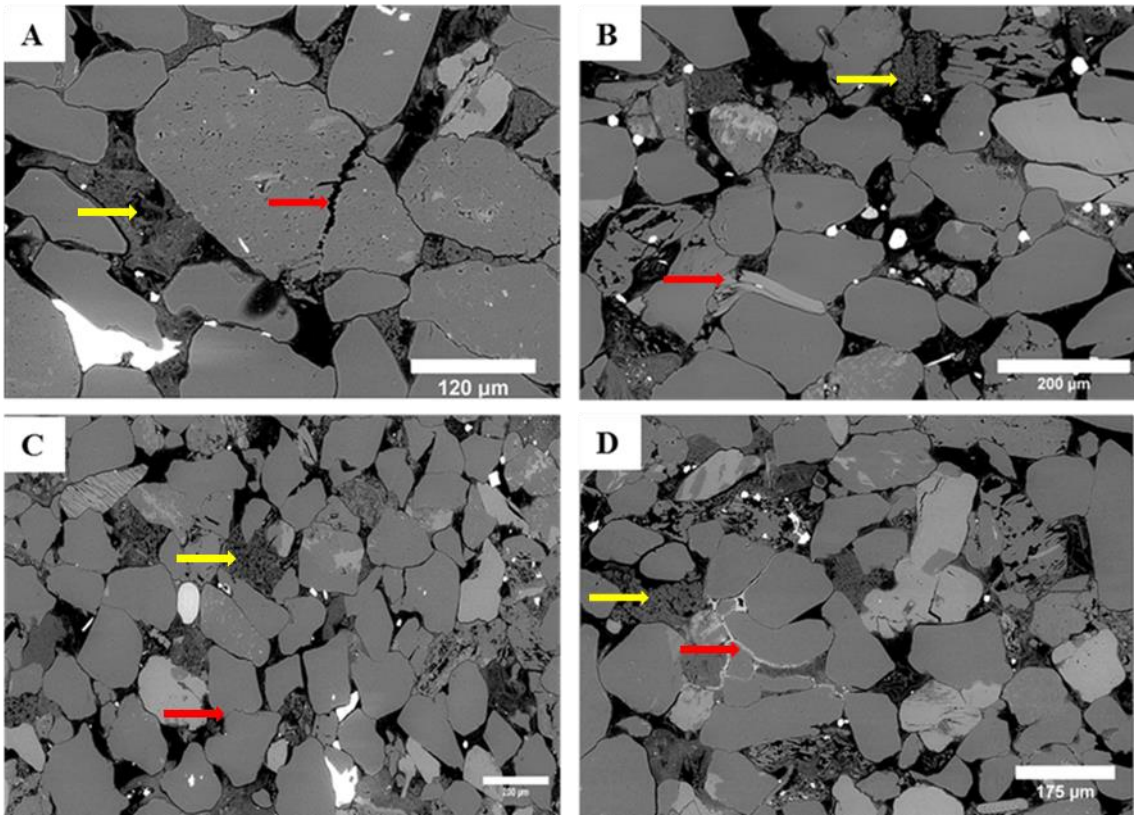

Figure 4-28. Backscattered electron images: A, B, C and D: Showing characteristics of compaction state (red arrows) (such as bending of mica grains, squeezed clay cement between grains, grain contact dissolution with sutured contacts and grain fracturing) and uncompacted pores and highly microporous kaolinite within the same field of view of one sample (yellow arrows) .

In the four studied wells, the Fulmar Formation lies directly on the Skagerrak Formation and both formations are sandstones with no fluid barrier; the overall RFT data indicates similar pressure and fluid communication throughout the field. This may indicate that the two formations may have developed overpressure at same time. The published model for the Fulmar Formation overpressure suggests that the overpressure was most likely to have been developed at burial depth of 3 km (Wilkinson et al., 2014). This means the development of overpressure occurred after the creation of the Mid-Cimmerian Unconformity and therefore any expected diagenetic change related to this unconformity surface should not have been resisted or inhibited by this late development of overpressure. Moreover, according to (Stricker and Jones, 2016) there would be almost no effect on compaction if overpressure occurred at depths greater than 2500 mbsf, and, again, this would not be the case if the feldspar grains were dissolved during the creation of the unconformity surface in the area of study, which was at a much shallower depth.

Therefore, it seems that whether compaction was resisted by an abundant quartz overgrowth or by the development of overpressure, the dissolution of feldspar grains and creation of secondary pores, which in many cases were associated with booklets of the highly microporous in-situ kaolinite within the Skagerrak Formation Sandstones were unlikely to have been formed as a result of the influx of meteoric waters through the Mid-Cimmerian Unconformity and most likely to have been formed at a burial depth of not less than 2 km.

Additionally, uplifted and exposed sedimentary rocks that have been subjected to meteoric waters are usually prone to erosion as well, and the rate of this erosion depends on many factors, for example, the properties of the exposed material, topography and climate of the area. Therefore, it is important to bear in mind that the expected effect of meteoric water on the exposed sedimentary rocks will be only preserved if the rate of erosion was less than the rate of meteoric water penetration and alteration, otherwise, any diagenetic effect of these waters (e.g. dissolution or kaolinitization of minerals) on sedimentary rock will be eroded and is unlikely to be seen (Bjorkum et al., 1990). Hence, it is possible that the rate of erosion of the Skagerrak sandstones underlying the Mid-Cimmerian Unconformity was higher than the rate of meteoric water penetration and, therefore, there was no relationship between the observed diagenesis products and the formation of the Mid-Cimmerian Unconformity.

4.6.2.3 Third scenario: The influx of acidic component produced by thermal maturation of organic matter or by addition of CO_2 that may form as a result of thermal maturation of organic matter

This scenario attributes the dissolution of unstable minerals (mainly feldspars) to the influx of organic acids that may have been produced by thermal maturation of organic matter and/or by the Carbon Dioxide (CO_2) that may form as a result of thermal maturation of organic matter. The hypothesis that organic acids and carbon dioxide released as a result of thermal maturation of source rocks may have had significant influence on sedimentary rocks has been mentioned by many authors (Bjorlykke and Aagaard, 1992). According to (Burley, 1986), dissolution of grains and precipitation of kaolinite in the Tartan and Piper fields of the North Sea was been mainly generated as a result of the generation and migration of organic acids before the maturation and

production of hydrocarbons. He also assumed that acidic pore fluid may migrate upwards for long vertical distances, up to 1000m, before reaching the potential reservoir. However, some doubts about this hypothesis have been raised by other researchers: for example, based on mass balance calculations (Giles and Marshall, 1986) found that the generated amount of the organic acids is insufficient to cause the observed leaching and dissolution of framework grains and cements in sedimentary rocks. The source rocks are also surrounded by carbonate and feldspar minerals that may react with the generated acidic fluids, so that the generated acidic fluids may be neutralized and lose their corrosive power before reaching the potential reservoir rocks (Lundegard et al., 1984, Bjorlykke, 1984).

Bjørlykke and Aagaard, (1992) point out that there is no relation between the degree of dissolution, volume of diagenetic kaolinite and distance to the source rocks; for example Fulmar and Claymore sandstone formations, which are very close to the Kimmeridge Clay Formation, do not show high dissolution of framework grains and rarely contain diagenetic kaolinite (Bjorlykke and Aagaard, 1992). If the generation of acidic fluids from the source rock is a possible mechanism for the dissolution of feldspar grains and precipitation of kaolinite, it is difficult to explain why these two sandstone formations are not affected by this mechanism, as they are so close to the mature Kimmeridge Clay source rock in the Upper Jurassic.

On the other hand, more recent studies have indicated that the total porosity of the Fulmar formation is decreasing rapidly below the top of the sealed Kimmeridge Clay source rock, suggesting that the spatial variation of reservoir porosity is related to the Kimmeridge Clay Formation above it (Wilkinson and Haszeldine, 2011). These authors suggest that, as oil charge will take place starting from the closest sandstone of the reservoir to the top source rock, the highest porosity in Fulmar Formation was just below the seal and decreasing downward, indicating that the hydrocarbon charge from the overlying seal/source has preserved porosity in the topmost layers of the Fulmar Formation. However, another possible mechanism can be suggested for this pattern of porosity underneath the overlying mature source rocks. That is the possibility that the acidity of the generated hydrocarbons was very high and affected the surrounding Fulmar Formation to cause grain dissolution and thus enhance the reservoir's porosity. This

scenario can also be accepted, as the acidity level of the fluid will decrease downward and become saturated with the interacting minerals with depth and time.

In the area of study, all the studied samples were taken from the Skagerrak Formation just below the Mid-Cimmerian Unconformity; the Skagerrak sandstones lie below the above Upper Jurassic Fulmar sandstone formation and are underlain by the Upper Permian thick Zechstein halite. The closest source rocks or shale to Skagerrak sandstone are the Kimmeridge Clay source rocks located in the Upper Jurassic. As mentioned above, this thick mature source rock is expected to be very mature and may produce highly acidic fluids which can interact with unstable minerals leading to the dissolution of these minerals and therefore enhancing the porosity of the reservoir below. However, it is not clear yet if this is the case for the studied Skagerrak Sandstones or not, as this source rock is separated from the studied Skagerrak sandstone by the Fulmar sandstone formation.

In addition, SEM images for the area of study have given clear evidence that the dissolution of feldspar grains post-date the majority of the mechanical compaction and/or were preserved from any further diagenetic processes. Moreover, it was clear that in many cases the increase of porosity due to feldspar grain dissolution was not associated with precipitation of reaction products (such as kaolinite, illite etc.). This may indicate that the reaction products resulting from the dissolution of grains were removed from the sandstones and transported to other places by pore fluid flow while the sandstone formation was becoming overpressured. This removal of produced products will lead to higher porosity and must have been occurring in an open system where pore fluid can migrate and remove the potential generated products. From all of these considerations, it is seems that the observed late generation of secondary porosity was preserved by the infill of hydrocarbons in highly overpressured sandstone. This secondary porosity would have occurred due to an aggressive fluid migration which was possibly generated from the Kimmeridge Clay Formation.

4.6.2.4 Fourth scenario: The release of organic acid and CO_2 that may form as a result of oil biodegradation

This scenario considers the dissolution of framework grains (particularly feldspar) to be caused by the organic acids and CO_2 that may have formed as a result of oil biodegradation. Biodegradation of oil is usually associated with the increase of hydrocarbon acidity caused by organic acids and CO_2 generation as a result of bacterial metabolism (Ehrenberg and Jakobsen, 2001). These organic acids and CO_2 can cause alteration and dissolution to some framework grains and carbonate cement in the sedimentary rocks and may form in both source rocks (mentioned above) and reservoir rocks. Oil biodegradation occurs as a result of crude oil alteration caused by living microorganisms (commonly bacteria); this will lead to generation of organic acids and CO_2 and, therefore, more acidic oil (Taylor et al., 2001). One of the most significant alteration processes in subsurface reservoirs is oil degradation (Wenger et al., 2002)

In subsurface reservoirs, most oil biodegradation processes occur within the transition zone (oil water contact), as within this area the chemical interaction of hydrocarbon with water and minerals may lead to the generation of organic acids and carbon dioxide CO_2 in the reservoir, similarly to the creation of organic acids and CO_2 from the source rocks (Head et al., 2003). An example of the effect of oil degradation on reservoir rocks is the dissolution of plagioclase and formation of kaolinite in the Gullfaks Field (Ehrenberg and Jakobsen, 2001); another example is the formation of carbonate cement in the Forth and Balmoral fields, which is assumed to be related to the oil degradation process at OWC (Watson et al., 1995).

In the area of study, the transition zone or the field OWC is assumed to be at 10430 ft TVSS, Unfortunately, none of the collected samples from the four studied wells were within the transition zone, except those from one well. However, it was interesting that this well was Well 21/18-6, which was the only well showing correlation between the dissolution of feldspar and the creation of secondary porosity toward the unconformity surface. The depth of the unconformity surface in this well was at 10415.5 ft, while the depth of OWC was expected to be at 10430 ft. It is worth noting that the previously mentioned correlation between the generated secondary porosity and the dissolution of feldspar grains toward the unconformity surface was observed only within the first 15 ft

below the unconformity surface, that is, just between the unconformity surface and the OWC. This is may indicate that, with respect to the oil biodegradation hypothesis, the dissolution of feldspar within this area can be related to the biodegradation of oil in this transition zone. Therefore, this is may explain why only Well 21/18-6 showed a correlation between the dissolution of feldspar and the creation of secondary porosity toward the unconformity surface.

4.6.3 Origin and timing of kaolinization

In Skagerrak sandstones, kaolinite was observed in all the studied wells. In most samples kaolinite was observed in association with the dissolution of feldspar filling pore spaces and in some other cases it was intermixed with other clay minerals. As mentioned before, two types of kaolinite were observed: 1- intermixed with other clay minerals (such as illite) filling pore spaces, which could be either detrital kaolinite or formed by early diagenetic processes (Figure 4-17 A); 2- in regular crystals stacked in "booklets" or vermicular habit and filling pore spaces (Figure 4-17 B and C). The latter which were commonly recognised as a microporous mass of blocky kaolinite within pore spaces, were most likely to have been formed as result of feldspar alteration and dissolution and usually appeared with hint of the grain outline (Figure 4-17 D).

Although, most of the observed kaolinite within the Skagerrak sandstones was interpreted to have been formed as a result of alteration and replacement of feldspar grains, the increase in the amount of kaolinite was not associated with a decrease in feldspar content in all the studied wells, with the exception of Well 21/18-6, which showed some correlation (Figure 4-19). This overall lack of correlation between feldspar content, which is expected to be most common source of silica and aluminium for precipitation of kaolinite, and kaolinite content in Skagerrak sandstones can be related to: 1- initial variability of the amount of feldspar, 2- Alteration and kaolinitization of other minerals such as micas and silicate rock fragments, and 3- the presence of other sources of silicate minerals from outside the Skagerrak sandstones (such as fluid flow with high silica content).

Although two types of kaolinite were observed in the area of study, backscattered images (BSE images) of polished sections showed that most of the kaolinite present was formed in situ and related to late diagenetic processes. Most of the evidence supported this hypothesis, including:

1. The vermicular textures and delicate euhedral booklets observed in most samples.
2. The growths of kaolinite between the pre-existing sheets of mica
3. Most studied samples of Skagerrak sandstone formations showed oversized secondary pores containing kaolinite; the generated kaolinite within these pores in most of the studied samples was associated with high microporosity and showed no signs of compaction, despite the great depth of burial which exceeds 3000m.
4. The absence of a systematic increase of kaolinite volume toward the unconformity surface. Although much of the evidence indicates that most of the observed kaolinite was formed in situ, no obvious vertical distribution trend of clay (kaolinite) content toward the unconformity surface was observed (Figure 4-18). However, if the creation of these kaolinites was related to the influx of meteoric waters through the Mid-Cimmerian unconformity, systematic vertical change toward the unconformity surface would be expected and it is difficult to explain why amount of kaolinite does not increase toward the unconformity surface. Furthermore, in many cases the opposite result was determined: for example, SEM images from Well 21/18-4 show that amount of in situ diagenetic kaolinite in sample 19/b2 at depth 10714.5 ft, which lies about 15 ft from the unconformity surface, was higher than the amount of kaolinite in sample 15/b2 at a depth of 10698.75 ft, which was lying immediately below the unconformity surface, and again, if the formation of kaolinite was related to the creation of the Mid-Cimmerian Unconformity the opposite pattern would be expected.

All this evidence contradicts the possibility that the alteration and replacement of feldspar grains and creation of kaolinite in the Skagerrak Formation to be due to the influx of meteoric water shortly after the deposition of Skagerrak sandstone sediments or during the creation of the Mid-Cimmerian Unconformity. Therefore, it seems that the observed kaolinite in the studied Skagerrak sandstone, which formed as a result of feldspar dissolution and replacement, was most likely to be formed as a result of late diagenetic processes at the same time as feldspar dissolution and most likely occurred due to an aggressive fluid attack.

4.7 Conclusion

Petrographic analysis of more than forty sandstone thin-sections from four wells in the Skagerrak Formation in the Kittiwake Field of the North Sea indicated that the secondary porosity was most likely to have been formed by the post-depositional dissolution of silicate minerals (particularly feldspar). Petrographic observations showed several pieces of evidence for this dissolution of minerals, including the oversized pores, partial and complete dissolution of detrital grains and corroded grain margins. Significant amounts of feldspar grains had been dissolved from the Skagerrak Formation; this dissolution was recognised in most of the analysed samples within the area of study and was the main cause of the creation of secondary porosity. SEM images of polished thin-sections for the area of study provided clear evidence that the dissolution of feldspar grains post-dated most of the mechanical compaction and/or were preserved from any further diagenesis process. This evidence includes: 1- the vermicular textures and delicate euhedral kaolinite booklets observed in most samples, despite depths greater than 3300 m; 2- the growth of kaolinite between the pre-existing sheets of mica and 3- oversized secondary pores containing kaolinite; the generated kaolinite within these pores was associated with high microporosity and showed no signs of compaction, despite the great depth of burial. Therefore, most of petrographic evidence demonstrates late dissolution of feldspar grains and that most of the created and enhanced secondary porosity was related to this dissolution of feldspar grains. However, the issue at hand was to detect the main cause of this dissolution and to see if it is related to the presence of the Mid-Cimmerian Unconformity on the top of Skagerrak formation in Kittiwake Field or not. The influx of meteoric waters during the formation of the Mid-Cimmerian Unconformity was considered. However, after the analysis of the collected samples, there are several lines of evidence suggesting that this hypothesis is not viable and that the dissolution and creation of secondary pores is not related to the unconformity surface. This evidence includes:

1- The absence of a systematic decrease of feldspar volume and increase of secondary porosity toward the unconformity surface.

2- The presence of delicate structures of feldspar grains with no signs of compaction: if the dissolution of these grain was related to the influx of waters from the Mid-Cimmerian Unconformity during the Early to Mid-Jurassic period, it is very difficult

to explain how these dissolution remnants of feldspar grains resisted the expected major mechanical compaction forces that may have occurred due to the burial depth, which exceeds 3000m.

3- The absence of a systematic increase in kaolinite volume toward the unconformity surface. Although most of the observed kaolinite was formed in situ and related to late diagenetic process, no obvious vertical distribution trend of clay (kaolinite) content toward the unconformity surface was observed. However, if the creation of this kaolinite was related to the influx of meteoric waters through the Mid-Cimmerian unconformity, systematic vertical change toward the unconformity surface would be expected.

Based on this and since all the signs indicate that the dissolution of feldspar grains occurred at a late stage and post-dated most of the mechanical compaction, this clearly suggests that there is no relationship between the formation of the Mid-Cimmerian Unconformity on top of Skagerrak Sandstones and the enhancement of secondary porosity underneath. Therefore, it can be concluded that the late dissolution of the feldspar grains and the generation of secondary porosity are most likely to be related to highly acidic fluids that may have been generated either:

1- Within the source rock and transported to the studied sandstones to interact with the reservoir minerals, thus generating the late secondary pores while the reservoir was highly overpressured: this aggressive fluid had possibly migrated from the nearby Kimmeridge Clay Formation.

2- Within the reservoir as a result of oil biodegradation in the transition zone. More studies are required to confirm which one of these hypothesis is the main cause for this change of the reservoir characteristics.

Chapter 5 Case Study 2: The role of the Base-Cretaceous Unconformity in the distribution of porosity and kaolinite in Brent Group sandstones of the Tampen Spur area, Northern North Sea

5.1 The Base-Cretaceous Unconformity

The Jurassic – Cretaceous synrift sediments in the North Sea are separated from the postrift sediments by the Base-Cretaceous Unconformity (otherwise called the Late Cimmerian Unconformity). The unconformity is an easily identifiable surface in wireline logs and seismic reflection data and has a distinct character and is classified as the most important regional marker in the North Sea area (Figure 5-1). Therefore, it has been used as reference horizon to map and/or correlate the main structures of the Norwegian part of the North Sea. The unconformity was formed as a result of several local and/or regional processes associated with the transition of the Northern North Sea from synrift to postrift phase of the Jurassic–Cretaceous sequences (Kyrkjebø et al., 2004).

The unconformity displays a significant variability at both local and regional scale, with variation in the geometry of the sediment layers and stratigraphic units below and above the unconformity. The variation in the characteristics of this unconformity is not just regional: its variation has been observed even within one basin. This variation may be related to different factors, including the geometry of the basin, the geographical position of the unconformity within this basin, the presence of faults and the variation of heat flow (Kyrkjebø et al., 2004). Therefore, the Base-Cretaceous Unconformity has been classified as disconformity in some basins and as an angular unconformity in others, based on the structure position of the unconformity within each basin.

In the Tampen Spur area, the Base-Cretaceous Unconformity has been classified as an angular unconformity, in most cases. However, some local variation was observed as well; this could be related to the rotation of fault blocks, erosion and/or sediment supply. The duration of this unconformity hiatus varies from 4 Ma to a maximum of 100 Ma, recorded in the Tampen Spur area, particularly in the studied Gullfaks Field separating the Upper Cretaceous sediments from the Middle Jurassic sediments of the Brent Group,

with the exception of some locations where up to 100 m of the Upper Jurassic Heather Formation was locally preserved (Horstad et al., 1995).

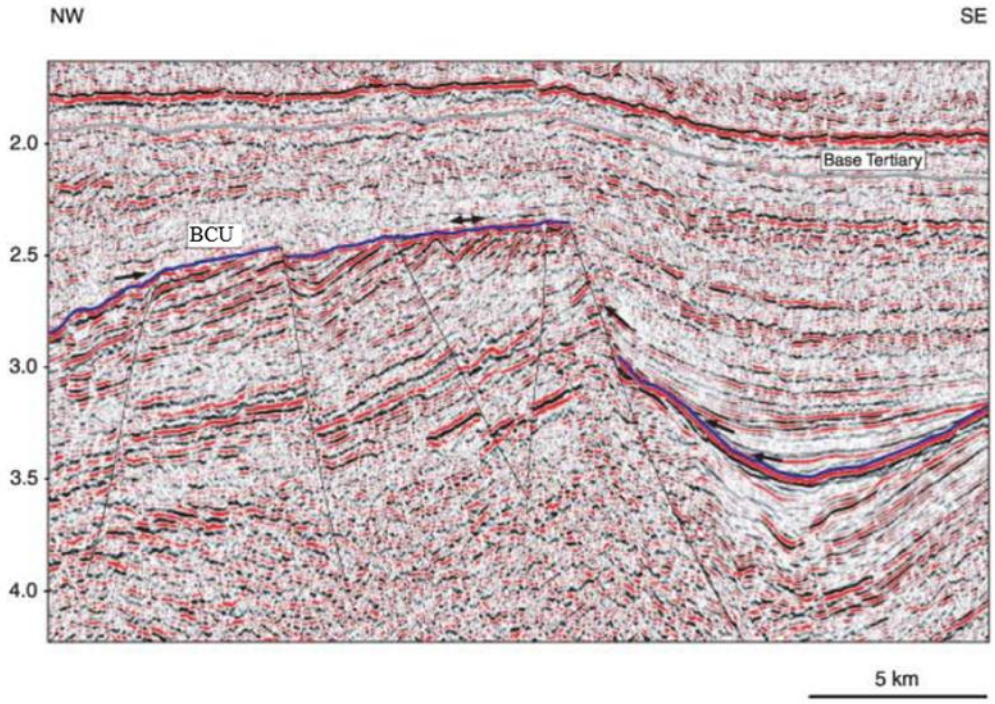

Figure 5-1. Seismic reflection data for the Base-Cretaceous Unconformity (blue) in the top of rotated fault block of Snorre Field (Kyrkjebø et al., 2004).

5.2 Introduction to the Tampen Spur area

The Tampen Spur area is located in the northern section of the Norwegian North Sea, it lies between the Viking Graben and East Shetland (Figure 5-2). The Tampen Spur area has a series of oil and gas fields with various reservoir depths ranging from less than 2 km to more than 4 km depths and with different types of hydrocarbons ranging from light alkaline crude oil to biodegraded oil (Figure 5-3). Some of the largest of these fields are the Statfjord Field, the Gullfaks Field and the Snorre Field. The Statfjord Field is one of the largest oilfields in the area and contains three main reservoirs: the Brent Group, the Cook Formation and the Statfjord Formation (Spencer et al., 1987). In the Gullfaks Field, which was discovered in 1978, the main reservoir units are within the Brent Group, which contain about 80% of the reserves. The Snorre Field was discovered in 1979 and is located in the north of the Tampen Spur area. In addition to these three fields, smaller fields have been discovered in the area, e.g. the Vigdis, Statfjord Ost, Statfjord Nord, Tordis and

Gullfaks Vest fields. The Tampen Spur area is a highly structured area and is surrounded by several mature source rocks in downfaulted blocks; therefore, many of the fields in this area which are lying adjacent to these source rocks may be filled from multiple directions (Horstad et al., 1995).

As the main target of this study is to examine the possible diagenetic effect of unconformities on the sediments underneath, the study has focused only on the Middle Jurassic Brent Group sediments which lie below the Base-Cretaceous Unconformity (BCU). A number of wells within the Tampen Spur area which include Brent Group sediments have been chosen for this study; most of these wells are particularly within the Gullfaks Field, as it is the most positive structural element in the Tampen Spur area (Bjørkum et al., 1990). However, other wells located in surrounding fields are studied as well, such as the Snorre Field, Vigdis Field, Statfjord Nord Field and Gullfaks Vest Field.

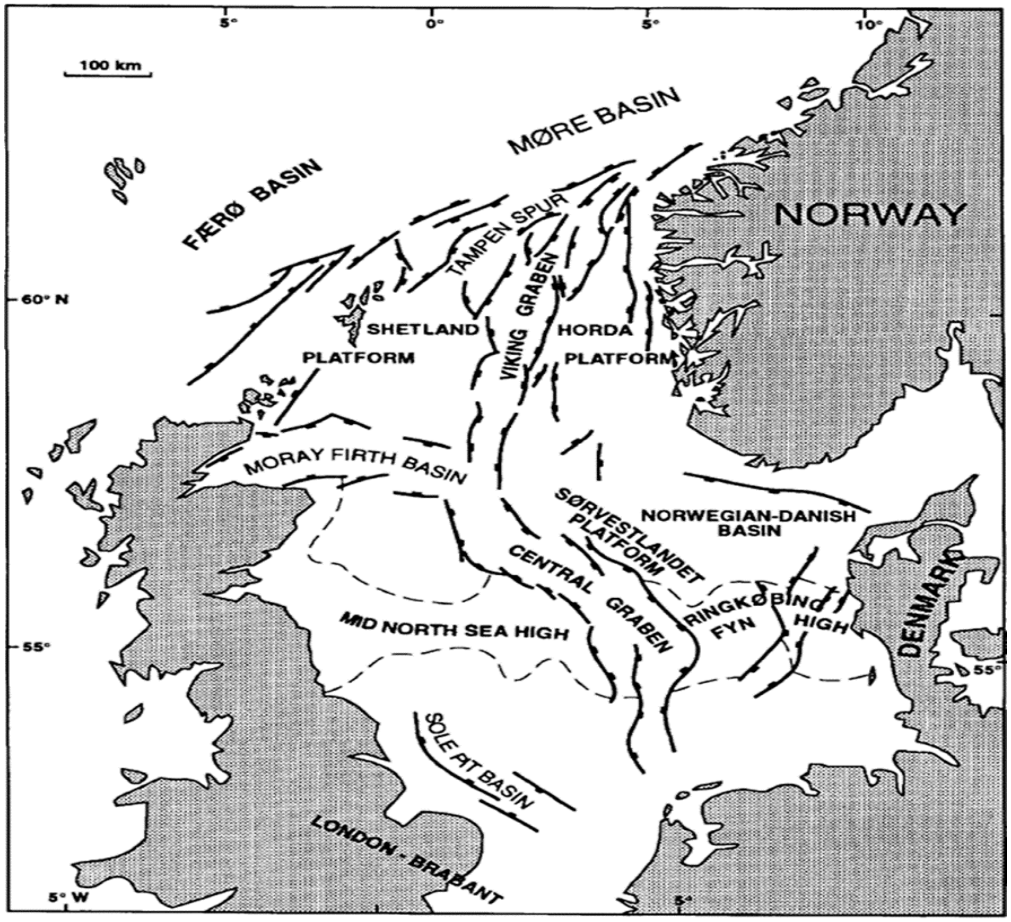

Figure 5-2 Location map of the Tampen Spur area in the North Sea (Horstad et al., 1995).

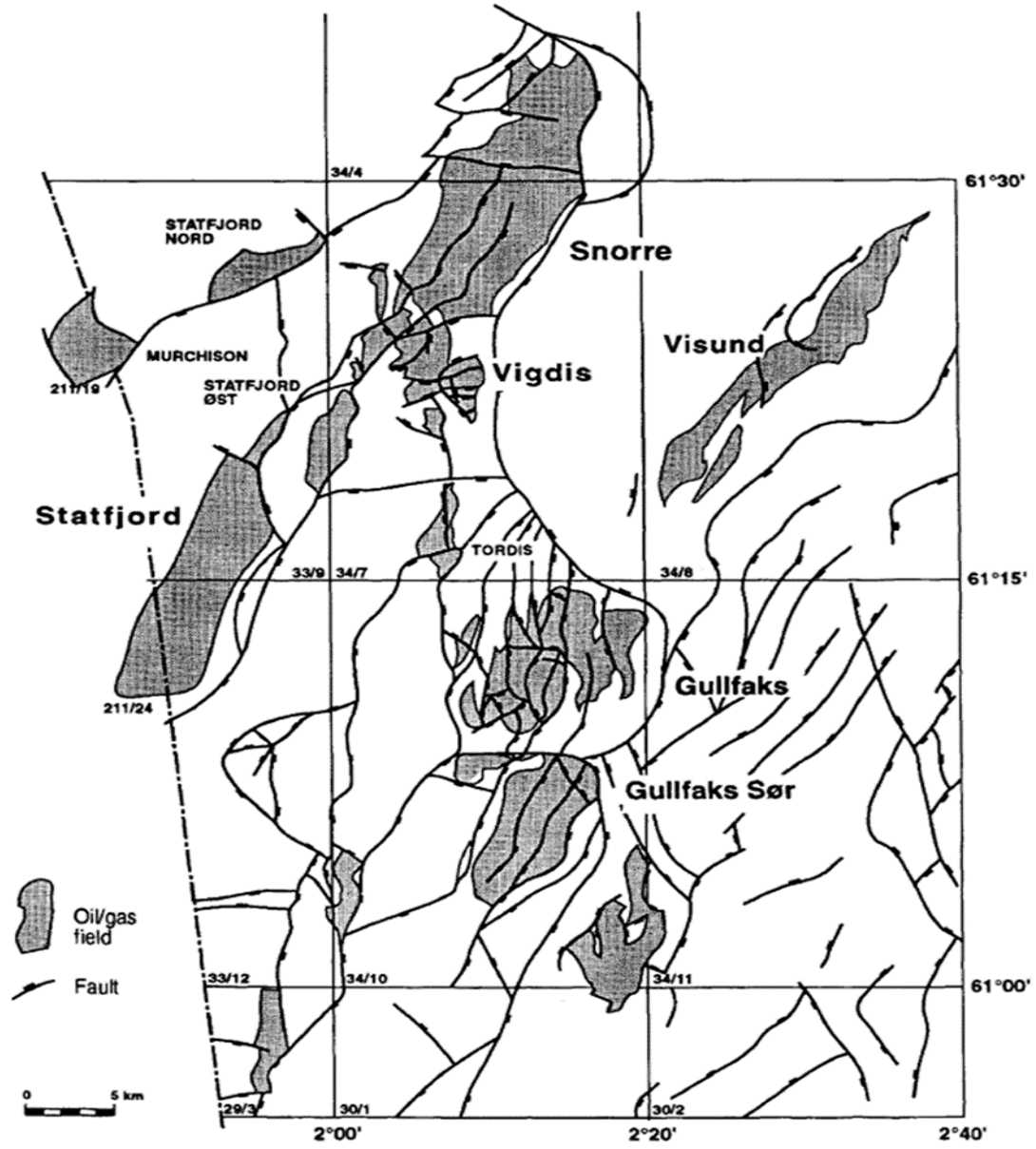

Figure 5-3 Giant fields in the Tampen Spur area (Horstad et al., 1995).

5.3 Stratigraphy of the Brent Group in Tampen Spur area

The Brent Group represents more than 200 m thickness of deltaic sediments and ranges in age from Aalenian to Bathonian. The group spreads across the North Sea over 200 km from the south to the north. The main sources of these clastic materials are believed to be related to the uplift of the Late Triassic to Mid Jurassic of the Mid North Sea High in the Central North Sea (Eschard et al., 1993). In the Tampen Spur area, the Brent Group is deposited unconformably above the Drake Formation of the Dunlin Group and sealed by the Heather Formation. The Brent Group is interpreted as deltaic and shallow marine

deposits and it has been divided into five different formations: the Broom, Rannoch, Etive, Ness and Tarbert formations (Figure 5-4). These formations are variable in their lithology, thickness and reservoir characteristics (Harwood et al., 2013).

5.3.1 Broom Formation

In the Tampen Spur area, the Broom Formation contains mudstone with thin layers of sandstone and is interpreted to be formed in an open marine environment during a transgressive event. For instance, in the Gullfaks Field, the Broom Formation consists mainly of 5-15 m of mudstone or shale interbedded with thin layers of sandstone. The thin layers of sandstone are usually cemented and have limited connection with the overlying Rannoch Sandstone.

5.3.2 Rannoch Formation

The Rannoch Formation lies between the Broom Formation below and the overlying Etive Formation and is interpreted to have been deposited in a shoreface environment and consists of fine-grained sandstones. In the southern part of the Tampen Spur, such as in the Gullfaks Field, the Rannoch Formation ranges in thickness from 50 to 90 m and is considered to be coarsening and shallowing upward from an offshore to upper shoreface environment, whereas in the northern part of the study area the Rannoch Formation grades laterally to offshore shale. The formation can be subdivided into three units, designated R1, R2 and R3 (Ehrenberg and Jakobsen, 2001). The lower unit, R1, contains less mud and is clearly coursing upward; sediments in this unit usually show bioturbation, hummocky cross-stratification and small-scale ripples, with the presence of laterally extensive carbonate cemented layers. The two overlying units, R2 and R3, are fine to medium grain sized sandstones and are considered to be good to very good reservoir sandstones; they also have some sedimentary structures, such as hummocky cross-stratification and small-scale ripples with the presence of some carbonate cemented layers (Petterson et al., 1990).

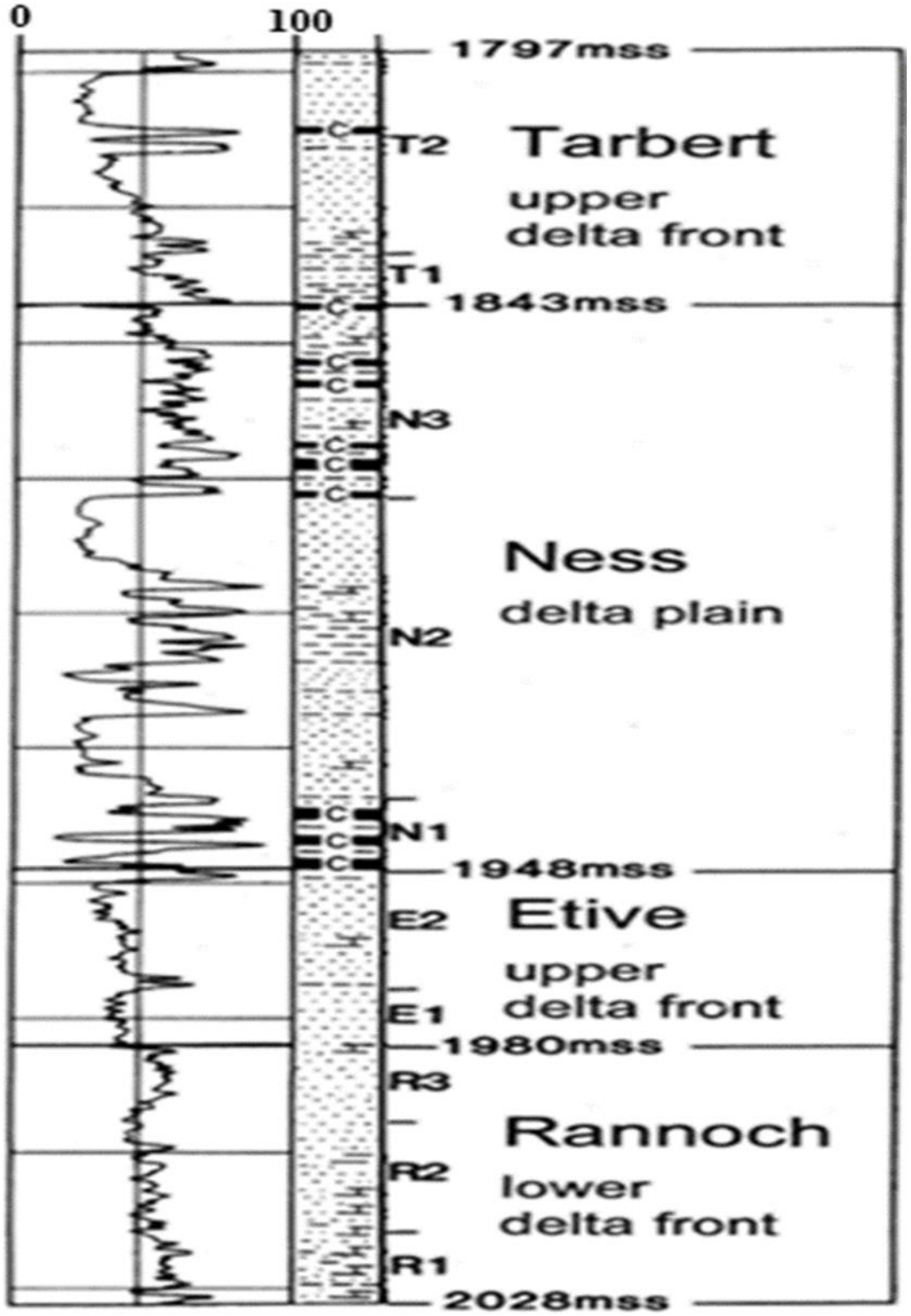

Figure 5-4. The stratigraphy of the Brent Group as represented by Well 34/10-8 in the Gullfaks Field. (C = coal beds). Modified from (Ehrenberg and Jakobsen, 2001).

5.3.3 Etive Formation

The Etive Formation, which lies between the underlying Rannoch Formation and the Ness Formation above, usually comprises medium- to coarse-grained sandstones with possible thickness ranging from 15-40 m. The formation represents a complex depositional environment of high energy beach environment and has been described as having excellent reservoir quality.

5.3.4 Ness Formation

The Ness Formation, which lies above the Rannoch Formation, consists mainly of interbedded shale, siltstone, coals and sandstone; the sandstone is usually fine to coarse grained in size, deposited in coastal plain or delta plain environments (Harwood et al., 2013). In the Gullfaks Field, the Ness Formation reaches a thickness of 85-110 m and is subdivided into three units. Unit 1 represents the lower part of Ness Formation and comprises interbedded mudstone, coals and sandstone; the sandstone channels may communicate locally with the Etive Formation sandstones underneath. Unit 2 is dominated by a number of upward coarsening sandstone layers, indicating good reservoir quality. Unit 3 represents the top of the Ness Formation and the end of progradation of the Brent delta in the area of the Gullfaks Field; it consists mainly of claystone and coals, but in some cases sandstones are present.

5.3.5 Tarbert Formation

The Tarbert Formation marks the top formation of the Middle Jurassic Brent Group and consists of fine- to coarse-grained sandstones interbedded with coals and mudstones. These sediments are suggested to have been deposited in complex depositional environments and can be shoreface, offshore or coastal plain environments (Glennie, 2009). In the Tampen Spur area, the Tarbert Formation is represented by alternate coarsening and upward shallowing coastal layers and changes toward the north into deep marine sediments which mark the start of the Heather Formation.

- The Heather Formation may occur lying conformably or unconformably above the Brent Group, depending on the tilted block arrangement. It consists mainly of mudstones formed in offshore environments. In the area of study, the base of the

Heather Formation is in contact with the top of the Tarbert Formation. However, in many cases the Base-Cretaceous Unconformity (BCU) has eroded the Heather Formation and separated the Brent Group from the overlying sediments.

5.4 Sedimentological analysis

11 wells from the Tampen Spur area in the Northern North Sea were studied; however, only 9 of them are described in detail in this study. All the selected wells for this study cross the Base-Cretaceous Unconformity. Most of these wells are particularly from Gullfaks Field, as it is the most positive structural element in the area of study, but other wells located in neighbouring fields such as the Snorre Field, Vigdis Field, Statfjord Nord Field and Gullfaks Vest Field are also included. Sedimentological core description was performed for the 9 selected wells detailing the observations of sediment details and interpretation of facies.

The following section presents the results of sedimentological description that was performed for more than 608 m of core length from the selected wells.

5.4.1 Sedimentological analysis results

Full sedimentolgical core descriptions were performed for the 9 studied wells (Figure 5-5, Figure 5-6, Figure 5-7, Figure 5-8, Figure 5-9, Figure 5-10, Figure 5-11, Figure 5-12 and Figure 5-13). As the main target of this study is to investigate the possible diagenetic effect of the Base-Cretaceous Unconformity on the sediments underneath, the study has focused only on the Brent Group sediments that lie below this unconformity. The 9 studied wells have similar facies and consist mainly of one or more of the five different formations of the Brent Group: the Broom, Rannoch, Etive, Ness and/or Tarbert Formations. In most of the studied wells, the Base-Cretaceous Unconformity were observed separating one or more of these formations from the overlying sediments. This study concentrated only on the formations which have been sampled (Rannoch, Etive and Tarbert).

Rannoch Formation

This formation marks the second, lower, formation within the Brent Group sandstones, it has appeared in three of the 9 studied wells, Well 34/10-1 and Well 34/10-4 located in the Gullfaks Field and in Well 33/09-13 in the nearby Statfjord Nord Field. In the three wells, the cored Rannoch interval consists mainly of very fine to fine-grained sandstones. Some sedimentary structures such as cross-bedding, lamination and bioturbation of the sandstone have been observed in some parts of the Rannoch Formation, especially in the lower part of the formation. Erosion boundaries have been recognised frequently, with the presence of carbonate cemented layers within the cored interval, Especially in Well 33/9-13. The whole interval is considered to have been deposited in delta environments.

Etive Formation

This formation appears in two of the studied wells, Well 34/10-1 in the Gullfaks Field and Well 34/7-16 in the Vigdis field in the North of the studied area. In the two wells, the cored Etive interval consists mainly of homogeneous medium to coarse-grained sandstones, with the exception of Well 34/10-16, which is interrupted by a one metre thick band of shale in middle of the interval at depth 2409 m. The sandstones are brown to grey, oil stained, and poorly to well cemented. Sedimentary structures are very rare in the Etive Formation.

Tarbert Formation

This formation, which marks the top formation of the Brent Group, was encountered in six of the studied wells, Well 34/10-1 and Well 34/10-8 in Gullafaks Field, Well 34/10-34 in the nearby Gullfaks Vest Field, Well 34/7-20 in the Snorre Field, Well 34/7-19 in the Vigdis Field and finally in Well 30/6-10A in the Oseberg Field. In Wells 34/10-1, 34/10-8 and 34/10-34, the Tarbert Formation consists mainly of sandstones with thin layers of shale and/or coal, especially in the lower part of Well 34/10-34. The sandstones are dark grey to brown, fine- to medium-grained sandstones and occasionally coarse particularly, in Well 34/10-1, whereas in Wells 34/7-20 and 34/7-19, the Tarbert Formation consists mainly of very fine-grained sandstones, light to dark grey in colour. In Well 34/7-19, some sedimentary structures such as lamination and bioturbation of sandstone have been observed.

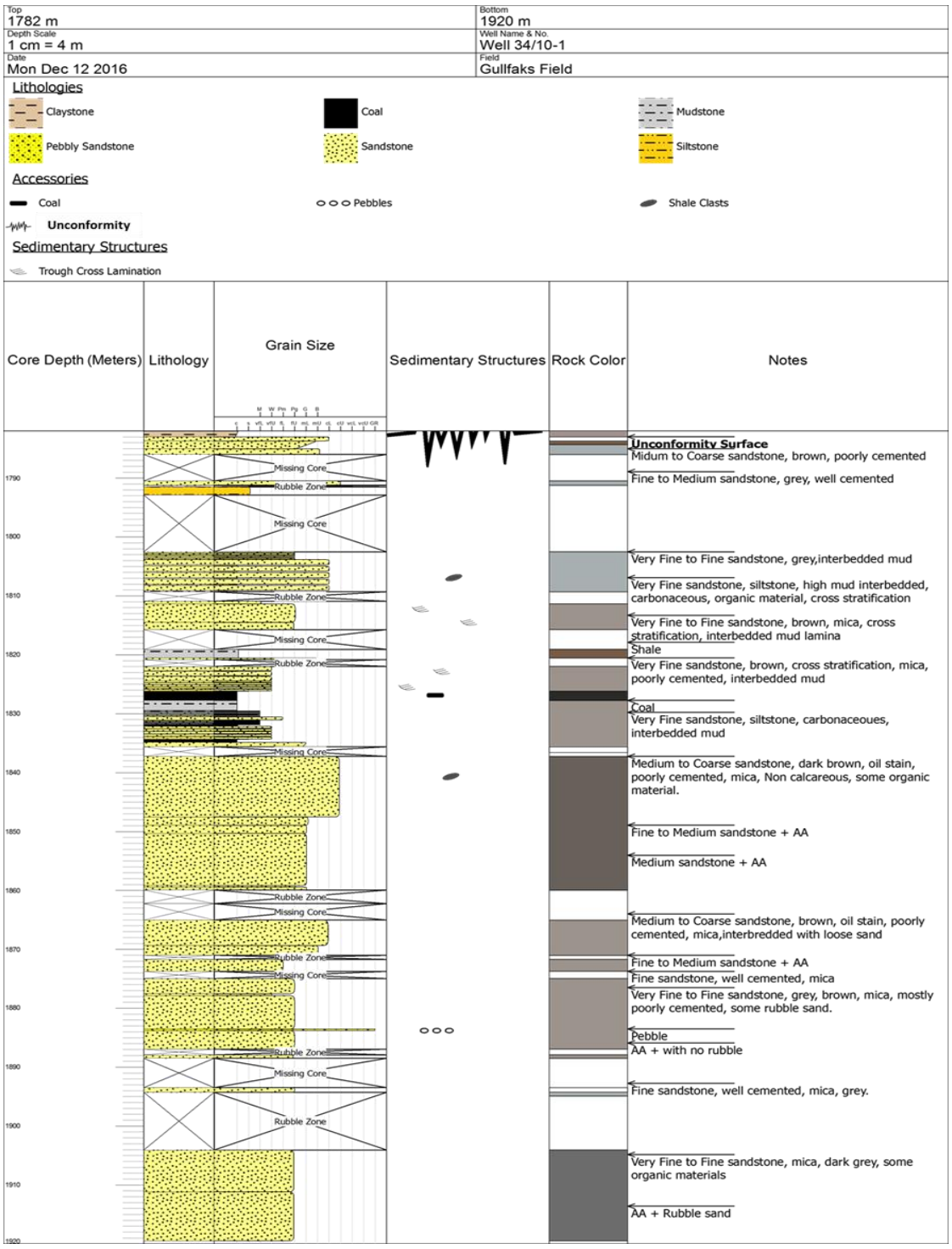

Figure 5-5. Sedimentological core descriptions of the Tarbert, Ness, Etive and Rannoch Formations in Well 34/10-1 in the Gullfaks Field. The Base-Cretaceous Unconformity is recognised at a depth of 1783 m, just above the top of the Tarbert Formation and separating these formations from the Upper Cretaceous Shetland Group.

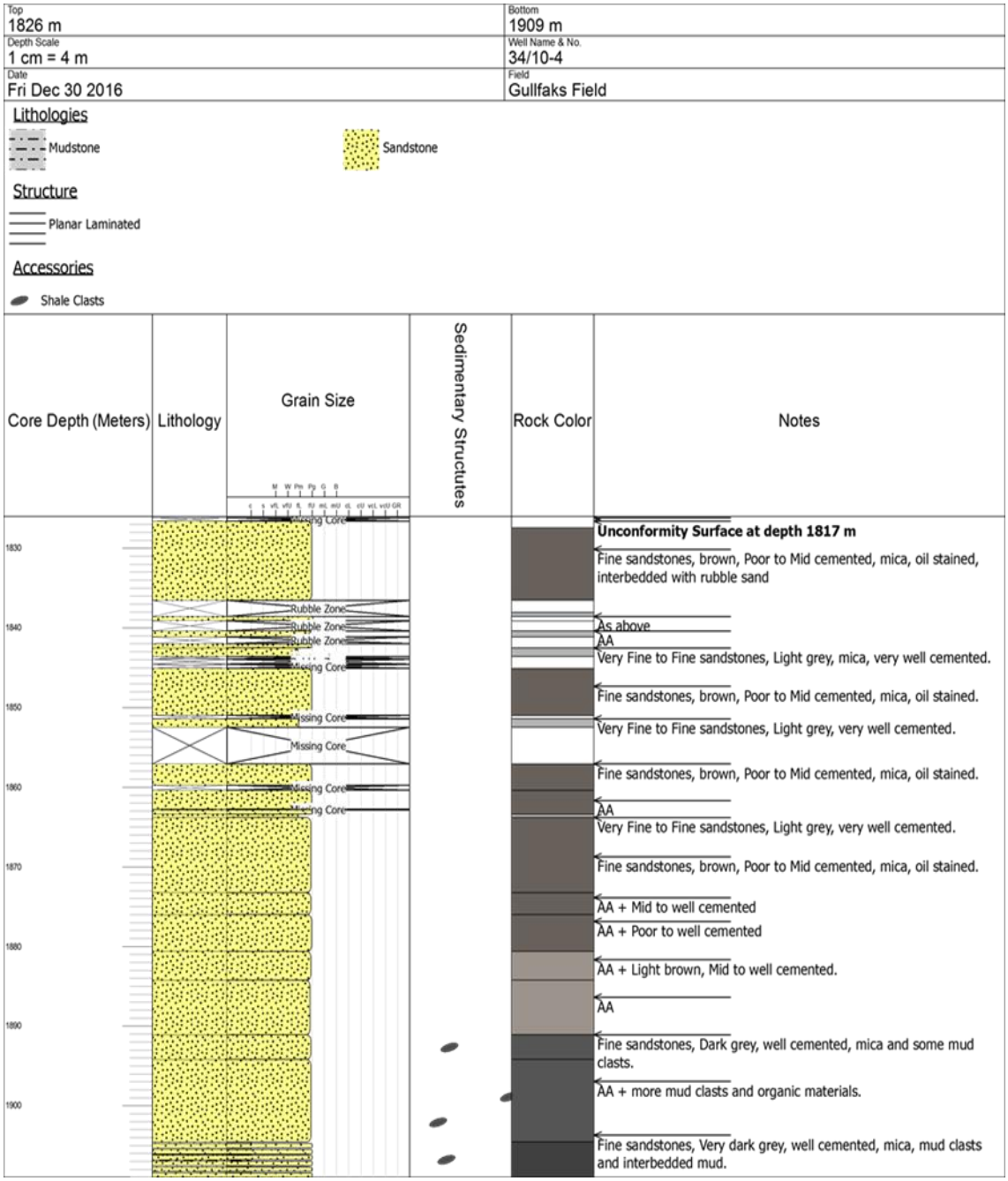

Figure 5-6. Sedimentological core descriptions of the Rannoch Formation in Well 34/10-4 in the Gullfaks Field. The Base-Cretaceous Unconformity is recognised at a depth of 1817 m, directly above the top of Rannoch Formation, separating the Rannoch Formation from the Upper Cretaceous Shetland Group.

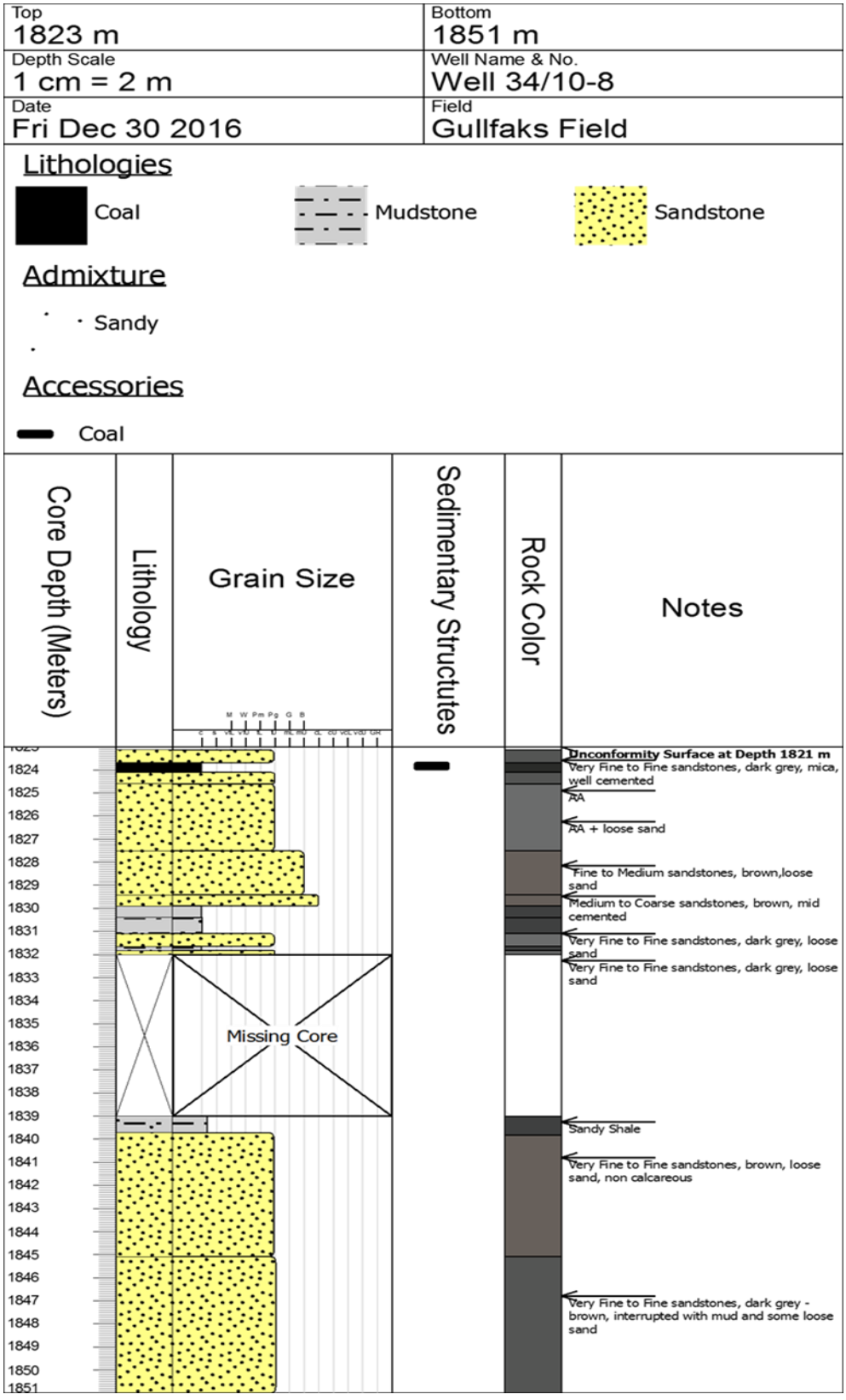

Figure 5-7. Sedimentological core descriptions of the Tarbert Formation in Well 34/10-8 in the Gullfaks Field. The Base-Cretaceous Unconformity is recognised at a depth of 1821 m, about 2 metres above the top of Tarbert Formation, separating the Tarbert Formations from the Upper Cretaceous Shetland Group.

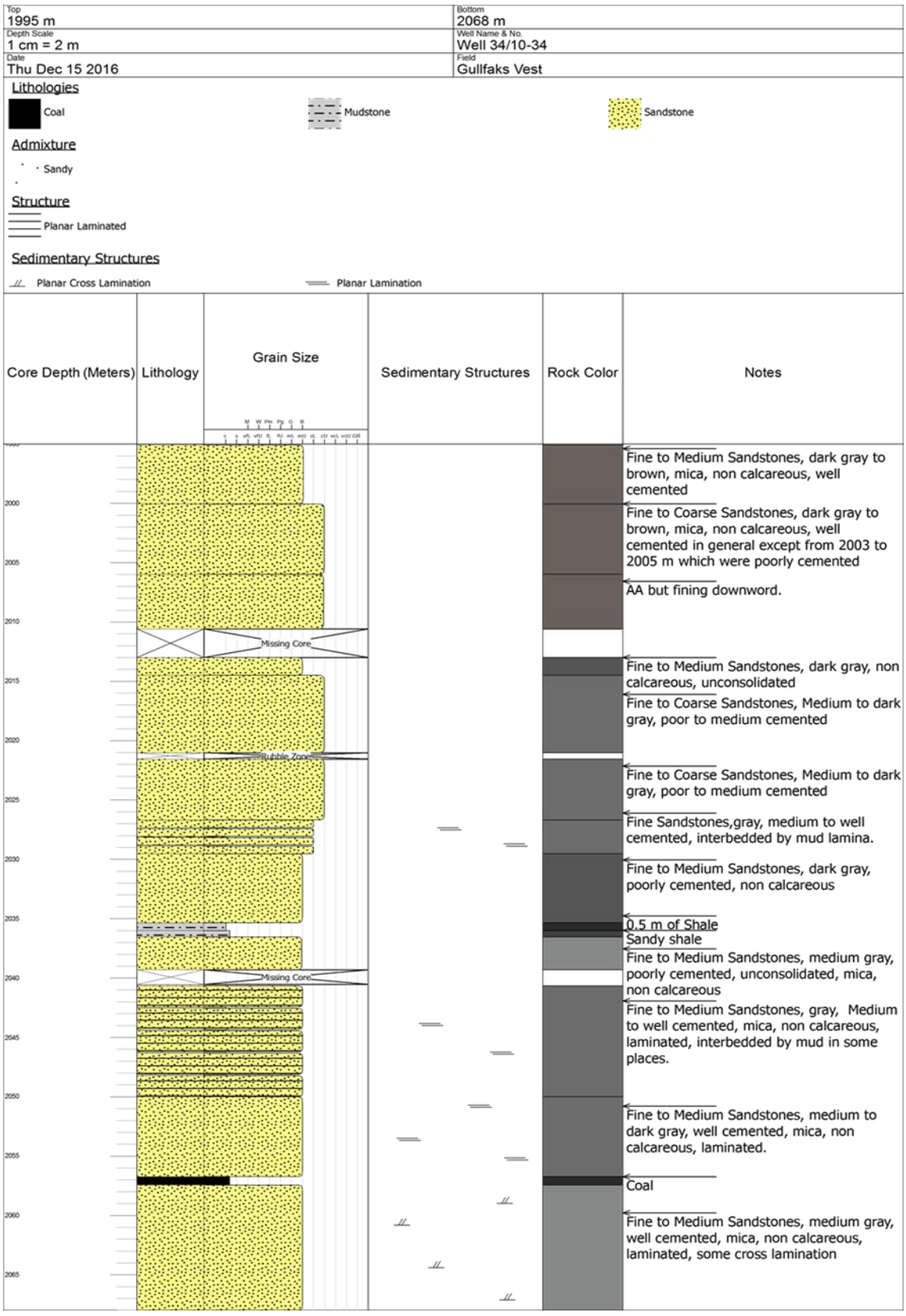

Figure 5-8. Sedimentological core descriptions of the Tarbert Formation in well 34/10-34 in the Gullfaks Vest Field. The Base-Cretaceous Unconformity is located at depth 1990.5 m, about 5 meters above the top of Tarbert Formation separating the Tarbert Formation from the Upper Cretaceous Shetland Group.

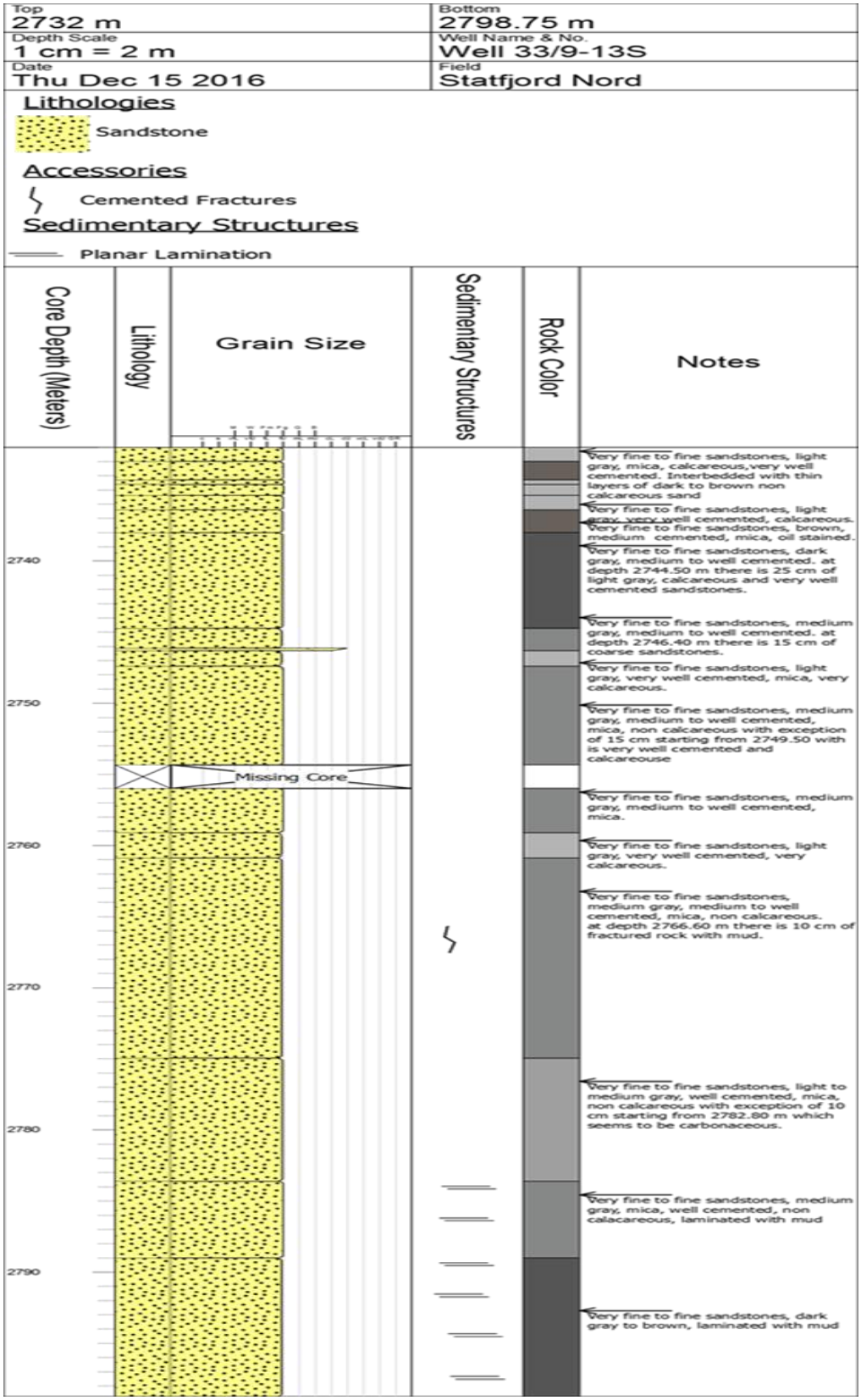

Figure 5-9. Sedimentological core descriptions of the Rannoch Formation in well 33/9-13S in the Statfjord Nord Field. The Base-Cretaceous Unconformity is located at depth 2726.5 m, about 5.5 meters above the top of the Formation separating the Rannoch Formation from the Cretaceous Cromer Knoll Group.

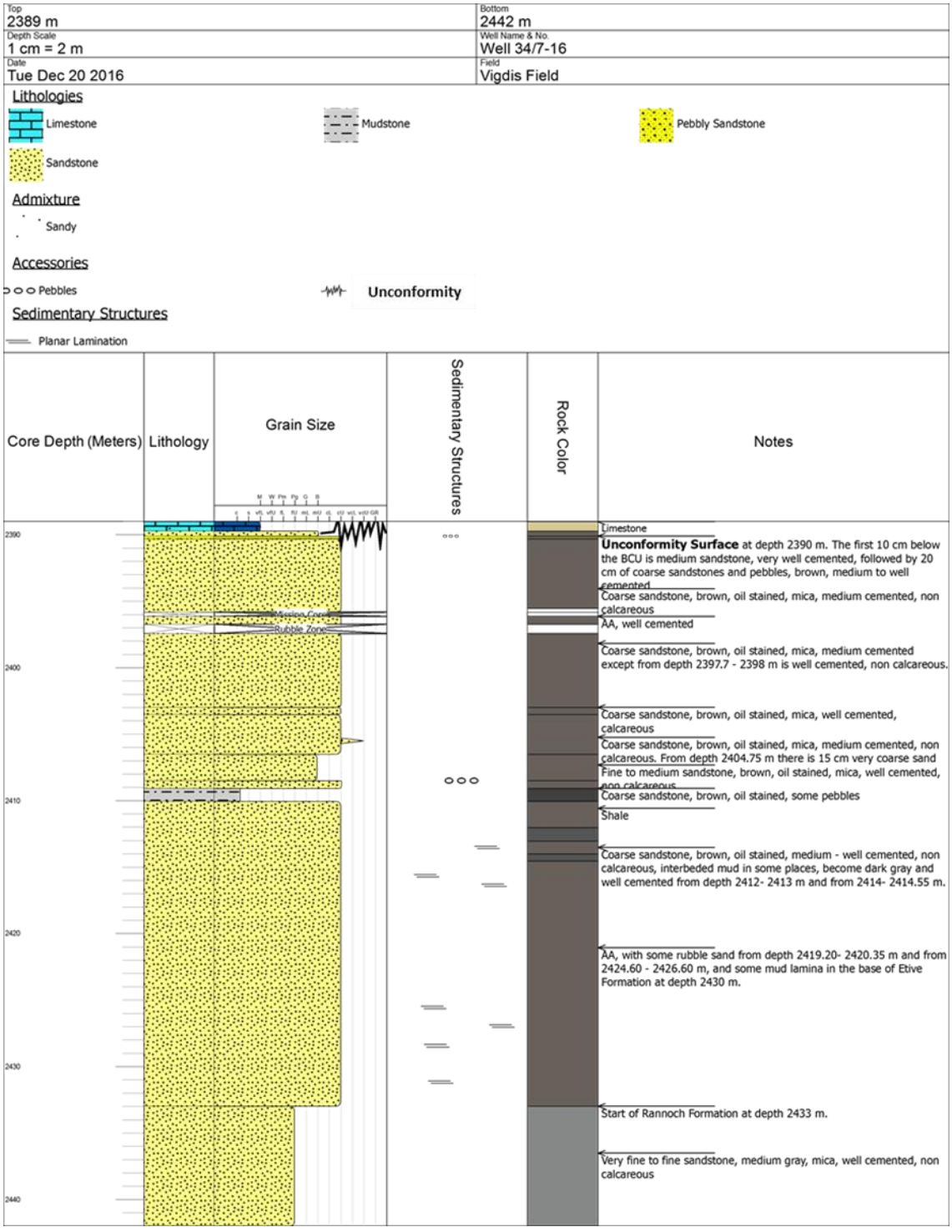

Figure 5-10. Sedimentological core descriptions of the Etive Formation in well 34/7-16 in the Vigdis Field. The Base-Cretaceous Unconformity is located at depth 2390 m, separating the Etive Formation from the Cretaceous Cromer Knoll Group.

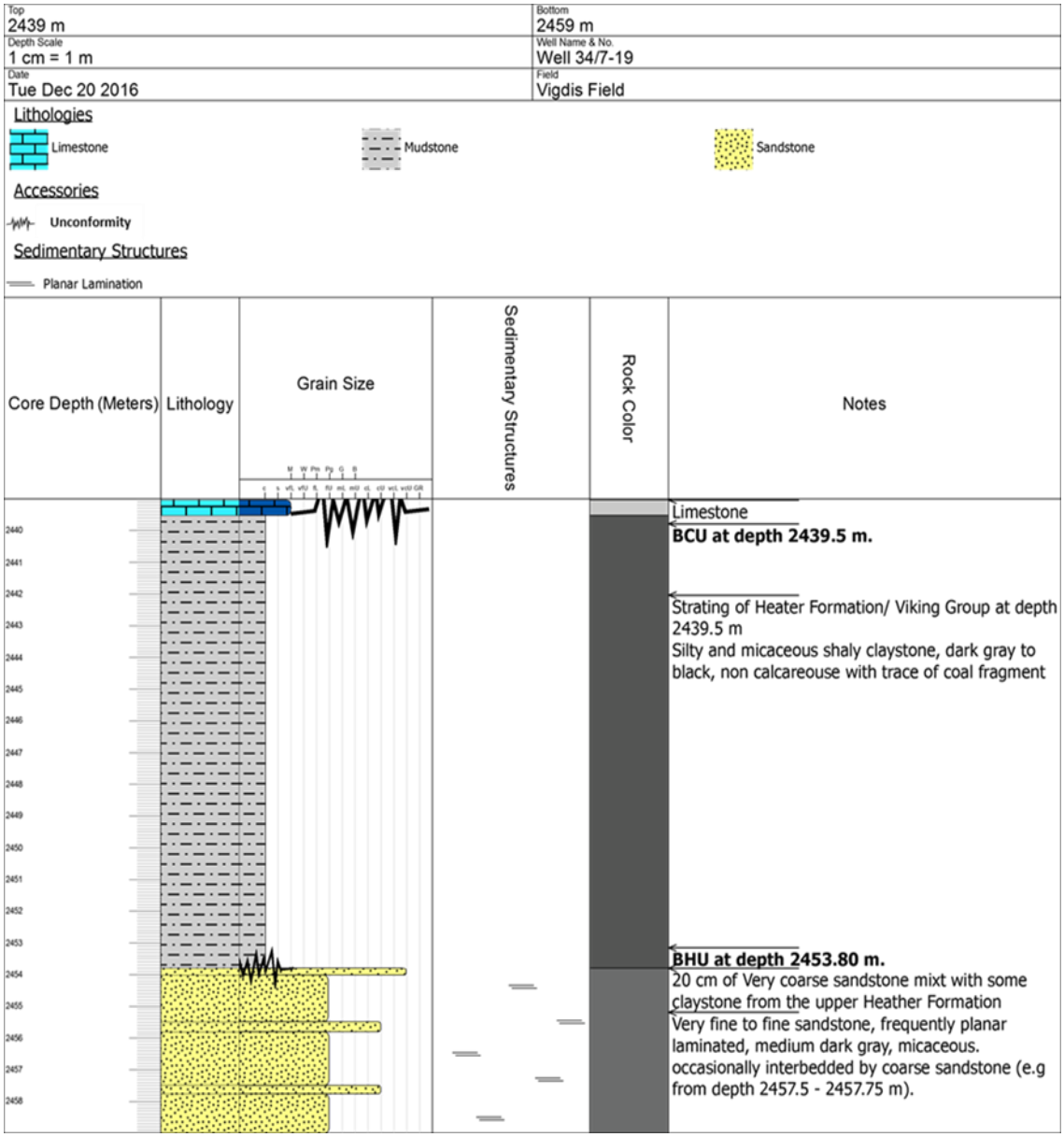

Figure 5-11. Sedimentological core descriptions of the Tarbert Formation in well 34/7-19 in the Vigdis Field. Two unconformities have been detected in this core intervals, the Base-Cretaceous Unconformity is located at depth 2439.5 m, separating the Heather Formation from the Cretaceous Cromer Knoll Group. The Base Heather Unconformity is located directly above the Tarbert Formation at depth 2453.80 m and separating the Tarbert Formation from the above Heather Formation.

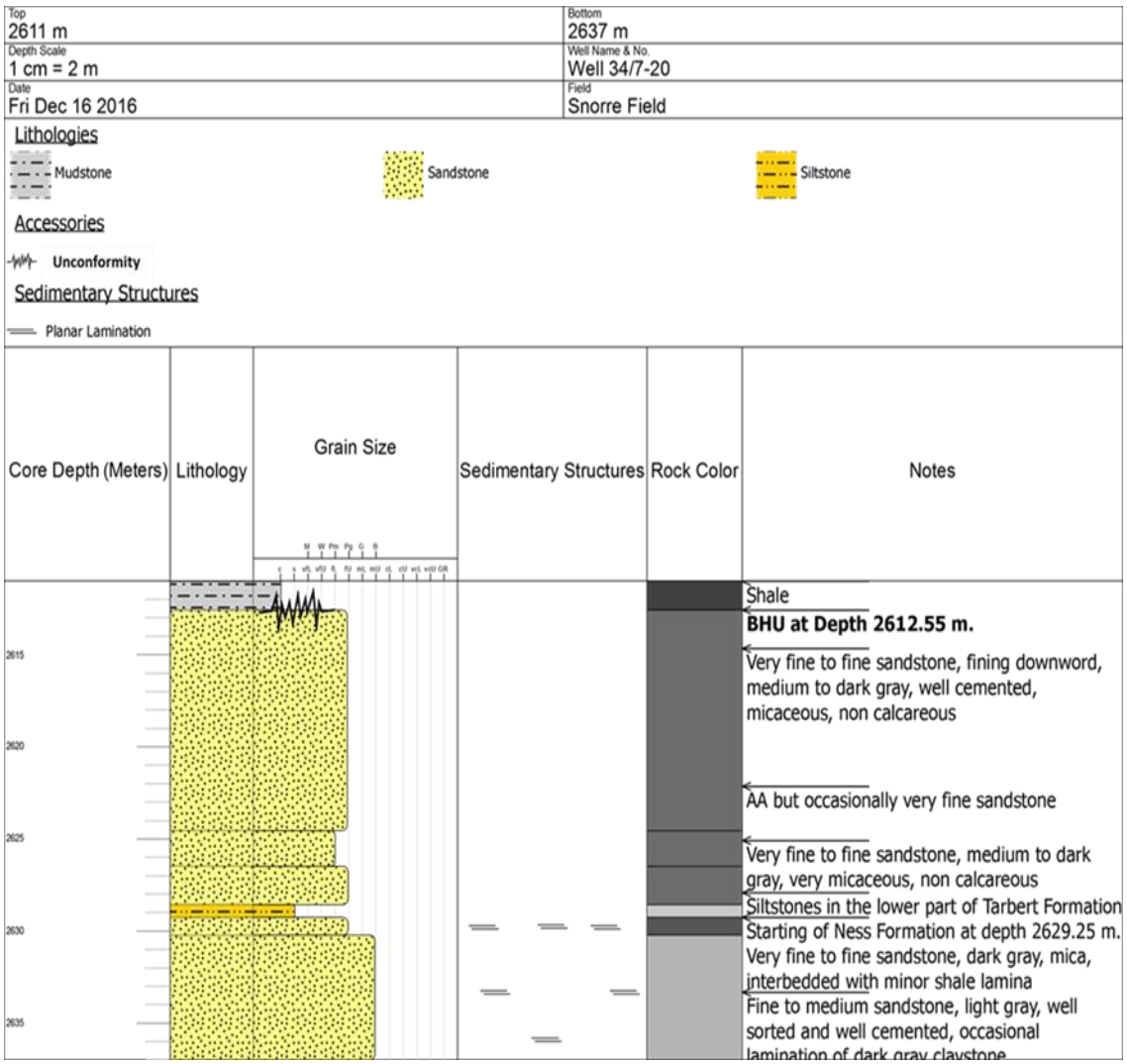

Figure 5-12. Sedimentological core descriptions of the Tarbert Formation in well 34/7-20 in the Snorre Field. The Base Heather Unconformity is located at depth 2612.5 m, directly above the top of the Tarbert Formation separating the formation from the Upper Jurassic Heather Formation.

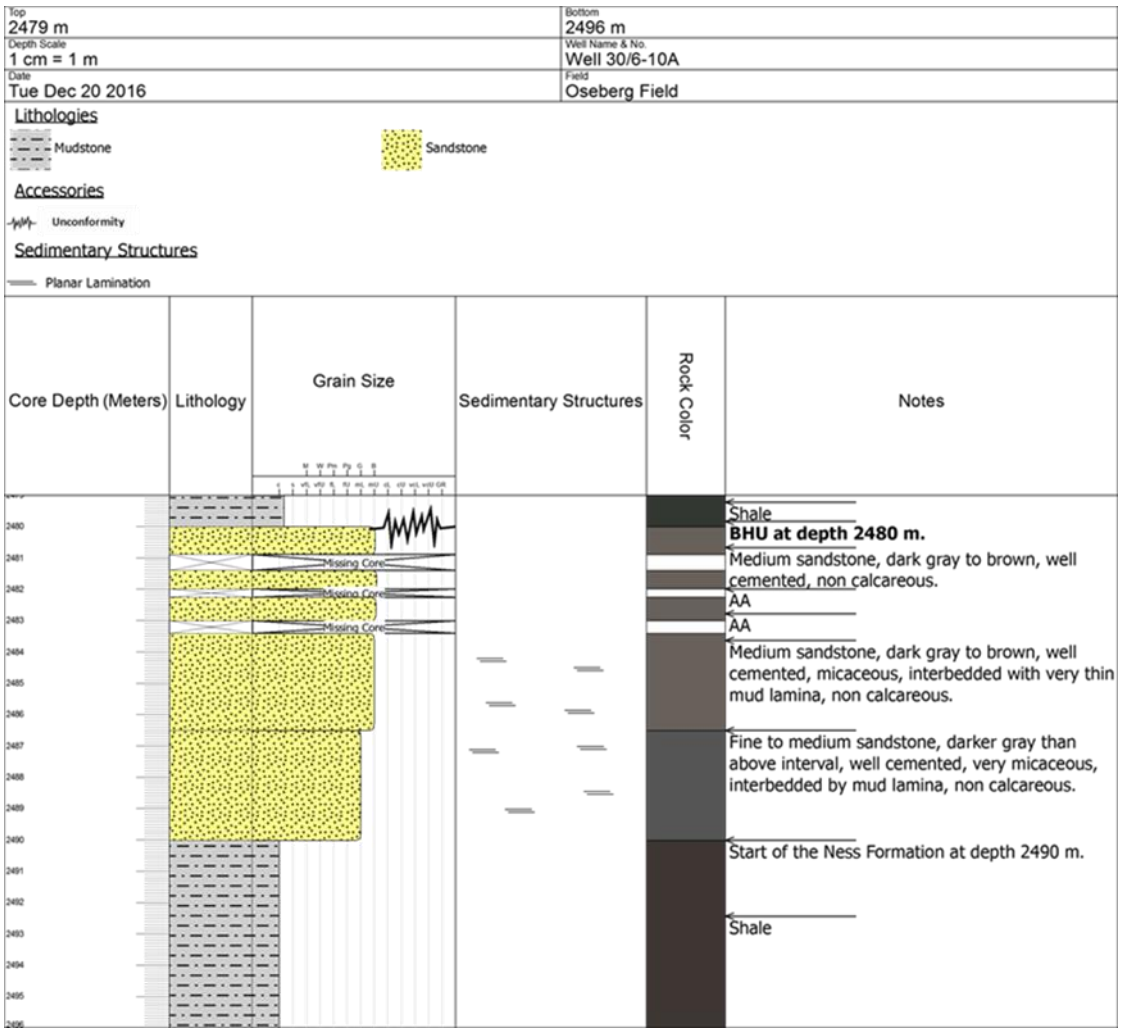

Figure 5-13. Sedimentological core descriptions of the Tarbert Formation in well 30/6-10 A in the Oseberg Field. The Base Heather Unconformity is located at depth 2480 m, directly above the top of the Tarbert Formation separating the formation from the above Viking Group Heather Formation.

5.5 Petrographic Analysis

Petrographic analysis was employed to identify the lithological texture, mineralogy, porosity and classification of sandstones. More than 43 core samples were taken from the selected wells in the studied area. All samples were taken from Middle Jurassic Brent Group sandstones. The main petrographic analysis for these wells was carried out using optical microscopy and scanning electron microscopy (SEM).

The sampling interval chosen for this petrographic study was taken in accordance with the location of the unconformity surface, starting from the point closest to the unconformity surface and going deeper in a vertical order. This was done in order to

undertake a vertical comparison analysis and to study the possible relationship between the unconformity surface and the physical properties of the sediments beneath. It also allowed a comparison between the characteristics of similar facies and formations of the Brent Group sandstone lying directly below the unconformity surface and the ones lying far away from the unconformity surface. For instance, the Base-Cretaceous Unconformity lies directly above the top of the Rannoch Formation in Wells 34/10-4 and 33/9-13, whereas in Well 34/10-1 the Base-Cretaceous Unconformity surface is located more than 70 m above the top of the Rannoch Formation.

5.5.1 Lithological Texture

The textures, grain size and sorting characteristics of the Brent Group sandstone facies are summarized in Table 5-1. Three main formations were observed in the studied wells of the Tampen Spur area: the Rannoch, Etive and Tarbert Formations. Each sample taken from these formation was described in detail. Each sample has been given a facies code which briefly indicates the sedimentary texture of the sandstone from which it was taken, and therefore all samples with similar sedimentary texture and microscopic characteristics can be easily observed and compared. Facies codes are given in the lithological textures table (Table 5-1) and compositional analysis tables (Table 5-2 to Table 5-10), together with the data for the petrographic characteristics of each studied sample.

The Rannoch sandstones are almost homogeneous and variability of grain-size across all the studied wells is limited. Most of the sampled sandstones range from very fine to fine-grained sand, which is subangular to subrounded and medium to well-sorted.

The Etive sandstones also show similar grain size of the sandstones in all the studied wells and consist mainly of medium- to coarse-grained sandstones, with the exception of Well 34/10-16, which has been interbedded by a one metre thick layer of shale in middle of the interval at a depth of 2409 m. The sandstones are classified as subangular to subrounded and well-sorted.

Based on the grain size, the Tarbert Formation can be subdivided into two facies of sandstone, fine to medium-grained sandstones with occasionally coarse-grained intervals, particularly in Well 34/10-4, and very fine to fine-grained sandstones, occasionally coarse, particularly in Well 34/7-19. Both sandstone facies are subangular to subrounded and moderately into well-sorted.

Table 5-1. Summary of lithological textures of Brent Group sandstones. VF = very fine sand. FS = fine sand. MS = medium sand. CS = coarse sand. M –W = medium to well-sorted and W= well-sorted. SA-SR = subangular to subrounded grains

Formation Name	Facies Code	Grain Size	Sorting	Roundness
Rannoch	2	VF-FS	M-W	SA-SR
Etive	6	M-CS	W	SA-SR
Tarbert	2 + 4	VF-FS + F-MS	M-W	SA-SR

5.5.2 Sandstone Classification

In the Tampen Spur area, all the studied samples were taken from three Formations: Rannoch, Etive and Tarbert; therefore, the classification represents only the components of sandstones in these three formations of the Brent Group. All the analysed samples which were taken for this study are sandstones. The range of sandstone types identified from the 43 thin-sections is shown in Figure 5-14; apart from the main framework grains of quartz, feldspar and rock fragments, the most common accessory mineral is mica. Using the Pettijohn (1975) classification scheme (where polycrystalline quartz is counted as rock fragments, see Appendix B.2), in general the Brent Group sandstones are classified as arkosic to lithic arkose sandstones. However, in more detail, the very fine to fine sandstone facies of the Rannoch Formation, which represents three of the analysed wells, 34/10-1, 34/10-4 and 33/9-13, is classified to be arkose sandstones. Most of the medium to coarse sandstones of the Etive Formations are lithic arkose, whereas the sandstones of the Tarbert Formation (which are subdivided into two different facies of sandstones, fine to medium sandstones, occasionally coarse, particularly in Well 34/10-4 and very fine to fine sandstones, occasionally coarse, particularly in Well 34/7-19) are classified to be arkosic to lithic arkose sandstones, depending on the grain size. The trend of increasing rock fragments and polycrystalline quartz with increasing grain size is typical for terrigenous sediments, according to Pettijohn et al. (1972).

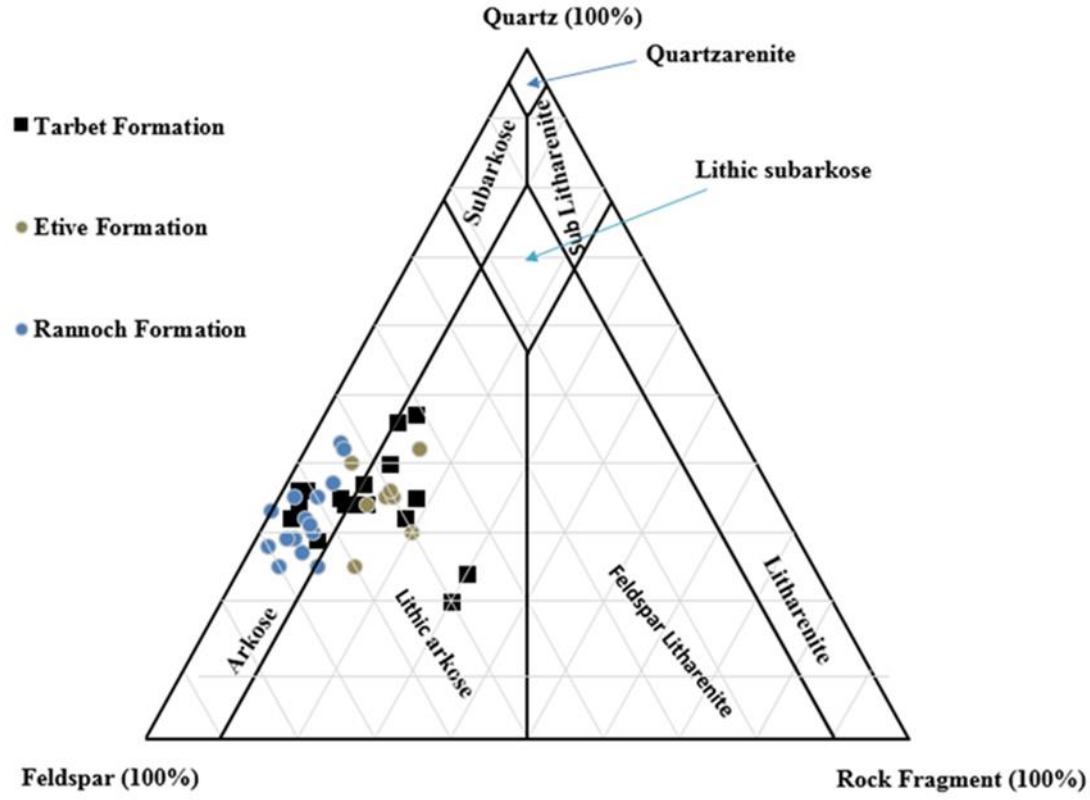

Figure 5-14. Sandstone classification diagrams, all the samples fall in the arkose and lithic arkose fields (modified from Pettijohn et al., 1972).

5.5.3 Quantitative analysis

Quantitative analysis of sandstones was carried out to quantify and determine the percentage of framework grains, cements and the porosity observed in each studied sample. The quantitative analysis of the studied samples are summarized in nine tables each table represents the petrographic results of several samples from particular well within the studied area (Table 5-2 to Table 5-10).

Table 5-2. Petrographic analysis data for Well 33/9-13

Sample n.	Depth (m)	Facies	CONSTITUENT (%)								Total (%)
			Porosity %	Framework minerals %			Accessory minerals %	Cements %		Others %	
				Quartz	Feldspar	Rock Fragment	Mica	Calcite	Clay	Iron Oxide	
1	2732	2R	1	35	9	2	13	38	0	2	100
2	2733.5	2R	24	25	8	5	13	12	10	3	100
3	2738	2R	24	43	8	4	6	5	7	4	100
4	2743.9	2R	17	42	7	5	6	7	8	8	100
5	2750	2R	25	31	7	6	10	10	7	4	100
6	2767.9	2R	18	37	9	6	9	13	6	2	100

Table 5-3. Petrographic analysis data for Well 34/7-20

Sample n.	Depth (m)	Facies	CONSTITUENT (%)								Total (%)
			Porosity %	Framework minerals %			Accessory minerals %	Cements %		Others %	
				Quartz	Feldspar	Rock Fragment	Mica	Calcite	Clay	Iron Oxide	
1	2612.8	2T	20	36	7	3	15	0	12	7	100
2	2615.5	2T	22	36	14	2	12	0	9	5	100
3	2620.5	2T	18	34	10	3	14	0	14	7	100

Table 5-4. Petrographic analysis data for Well 34/7-19

Sample n.	Depth (m)	Facies	CONSTITUENT (%)								Total (%)
			Porosity %	Framework minerals %			Accessory minerals %	Cements %		Others %	
				Quartz	Feldspar	Rock Fragment	Mica	Calcite	Clay	Iron Oxide	
1	2453.92	8T	12	20	4	30	3	0	30	1	100
2	2455.6	8T	14	24	7	30	2	0	22	1	100
3	2465.5	2T	24	32	9	3	9	0	20	3	100

Table 5-5. Petrographic analysis data for Well 34/7-16. Samples 5, 6 and 7 are below a shale layer and show no difference compared with above sample.

Sample n.	Depth (m)	Facies	CONSTITUENT (%)								Total (%)
			Porosity %	Framework minerals %			Accessory minerals %	Cements %		Others %	
				Quartz	Feldspar	Rock Fragment	Mica	Calcite	Clay	Iron Oxide	
1	2390.07	6E	7	40	7	7	1	35		3	100
2	2390.65	6E	37	34	5	12	1	3	7	1	100
3	2393.8	6E	28	35	8	14	1	5	7	2	100
4	2409.1	3-7E	26	30	8	20	2	7	5	2	100
5	2410.8	6E	24	42	7	15	1	6	3	2	100
6	2416.7	6E	20	35	8	15	2	10	4	5	100
7	2429.8	6E	22	36	9	14	3	5	8	3	100

Table 5-6. Petrographic analysis data for Well 34/10-8

Sample n.	Depth (m)	Facies	CONSTITUENT (%)								Total (%)
			Porosity %	Framework minerals %			Accessory minerals %	Cements %		Others %	
				Quartz	Feldspar	Rock Fragment	Mica	Calcite	Clay	Iron Oxide	
1	1823.3	4T	25	37	6	10	2	3	15	5	100
2	1824.5	1-5T	7	34	6	9	12	5	25	7	100
3	1846.4	2T	14	29	6	8	15	7	28	0	100

Table 5-7. Petrographic analysis data for Well 34/10-34

Sample n.	Depth (m)	Facies	CONSTITUENT (%)									Total (%)
			Porosity %	Framework minerals %			Accessory minerals %		Cements %		Others %	
				Quartz	Feldspar	Rock Fragment	Mica	Opaque Minerals	Calcite	Clay	Iron Oxide	
1	1995	4T	25	40	7	12	1	0	11	3	1	100
2	2000	4T	18	34	8	10	0	4	19	7	0	100
3	2009	3-7T	24	32	9	18	2	0	0	8	1	100

Table 5-8. Petrographic analysis data for Well 34/10-4

Sample n.	Depth (m)	Facies	CONSTITUENT (%)								Total (%)
			Porosity %	Framework minerals %			Accessory minerals %	Cements %		Others %	
				Quartz	Feldspar	Rock Fragment	Mica	Calcite	Clay	Iron Oxide	
1	1826.5	2R	30	30	5	7	8	12	6	2	100
2	1835	2R	28	27	8	7	10	11	7	2	100
3	1841.8	2R	33	29	5	5	8	11	7	2	100
4	1843.1	2R	1	29	8	4	7	49	0	2	100
5	1848.4	2R	27	32	8	5	6	12	8	2	100
6	1868.1	2R	26	35	7	5	5	14	6	2	100
7	1898	2R	25	28	7	2	10	19	7	2	100

Table 5-9. Petrographic analysis data for Well 34/10-1

Sample n.	Depth (m)	Facies	CONSTITUENT (%)								Total (%)
			Porosity %	Framework minerals %			Accessory minerals %	Cements %		Others %	
				Quartz	Feldspar	Rock Fragment	Mica	Calcite	Clay	Iron Oxide	
1	1783.1	6T	20	35	6	18	1	15	5		100
2	1784	4T	0	34	6	12	1	45	0	2	100
3	1785.1	4T	22	35	6	8	2	22	3	2	100
4	1840.2	6E	22	42	6	15	1	0	12	2	100
5	1867.7	6E	40	25	5	15	1	0	12	2	100
6	1877.65	2R	15	25	7	10	12	30	0	1	100
7	1880.3	2R	30	29	6	5	10	7	11	2	100
8	1916.3	2R	30	33	6	0	9	12	8	2	100

Table 5-10. Petrographic analysis data for Well 30/6-10A

Sample n.	Depth (m)	Facies	CONSTITUENT (%)									Total (%)
			Porosity %	Framework minerals %			Accessory minerals %		Cements %		Others %	
				Quartz	Feldspar	Rock Fragment	Mica	Opaque Minerals	Calcite	Clay	Iron Oxide	
1	2480	5T	18	47	11	12	2	0	0	8	2	100
2	2483.5	5T	18	46	12	10	3	4	trace	9	2	100

5.5.3.1 Mineralogy

This section will describe in detail the main composition of the studied Brent Group sandstones, based on the point counted results of the 43 studied samples.

5.5.3.1.1 Framework Minerals

1. Quartz

The main framework grains in the studied sandstone samples were quartz. Only monocrystalline quartz is counted as quartz grains in all samples, any polycrystalline grains are considered as rock fragments. Some samples showed cracked and corroded quartz grains, with partial dissolution of the edge of the grains, in some cases. The percentage of quartz grains ranged from 25 to 42%. Sutured boundaries between the quartz grains were observed in some samples, which may indicate compaction processes (Figure 5-15 A).

2. Feldspar

The majority of the feldspar grains which appeared in the studied samples were K-feldspar, with less common plagioclase and microcline. Most of these feldspar grains exhibited variable degrees of alteration, replacement and partial to complete dissolution (Figure 5-15 A). In many cases complete dissolution of feldspar grains was observed and only the outline of the grains still appeared (Figure 5-15 B). In addition, in many cases the partial and complete dissolution of some grains had been followed by precipitation of kaolinite (Figure 5-15 C) or authigenic calcite, filling the intragranular pores (Figure 5-15 D). Some feldspar grains which were presumably originally calcium plagioclase had been replaced partially or completely by authigenic calcite (Figure 5-15 E). In most of the studied sandstone samples there was no significant variation in the volume and distribution of feldspar grains, which ranged from 5 to 9%, except in Wells 34/7-20 and 30-6-10A, where feldspar volume increased to 14%.

3. Rock Fragments

Because polycrystalline quartz grains were considered as rock fragments in this study, the most common rock fragments found in most of the analysed samples within the Brent

Group Formation were polycrystalline quartz. However, other sedimentary rock fragments were observed as well. The petrographic analysis showed that the coarser sand comprised the greater proportion polycrystalline quartz; this was observed particularly in the coarse sandstones of the Tarbert Formation, in Well 34/7-19.

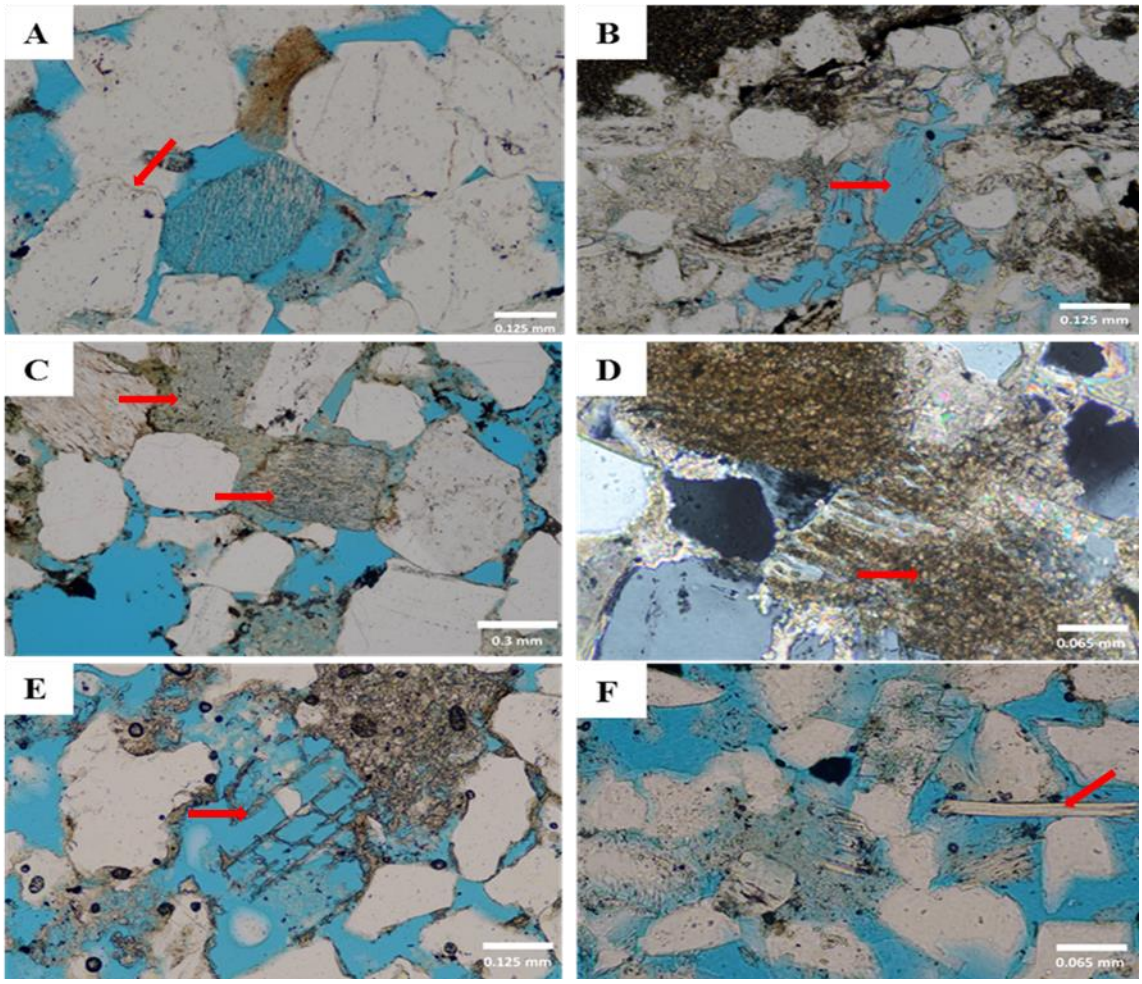

Figure 5-15. Photomicrographs showing different petrographic features observed in the studied sandstones. **A.** Medium-grained sandstone showing corroded quartz grains and signs of compaction represented by the sutured boundaries between quartz grains: Wells 30/6-10A, 2480 m. **B.** Very fine to fine-grained sandstone facies showing complete dissolution of feldspar: Wells 34/10-1, 1877.6 m. **C**. Kaolinite within a pore space; the shape and size of the filled pores indicate that this kaolinite has formed as a result of feldspar dissolution: Well 34/10-1, 1840.2 m. **D**. Dissolved feldspar grains which have been followed by precipitation of authigenic calcite: Well 34/10-4, 1843.10. **E**. Detailed view showing almost complete dissolution of calcareous feldspar grain and replacement by authigenic calcite: Well 34/10-1, 1785.10 m. **F**. Flakes of mica between detrital grains: Well 34/10-1, 1916.30 m.

5.5.3.1.2 Accessory Minerals

Mica

Mica may form in distinctive flakes parallel to the beds and lamination planes and with burial can be deformed and compacted between detrital grains (Figure *5-15* F). The most common mica in the Brent Group sandstones is muscovite; in the analysed thin-section and under cross-polarized light it appears in bright blue to yellow and in plane polarized light it is colourless. Biotite, which is commonly strongly brown or green coloured was also observed in some samples. Diagenetic mica was observed in many samples as well, it may have been formed by replacement of some feldspar grains.

There was significant variation in the distribution and contents of mica in the studied sandstone facies of the Brent Group. For instance, 6-15% mica was determined in the very fine to fine-grained sandstone of the Rannoch and Tarbert formations, whereas in the medium to coarse-grained sandstones of Etive and Tarbert Formations the content of mica was much less and did not exceed 3%, at most. It was clear that this variation in mica content appeared to be proportional to grain size, which can be related to the depositional process rather than to the provenance, and the finer the grain size the more abundant the mica.

5.5.3.1.3 Authigenic Mineralogy

1. **Calcite cement**

Most of the studied sandstone samples of the Brent Group contained calcite cement ranging from 6% up to 49%, with the exception of some samples where only a trace of calcite was observed. Different types of calcite cement were observed in the studied sandstone samples, including scattered patches of calcite cement and extensively cemented sandstone layers. This variation in the amount and distribution of calcite cement is possibly based on the different location of the selected samples, as cemented layers within the cored interval of the Brent Group have been observed frequently. In some samples, calcite was observed as a blocky spray and poikilotopic habits, replacing some of the framework grains and filling the pore space or filling intragranular pores within micas (Figure 5-16 A) and feldspar grains (Figure 5-15D), indicating that the precipitation

of calcite post-dated feldspar dissolution. On the other hand, the patchy distribution of calcite cement, the etched boundary of some of the calcite crystals and the dissolution of the calcite cements that have precipitated in the intragranular pores may indicate a late dissolution phase of calcite and consequent enhancement of the porosity (Figure 5-16 B).

Based on this, calcite cement within the Brent Group sandstones in the Tampen Spur area can be divided into two types of calcite cement:

1. Early calcite cement: poikilotopic and intergranular calcite cement can be interpreted as representing early diagenetic processes, which may support the other detrital framework grains and prevent later diagenetic processes.
2. Late calcite cement: calcite which has been formed by alteration and replacement of feldspar grains or that has filled dissolution pores indicates that this cementation was formed later and post-dates the dissolution process.

These points suggest that the sandstones may have gone through multiple early and late diagenetic processes and that the calcite in these sandstone represented more than one precipitation phase.

2. Siderite

Siderite occurs in sandstones as scattered crystals to microcrystals, it usually appears in rhombic crystals of brownish colour but sometimes the rhombs become irregular or highly altered. It is usually found in association with calcite cement and may show alteration associated with iron oxide and sometimes with mica alteration. In the area of study, siderite was observed in many samples and in various habits: in small crystals between framework grains associated with iron oxide (Figure 5-16 C), in association with calcite cement and within the expanded mica grains (Figure 5-16 D).

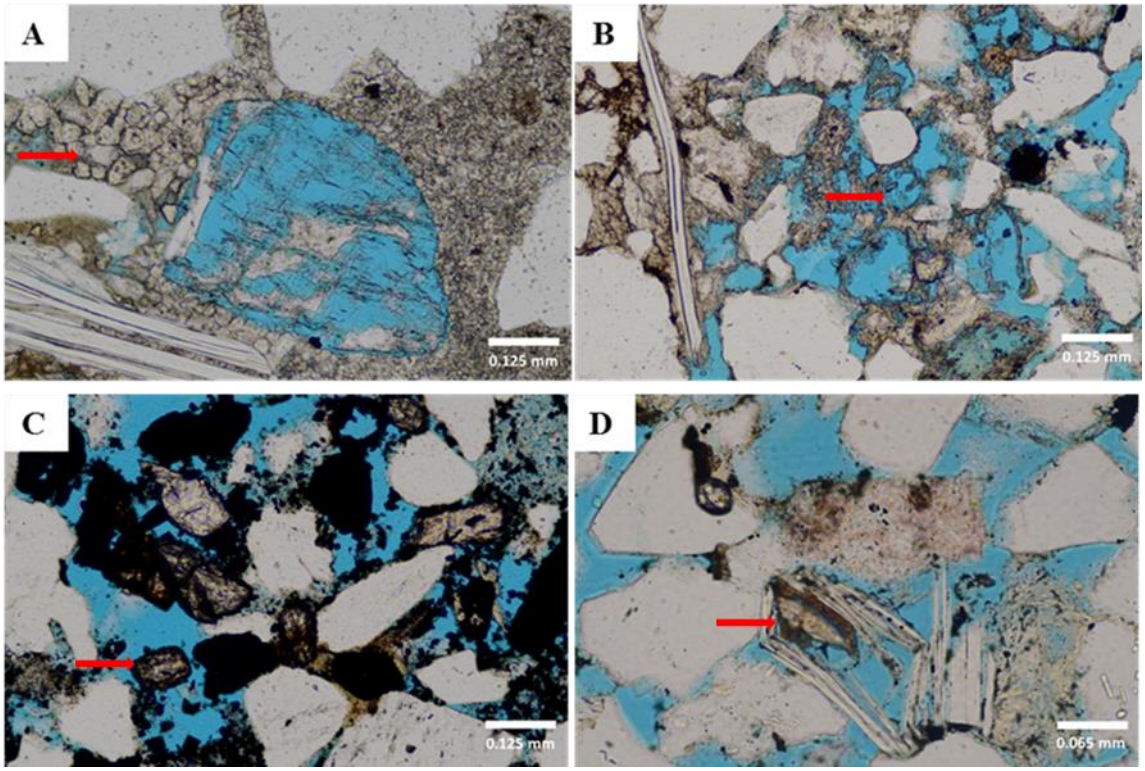

Figure 5-16. Optical micrographs showing: **A**. Calcite cement filling the intergranular pores: Well 34/7-16, 2390.07 m. **B**. Late dissolution of calcite cement: Well 34/10-1, 1785.10 m. **C**. Rhombic crystals of siderite cement associated with iron oxide; these occur within the pore space, reducing the volume of porosity: Well 34/10-34, 2000 m. **D**. Growth of siderite among the expanded grains of mica: Well 33/9-13, 2738 m.

3. Kaolinite

In the area of study, clay minerals were not common and in most samples the most abundant cement type was calcite. However, some clay cement also occurred in many samples. One of the most common clay minerals within the Brent Group is kaolinite. It occurs as patches in association with altered detrital grains, particularly feldspars and usually has similar sizes to the original grains (Figure 5-17 A). Kaolinite may form as patches and is usually seen as deformed kaolinite between adjacent framework grains (Figure 5-17 B). These types of kaolinite usually occupy intergranular porosity or are found within secondary porosity that may have been formed by dissolution of framework grains. Kaolinite may also occur in irregular crystals in association with altered detrital mica flakes, where it is usually poorly developed (Figure 5-17 C).

4. **Pyrite and Iron oxide**

This widely distributed authigenic mineral has been observed in almost all the studied sandstone samples. Most of the samples showed a low percentage of pyrite, ranging from 1 - 3%. However, in some samples it reached 8%. Pyrite was observed as clusters of black cubic crystals within pores or in association with other clay minerals and as dense nodules, framboids, or in amorphous form in some other samples.

5.5.3.2 Porosity

The porosity of the sandstones can be either, primary or secondary in origin and sometimes both of these forms may appear. Visual distinction between primary and secondary porosity types is sometimes difficult. Different types of secondary porosity were observed within the studied samples of the Brent Group sandstones: these included (1)- intragranular porosity formed as a result of partial or complete dissolution of detrital grains (particularly feldspar) or calcite cement and (2)- intercrystalline porosity; commonly microporosity observed within and between kaolinite crystals.

The point counted porosities of the Brent Group sandstones which were obtained from the 43 studied thin-section samples were relatively high, especially in the sandstone samples with low carbonate cement (Table 5-11). The point counted porosity volume here includes both primary and secondary porosity. It is also worth mentioning that very high porosity may be attributed to grains being plucked during sample preparation.

1. **Macroporosity**

Macroporosity includes two main pore types which have been observed, intergranular and intragranular pores. In the area of study, the intergranular porosity represents the primary porosity and commonly exists as pores between framework detrital grains as was observed in most of the analysed samples. Intergranular porosity was well interconnected in most samples, except in the samples containing a high volume of calcite cement.

Intragranular porosity represented a high percentage of the total volume of porosity; it had been developed mainly by partial to complete dissolution of detrital grains (particularly feldspars) (Figure 5-16 A). Some of the feldspar grains which had been dissolved completely were outlined by clays. However, in many cases, dissolution of feldspar grains was associated with precipitation of calcite cement (particularly where the

dissolved grain was plagioclase) and/or formation of kaolinite (where the dissolved grain was a k-feldspar), filling the created intragranular pores (Figure 5-15 C and E). Another detected porosity type was intragranular porosity formed by the dissolution of calcite cement, which was fairly extensive in many samples (Figure 5-16 B). These intragranular porosity types may enhance reservoir quality.

Table 5-11. Petrographic analysis data of porosity volume below the unconformity surface in the studied wells.

Well 34/10-1		Well 34/10-4		Well 34/7-16		Well 33/9-13		Well 34/10-8		Well 34/10-34		Well 34/7-19		Well 34/7-20		Well 30/6-10A	
BCU at 1783 m		BCU at 1817 m		BCU at 2390 m		BCU at 2726.5 m		BCU at 1821 m		BCU at 1990.5 m + BHU at 1992.5 m		BCU at 2439.5 m + BHU at 2453.80 m		BHU at 2612.5 m		BHU at 2480 m	
Depth (m)	Porosity %	Depth (m)	Porosity %	Depth (m)	Porosity %	Depth (m)	Porosity %	Depth (m)	Porosity %	Depth (m)	Porosity %	Depth (m)	Porosity %	Depth (m)	Porosity %	Depth (m)	Porosity %
1783.1	20	1826.5	30	2390.0	7	2732	1	1823	0	1995	25	2453.9	12	2612.8	20	2480	18
1784	0	1835	28	2390.6	37	2733.5	24	1823.3	25	2000	18	2455.6	14	2615.5	22	2483.5	18
1785.1	22	1841.8	33	2393.8	28	2738	24	1824.5	7	2009	24	2465.5	24	2620.5	18		
1840.2	22	1843.1	1	2409.1	26	2743.9	17	1846.4	14								
1867.7	40	1848.4	27	2410.8	24	2750	25										
1877.6	15	1868.1	26	2416.7	20	2767.9	18										
1880.3	30	1898	25	2429.8	22												
1916.3	30																

2. Microporosity

Micropores is the presence of small pores that are usually associated with altered detrital grains and/or authigenic clays (Ulmer-Scholle et al., 2014). Identification of micropores within the analysed sandstone samples under the microscope was facilitated by the presence of blue impregnating resin within the very small pores. In the area of study, two types of micropores were observed in the Brent Group sandstones. The first microporosity type was the micropores that were associated with the authigenic clays, mainly within kaolinite crystals (Figure 5-17 D). The second type of microporosity was represented by the micropores observed within partially dissolved feldspar grains (Figure 5-17 E) and/or in between the expanded flakes of mica (Figure 5-17 F).

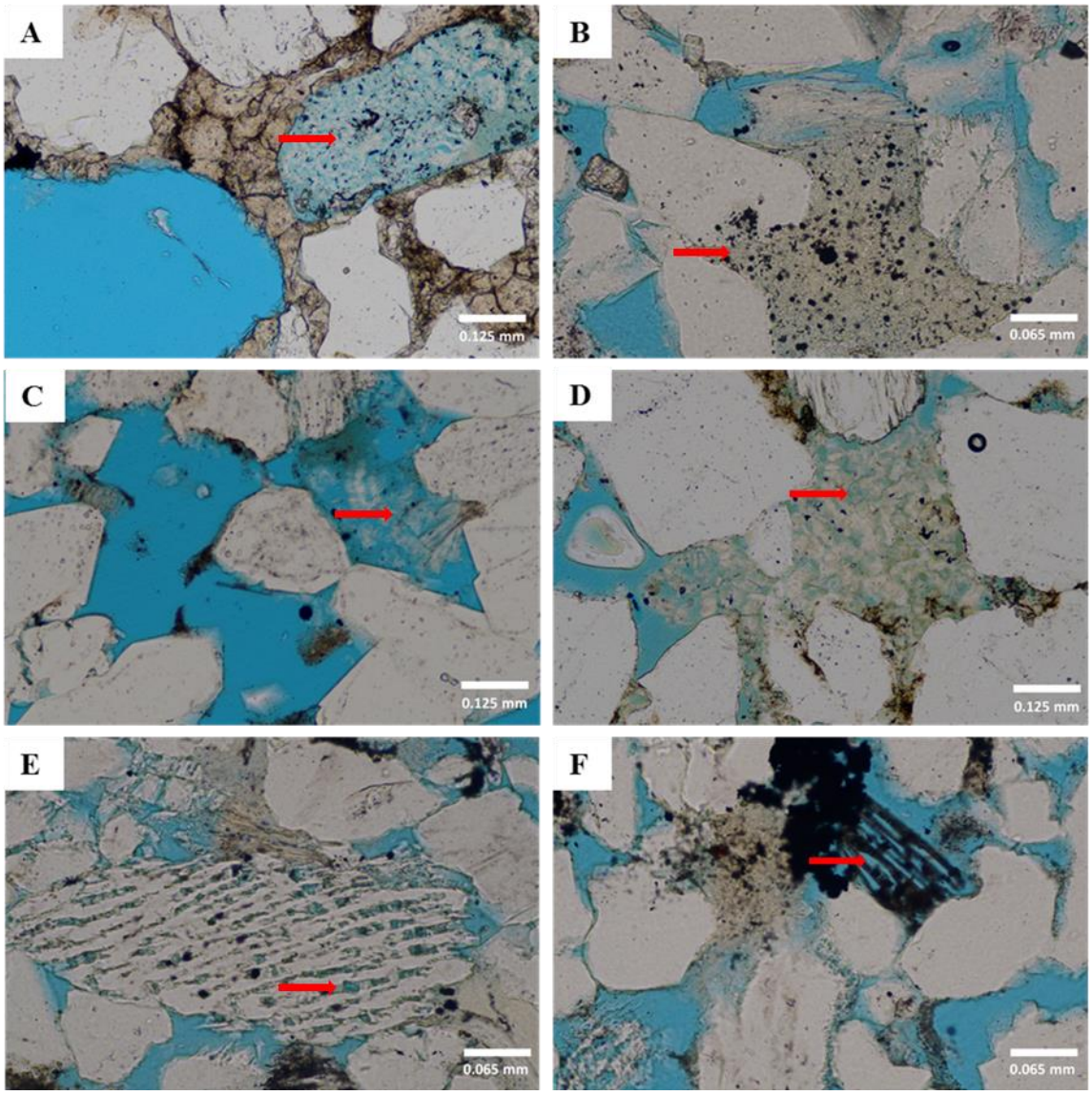

Figure 5-17. Optical micrographs images showing: **A**. Blocky kaolinite within a pore space: the shape and size of the filled pores indicate that this kaolinite has formed as a result of feldspar dissolution: Well 34/7-16, 2390.07 m. **B.** Aggregate of kaolinite booklets which were deformed and squeezed between grains and associated with some iron oxide: Well 33/9-13, 2750 m. **C**. Expanded and partially dissolved mica grain associated with precipitation of kaolinite: Well 30/6-10A, 2480 m. **D**. Microporosity associated within kaolinite crystals: Well 34/7-16, 2390.65 m. **E**. Microporosity observed within partially dissolved feldspar grains: Well 33/9-13, 2767.90 m. **F**. Microporosity between the expanded flakes of mica: Well 34/7-19, 2465.50 m.

5.6 Spatial distribution of minerals and porosity in Brent Group below the Base-Cretaceous Unconformity

This section will focus on the pattern of vertical distribution of unstable minerals and the reservoir properties of the Brent Group Sandstones below the Base-Cretaceous Unconformity. This mainly includes the pattern of vertical distribution of feldspar, kaolinite, carbonate cement and porosity in the studied wells. This will allow me to investigate the presence of any significant change in sandstone characteristics of the Brent Group below the unconformity surface and to study the possible relationship between these changes and the unconformity surface above. To do this, characteristics of Rannoch, Etive and Tarbert sandstones were studied separately, a different number of samples was selected from each formation, based on the location of the Base-Cretaceous Unconformity.

5.6.1 Rannoch Formation

16 samples were taken from this formation and studied in detail. These samples were divided between three different wells, Wells 34/10-1 and 34/10-4 in the Gullfaks Field and Well 33/9-13 in the nearby Statfjord Nord Field. Since the Rannoch Formation has been truncated by the Base-Cretaceous Unconformity in Well 34/10-1 and Well 33/9-13, any significant diagenetic effect related to the unconformity surface should be detected and seen in these two wells and should be much higher than any possible effect in Well 34/10-1 where the Base-Cretaceous Unconformity is lying more than 90 m above the top of the Rannoch Formation. Therefore, distribution of minerals and porosity in this formation were investigated in each of the three wells and compared with the other wells to study the possible diagenetic effect of the Base-Cretaceous Unconformity on the Rannoch sandstones.

5.6.1.1 Feldspar

No systematic variation (vertical trend) in the volume and distribution of feldspar grains toward the unconformity surface were observed in the Rannoch sandstones, with the volume of feldspar in the Rannoch Formation ranging between 5 – 9% in the three studied wells (Table 5-12).

Evidence for the partial and complete dissolution of the feldspar grains was observed in all the studied wells for the Rannoch Formation (Figure 5-18). However, the feldspar content did not show any systematic change in relationship to the unconformity surface (Figure 5-19). If the dissolution of feldspar grains was caused by the penetration of meteoric water through the Base-Cretaceous Unconformity, systematic vertical change of the feldspar volume would be expected and the amount of alteration and dissolution of feldspar grains should be much higher in the Wells 34/10-4 and 33/9-13, where Rannoch sandstones are directly truncated by the unconformity surface, compared to Well 34/10-1, where the Rannoch sandstones are separated from the unconformity surface by more than 90 m of sediments of the Etive, Ness and Tarbert Formations.

Table 5-12. Petrographic analysis data of feldspar content below the Base-Cretaceous Unconformity in Wells 34/10-1, 34/10-4 and 33/9-13.

Well 34/10-1			Well 34/10-4			Well 33/9-13		
BCU at 1783 m			BCU at 1817 m			BCU at 2726.5 m		
Depth (m)	Distance from BCU (m)	Feldspar %	Depth (m)	Distance from BCU (m)	Feldspar %	Depth (m)	Distance from BCU (m)	Feldspar %
1877.65	94.6	7	1826.5	9.5	5	2732	5.5	9
1880.30	97	6	1835	18	8	2733.5	7	8
1916.30	133.3	6	1841.80	24.8	5	2738	11.5	8
			1843.10	26.1	8	2743.9	17.4	7
			1848.40	31.4	8	2750	23.5	7
			1868.10	51.1	7	2767.9	41.4	9
			1898	81	7			

It is also important to mention that the Rannoch sandstones were shown to bear plagioclase in some samples, which was included in the total point counted feldspar volume. Samples which showed the presence of plagioclase within their composition in the Rannoch Formation were mainly from Well 34/10-4 and present mainly in the upper part of the formation, whereas plagioclase was almost absent in the Rannoch sandstone of Well 34/10-1.

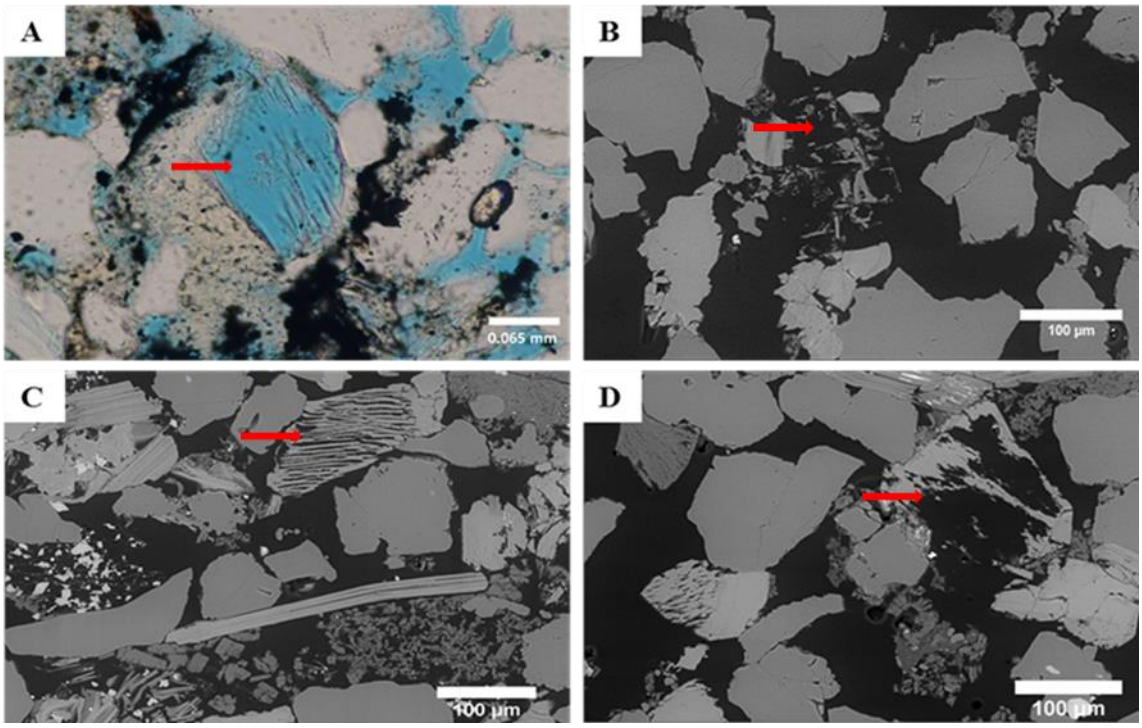

Figure 5-18. Thin-section photomicrographs and backscattered electron images from the three studied wells for the Rannoch Formation: **A** and **B**. Partially to complete dissolution of feldspar grain: Well 33/9-13, 2743.90 m and Well 34/10-4, 1830 m, respectively. **C** and **D**. BSE image showing partial dissolution of feldspar grains: Well 34/10-4, 1830 m and Well 34/10-1, 1885.30 m, respectively.

This observation is compatible with the XRD data mentioned in previous studies on these two wells (Ehrenberg and Jakobsen, 2001). Their XRD study showed the presence of plagioclase within the upper part of the Rannoch Formation in Well 34/10-4 and absence of plagioclase in Well 34/10-1 (Figure 5-20). If the dissolution of feldspar, including plagioclase grains, has a relationship with the Base-Cretaceous Unconformity, it is difficult to explain why plagioclase grains are present in Well 34/10-4, particulary in the top part which lies closest to the unconformity surface, and yet are not present in Well 34/10-1 which is more than 90 m away. In the case of unconformity related dissolution, the opposite trend is expected and plagioclase should be more common in the well further from the unconformity than in the other.

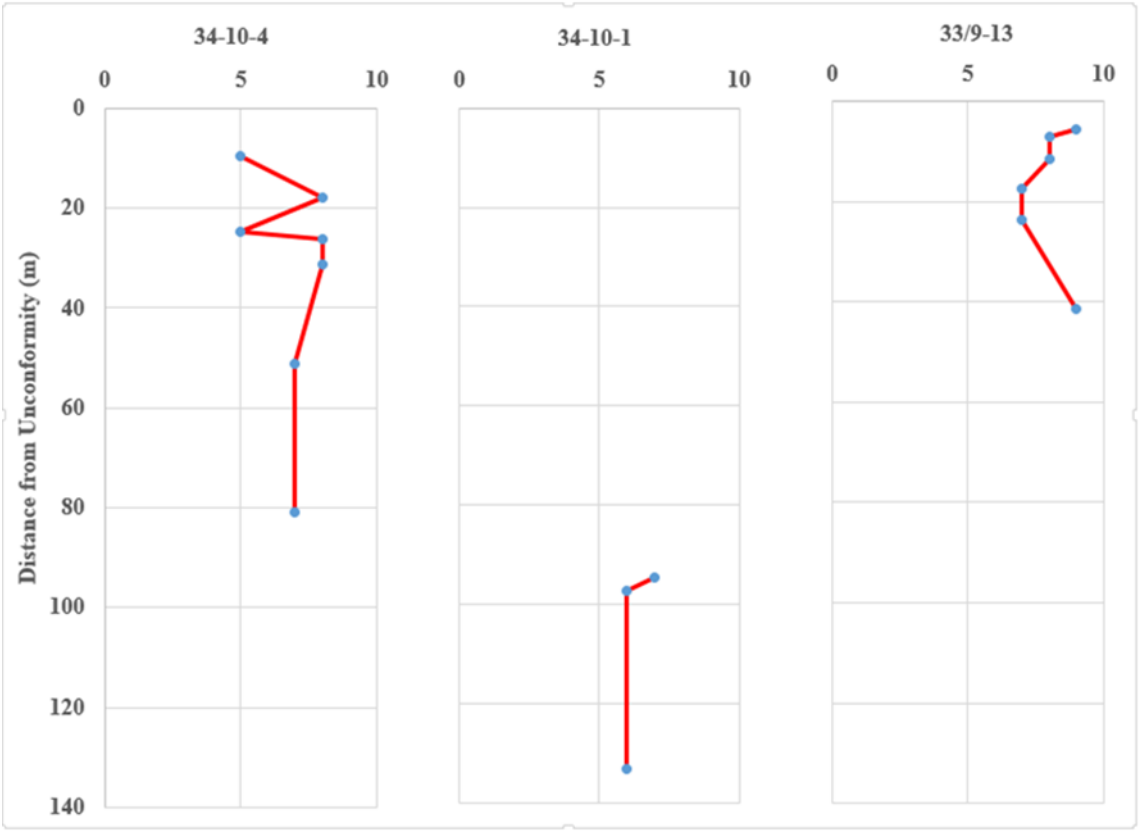

Figure 5-19. The volume and distribution of feldspar in the Rannoch Formation for the three studied wells. No systematic change in the volume and distribution of the feldspar toward the unconformity surface is observed. Although the BCU is located directly above the top of Rannoch Formation in Wells 34/10-4 and 33/9-13 the content of feldspar in these wells is not less than in Well 34/10-1, where the BCU is located more than 90 m above the top of Rannoch Formation.

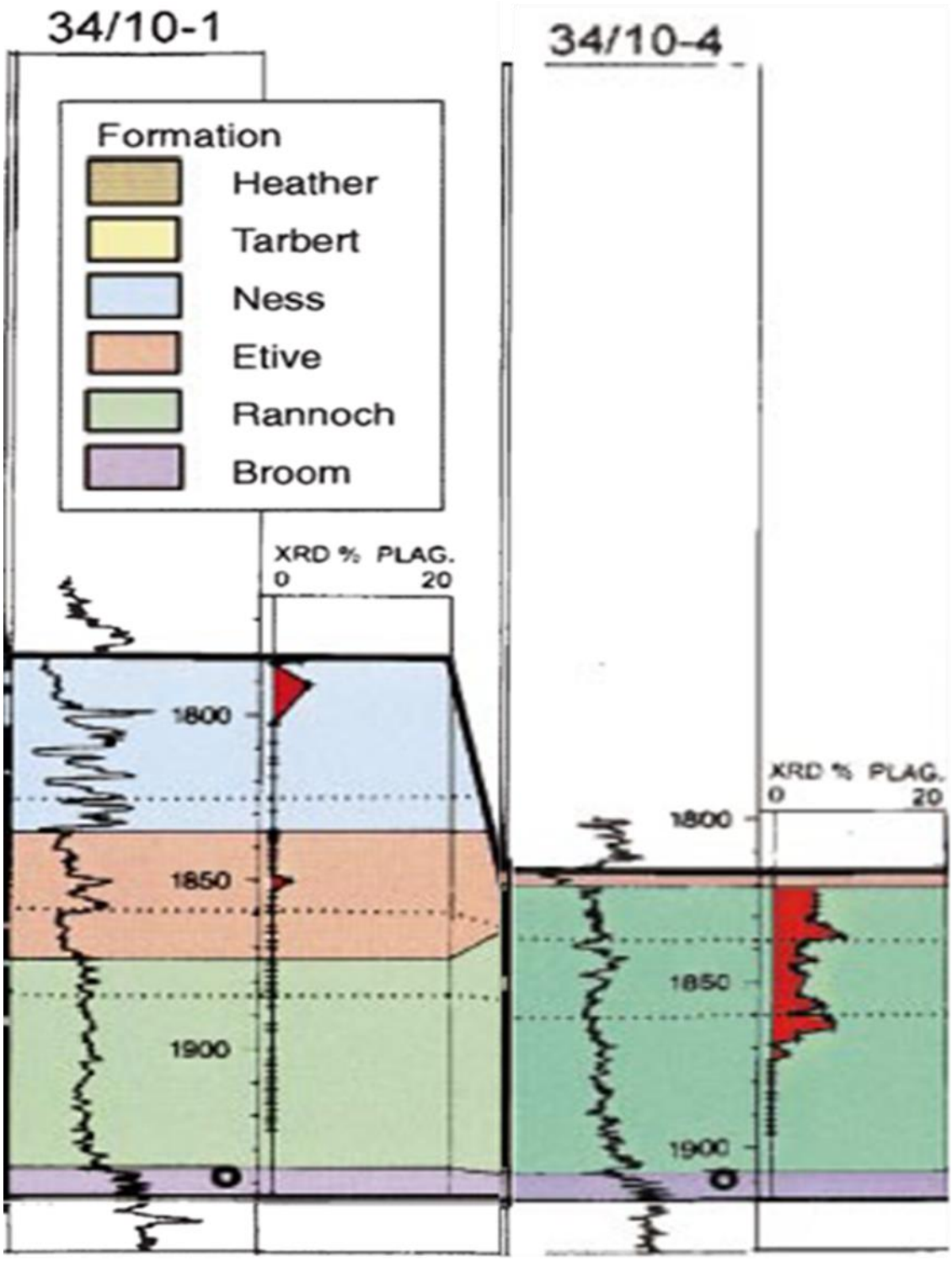

Figure 5-20. Vertical distribution of plagioclase within the Brent Group in Wells 34/10-1 and 34/10-4. The thick line above the coloured section indicates the Base-Cretaceous Unconformity. Modified from (Ehrenberg and Jakobsen, 2001).

5.6.1.2 Kalonite

The most common clay mineral identified within Rannoch sandstones in the three studied wells is kaolinite. In many cases kaolinite was observed in association with the altered and dissolved feldspar grains filling secondary pore spaces and usually appeared with a hint of the original grain outline (Figure 5-21 A). The evidence indicates that most of the observed kaolinite was formed in situ and related to late diagenetic processes (including euhedral booklets and high microporosity within kaolinite masses) (Figure 5-21 B and C). However, other types of kaolinite which may indicate early diagenetic or detrital origins were observed as well (Figure 5-21 D).

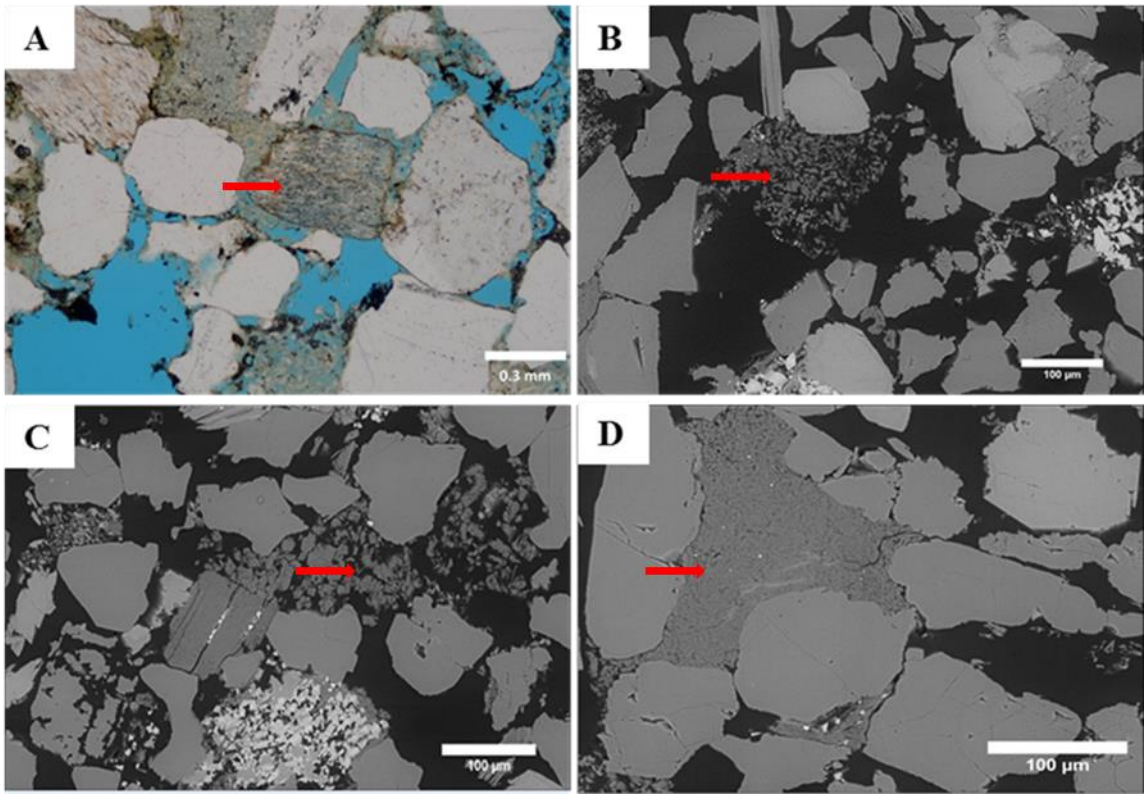

Figure 5-21. Thin-section photomicrographs and backscattered electron images: **A**. Photomicrographs showing kaolinite within a pore space; the shape and size of the filled pores indicate that this kaolinite has formed as a result of feldspar dissolution: Well 34/10-1, 1840.20 m. **B** and **C**. BSE images of euhedral booklets of kaolinite associated with high microporosity within kaolinite masses and indicating that kaolinite was formed in situ and related to late diagenetic processes: Well 34/10-4, 1830 m and Well 34/10-4, 1858.80 m, respectively. D. Aggregate of kaolinite booklets squeezed between grains and can be early diagenetic or detrital kaolinite: Well 34/10-4, 1830 m.

It was not feasible to distinguish the authigenic (in situ) kaolinite from the early diagenetic and/or detrital kaolinite and to detect the volume and distribution of kaolinite within the Rannoch Formation in each well. Therefore, the result of point counted clay minerals (Table 5-13) has been used to study the distribution patterns of clay (including kaolinite) below the Base-Cretaceous Unconformity in the area of study (Figure 5-22). The figure shows no obvious vertical trend in the distribution of clay (kaolinite) content toward the unconformity surface. If the formation or distribution of kaolinite was related to the presence of the Base-Cretaceous Unconformity or formed as a result of meteoric water penetrating through the unconformity surface, the kaolinite content should be much higher in Well 34/10-4 and Well 33/9-13 than in Well 34/10-1 and should increase upwards toward the unconformity surface.

Table 5-13. Petrographic analysis data of clay content below the Base-Cretaceous Unconformity in Wells 34/10-1, 34/10-4 and 33/9-13.

Well 34/10-1			Well 34/10-4			Well 33/9-13		
BCU at 1783 m			BCU at 1817 m			BCU at 2726.5 m		
Depth (m)	Distance from BCU (m)	Clay %	Depth (m)	Distance from BCU (m)	Clay %	Depth (m)	Distance from BCU (m)	Clay %
1877.65	94.6	0	1826.5	9.5	6	2732	5.5	0
1880.30	97	11	1835	18	7	2733.5	7	10
1916.30	133.3	8	1841.80	24.8	7	2738	11.5	7
			1843.10	26.1	0	2743.9	17.4	8
			1848.40	31.4	8	2750	23.5	7
			1868.10	51.1	6	2767.9	41.4	6
			1898	81	7			

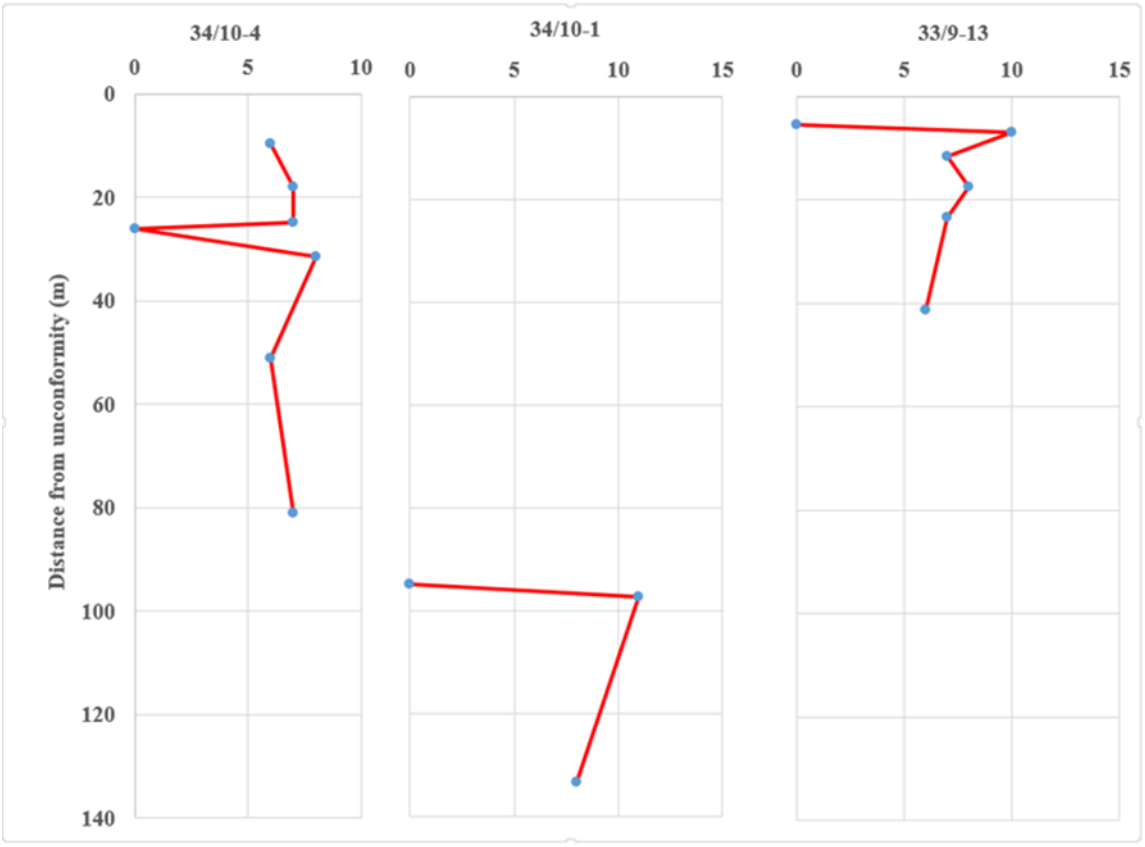

Figure 5-22. Distribution patterns of clay minerals (includes kaolinite) toward the Base-Cretaceous Unconformity in the Rannoch sandstones.

5.6.1.3 Carbonate Cement

The volume of carbonate cements in the Rannoch Formation ranged from 5% up to 19% in most samples, with the exception of some samples which were highly cemented and where calcite content reached 38% (Table 5-14). Counted calcite included early calcite cement formed as poikilotopic habits exhibiting early diagenetic processes filling the intergranular pores and supporting the detrital framework grains (Figure 5-23 A), and late calcite cement which formed due to the replacement of some feldspar grains or that had filled the dissolved pores after partial or complete dissolution of some feldspar grains (Figure 5-15 D and E). Siderite cement was observed in some samples as small crystals between the framework grains in association with calcite cement (Figure 5-23 B) or as rhombic crystals within the expanded grains of mica and filling the pore space, thus reducing the volume of porosity (Figure 5-16 A). Some of the calcite cements that had precipitated in the intergranular pores and in the intragranular pores had been dissolved; this may have occurred due to another phase of dissolution, which is interpreted to post-

date compaction (Figure 5-23 C and D). This dissolution of the calcite cements has led to the porosity enhancement of the Rannoch sandstones, whereas low porosity values were encountered in the sandstone samples that were tightly cemented by calcite.

No vertical systematic variation in the amount and distribution of carbonate cements (particularly calcite) toward the unconformity surface in the Rannoch sandstones were recognised (Figure 5-24). If there is relationship between the Base-Cretaceous Unconformity and the distribution and dissolution of carbonate cements in the Brent Group sandstones, systematic vertical change of the calcite toward the unconformity surface would be expected, and the amount of calcite cement should decrease upward toward the unconformity surface, particularly in samples closest to the unconformity surface.

Table 5-14. Volume and distribution of carbonate cements below the Base-Cretaceous Unconformity in Wells 34/10-1, 34/10-4 and 33/9-13.

Well 34/10-1			Well 34/10-4			Well 33/9-13		
BCU at 1783 m			BCU at 1817 m			BCU at 2726.5 m		
Depth (m)	Distance from BCU (m)	Carbonate % Calcite and Siderite	Depth (m)	Distance from BCU (m)	Carbonate % Calcite and Siderite	Depth (m)	Distance from BCU (m)	Carbonate % Calcite and Siderite
1877.65	94.6	30	1826.5	9.5	12	2732	5.5	38
1880.30	97	7	1835	18	11	2733.5	7	12
1916.30	133.3	12	1841.80	24.8	11	2738	11.5	5
			1843.10	26.1	49	2743.9	17.4	7
			1848.40	31.4	12	2750	23.5	10
			1868.10	51.1	14	2767.9	41.4	13
			1898	81	19			

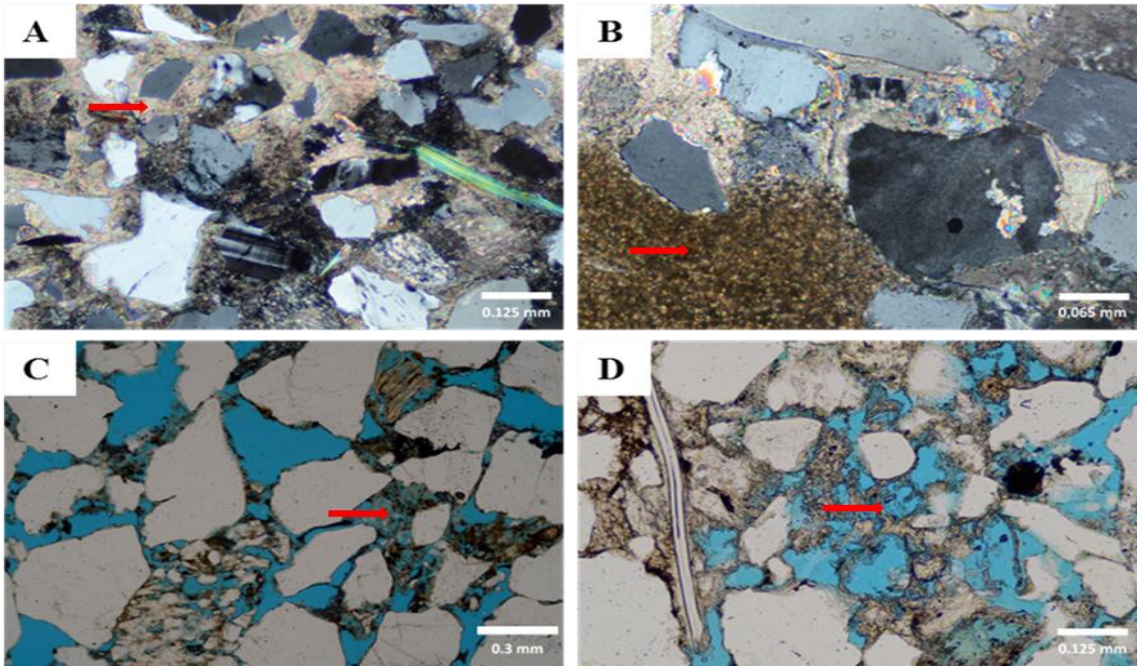

Figure 5-23. Optical micrograph images for the Rannoch sandstones: **A**. Calcite cement formed as poikilotopic habits illustrating early diagenetic process filling the intergranular pores and supporting the detrital framework grains: Well 33/9-13, 2732 m. **B**. Siderite appears in microcrystals size mixed with clay, brown-coloured, and associated with poikilotopic calcite cement: Well 34/10-4, 1843.10 m. **C** and **D**. Late dissolution of calcite cement which is interpreted to post-date compaction: Well 34/10-1, depth 1840.20 m and 1785.10 m respectively.

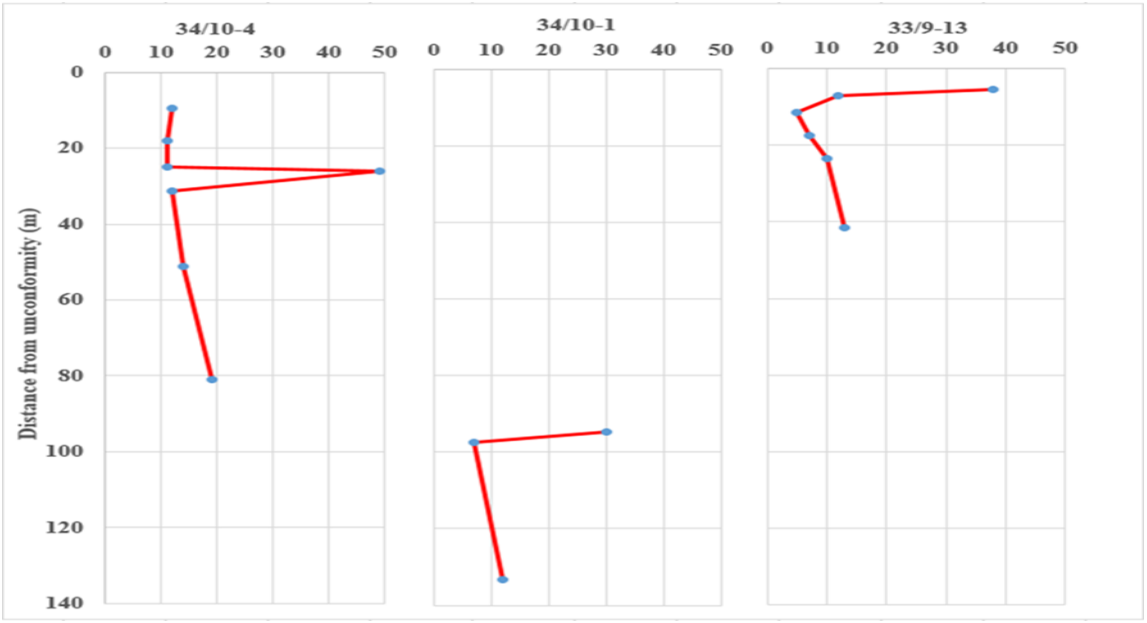

Figure 5-24. The distribution of carbonate cement under the Base-Cretaceous Unconformity in the three studied wells.

5.6.1.4 Porosity

Different types of porosity were observed within the studied samples of the Rannoch Formation. Primary porosity (intergranular) and secondary porosity, which includes: intragranular porosity formed due to the partial or complete dissolution of detrital grains (particularly feldspar), intragranular porosity formed by the dissolution of calcite cement and intercrystalline porosity (commonly microporosity) observed within and between kaolinite crystals. The point counted porosity values here included the total value of the different observed porosities, intergranular, intragranular and microporosity (Table 5-15). The correlation between measured core porosity and a visible point counted modal porosity for two of the studied wells shows that both porosity values are related (Figure 5-25).

Table 5-15. Value and distribution of porosities in the Rannoch Formation below the BCU.

Well 34/10-1			Well 34/10-4			Well 33/9-13		
BCU at 1783 m			BCU at 1817 m			BCU at 2726.5 m		
Depth (m)	Distance from BCU (m)	Porosity %	Depth (m)	Distance from BCU (m)	Porosity %	Depth (m)	Distance from BCU (m)	Porosity %
1877.65	94.6	15	1826.5	9.5	30	2732	5.5	1
1880.30	97	30	1835	18	28	2733.5	7	24
1916.30	133.3	30	1841.80	24.8	33	2738	11.5	24
			1843.10	26.1	1	2743.9	17.4	17
			1848.40	31.4	27	2750	23.5	25
			1868.10	51.1	26	2767.9	41.4	18
			1898	81	25			

A high percentage of intergranular porosity was observed in most of the analysed samples within the Rannoch sandstones; this porosity had been enhanced by the dissolution of carbonate cements (particularly calcite) and/or some detrital grains (particularly feldspars) (Figure 5-26). However, in many cases, the dissolution of feldspar grains was associated with precipitation of calcite cement (particularly in plagioclase) and/or formation of kaolinite, filling the produced intragranular pores and reducing the potential volume of enhanced secondary porosity.

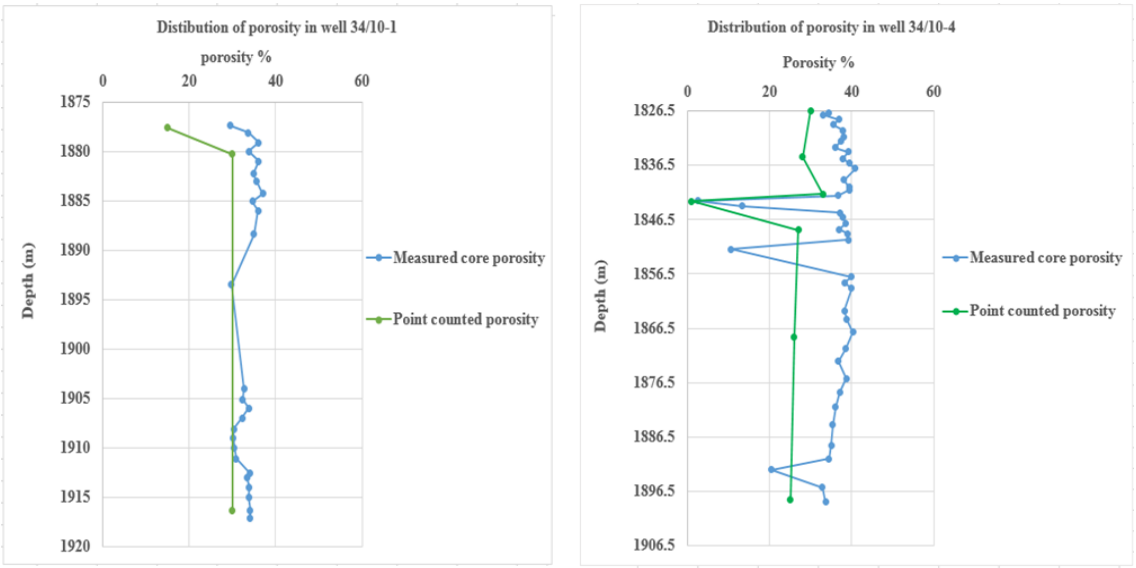

Figure 5-25. Positive correlation between measured core porosity and the point counted porosity for two of the studied wells, indicating that both porosity values are related.

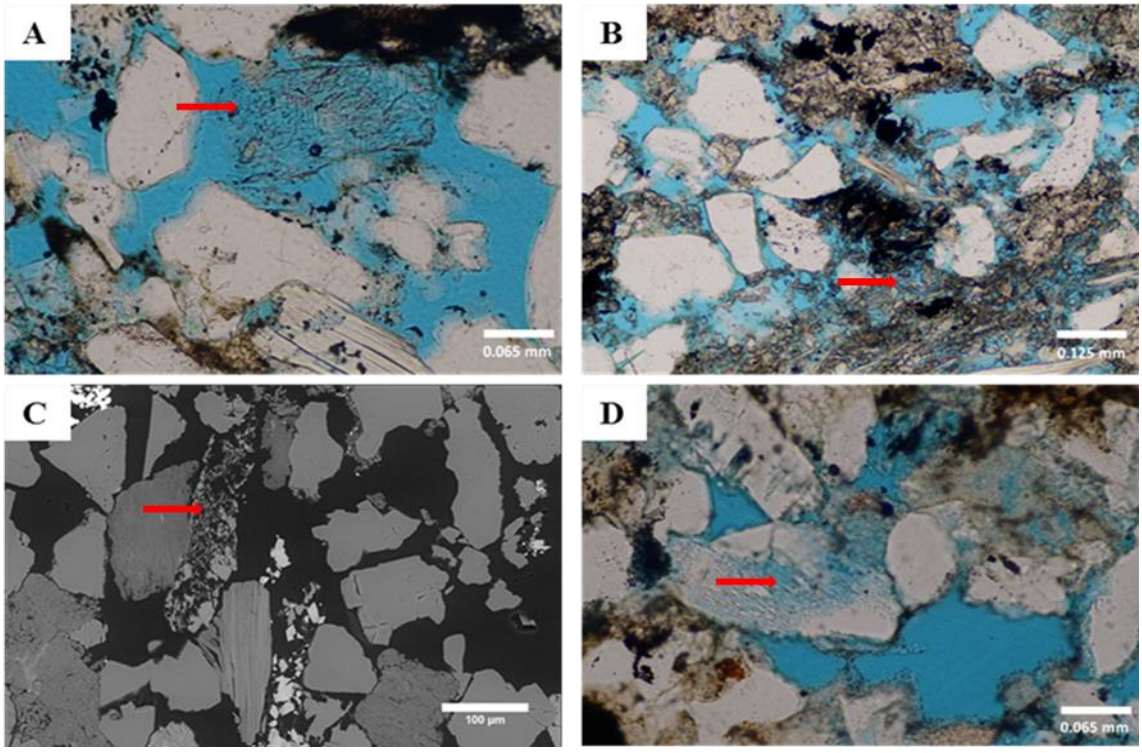

Figure 5-26. Degrees of dissolution of feldspar grains and/or carbonate cement and the formation of secondary porosity within the Rannoch Formation in the Brent Group. **A**. An almost complete dissolution of feldspar grain and enhancement of porosity: Well 33/9-13, 2733.5 m. **B**. Dissolution of carbonate cement (particularly calcite) and enhancement of porosity: Well 33/9-13, 2733.5 m. **C** and **D**. Feldspar grains dissolution and enhancement of porosity: Well 34/10-4, 1830 m and Well 34/10-1, 1916.30 m respectively.

The petrographic analysis results for the three studied wells indicate that the porosities of Rannoch sandstones may have negative correlation with carbonate cements (Figure 5-27), since the porosities are relatively high (> 30%) in the sandstone samples which have low values of carbonate cements and very low (< 1%) in the samples of sandstones which are tightly cemented by carbonate cements (commonly calcite). However, no systematic variation in the values and distribution of porosities toward the Base-Cretaceous Unconformity was observed (Figure 5-28).

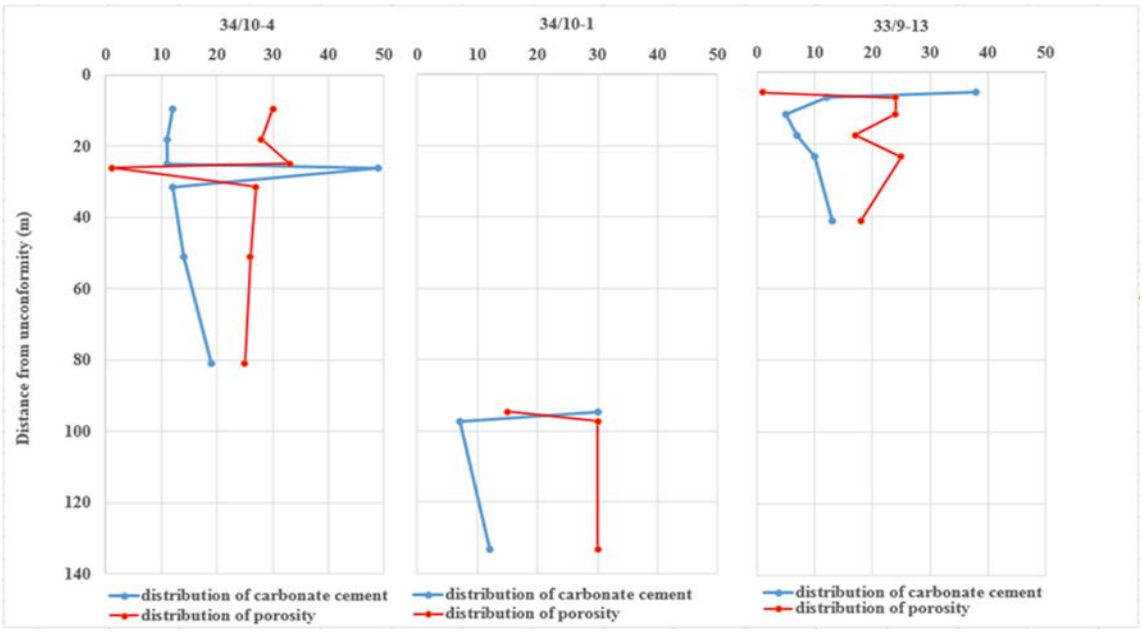

Figure 5-27. A negative correlation between porosity and carbonate cement in the Rannoch Formation.

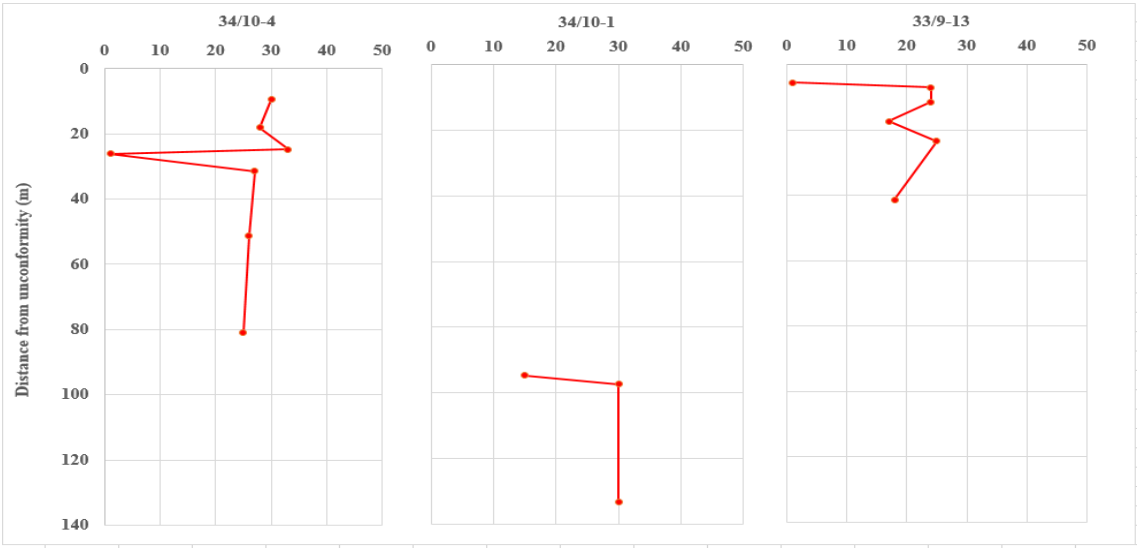

Figure 5-28. The distribution of porosity below the unconformity surface in the three studied wells.

5.6.2 Etive Formation

Nine sandstone samples were taken from two different wells to study the diagenetic effect of Base-Cretaceous Unconformity on the sandstones of the Etive Formation. The two studied wells were: Well 34/10-1 in the Gullfaks Field and Well 34/7-16 in the Vigdis Field to the north of the Gullfaks Field. The Base-Cretaceous Unconformity is situated at the top of the Etive Formation in Well 34/7-16 and about 57 m above the top of the Etive Formation in Well 34/10-1 and separated from the unconformity by the presence of the Ness and Tarbert Formations. Therefore, any possible diagenetic effect related to the unconformity surface should be detected and observed in the sandstone samples of Well 34/7-16 and should be higher than any possible effect in Well 34/10-1. Distribution of minerals and porosity in this formation were investigated in each well and compared with those of the other well to study the possible diagenetic effects of the Base-Cretaceous Unconformity on the Etive sandstones.

5.6.2.1 Feldspar

Most of the studied samples of the Etive Formation were taken from Well 34/7-16, starting from the closest point to the Base-Cretaceous Unconformity. However, other samples were taken from Well 34/10-1 for correlation and comparison between the two wells. In both wells, the volume of feldspar in the Etive Formation ranged between 5 – 9% (Table 5-16).

Table 5-16. Petrographic analysis data of feldspar content below the Base-Cretaceous Unconformity in Wells 34/10-1 and 34/7-16.

Well 34/10-1			Well 34/7-16		
BCU at 1783 m			BCU at 2390 m		
Depth (m)	Distance from BCU (m)	Feldspar %	Depth (m)	Distance from BCU (m)	Feldspar %
1840.20	57.2	6	2390.07	0.07	7
1867.70	84.7	5	2390.65	0.65	5
			2393.80	3.8	8
			2409.10	19.1	8
			2410.80	20.8	7
			2416.70	26.7	8
			2429.80	39.8	9

Although the Base-Cretaceous Unconformity occurs at the top of the Etive Formation in Well 34/7-16, the feldspar content was not less than in Well 34/10-1, where the Base-Cretaceous Unconformity lies more than 57 m above the top of the Etive Formation, with the presence of two other formations between the unconformity and the Etive Formation. Furthermore, alteration and partial to complete dissolution of the feldspar grains were observed in both wells (Figure 5-29 A and B), whereas, if the dissolution of feldspar grains was caused by the penetration of meteoric water through the Base-Cretaceous Unconformity, systematic vertical change of the feldspar volume toward the unconformity would be expected and the amount of altered and dissolved feldspar grains should be much higher in Well 34/7-16 than in Well 34/10-1.

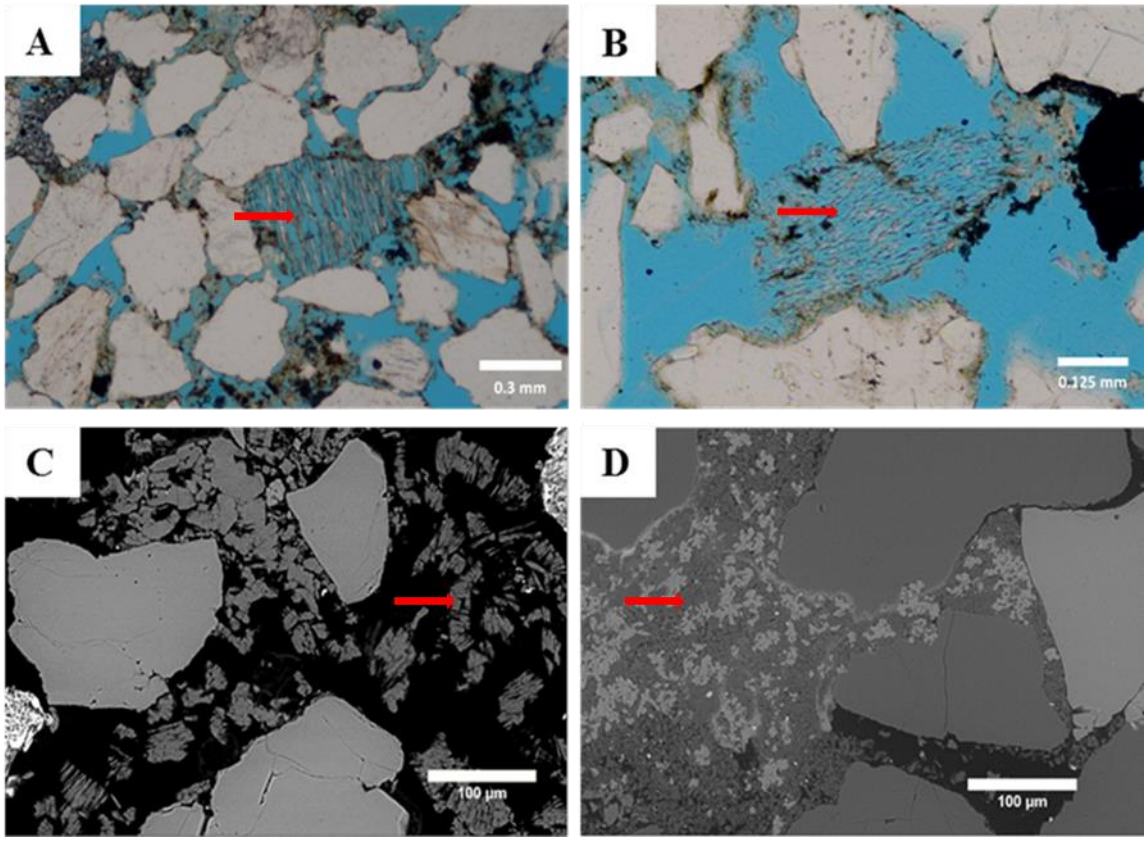

Figure 5-29. **A** and **B**. Showing dissolution of feldspar grains and enhancement of porosity in Wells 34/10-1, 1840.20 m and 34/7-16, 2393.80 m, respectively. **C**. BSE showing euhedral booklet of kaolinite formed in situ in Well 34/7-16, 2416.70 m. **D**. BSE showing early diagenetic or detrital kaolinite squeezed between grains in Etive Formation of Well 34/7-16, 2416.70 m.

On the other hand, a shale layer was observed within the Etive Formation at depth 2409 m in Well 34/7-16, separating the upper part of the Etive sandstone from the lower part. This shale layer is expected to have acted as a barrier preventing the meteoric water from moving downward from the unconformity surface to the lower part of the Etive sandstone and therefore preventing the possible diagenetic effect of the unconformity on the distribution and dissolution of feldspar grains below this layer. As this is not the case, and because no vertical systematic change toward the unconformity surface was observed (Figure 5-30), it seems unlikely that the distribution and dissolution of feldspar grains in the Etive Formation was caused by a diagenetic process related to the unconformity.

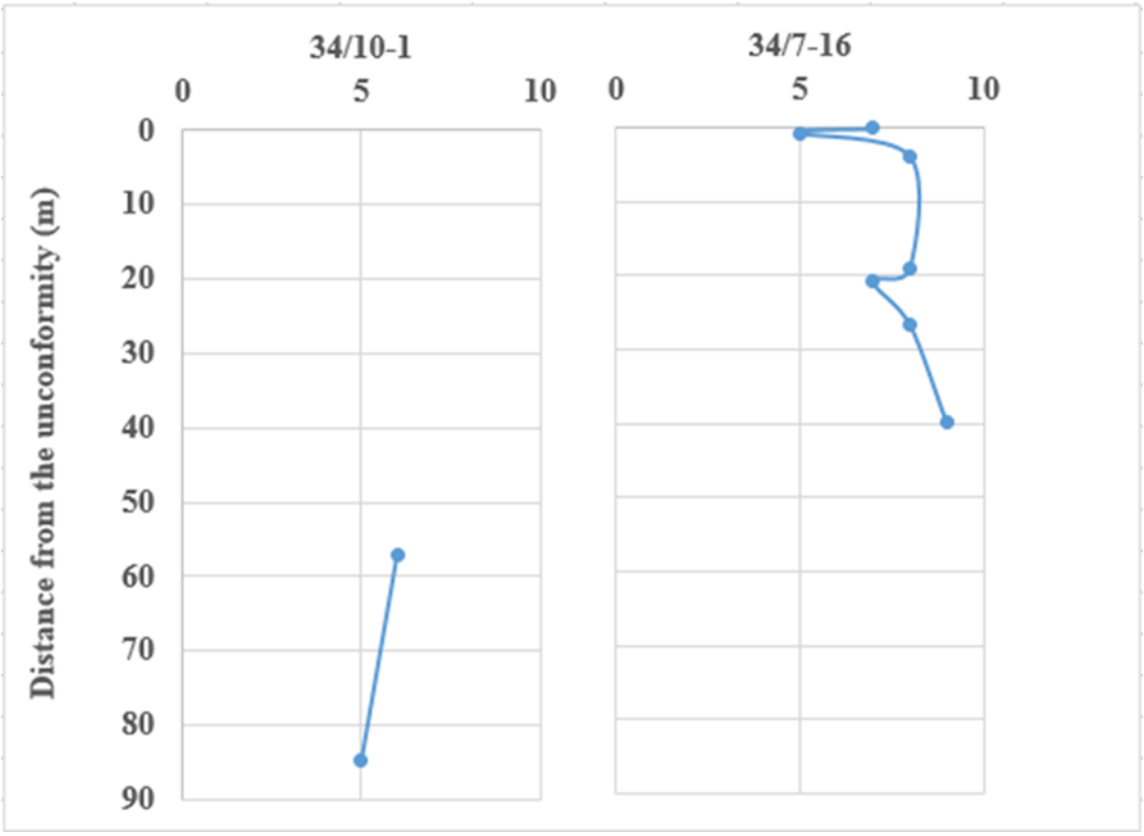

Figure 5-30. The distribution of feldspar grains within Etive Formation below the BCU in the two studied wells for Etive Formation.

5.6.2.2 Kaolinite

Kaolinite is the dominant clay mineral within the Etive Formation in both the studied wells. Therefore, the result for point counted clay minerals within the Etive Formation (Table 5-17) has been used to obtain the vertical distribution patterns of clay (including kaolinite) below the Base-Cretaceous Unconformity. Two types of kaolinite were

observed: in situ kaolinite, formed in association with the altered and dissolved feldspar grains or filling the produced pore spaces, and/or detrital or early diagenetic kaolinite, intermixed with other clay minerals between adjacent framework grains, filling pore spaces (Figure 5-29 C and D). The distribution and content of kaolinite in the Etive Formation in Wells 34/7-16 and 34/10-1 is plotted in Figure 5-31. Although the Base-Cretaceous Unconformity is situated at the top of the Etive Formation in Well 34/7-16, the volume of kaolinite in this well is not higher than the volume of kaolinite in Well 34/10-1, where the Base-Cretaceous Unconformity is situated more than 57 m above the top of the Etive Formation. Moreover, there was no systematic variation in the values of kaolinite toward the unconformity surface in both wells. If the formation or distribution of the kaolinite was related to the presence of the Base-Cretaceous Unconformity or formed as a result of meteoric water penetrating through the unconformity surface, the kaolinite content should be much higher in Well 34/7-16 compared with that in Well 34/10-1 and should be increasing upward towards the unconformity surface.

Table 5-17. Petrographic analysis data of clay content (includes kaolinite) below the Base-Cretaceous Unconformity in Wells 34/10-1 and 34/7-16.

Well 34/10-1			Well 34/7-16		
BCU at 1783 m			BCU at 2390 m		
Depth (m)	Distance from BCU (m)	Clay %	Depth (m)	Distance from BCU (m)	Clay %
1840.20	57.2	5	2390.07	0.07	4
1867.70	84.7	6	2390.65	0.65	7
			2393.80	3.8	7
			2409.10	19.1	5
			2410.80	20.8	3
			2416.70	26.7	4
			2429.80	39.8	8

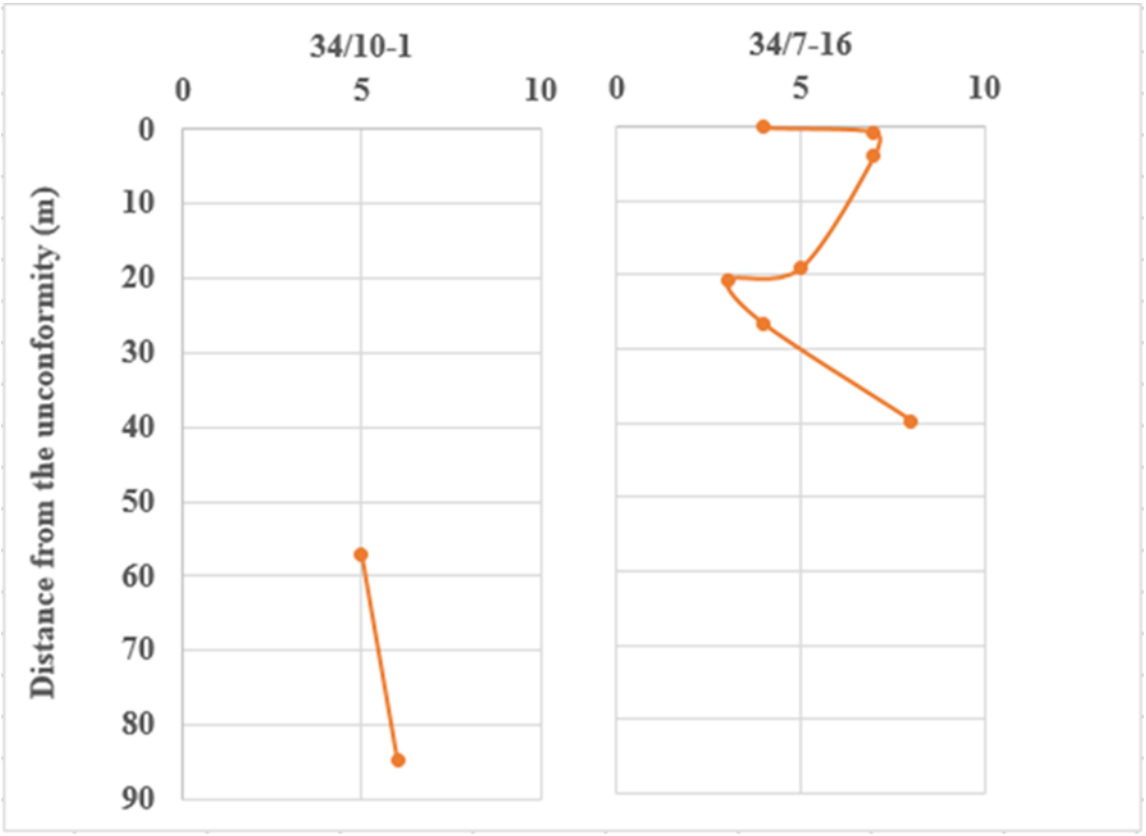

Figure 5-31. Distribution of clay minerals (includes kaolinite) toward the Base-Cretaceous Unconformity for the Etive sandstones in both wells.

5.6.2.3 Carbonate Cement

The volume of carbonate cements in the Etive Formation ranged from 3% up to 7% in both studied wells, with exception of some samples which were highly cemented when it reached 31% (Table 5-18). No pattern of carbonate cementation was observed in the Etive sandstones. This may attributed to the variation in the depositional composition of sandstones (Figure 5-32). For instance, at depth 2390.07 m in Well 34/7-16, the content of calcite cement in sample 1, which was situated directly below the Base-Cretaceous Unconformity was much higher than the rest of samples, which were located more than 20 m below the unconformity surface and separated from the above sample by a shale layer. Furthermore, the dissolution of carbonate cements increased downward, where high degradation and dissolution of calcite cement were observed. If this distribution and dissolution of calcite cement in the Etive sandstone was related to the diagenetic effect of the Base-Cretaceous Unconformity, the opposite trend would be expected, and the

amount of calcite cement should decrease upward toward the unconformity surface, particularly in samples closest to the unconformity surface.

Table 5-18. Petrographic analysis data of carbonate cement content below the Base-Cretaceous Unconformity in Wells 34/10-1 and 34/7-16.

Well 34/10-1			Well 34/7-16		
BCU at 1783 m			BCU at 2390 m		
Depth (m)	Distance from BCU (m)	Carbonate % Calcite and Siderite	Depth (m)	Distance from BCU (m)	Carbonate % Calcite and Siderite
1840.20	57.2	7	2390.07	0.07	31
1867.70	84.7	6	2390.65	0.65	3
			2393.80	3.8	5
			2409.10	19.1	7
			2410.80	20.8	6
			2416.70	26.7	10
			2429.80	39.8	5

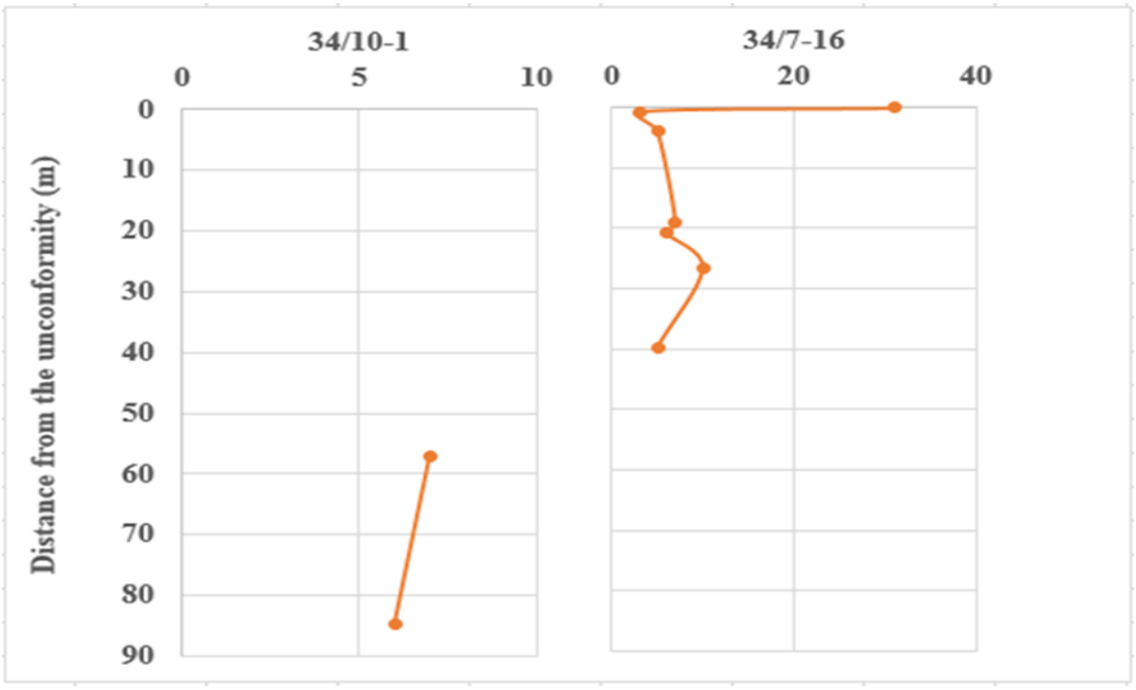

Figure 5-32 Distribution patterns of carbonate cement toward the Base-Cretaceous Unconformity for the Etive sandstones in both wells.

5.6.2.4 Porosity

The petrographic analysis results for the two studied wells showed high variation in the porosity values, which ranged between 7-40%. This included the different observed porosities, intergranular, intragranular and microporosity (Table 5-19). This variation in the value of porosities is most likely to be related to amount of carbonate cement, since the porosities were relatively high (> 40%) in the sandstone samples which had low values of carbonate cements and were low (< 7%) in the sandstone samples which were tightly cemented by carbonate cements (commonly calcite). In addition to that, it is worth mentioning that the very high porosity observed in some samples (such as the sample at depth 1867.70 in Well 34/10-1) may be related to sample preparation issues and do not reflect the correct value of porosity. However, in general, no clear pattern of variation in the porosities toward the Base-Cretaceous Unconformity was recognised (Figure 5-33). Furthermore, despite the presence of a shale layer within the Etive Formation which separates the lower part of the formation from any connection with possible digenetic processes related to the unconformity surface, no variation in the porosities between the two sandstone units were observed. More dissolution and higher porosities would be expected in the upper unit if the secondary porosity was formed by diagenetic process related to the Base-Cretaceous Unconformity.

Table 5-19. Petrographic analysis data of porosities volume below the Base-Cretaceous Unconformity in wells 34/10-1 and 34/7-16.

Well 34/10-1			Well 34/7-16		
BCU at 1783 m			BCU at 2390 m		
Depth (m)	Distance from BCU (m)	Porosity %	Depth (m)	Distance from BCU (m)	Porosity %
1840.20	57.2	22	2390.07	0.07	7
1867.70	84.7	40	2390.65	0.65	37
			2393.80	3.8	28
			2409.10	19.1	26
			2410.80	20.8	24
			2416.70	26.7	20
			2429.80	39.8	22

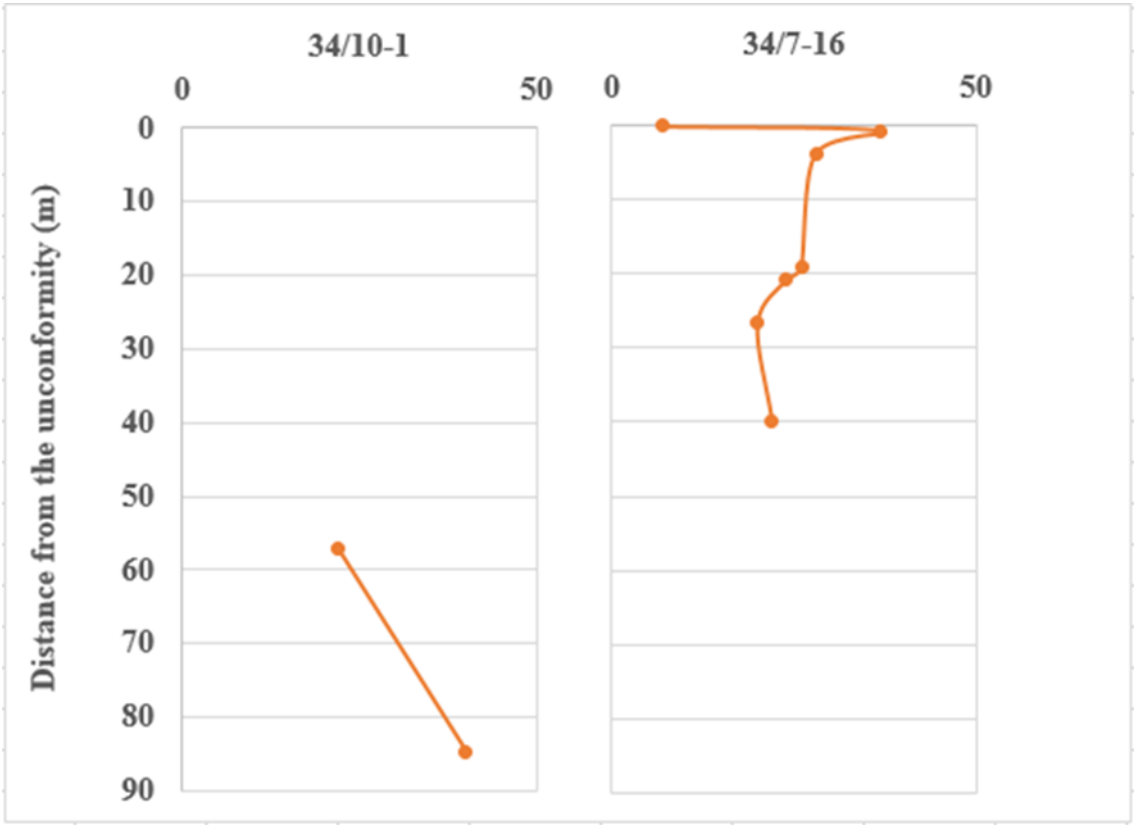

Figure 5-33. The distribution of total porosity in the Etive Formation below the Base-Cretaceous Unconformity.

5.6.3 Tarbert Formation

18 sandstone samples distributed between six wells in the area of study were taken from the Tarbert Formation to study the possible diagenetic effect of the Base-Cretaceous Unconformity. The main mineralogy composition of Tarbert Formation in these wells has been mentioned in section 5.5.3 above. This section deals with the distribution of these minerals and porosities in Tarbert Formation to examine the possible diagenetic effect of the Base-Cretaceous Unconformity.

5.6.3.1 Feldspar

The contents of feldspar in the Tarbert Formation were 4-14% in the six studied wells (Table 5-20). Partial to complete dissolution of the feldspar grains was observed in the six studied wells. There is no obvious pattren of variation in distribution of feldspar below the unconformity surface (Figure 5-34). For example, altough the Base-Cretaceous Unconformity is located at the top of Tarbert Formation in Wells 34/10-1 and 34/10-8, the content and rate of feldspar dissolution did not show systematic vertical decrease

toward the Base Cretacous Unconformity. On the other hand, in Wells 34/10-34 and 34/7-19, where the Base-Cretaceous Unconformity is located 4.5 m and 14.4m respectivly above the top of the Tarbert Formation, the content of feldspar grains seems to be increasing downward. In both of these wells shales of Heather Formation lie between the top of the Tarbert Formation and the unconformity surface. Therefore, this variation in the content of feldspar grains can be interpreted as primary depositional characteristics and reflect varition in sand composition.

Table 5-20. Petrographic analysis data of feldspar content below the Base-Cretaceous Unconformity in six studied wells.

Well 34/10-1		Well 34/10-8		Well 34/10-34		Well 34/7-19		Well 34/7-20		Well 30/6-10A	
BCU at 1783 m		BCU at 1821 m		BCU at 1990.5 m + BHU at 1992.5 m		BCU at 2439.5 m + BHU at 2453.80 m		BHU at 2612.5 m		BHU at 2480 m	
Depth (m)	Feldspar %	Depth (m)	Feldspar %	Depth (m)	Feldspar %	Depth (m)	Feldspar %	Depth (m)	Feldspar %	Depth (m)	Feldspar %
1783.10	6	1823.3	6	1995	7	2453.9	4	2612.8	7	2480	11
1784	6	1824.5	6	2000	8	2455.6	7	2615.5	14	2483.5	12
1785.10	6	1846.4	6	2009	9	2465.5	9	2620.5	10		

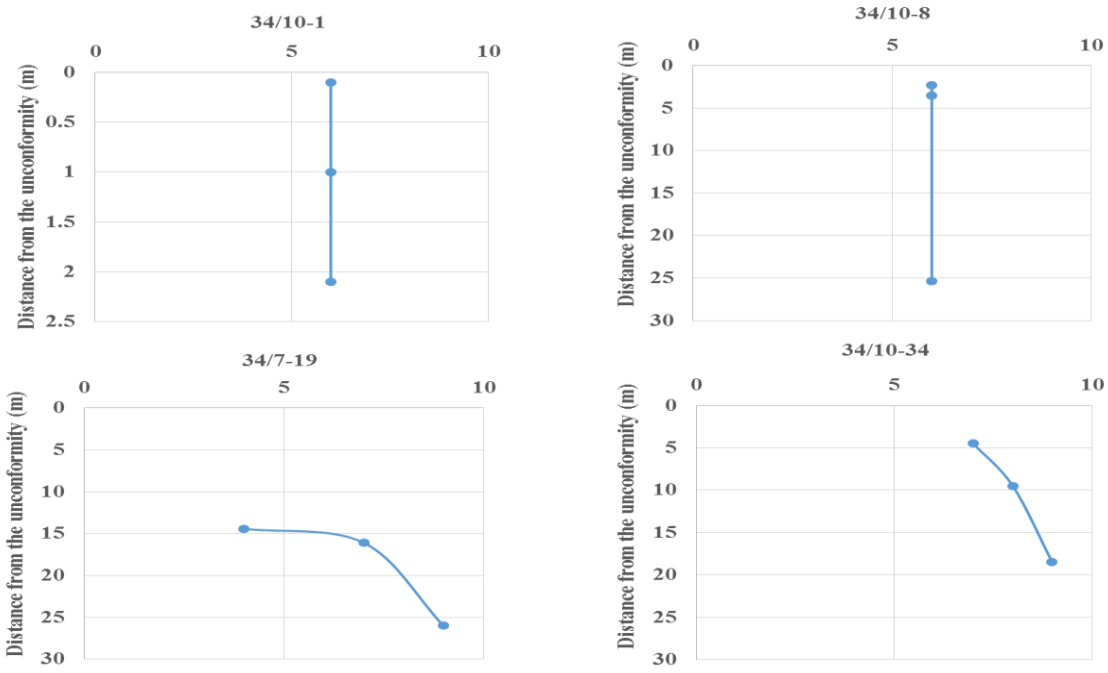

Figure 5-34. Feldspar contents below the Base-Cretaceous Unconformity in four of the six studied wells.

5.6.3.2 Kaolonite

The most dominant clay type in the 18 sandstone samples of the Tarbert Formation was kaolinite, with content of 0-19%, and up to 27% in very coarse sandstone samples in Well 34/7-19 kaolinite (Table 5-21). Most of the observed kaolinite was formed as a result of alteration and replacment of feldspar grains and filling of the produced pore spaces. Although the Base-Cretaceous Unconformity lies directly at the top of the Tarbert Formation in Wells 34/10-1 and 34/10-8, their kaolinite content was not higher than in sediments in Wells 34/10-34 and 34/7-19, where the Base-Cretaceous Unconformity is located 4.5 m and 14.4 m respectivly above the top of the Tarbert Formation (Figure 5-35). In both of these wells, shales of the Heather Formation lie between the top of Tarbert Formation and the unconformity surface. In addition to that, Well 34/10-34 shows a downward increase in the content of kaolinite, whereas if the formation of kaolinite is related to the diagenatic processes of the Base-Cretaceous Unconformity the opposite trend would be expected (Figure 5-35).

Table 5-21. Petrographic analysis data of clay (commonly kaolinite) content below the Base-Cretaceous Unconformity in the Tarbert Formation within the six studied wells.

Well 34/10-1		Well 34/10-8		Well 34/10-34		Well 34/7-19		Well 34/7-20		Well 30/6-10A	
BCU at 1783 m		BCU at 1821 m		BCU at 1990.5 m BHU at 1992.5 m		BCU at 2439.5 m BHU at 2453.80 m		BHU at 2612.5 m		BHU at 2480 m	
Depth (m)	Clay %	Depth (m)	Clay %	Depth (m)	Clay %	Depth (m)	Clay %	Depth (m)	Clay %	Depth (m)	Clay %
1783.10	5	1823.30	8	1995	3	2453.9	27	2612.8	8	2480	6
1784	0	1824.5	14	2000	7	2455.6	19	2615.5	5	2483.5	5
1785.10	3	1846.40	14	2009	8	2465.5	15	2620.5	7		

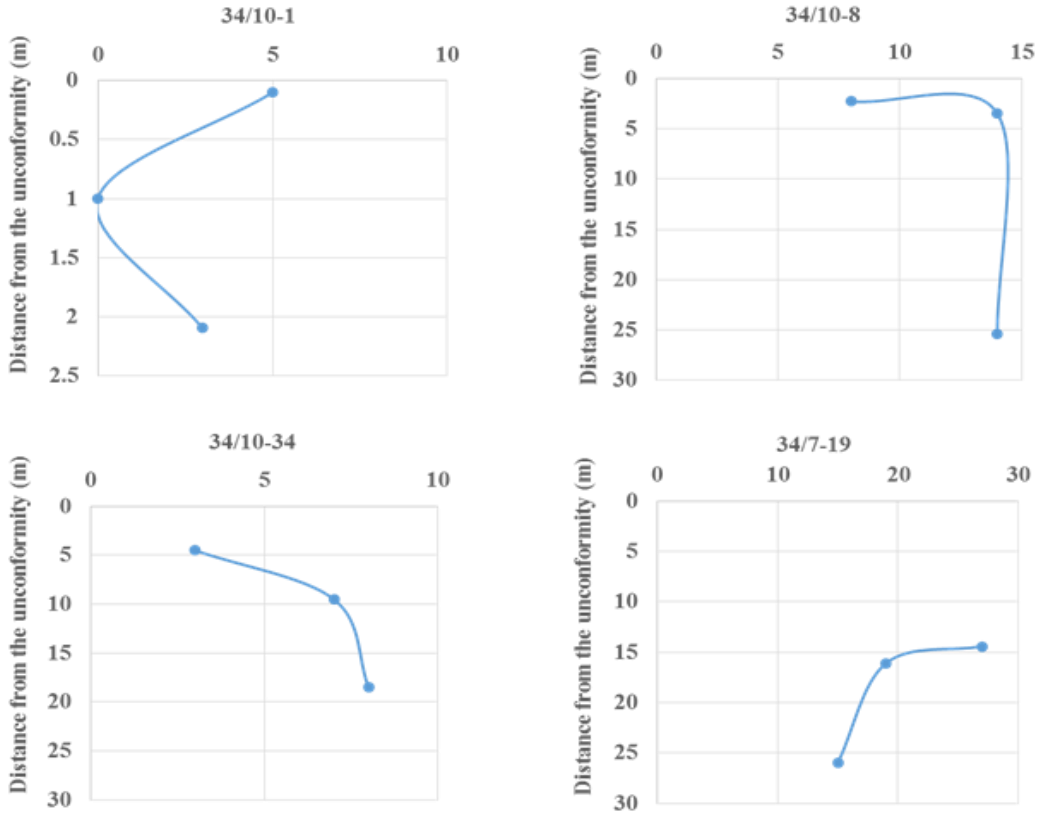

Figure 5-35. The distribution of clay (particularly kaolinite) below the Base-Cretaceous Unconformity in the Tarbert Formation within four of the six studied wells.

5.6.3.3 Carbonate Cement

No vertical systematic variation in the amount and distribution of carbonate cements (particularly calcite) toward the unconformity surface were recognised in the Tarbert sandstones of the studied wells (Table 5-22). Some sandstone samples were tightly cemented by calcite cements, >45% (such as sample 2, depth 1784 m in Well 34/10-1) and others were poorly cemented, <7% (such as sample 2, depth 1823.30 m in Well 34/10-8); in both cases the samples were taken 1 m and 2.3 m respectively below the Base-Cretaceous Unconformity. A systematic decrease of the carbonate cements toward the unconformity surface is expected, especially in samples closest to the unconformity surface. However, the distribution of carbonate cements below the unconformity surface in the Tarbert Formation was not found to be systematic (Figure 5-36) and was most likely to have been formed as a result of the variation in the depositional composition of the sandstones and not related to the diagenetic effect of the Base-Cretaceous Unconformity.

Table 5-22. Petrographic analysis data of carbonate cement (commonly calcite) content below the Base-Cretaceous Unconformity in four of the six studied wells.

Well 34/10-1		Well 34/10-8		Well 34/10-34		Well 34/7-19	
BCU at 1783 m		BCU at 1821 m		BCU at 1990.5 m BHU at 1992.5 m		BCU at 2439.5 m BHU at 2453.80 m	
Depth (m)	Carbonate % Calcite and Siderite	Depth (m)	Carbonate % Calcite and Siderite	Depth (m)	Carbonate % Calcite and Siderite	Depth (m)	Carbonate % Calcite and Siderite
1783.10	15	1823.30	7	1995	11	2453.9	3
1784	45	1824.5	11	2000	19	2455.6	3
1785.10	22	1846.40	6	2009	6	2465.5	5

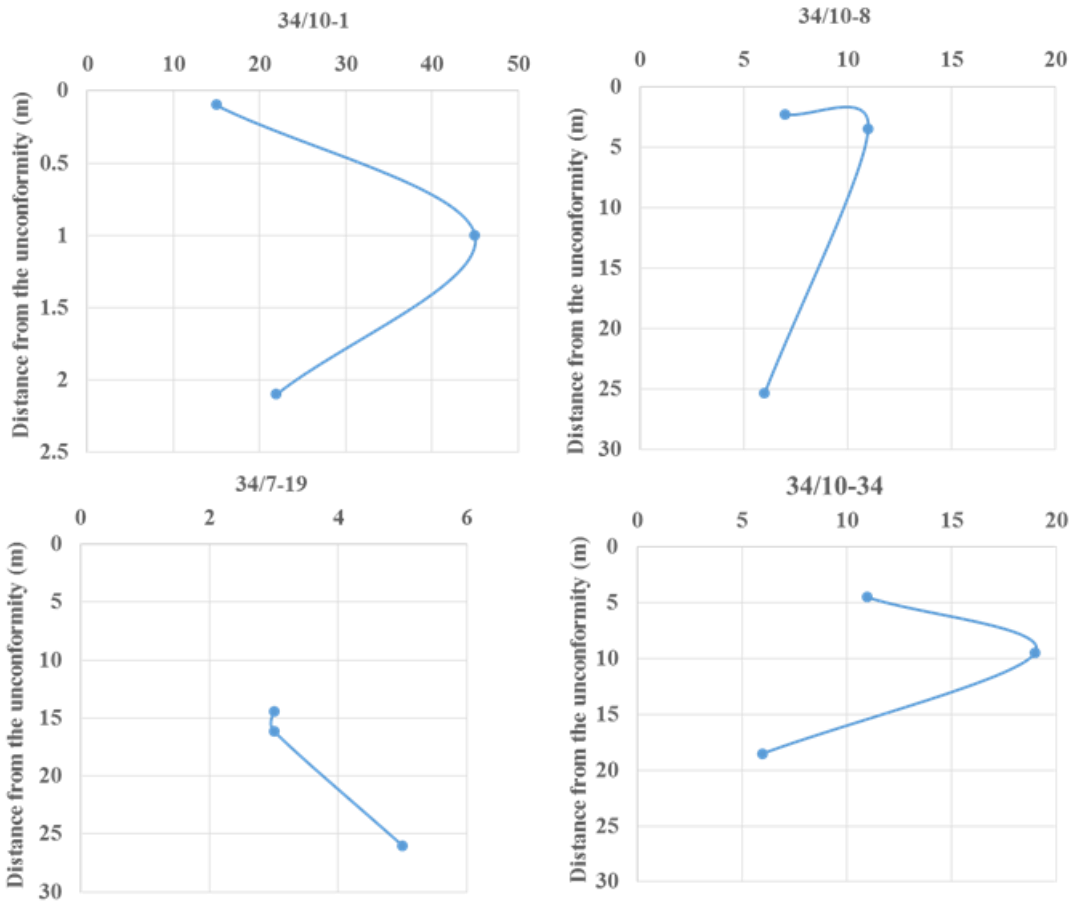

Figure 5-36. Carbonate cement distribution (commonly calcite) below the Base-Cretaceous Unconformity in four of the six studied wells.

5.6.3.4 Porosity

High variations in the value of porosity were recognised in the Tarbert sandstones; this included the different observed porosity types, intergranular, intragranular and microporosity (Table 5-23). Samples with high porosity value are commonly associated with the dissolution of carbonate cements (particularly calcite) and/or some detrital grains (particularly feldspars), forming intragranular porosity. However, in many cases, this dissolution was associated with precipitation of calcite cement and/or formation of kaolinite filling the produced intragranular pores and reducing the potential volume of enhanced secondary porosity. For example, in Well 34/10-1, the porosity of the Tarbert sandstones was very low, < 1% in the carbonate cemented sandstone samples, and was higher (> 22%) in the sandstone samples with lower amounts of carbonate cements.

The petrographic analysis results for the six studied wells indicate that there was no systematic variation in the values and distribution of porosities toward the Base-Cretaceous Unconformity (Figure 5-37). Thus, the distribution of porosities in the Tarbert Formation is most likely to be related to the variation of the sandstones' composition and mainly controlled by the dissolution of some minerals and precipitation of others.

Table 5-23. Petrographic analysis data of the porosities volume below the Base-Cretaceous Unconformity in six studied wells.

Well 34/10-1		Well 34/10-8		Well 34/10-34		Well 34/7-19		Well 34/7-20		Well 30/6-10A	
BCU at 1783 m		BCU at 1821 m		BCU at 1990.5 m BHU at 1992.5 m		BCU at 2439.5 m BHU at 2453.80 m		BHU at 2612.5 m		BHU at 2480 m	
Depth (m)	Porosity %	Depth (m)	Porosity %	Depth (m)	Porosity %	Depth (m)	Porosity %	Depth (m)	Porosity %	Depth (m)	Porosity %
1783.10	20	1823.30	25	1995	25	2453.9	12	2612.8	20	2480	18
1784	0	1824.5	7	2000	18	2455.6	14	2615.5	22	2483.5	18
1785.10	22	1846.40	14	2009	24	2465.5	24	2620.5	18		

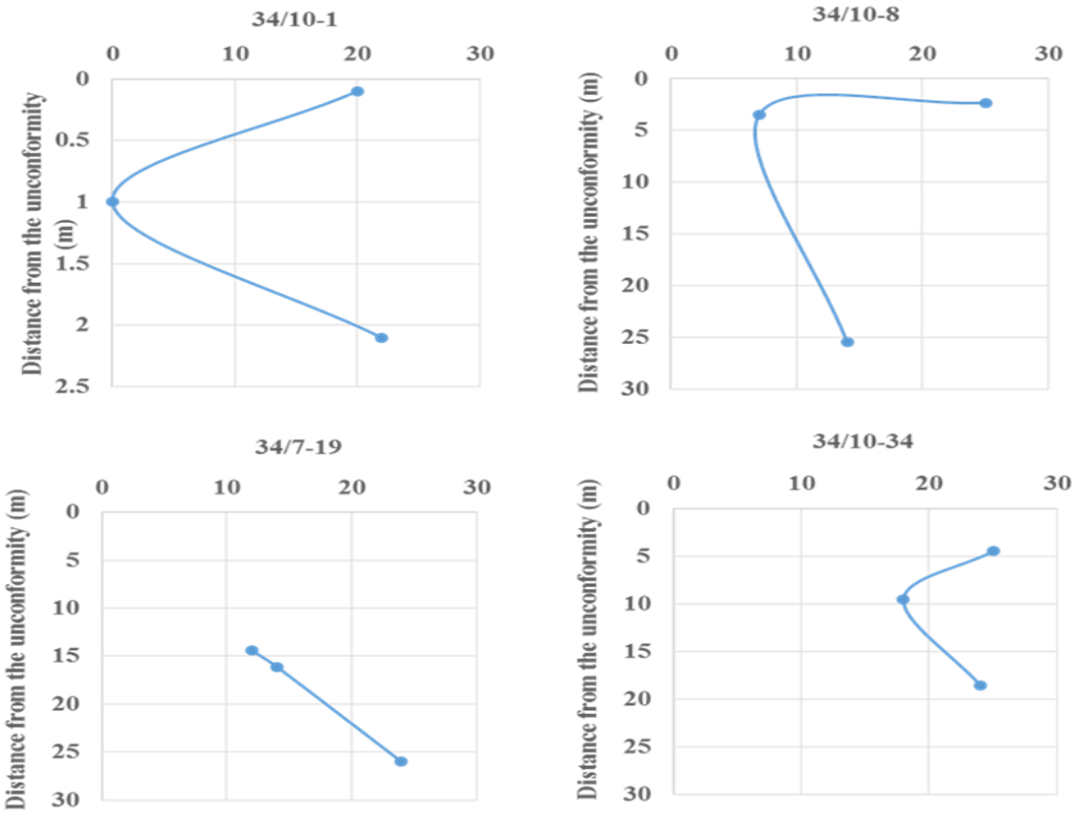

Figure 5-37. Distribution of porosity below the Base-Cretaceous Unconformity in four of the six studied wells.

5.7 Discussion of results

The effect of diagenesis on the spatial and temporal distribution of minerals and porosity in the Brent Group sandstones underneath the Base-Cretaceous Unconformity has been studied. Although it is difficult to detect the duration and exact time of the diagenetic processes, paragenetic phases for diagenetic alterations have been established based on the petrographic composition and textural relationships and by investigating the different potential mechanisms that may cause dissolution of minerals and precipitation of others in the Brent Group.

5.7.1 Potential mechanisms for the dissolution of minerals and precipitation of others in the Brent Group

According to (Ehrenberg and Jakobsen, 2001), four common mechanisms may explain and can be considered for the nature and timing of post-depositional framework grains and cement dissolution in sandstone sediments:

1. Influx of meteoric water shortly after the deposition of sediments
2. Influx of meteoric water during erosion or Late Jurassic uplift
3. Influx of acidic components produced by thermal maturation of organic matter or by addition of CO_2 that may form as a result of thermal maturation of organic matter
4. By release of organic acid and CO_2 that may form as a result of oil biodegradation.

These mechanisms were explained in detail in Chapter 4, section 4.6.1.

5.7.2 Origin and timing of dissolution and production of secondary porosity

Detailed petrographic analysis showed that there are several lines of evidence for the creation of secondary porosity in the studied Middle Jurassic Brent Group sandstones (as mentioned in section 5.6 above). This porosity was formed mainly due to the partial or complete dissolution of feldspar grains and/or carbonate cements (particularly calcite). This dissolution was observed in most of the analysed samples and was the main cause of secondary porosity. As mentioned before, this post-depositional dissolution of feldspar grains and carbonate cements may be caused by several mechanisms; this section will discuss the four possible scenarios that may explain the origin and timing of the post-depositional dissolution in the Brent Group sandstones, including the influx of meteoric water through the Base-Cretaceous Unconformity.

5.7.2.1 The first scenario: The influx of meteoric water shortly after the deposition of sediments

Similar results to case study 4 were obtained from this case study. In line with the discussion on section 4.6.2.1, the assumption of Acidic meteoric water affecting the rocks shortly after their deposition and burial, leading to dissolution of unstable minerals and enhancement of porosity was again disproved. This is based on the following findings:

Firstly, the ability of meteoric water to leach and dissolve minerals is most likely to be limited and decrease with depth, because meteoric water when start to penetrate will usually be under-saturated and with interaction between these waters and minerals the water will rapidly become saturated (Bjorlykke and Aagaard, 1992).

Secondly, if penetration of acidic meteoric water occurring directly after deposition of Middle Jurassic Brent Group sediments is the main reason for the observed dissolution of minerals, the produced secondary pores would be most likely to be destroyed by compaction processes, whereas oversized secondary pores which were almost the same size as the other surrounding framework grains were observed within many of the analysed samples of Brent Group sandstones (Figure 5-17 A and C). It is difficult to explain why these oversized pores have not been affected by compaction, despite the current depth of burial, which exceeds 2700 m in some wells.

Thirdly, the petrographic analysis results show that some of the dissolved feldspar grains have been replaced by kaolinite; the generated kaolinite is located within the produced pore space and associated with microporosity, indicating no signs of compaction, despite the depth of burial. Furthermore, in some samples oversized pores and/or booklets of kaolinite associated with microporosity that have not been affected by compaction process were observed, with some compaction signs within the same field of view (Figure *5-21* A and B), indicating that this dissolution and formation of kaolinite within the secondary pores is most likely to be late dissolution and post-date the compaction process.

All this cumulative evidence disproves the possibility that the observed dissolution of feldspar grains and/or carbonate cements and enhancement of porosity in Brent Group sandstones were caused by the influx of meteoric water shortly after the deposition of Middle Jurassic Brent Group sediments.

5.7.2.2 The second scenario: The influx of meteoric water during erosion or uplift

Late diagenetic processes (telodiagensis) are expected to occur when sedimentary rocks which have undergone early (eogenetic) and mid-diagenetic (mesogenetic) processes are uplifted or eroded and subjected to the effect of meteoric waters. As mentioned before, the extent and distribution of meteoric waters underneath the unconformities' surfaces are controlled by many factors (Figure 4-24 in chapter 4). However, although penetration of meteoric waters has been observed, reaching a depth of more than 2000 m in sedimentary rocks, the thickness of the pervasive late diagenetic influence of these waters below unconformity surfaces usually varies between ten to hundreds of metres and the

influence is expected to increase systematically toward the unconformity surface (Emery et al., 1990, Shanmugam, 1990).

In the area of study, the dissolution of framework grains (commonly feldspar) and carbonate cements (commonly calcite) was observed at various depths regardless of the sample position relative to the unconformity. As most of petrographic evidence demonstrates the late dissolution of framework grains and carbonate cements, it seems to be that this dissolution is the main cause of the enhancement of porosity in the Brent Group sandstones. However, in many cases this dissolution was associated with the precipitation of pore-filling kaolinite and/or calcite cements, which relatively lead to a decrease in the total porosity of Brent Group sandstones.

In the Tampen spur area, the Base-Cretaceous Unconformity is located above the studied Brent Group Formations, and some of the formations are truncated directly by this unconformity surface and others are separated from this unconformity by the Upper Jurassic Heather Formation. As the main issue is to detect the main cause of this dissolution and to examine if it is related to the presence of the Base-Cretaceous Unconformity on the top of Brent Group formations in the Northern North Sea or not, which is the main hypothesis on which this study was based, all the analysed samples were taken at regular intervals with depth, starting from the point closest to the unconformity surface and going deeper. Thus, any possible diagenetic change in relationship to this unconformity surface would be expected to be in systematic order, which means that any observed changes are expected to increase with proximity to this unconformity surface. Furthermore, each formation from the three studied formations of the Brent Group has been studied in two different cases: case 1: when it lies directly below the Base-Cretaceous Unconformity, and case 2: when the formation has been separated from the unconformity surface by other formation/s.

Based on this hypothesis, a systematic vertical diagenetic change toward the unconformity surface is expected, and dissolution of framework grains and carbonate cements should increase upward toward the unconformity, particularly in samples closest to the unconformity surface. After detailed analysis of the collected samples for each formation and the comparison between the results of the samples collected from the formation lying directly below the unconformity surface and other samples collected from

the same formation but in different wells and separated from the unconformity by other facies, it seems that there are several lines of evidence suggesting that the dissolution and creation of secondary porosity is not related to the unconformity surface. Some of these evidence are:

Firstly, no vertical systematic variation (vertical trend) in the volume and distribution of framework grains and carbonate cements or in the volume and distribution of porosity toward the unconformity surface have been observed in any of the studied formations, regardless of how close these formations are to the unconformity surface. Although dissolution of minerals has been observed in almost all the studied formations of the Brent Group, none of these studied formations has shown systematic vertical change toward the unconformity surface. For instance, although the Base-Cretaceous Unconformity lies directly at the top of Rannoch Formation in Wells 34/10-4 and 33/9-13, their total porosity values including the porosity generated by the dissolution of minerals was not higher than in Wells 34/10-1, where the Base-Cretaceous Unconformity is located more than 94 m above the top of Rannoch Formation (Figure 5-28).

Another example is the contents and distribution of minerals and porosity in the Etive Formation. Although the Base-Cretaceous Unconformity is situated at the top of the Etive Formation in Well 34/7-16, its feldspar and carbonate cements contents were found to be not less than in Well 34/10-1, where the Base-Cretaceous Unconformity is situated more than 57 m above the top of the Etive Formation. Furthermore, the dissolution of carbonate cements increased downward and high degradation and dissolution of calcite cement were observed. If the dissolution of feldspar grains and carbonate cements were related to the penetration of meteoric water through the Base-Cretaceous Unconformity, systematic vertical change toward the unconformity would be expected and the amount of dissolution and porosity should be much higher in Well 34/7-16 than in Well 34/10-1 (Figure 5-33).

Similarly, results from the analysed 18 sandstone samples of the Tarbert Formation showed no systematic variation (vertical trend) in the volume and distribution of feldspar grains or carbonate cements toward the unconformity surface. Comparison was made between the wells where the Base-Cretaceous Unconformity is situated directly on the top of the Tarbert Formation and the wells where the unconformity is situated metres above the top of Tarbert Formation and separated by layers of sediments, including the

shale layer of the Heather Formation. This comparison focused on the type and rate of diagenetic effects (including the dissolution of minerals and enhancement of porosity) in each well and the possible relationship between these diagenetic changes and the location of the Base-Cretaceous Unconformity. For instance, in Wells 34/10-1 and 34/10-8, where the Base-Cretaceous Unconformity is located at the top of Tarbert Formation, the rate of dissolution and the created porosity was not higher than that in Wells 34/10-34 and 34/7-19, where the Base-Cretaceous Unconformity is located 4.5 m and 14.4 m respectively above the top of Tarbert Formation, and in both cases did not change systematically toward the unconformity surface (Figure 5-37). If the dissolution of minerals and the enhancement of porosity were related to the Base-Cretaceous Unconformity, higher rates of dissolution and porosity would be expected to be observed in the wells located directly below the unconformity surface than in wells separated from the unconformity surface by other sediments, including the Heather shale.

Secondly, if the observed dissolution of framework grains and carbonate cements were related to the presence of the unconformity surface, the secondary porosity, including the oversized pores generated from this dissolution, would be expected to be at least partly destroyed by compaction processes at this depth of burial.

Instead of that, in most of the analysed sandstone samples the shape of the partly and completely dissolved feldspar grains and the generated oversized pores which were observed to have a similar size to the surrounded grains still existed and did not show any compaction signs; these dissolved remnants of feldspar grains are usually delicate structures and may easily be destroyed under any mechanical compaction process. Even with possibility that there had been an early cement formed before the creation of the unconformity surface and that it may have been sufficiently strong to prevent complete compaction to the unconformity related secondary pore spaces, it is very difficult to explain how these remnant delicate structures of feldspar grains and oversized pores resisted the expected major mechanical compaction process that would be likely to form due to the depth of burial, which in some cases exceeds 2700 m (Figure 5-38). Furthermore, there were some signs of compaction within the same samples which contained undestroyed oversized pores.

Thirdly, in many cases the oversized pores created due to the dissolution of framework grains and carbonate cements are associated with the precipitation of clay (commonly kaolinite) that formed as a result of feldspar alteration; the generated kaolinite has filled the generated pores and is associated with a high percentage of microporosity. The presence of the high microporosity within the kaolinite indicates no major compaction has occurred over these sediments, despite the depth of their burial. Furthermore, the distribution of this kaolinite does not change systematically below the Base-Cretaceous Unconformity.

The second and third points of evidence indicate that the dissolution of framework grains and carbonate cements in the Brent Group post-dated the majority of mechanical compaction processes. An argument against this result may suggest that the abundance of quartz cement could have resisted the compaction. However, quartz cement which rarely forms at depths less than 1.5-2 km (Wilkinson et al., 2014) was not observed in the analysed samples. Furthermore, signs of compaction have already appeared in many samples: the presence of such signs of compaction together with uncompacted pores and/or remnant delicate structures of partially dissolved feldspar within the same field of view of one sample indicates that the dissolution of framework grains and the formation of highly microporous kaolinite are most likely to have post-dated the main mechanical compaction processes. Another argument may claim that the observed compaction signs may have been formed as a result of compaction processes that may have occurred before the creation of the unconformity surface. This hypothesis can be disproved by pointing out that the maximum thicknesses of Upper Middle Jurassic to Upper Jurassic depositions (the Viking Group Formation) that may have been deposited above the Brent Group in the Tampen spur area and later on eroded partly or completely by the Base-Cretaceous Unconformity vary from a few metres to a few hundreds of meters in all the studied wells. This thickness of sediments is not likely to cause the observed signs of compaction and possibly only the initial phase of compaction will take place. This leads to the conclusion that the observed digenetic changes including dissolution of framework grains and carbonate cements are not related to the Base-Cretaceous Unconformity that lies over the top of the Brent Group sandstones and were most likely to have taken place much later.

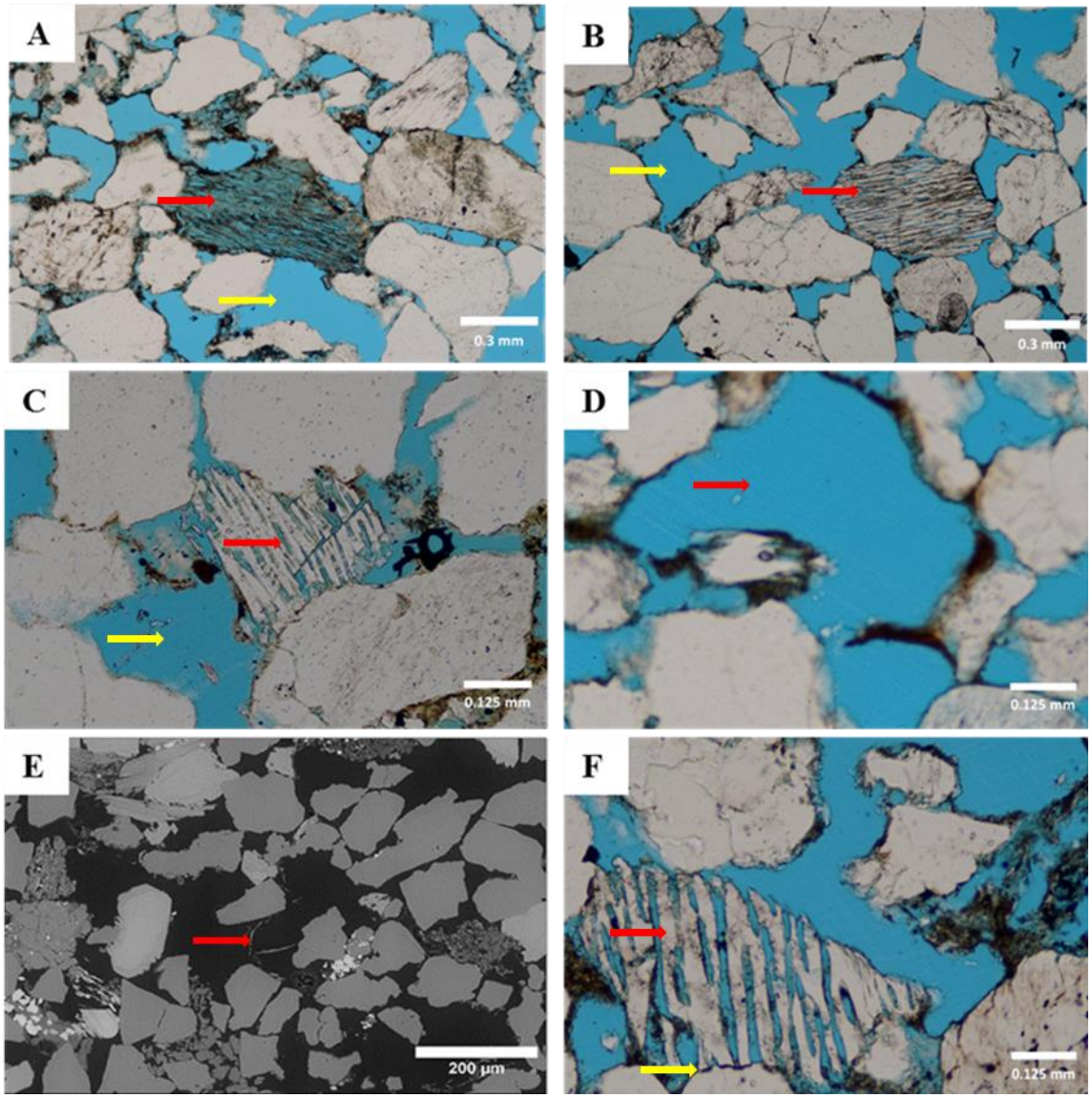

Figure 5-38. Thin-section photomicrographs and backscattered electron images: **A**, **B** and **C**. Showing partial to complete dissolution of feldspar grains in Wells 34/10-34, 2009 m, and 34/7-16, 2410.80 m (red arrows), respectively with the presence of compaction signs and uncompacted secondary pores (yellow arrows), despite the depth of burial which exceeds 2000 m. **D**. Showing the preservation of the oversized pores generated by dissolution at depth 1783.10 m in well 34/10-1, 1783.10 m. **E** and **F**. Showing uncompacted complete and partially dissolved feldspar grains and remnant delicate structures of feldspar grains with the presence of compaction signs in the same sample in Well 34/10-4, 1830 m and 34/10-34, 2009 m (yellow arrow), respectively.

Fourthly, petrographic analysis and comparison between two of the studied Rannoch Formations within the Brent Group in the Gullfaks Field have shown variation in the amount and distribution of plagioclase within the two formations. Petrographic analysis

of Rannoch sandstones samples showed presence of plagioclase within the upper part of the Rannoch Formation in Well 34/10-4, which lies directly below the Base-Cretaceous Unconformity, whereas, in Well 34/10-1 the Rannoch Formation, which lies more than 90 m below the unconformity surface, was plagioclase free. If the dissolution of feldspar, including plagioclase grains, is related to the diagenetic effect of the Base-Cretaceous Unconformity, it is difficult to explain why plagioclase grains occur in Well 34/10-4, and particularly in samples closest to the unconformity surface, and do not occur in Well 34/10-1, which is more than 90 m further away. The opposite trend is expected and volume of dissolved plagioclase should be higher in the well where the formation is closer to the unconformity than the other.

The petrographic results showed no evidence for the dissolution of framework grains and cements to be related to the Base-Cretaceous Unconformity. It may be worth mentioning that uplifted and exposed sedimentary rocks that were subjected to meteoric waters are usually prone to erosion as well; the rate of this erosion is controlled by many factors, for example properties of the exposed material, topography and climate of the area. Therefore, any possible diagenetic changes related to the penetration of meteoric waters through the Base-Cretaceous Unconformity which lies on the top of Brent Group would only be preserved if the rate of meteoric water penetration and alteration was higher than the rate of erosion, otherwise the diagenetic effect of these waters (e.g. dissolutions and enhancement of porosity) on the Brent Group sandstones will have been eroded and is unlikely to be seen.

5.7.2.3 The third scenario: The influx of acidic component produced by thermal maturation of organic matter or by addition of CO_2 that may form as a result of thermal maturation of organic matter

Organic acids and carbon dioxide may have significant influence on sedimentary rocks, especially in sandstones that may lie adjacent to mature source rocks, due to them causing dissolution of framework grains and carbonate cements (Bjorlykke and Aagaard, 1992). For instance, according to (Burley, 1986), generation and migration of organic acids is the main cause for the dissolution of grains and precipitation of kaolinite in the Tartan and Piper fields of the North Sea; he claimed that acidic pore fluids may migrate upward for long vertical distances of up to 1000 m before reaching the potential reservoir.

However, an argument against this hypothesis indicated that the generated acidic fluids would not be sufficient to cause a high amount of leaching and dissolution of framework grains and cements in sedimentary rocks and would most likely be neutralized and lose their corrosive power before reaching the potential reservoir rocks (Lundegard et al., 1984).

In the Tampen Spur area, many of the oilfields lie adjacent to several mature oil and gas source rocks. The studied Middle Jurassic Brent Group formations lie above the Lower Jurassic shales of Dunlin Group and below the Upper Jurassic marine shales of the Viking Group (Heather Formation and Draupne Formation). The Upper Jurassic Draupne Formation which is equivalent to the Kimmeridge Clay Formation is the main hydrocarbon source rock in the Tampen Spur area, whereas, the underlying Heather Formation is classified as Type II kerogen-rich source rock and has lower quality of kerogen compared to the Draupne Formation (Horstad et al., 1995).

The presence of Brent Group formations adjacent to and between these mature source rocks may enhance the idea of dissolution of framework grains and carbonate cements by the influx of organic acids that may have been produced by thermal maturation of organic matter and/or by the carbon dioxide (CO_2) that may have formed as a result of thermal maturation of organic matter. However, this does not seem to be applicable to the studied different formations of the Brent Group, because there is no evidence to indicate that the rates of dissolution of framework grains and carbonate cements are higher in proximity to the source rocks. If the generation of acidic fluid and/or carbon dioxide from the thermal maturation of organic matter in source rock is the main cause of the observed dissolutions and porosity enhancement, the sandstone formations closer to the mature source rock should show much higher dissolutions and greater enhancement of porosity compared with the formations that are separated from the source rock by distance or other formations. There should be also a systematic vertical change and higher porosity toward the mature source rocks. However, this has not been observed in the studied wells. Therefore, this hypothesis will remain possible but cannot be confirmed or denied and further analysis is required.

5.7.2.4 The fourth scenario: The release of organic acid and CO_2 that may form as a result of oil biodegradation

This scenario considers the dissolution of framework grains and/or carbonate cements to be caused by the organic acids (mainly carboxylic acids) that may have formed as a result of interaction of hydrocarbon with waters and/or bacterial degradation of hydrocarbon and organic matter (Morad et al., 2000). The generated organic acids and CO_2 may promote the alteration and dissolution of framework grains and carbonate cement and enhance porosities (Surdam et al., 1984). For instance, alteration of crude oil by living microorganisms (commonly bacteria) may cause biodegradation of oil, this may produce organic acids and CO_2 and therefore more acidic oil (Taylor et al., 2001).

Similarly to the process mentioned in the third scenario for the creation of organic acids and CO_2 from the source rocks, biodegradation of oil may occur in reservoirs within the transition zone (oil-water contact), where chemical interaction of hydrocarbons with water and minerals may produce and/or enhance carboxylic acids in the reservoir (Head et al., 2003). The generated carboxylic acids within the reservoir are considered to be one of the main factors for the dissolution and the enhancement of porosity in clastic reservoirs (Stoessell and Pittman, 1990). Furthermore, several authors have mentioned that, degradation of oil in reservoir rocks may play a significant role in influencing the distribution of clay and porosity in clastic reservoirs (Larter et al., 2006). For instance, the dissolution of plagioclase and creation of kaolinite in the Gullfaks Field (Ehrenberg and Jakobsen, 2001); another example is the formation of carbonate cement in the Forth and Balmoral fields which is assumed to be related to the oil degradation process at OWC (Watson et al., 1995). However, an argument against this theory suggested that mass balance calculations and the commonly low concentrations of organic acids in reservoirs, as well as the absence of obvious concentration of Al and Si raise uncertainty about the efficiency of these organic acids in enhancing the porosity in clastic reservoirs (Giles et al., 1994).

Petrographic analysis and comparison between the studied wells in the Gullfaks Field have shown that the amount and distribution of plagioclase within the Brent Group sandstones varies from well to another. For instance, the presence of plagioclase in some wells and its absence in other wells was very obvious. Petrographic analysis of Rannoch

Formation samples showed presence of plagioclase in Well 34/10-4, particularly in the upper part of the formation and the absence of plagioclase in Well 34/10-1. This observation is supported by the XRD data mentioned by Ehrenberg and Jakobsen (2001), in previous published work for the same wells (Figure 5-20). The authors concluded that, there is a complete absence of plagioclase in almost the whole Brent Group Formation in the southern section of the Gullfaks Field (Figure 5-39). They claimed that, the lateral transition in the composition of Brent Group from plagioclase bearing to plagioclase free over less than 5 km distance is unlikely to be due to the variation in the composition of depositional sand of Brent Group and most likely to be related to a diagenetic effect. Analysis of oil samples from different places within the Gullfaks Field shows that the oil belongs to different geochemical families. This variation in the composition of oil is assumed to be related to differing rates of biodegradation in various locations within Gullfaks Brent Group reservoirs (Horstad et al., 1995). Furthermore, they assumed that there is a correlation between the observed pattern of plagioclase distribution and the biodegradation of oil in the Gullfaks Field, particularly in Brent reservoirs. This pattern of plagioclase distribution is believed to be related to the variation in the composition of oil within the Gullfaks Field, where the most intensely biodegraded oils occur in the southern part of Gullfaks Field compared to the other parts of the field.

Their conclusion is compatible with my petrographic analysis results for the two studied wells in the Gullfaks Field. In both wells, the texture and composition of Rannoch sandstones was almost the same and the only difference was the presence of plagioclase in the upper part of the formation in Well 34/10-4 and its absence in Well 34/10-1. These results support the idea that variation of plagioclase is unlikely to be due to the variation in the composition of depositional sand of the Brent Group and most likely to be related to a diagenetic effect. This diagenetic effect, including the dissolution of framework grains (commonly feldspar) and carbonate cements (commonly calcite), which increased the total porosity values has been observed in most of the studied samples of both wells, regardless of how close these samples are to the unconformity surface. For instance, dissolution of feldspar grains and formation of authigenic kaolinite were not higher in Well 34/10-4, where the Base-Cretaceous Unconformity lies almost directly above the Rannoch Formation, than in Wells 34/10-1 where the unconformity lies more than 94 m above the top of Rannoch Formation. Furthermore, this conclusion is also enhanced by the results of the analysed sandstone samples from the Tarbert Formation in Well 34/10-

8; this well, which is located in the southern part of Gullfaks Field is also plagioclase free, similarly to Well 34/10-1.

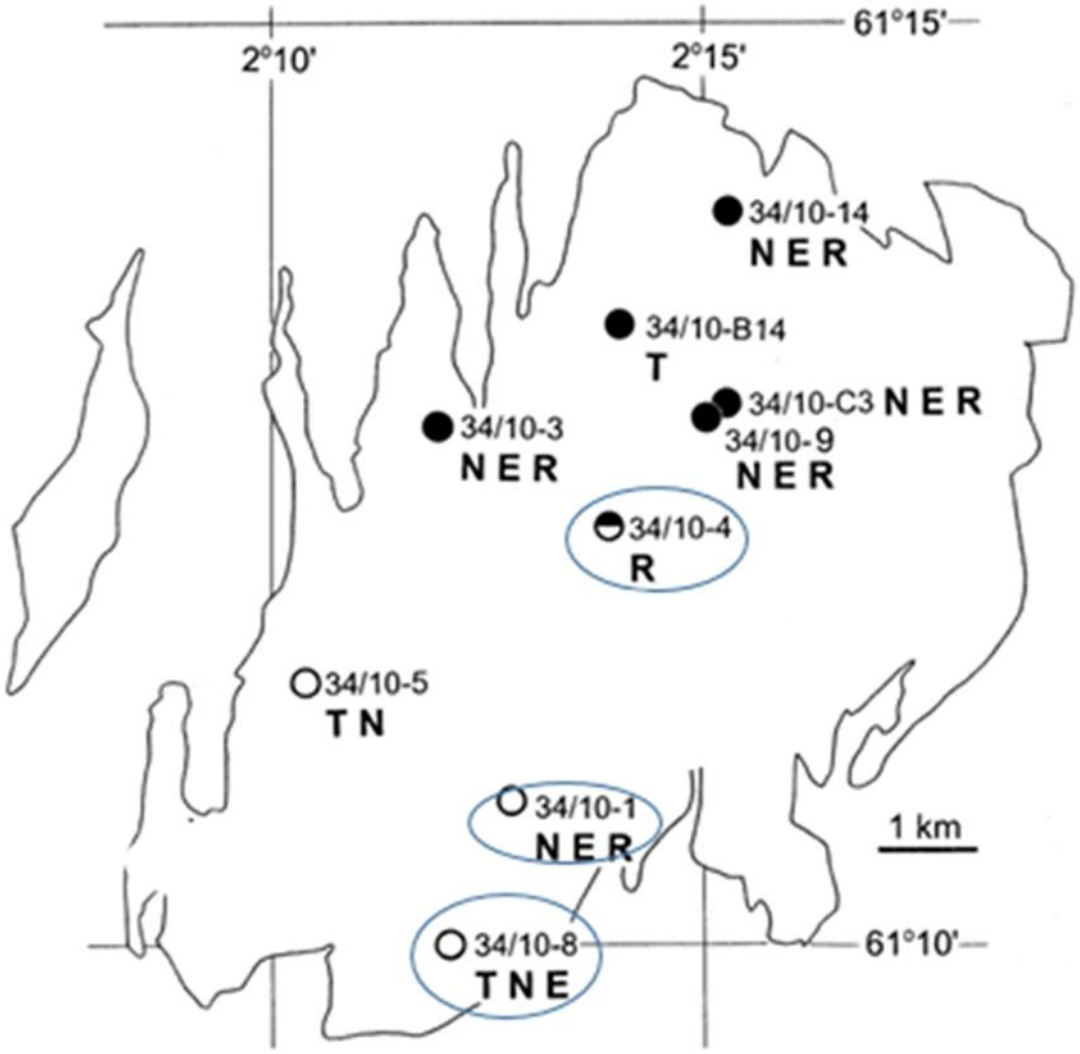

Figure 5-39. Locations of wells in the Gullfaks Field (includes the three studied wells) and distribution of plagioclase within the Brent Group in each of these wells. Open circles indicate wells with almost plagioclase free intervals; filled circles indicate wells where the bearing of plagioclase is in normal abundances, half-filled circles indicate the wells where plagioclase appears in the upper part of the Rannoch Formation and disappears in the lower part. The formations studied in each well are represented by letters (T = Tarbert, N = Ness, E = Etive and R = Rannoch). Modified from (Ehrenberg and Jakobsen, 2001).

After the discussion of the four possible scenarios, it seems that the hypothesis of leaching of grains by meteoric waters or organic acids released from the source rocks are not compatible with the observed distribution pattern of plagioclase free and plagioclase bearing sandstone intervals within the Brent Group. However, the correspondence between the wells that have plagioclase free intervals and their compositions of oil, which are considered to be highly biodegraded oil, indicates a link between the biodegradation of oil and the dissolution of plagioclase. Therefore, the acidic component formed from biodegradation of oil which has been proposed to be most intense in the southern part of the Gullfaks Field is the best scenario that may explain this pattern of plagioclase distribution.

5.7.3 Origin and timing of kaolinization

There is a considerable argument about the type of kaolinite in the Brent Group sandstones in the North Sea. According to (Glasmann, 1992), the most abundant digenetic clay in the Brent Group reservoirs is kaolinite and assumed that the association of kaolinite with significant dissolution of feldspar grains means that this kaolinite is most likely to be generated due to the flushing of meteoric waters through the major unconformity surfaces. Other authors have classified the kaolinite in the Brent Group reservoirs to be detrital and not diagenetic ((Bjorkum et al., 1990), while some have claimed that generation of kaolinite within Brent Group sandstones is related to the circulation of acidic fluid expelled from the nearby source rocks before the accumulation of hydrocarbons (Scotchman et al., 1989). However, an argument against this scenario claims that it is unlikely for the generated kaolinite to have occurred due to the circulation of organic acids and/or CO_2 produced from the nearby source rocks. Proponents of this idea suggest that the commonly low concentration of organic acids in reservoirs will raise uncertainty about the efficiency of these organic acids in enhancing the dissolution of grains and precipitation of kaolinite in clastic reservoirs (Giles et al., 1994).

In the Tampen Spur area, some of the observed kaolinite was in association with partly and/or completely dissolved detrital framework grains (commonly feldspar) filling the generated pore spaces. However, no correlation between the feldspar and the kaolinite content within the Brent Group sandstones has been observed in any of the studied wells. This lack of correlation in the content of feldspar and kaolinite may be attributed to: 1-

initial variability in the content of feldspar; 2- Alteration and kaolinitization of other minerals such as micas and/or silicate rock fragments; 3- the presence of two types of kaolinite authigenic and detrital.

In fact, two types of kaolinite were observed within the Brent Group sandstones in the Tampen Spur area, detrital or early diagenetic kaolinite, which was intermixed with other clay minerals between adjacent framework grains and filling pore spaces, and authigenic (in situ) kaolinite, which was formed as a result of alteration and dissolution of framework grains (commonly feldspar). Although it is difficult to distinguish between authigenic (in situ) kaolinite and detrital kaolinite and to detect the volume and distribution of each type within Brent Group sandstones for each well, there are several points in the petrographic evidence that indicate that many of the observed kaolinites within the Brent Group sandstones were formed in situ and related to late diagenetic processes. This evidence includes:

1. The vermicular textures and delicate euhedral booklets observed in many samples (Figure 5-29 C).
2. The growths of kaolinite between the pre-existing sheets of mica (Figure 5-17 C).
3. The generation of kaolinite within the oversized secondary pores and its association with a high proportion of micropores: the generated kaolinite shows no signs of compaction, despite the depth of burial which exceeds 2000 m in most cases (Figure 5-17 D).

All this body of evidence supports the hypothesis of the generation of kaolinite due to late diagenetic processes. However, the main aim of this study is to detect how this kaolinite has been formed and particularly to see if it is related to the Base-Cretaceous Unconformity or not.

Although it is difficult to detect the main cause for the late generation of kaolinite, most petrographic evidence shows that there is no relationship between the distribution and content of kaolinite and the Base-Cretaceous Unconformity. Some of these points of evidence are:

Firstly, the absence of a systematic increase of kaolinite content toward the unconformity surface in any of the studied wells (Figure *5-22*, Figure 5-31 and Figure 5-35). For instance, although the Base-Cretaceous Unconformity is situated directly over the top of

the Rannoch Formation in Well 34/10-4 and Well 33/9-13, the content of kaolinite in these two wells does not seem to be higher than the content of kaolinite in Well 34/10-1, where the Base-Cretaceous Unconformity is situated more 94 m above the top of Rannoch Formation. A similar type of distribution pattern of kaolinite is observed in the Etive Formation, where the Base-Cretaceous Unconformity is situated at the top of the Etive Formation in Well 34/7-16 and 57 m above the Etive Formation in Well 34/10-1. The volume of kaolinite observed in Well 34/7-16 was not higher than the volume of kaolinite in Well 34/10-1.

Another supporting piece of evidence is the content and distribution of kaolinite in the Tarbert Formation. Although the Base-Cretaceous Unconformity lies directly at the top of Tarbert Formation in Wells 34/10-1 and 34/10-8, their kaolinite content was not found to be higher than that in Wells 34/10-34 and 34/7-19, where the Base-Cretaceous Unconformity is located 4.5 m and 14.4 m respectively above the top of Tarbert Formation. In both of these wells, shales of the Heather Formation lie between the top of the Tarbert Formation and the unconformity surface. If the penetration of meteoric waters through the unconformity surface is the main cause of the observed kaolinite owing to the lower pH of meteoric waters and the greater degree of saturation, the content of kaolinite would be much higher in the formation that lies directly below the unconformity surface than in others, where the meteoric water becomes much less undersaturated and has a higher pH, and therefore, systematic change toward the unconformity surface would be expected.

Secondly, petrographic results of the Brent Group sandstones revealed the generation of kaolinite within the oversized secondary pores: these oversized secondary pores in many cases contain kaolinite associated with high microporosity and are interpreted to have been formed due to the dissolution of framework grains; however, they show no signs of compaction, despite the depth of burial which exceeds 2000 m in most cases. This may indicate that the dissolution of framework grains and carbonate cements and the formation of kaolinite are most likely to have occurred in the late stage, after the end of the majority of mechanical compaction processes and is therefore not related to the Base-Cretaceous Unconformity in the top of Brent Group sandstones.

All the evidence put forward disproves the hypothesis that the alteration and dissolution of framework grains and creation of kaolinite in Brent Group sandstones was formed as

a result of an influx of meteoric water shortly after their deposition or through the Base-Cretaceous Unconformity. Therefore, these results appear to support the pervious results in case study 1, and indicate that kaolinite may have been formed by circulation of acidic fluid (e.g. organic acids and/or CO_2) that were produced by the biodegradation of oil and/or thermal maturation of organic matter.

5.8 Conclusion

Petrographic analysis of more than 43 sandstone samples from the Brent Group in the Tampen Spur area indicated that a high amount of secondary porosity has been developed as a result of diagenetic processes. Post-depositional dissolution of framework grains and carbonate cements has been recognised in most of the analysed samples and was the main reason for the creation of secondary porosity and generation of authigenic kaolinite.

The observation of vermicular textures and delicate euhedral booklets of kaolinite and its association with high microporosity at depths exceeding 2000m is clear evidence for late diagenetic processes and disproves the hypothesis claiming that the enhancement of porosity and the formation of kaolinite could have been formed as a result of influx of meteoric water shortly after the deposition.

The other scenario that may explain the nature and timing of post-depositional dissolution of framework grains and cements and kaolinite formation in the Brent Group sandstones is the influx of meteoric waters through the Base-Cretaceous Unconformity. This hypothesis, which represents the main concern of this study, has been considered. However, after detailed analysis of the collected samples, there are several lines of evidence that suggest this hypothesis is not viable and that the dissolution of framework grains and creation of secondary pores and/or kaolinite are not related to the Base-Cretaceous Unconformity. Some of this evidence includes:

1. The absence of obvious systematic distribution of framework grains and/or carbonate cements relative to the Base-Cretaceous Unconformity.
2. The absence of vertical systematic variation (vertical trend) in the volume and distribution of enhanced porosity toward the Base-Cretaceous Unconformity.

3. No systematic increase in the content of kaolinite toward the Base-Cretaceous Unconformity has been observed in any of the studied formations, regardless of how close these formations are to the unconformity surface.
4. Diagenetic effects, including the dissolution of feldspar grains and formation of authigenic kaolinite, have been observed in most of the studied samples, regardless of how close these samples were to the unconformity surface. For instance, the dissolution of feldspar grains and formation of authigenic kaolinite were not higher in Well 34/10-4, where the Base-Cretaceous Unconformity lies almost directly above the Rannoch Formation, than in Well 34/10-1, where the unconformity lies more than 94 m above the top of Rannoch Formation.
5. The presence of evidence indicating that the dissolution of framework grains and/or cements and the formation of kaolinite occurred in a late stage and post-date the majority of mechanical compaction processes. For instance,
    a. The preservation of delicate euhedral booklets of authigenic kaolinite despite depths which exceed 2000 m.
    b. The preservation of uncompacted delicate crystal remnants lining the secondary pores from dissolved feldspar grains.
    c. The preservation of uncompacted and/or undestroyed oversized secondary pores despite depths which exceed 2000 m.

This evidence clearly suggests that there is no relationship between the enhancement of porosity and the formation of authigenic kaolinite and the Base-Cretaceous Unconformity located above the Brent Group sandstones. Based on this, it seems that the dissolution of the framework grains and/or cements and the generation of secondary porosity and authigenic kaolinite in the Brent Group sandstones are possibly related to high acidic fluids that may generated by either:

1. Thermal maturation of organic matter in surrounding source rocks and migrated to the Brent Group sandstones to interact with the reservoir minerals and enhance the porosity.
2. Interaction of hydrocarbon with waters and/or bacterial degradation of hydrocarbon and organic matter.

Chapter 6 Results from other North Sea wells

8 wells from the studied 32 wells looked at in this study did not fit into the geographical grouping of the two case studies presented in chapters 4 and 5. Therefore, these wells were selected for further discussion in this Chapter. 6 from these wells cross one particular unconformity surface named the Base Humber Unconformity. Well 3/3-N14 is located in the Ninian Field, Well 211/12a-14 is within the Magnus Field, Well 2/5-17 is in the Heather Field, Well 211/23-A21 is located in the Dunlin Field, Well 14/19-3 is located in the Claymore Field and Well 9/28-10A is in the Crawford Field. The other 2 wells cross a different unconformity surface called the Base Kimmeridgian Unconformity; these are Well 5/17-B2 in the Piper Field and Well 3/3/-N15 located in the Ninian Field.

6.1 Identified unconformities

6.1.1 Base Humber Group Unconformity (BHU)

This is a local unconformity surface observed in some wells separating one or more of the Middle Jurassic Brent Group formations from the overlying Humber Group marine depositions.

6.1.2 Base Kimmeridgian Unconformity (BKU)

This is a local unconformity surface separating the Upper Jurassic Piper formation from the overlying Kimmeridge Clay formation (e.g. in the studied Well 15/17-B2, the Piper Formation is overlain unconformably by the Upper Jurassic Kimmeridge Clay Formation.

6.2 Introduction to the studied wells

As in the two case studies reported in Chapters 4 and 5, samples were collected from each well at vertical intervals in proximity to the unconformity surface. All selected samples were prepared and observed under an optical microscope in the same way as the previous studied samples; details of the preparation of samples and analysis procedure are presented in Appendix A.2

Similar results were obtained from the petrographic analysis of all the wells. Accordingly, and for the purpose of brevity, only two wells (Well 2/5-17 and Well 15/17-B2, each crossing a different unconformity surface) have been chosen to illustrate the findings from the remaining wells. The details of the geography and geology of the two selected wells are referenced here for further reading (Kay, 2003, Penny, 1991, Schmitt and Gordon, 1991, Burley, 1986). Well 2/5-17 has been chosen to represent the 6 wells crossing the Base Humber Unconformity, while well 15/17-B2 has been chosen to represent the 2 wells crossing the Base Kimmeridgian Unconformity.

Therefore, this chapter will only show the petrographic results of the analysed samples for the chosen wells and discuss the distribution of the observed minerals and porosity below the unconformity surface which lies on the top of each studied interval. The petrographic analysis results for the other 6 wells are briefly presented in Appendix B.3. The study has focused mainly on the main composition and texture of each selected sample and whether there is systematic diagenetic change in these samples in proximity to the unconformity surface or not.

6.3 Well 2/5-17 in Heather Field

This well was drilled as an exploration well in the Heather Field to examine the Brent Group sandstone. The well penetrates Tertiary, Cretaceous, Jurassic strata and a few feet of Triassic strata. This well crosses the Base Humber Unconformity (BHU) which separates the Middle Jurassic Brent Group from the overlying Upper Jurassic Heather Formation at a depth of 10678ft. The coring interval started from the Heather Formation, just few feet above the detected BHU, and terminated within the Brent Group at a depth of 10830ft.

6.3.1 Sedimentological analysis

This section will present the results of sedimentological descriptions which have been conducted for the available core from the studied well, allowing the observation of sediment details and interpretation of facies. Sedimentological description (core logging) was carried out for more than 60 feet of the observed core. The description started with the determination of grainsize by visual comparison of small sandstone samples using the

Wentworth size classification scale. After the determination of grain sizes, lithology and sedimentary structures were described.

6.3.1.1 Sedimentological analysis results

Figure *6-1* illustrates the stratigraphic core descriptions of Well 2/5-17 located in the Heather Field. Two different groups were observed within the described core interval: the Brent Group and the overlying Humber Group. The Humber Group lies unconformably above the top formation of the Brent Group. This unconformity has been named the Base Humber Unconformity (BHU). Only the base of the Heather Formation was cored and observed within the Humber Group. The Heather Formation is interpreted to be a nearshore, shallow-marine shelf consisting mainly of fine to coarse cemented sandstone; it is medium to dark grey and calcareous with an abundance of fossils and bioturbation. The Brent Group comprises five formations, the Broom, Rannoch, Etive, Ness and Tarbert Formations; however, in this well, only the Tarbert Formation occurs; it consists mainly of fine to medium sandstone (occasionally fine to coarse) and is light grey, calcareous and variably well-cemented.

Although samples were collected from both formations (Heather and Tarbert formations) the Tarbert Formation is the main target of this study, because it lies directly below the detected Base Humber Unconformity. Samples were taken from this formation for further investigation and petrographic analysis, including the texture, minerology and porosity of the sandstone.

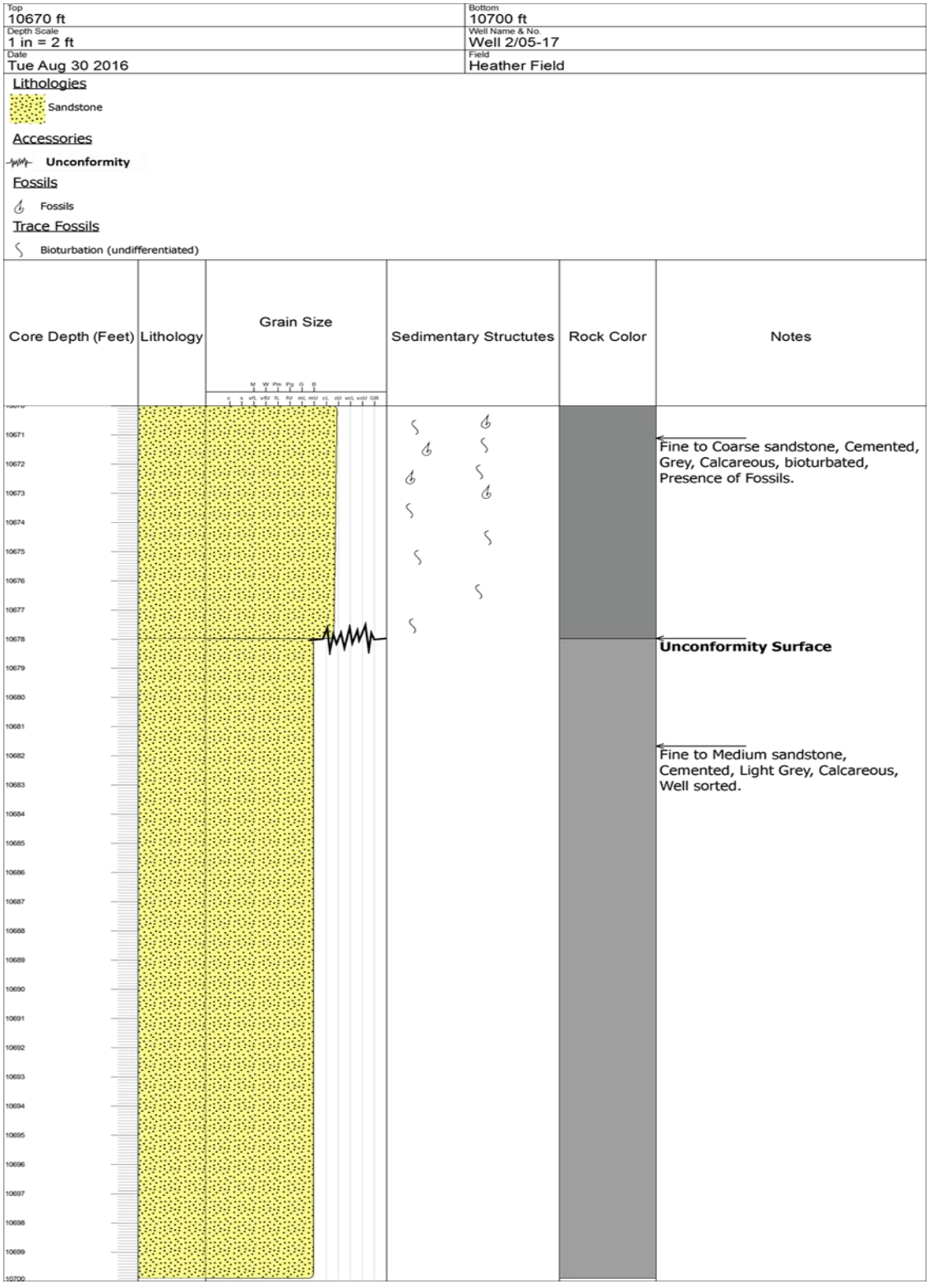

Figure 6-1. Sedimentological core descriptions of the Tarbert Formation in Well 2/5-17 in the Heather Field. The Base Humber Unconformity is recognised at depth 11678 ft, separating Tarbert Formation from the Upper Heather Formation.

6.3.2 Petrographic analysis

This section will present the results of the petrographic analysis, which allow the identification of the lithological texture, mineralogy and porosity of the sandstones.

6.3.2.1 Lithological Texture

Based on the grain size, two different sandstone facies were observed in the two studied formations: fine to medium sand, which was subangular to subrounded and moderately- to well-sorted, which represented the lower part of the Heather Formation, and fine to coarse sandstone, which was poorly- to moderately-sorted and subangular to subrounded, which represented the Tarbert Formation (Table 6-1).

Table 6-1. Showing the lithological texture of the two studied formations in Well 2/5-17. F-MS = fine to medium sand, F-CS= fine to coarse sand. P-M = poor to medium sorting, M-W medium to well-sorted. SA-SR= subangular to subrounded sand

Facies Code	Grain Size	Sorting	Roundness
3-7	F-CS	P-M	SA-SR
4	F-MS	M-W	SA-SR

6.3.2.2 Quantitative analysis

The main petrographic analysis data of the studied samples of Well 2/5-17 is summarized in Table 6-2.

Table 6-2. Petrographic analysis data for Well 2/5-17

Sample no.	Core Depth (ft)	Facies	CONSTITUENT (%)								Total %
			Porosity %	Framework Minerals			Accessory Minerals	Cement %		Others	
				Quartz	Feldspar	Rock Fragment	Mica	Calcite	Clay	Iron oxide and Pyrite	
19	10672.7	3-7	5	50	10	0	1	29	3	2	100
20	10673.3	3-7	6	52	10	0	0	28	2	2	100
21	10674	3-7	7	50	12	0	0	27	3	1	100
22	10678	4	10	45	11	0	1	27	4	2	100
40/B2	10678.5	4	2	51	8	2	3	18	8	8	100
23	10681.5	4	5	48	5	0	4	29	6	3	100
41/B2	10683.8	4	2	55	7	0	2	20	12	2	100
42/B2	10704	4	4	46	7	0	1	28	8	6	100

6.3.2.2.1 Minerology

This section will describe in detail the main composition of the studied samples.

6.3.2.2.1.1 Framework Minerals

The principal three detrital components within the studied samples were quartz, feldspar and rock fragments. In all the studied samples, the main observed quartz was monocrystalline quartz and the content of quartz ranged from 44 – 55%; some of these quartz grains were cracked and corroded (Figure 6-2 A). The feldspar content ranged from 10 to 12 % in the Heather Formation and from 5 – 8% in the Tarbert Formation. Identifying feldspars definitely without staining is difficult, but it is likely that the majority were potassium feldspar. Most of the observed feldspar grains in both formations exhibited variable degrees of alteration, replacement and in some cases partial or complete dissolution (Figure 6-2 B). The variation of feldspar content between the Heather and Tarbert formations is most likely to be related the variation in the facies and the origin composition of the deposited sand. The other components, apart from rock fragments, included mica and heavy minerals and the content varied from sample to sample, ranging in percentage from 0 to 8 %.

6.3.2.2.1.2 Authigenic minerals

Petrographic analysis of the studied samples showed that calcite cement was the most dominant cement type within the studied samples in both formations, and some samples were tightly cemented. All the studied sandstones samples contained calcite cement, ranging from 18 % up to 29%. Different types of calcite cement which may have been formed in different ways were observed, showing patchy and/or poikilotopic habits (Figure 6-2 C). This variation in the amount and type of calcite cement may indicate that calcite had been formed in two phases, probably early and late calcite cement. Only a small amount of clay cement was observed in most samples, ranging from 2-8%, with the exception of sample 41/B2 at 10683.8 ft from the Tarbert Formation, which contained about 12% of clay. Most of the observed clay seemed to be kaolinite, which most likely to have been formed in situ as a result of alteration and dissolution of framework grains. Some pyrite was seen as nodules in all samples but it was more abundant in the Tarbert Formation and ranging in percentage of 1 to 8% (Figure 6-2 D).

6.3.2.2.2 Porosity

Different types of porosity have been observed within the studied samples of both formations: primary (intergranular porosity) and secondary porosity. The secondary porosity includes intragranular porosity formed as a result of partial or complete dissolution of detrital grains, and microporosity, which usually appears as tiny pores (Figure 6-2 B). Some of the generated secondary porosity was followed by precipitation of either calcite or clay (particularly kaolinite) cements, reducing the total porosity of the sandstone. The observed porosity was higher in the Heather Formation than in the Tarbert Formation, with ranges of 5 to 10% in the Heather Formation and from 2 to 5% in the Tarbert Formation.

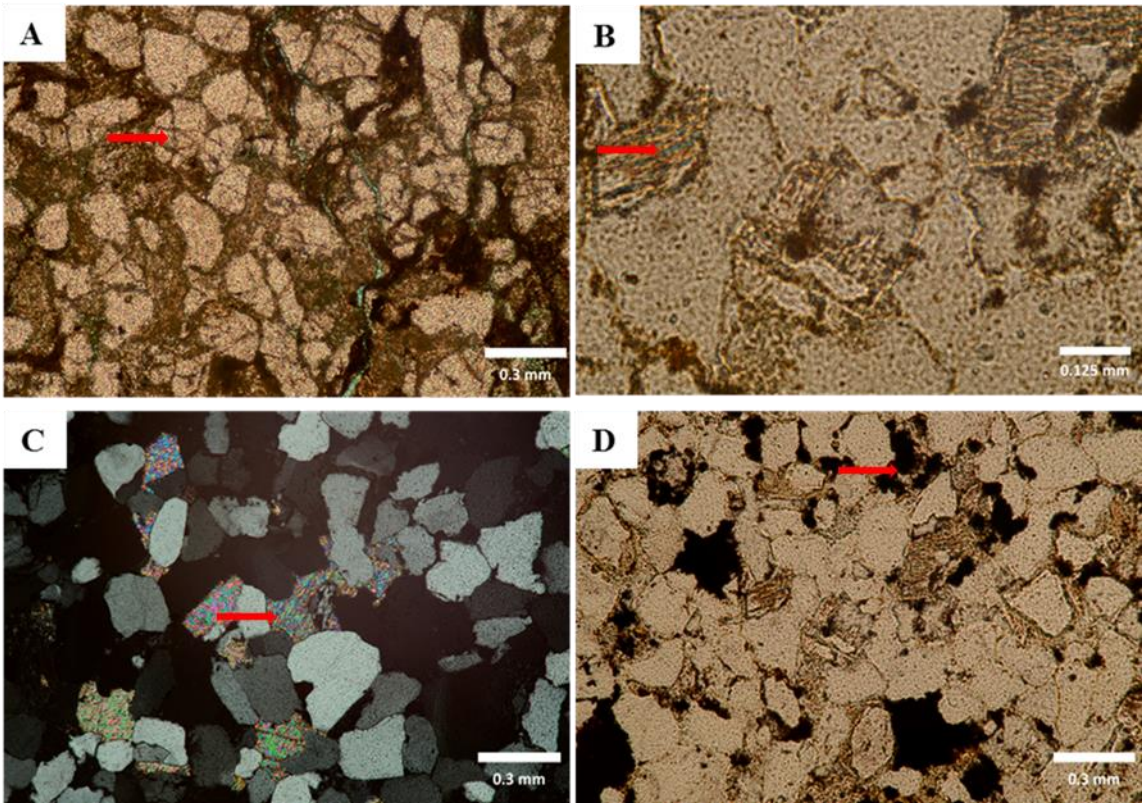

Figure 6-2. Thin-section photomicrographs Showing: **A**. corroded and fractured quartz grains: Well 2/05-17, 10678 ft. **B**. generation of microporosity due to the partial dissolution of feldspar grains: Well 2/05-17, 10678.5 ft. **C**. PPL image showing the occurrence of early calcite cement filling the intergranular pore space: Well 2/05-17, 10683.8 ft. **D**. abundance of pyrite nodules: Well 2/05-17, 10678 ft.

6.3.3 Spatial distribution of minerals and porosity below the Base Humber Unconformity

As the main target of this study is to examine the effect of the unconformity surface on the sediment lying underneath, this section will only focus on the samples selected from the Tarbert Formation, which lies directly below the Base Humber Unconformity. The vertical distribution pattern of unstable minerals and the porosity of sandstone under the unconformity surface in this formation have been examined to study whether there is a relationship between the Base Humber Unconformity and the distribution of the minerals and porosity within this formation or not.

6.3.3.1 Feldspar

The content of feldspar grains in the Tarbert Formation varies from sample to sample and ranges in volume from 5 to 8 %. Some of these feldspar grains have been altered and partly or completely dissolved. Petrographic evidence for this alteration and dissolution of feldspar grains was observed in the studied samples of both formations. In relationship to the unconformity surface, the feldspar content within the Tarbert Formation does not show systematic change toward the unconformity surface (Figure 6-3). Furthermore, the presence of some euhedral void spaces mimicking feldspar grains in this depth may indicate a late dissolution phase which post-dated the compaction processes.

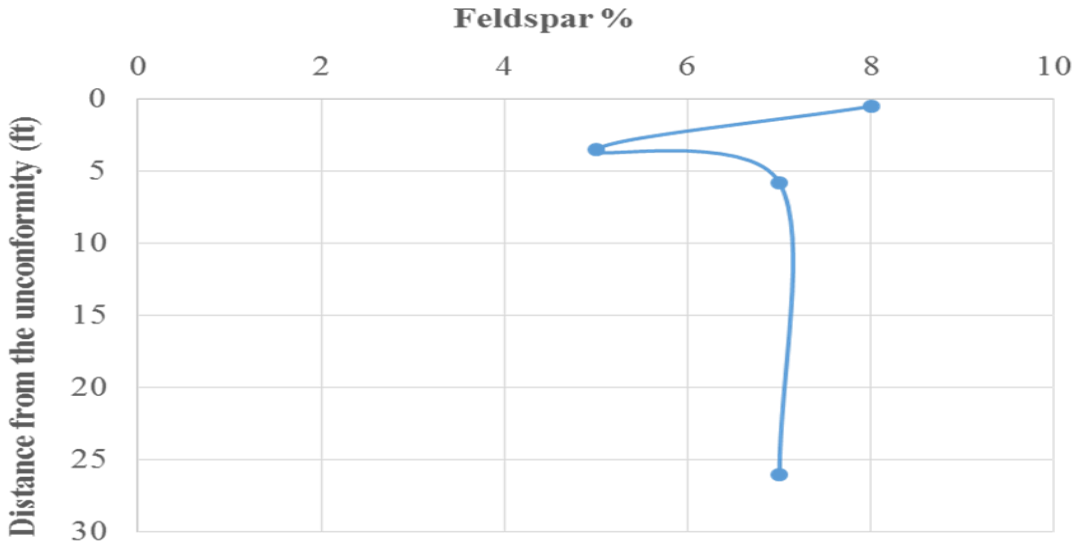

Figure 6-3. Distribution of feldspar grains below the Base Humber Unconformity in the studied well.

6.3.3.2 Kaolinite

Most of the observed clay within the analysed samples was kaolinite and seemed to be distributed irregularly and formed mainly due to the alteration and dissolution of framework grains (commonly feldspar) filling the generated pore space. A good correlation between the content of kaolinite and porosity in the Tarbert Formation was observed, the increase of kaolinite was associated with decrease in porosity (Figure 6-4). While, there is no correlation with the feldspar was observed (Figure 6-5).

The lack of correlation between the feldspar and kaolinite may be attributed to the present of other sources of kaolinite (mica, rock fragments and intraclasts). The petrographic evidence which indicates that the observed kaolinite was formed in situ includes the presence of booklets of kaolinite within the secondary pore spaces and the shape of these booklets, which in many cases appear as fresh patches and are un-deformed. Furthermore, these patches of kaolinite were mainly observed within the secondary pores and showed no signs of compaction, despite the depth of burial which exceeded 10678 ft. In relationship to the unconformity surface, it seems that there is no relationship between the formation of kaolinite and the position of the unconformity above the top of the Tarbert Formation. If the in situ generated kaolinite was related to the unconformity surface, the content of kaolinite would be expected to increase with proximity to the unconformity surface, whereas the petrographic analysis data do not show any vertical systematic change in the content of kaolinite toward the unconformity surface (Figure 6-6). Furthermore, the presence of fresh and unaltered kaolinite at this depth indicates that this kaolinite was most likely to have been formed in a late stage and post-dated the majority of the compaction processes.

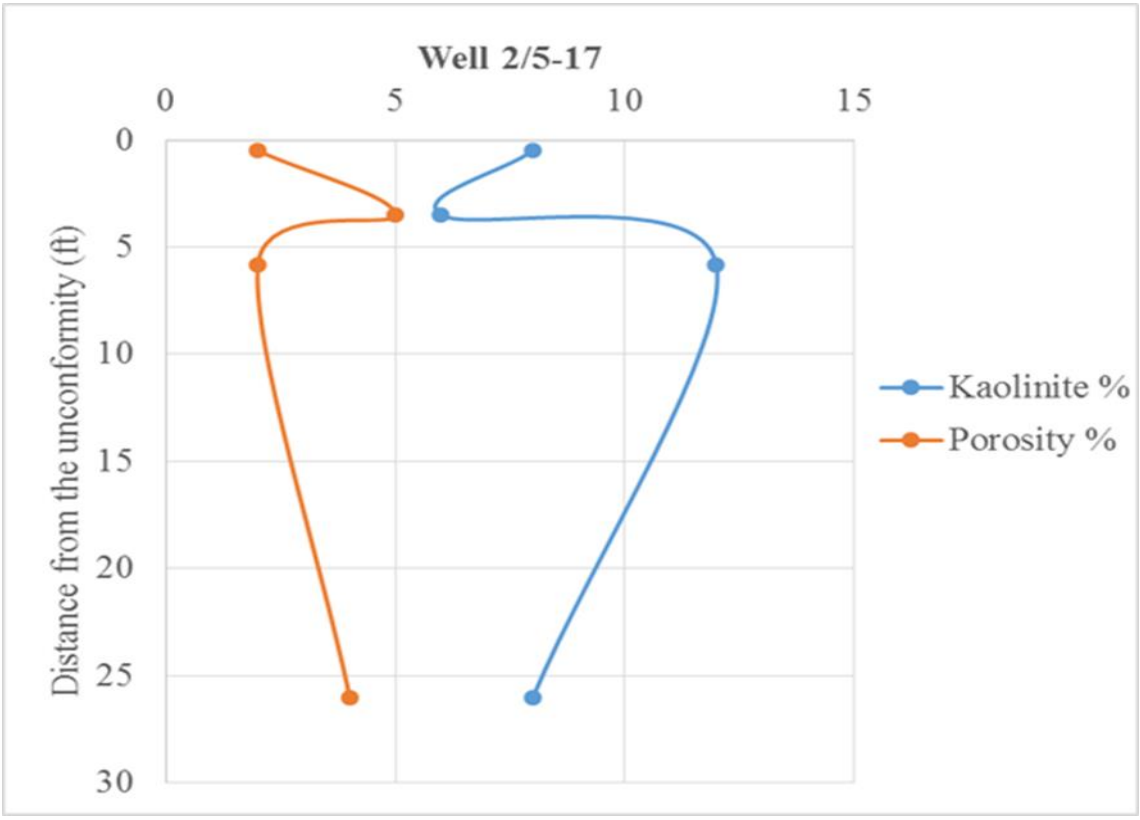

Figure 6-4. A correlation between the content of kaolinite and porosity in the Tarbert Formation below the unconformity surface.

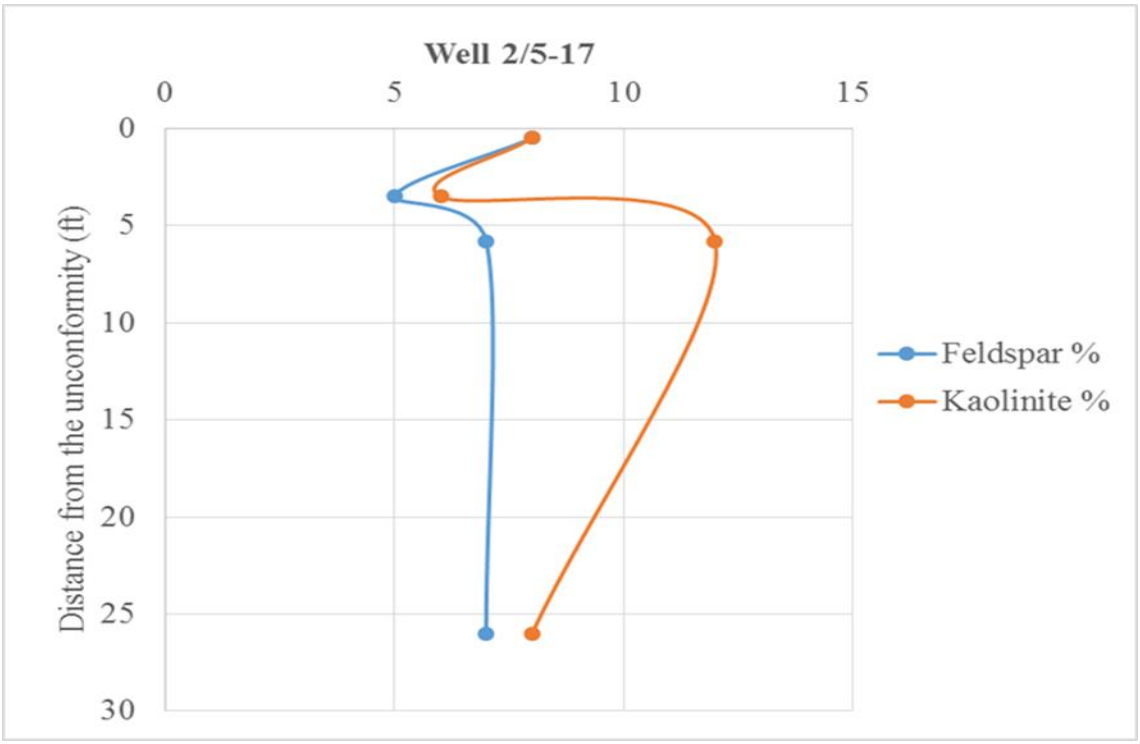

Figure 6-5. A correlation between the content of kaolinite and feldspar within the Tarbert Formation below the unconformity surface.

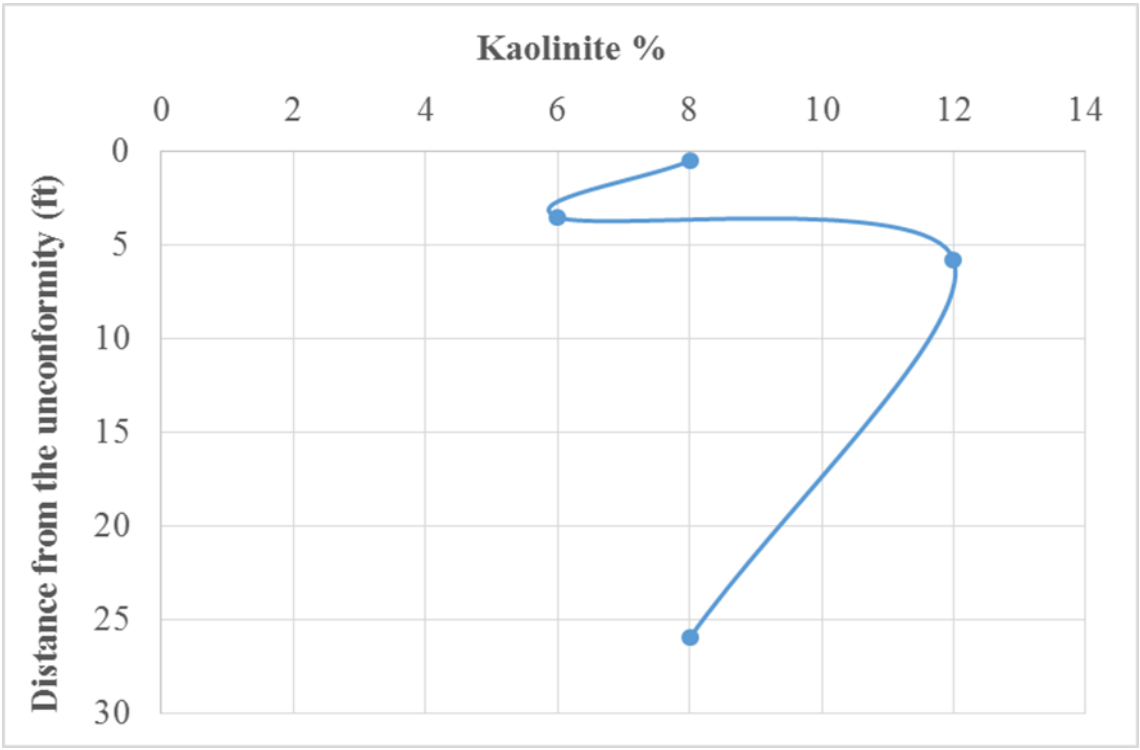

Figure 6-6. Distribution of kaolinite below the Base Humber Unconformity in the studied well.

6.3.3.3 Calcite

The volume of calcite cement in the Tarbert Formation ranged from 18% up to 29% (Table 6-2). This included the two observed types of calcite: early calcite cement formed as poikilotopic habits illustrating early diagenetic processes filling the intergranular pores and supporting the detrital framework grains and late calcite cement that has filled the secondary pores which formed due to the dissolution of some grains. Petrographic analysis indicated that the distribution of calcite cement was not constant throughout the Tarbert sandstone. However, no vertical systematic variation in the amount and distribution of calcite cement toward the unconformity surface in the Tarbert sandstones was recognised (Figure 6-7). If there was a relationship between the unconformity surface lies directly above the top of the Tarbert Formation and the distribution of calcite cement, systematic vertical change of the calcite toward the unconformity surface would be expected and the amount of calcite cement should decrease upward toward the unconformity surface. Furthermore, this type of calcite was observed even in the samples from the Heather Formation, which lies above the unconformity surface. Therefore, it

seems that it is unlikely that the variation in the distribution of calcite cement in Tarbert sandstone is related to the presence of the Base Humber Unconformity.

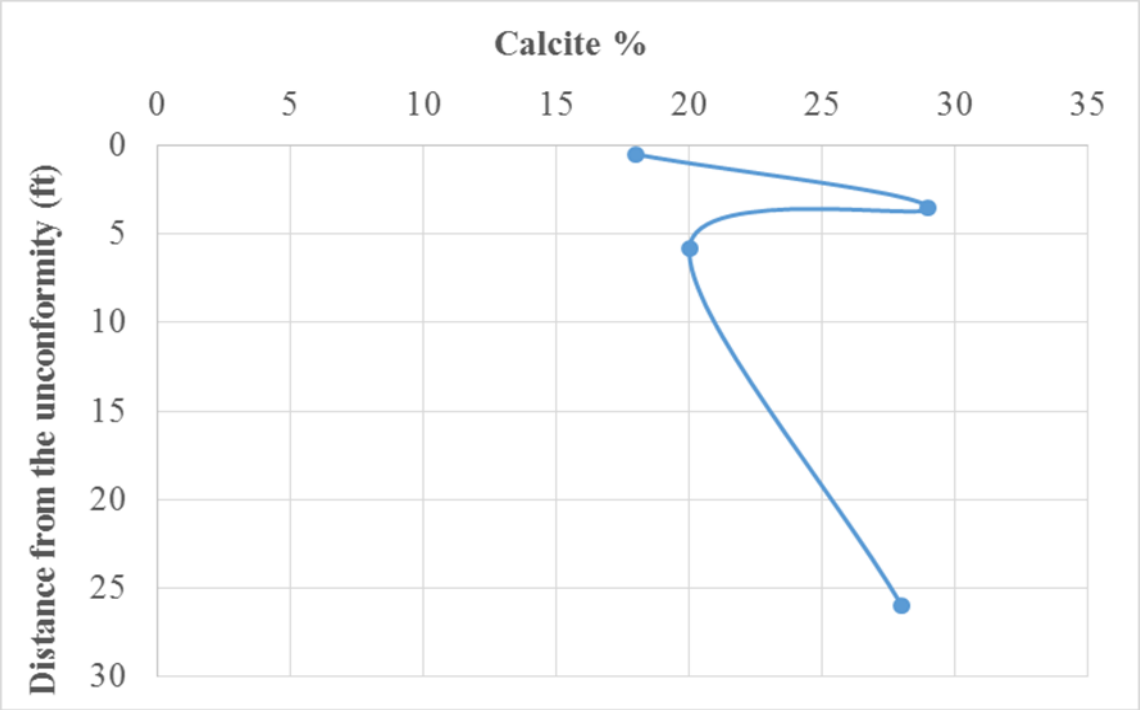

Figure 6-7. Distribution of calcite cement below the Base Humber Unconformity in the studied well.

6.3.3.4 Porosity

The measured helium porosity values of the cored intervals in Well 2/5-17 ranged between 1.7% and 15%, whereas, the petrographic analysis of the studied samples showed that porosity ranged from 2 to 5% within those from the Tarbert Formation. This variation between the two measured porosities is most likely to be related to the difficulty of quantifying the small pores size (such as microporosity among clay plates). Two different types of porosity were observed within the studied Tarbert Formation, primary and secondary porosity. Primary porosity was variable in the studied samples and based on the texture and cementation of each sample. The observed secondary pores, which included microporosity in the Tarbert Formation, were generated mainly due to the dissolution of unstable detrital grains (particularly feldspar) or to preservation of tiny pores among the kaolinite plates or within feldspar grains. The variation in the content of porosity in the Tarbert Formation did not change systematically below the unconformity surface (Figure 6-8). Petrographic analysis of the studied samples showed that the

porosity may have been controlled by primary (sedimentological) and secondary (diagenetic) factors: the grain size, sorting and characteristics of the sediment are important factors controlling the primary porosity. In addition, the type of detrital grains within the sediments and the presence of unstable grains have led to the generation of secondary porosity.

The main diagenetic factors which observed in the studied samples and controlling the porosity of the Tarbert Formation were dissolution of minerals (commonly feldspar) and cementation of others (particularly calcite and clay possibly (kaolinite). It seems that two phases of dissolution have contributed to the enhancement and generation of porosity. The first phase of dissolution dissolved the unstable grains and formed secondary porosity; this dissolution and generation of secondary pores may have been followed by precipitation of calcite cement. The second phase of dissolution seems to be the most important phase for the creation of the secondary porosity observed in the sandstone of the Tarbert Formation, this phase has been interpreted to be post-dated calcite cementation which dissolved only the feldspar grains and not the calcite cement. Petrographic evidence for this is the observation of oversized secondary pores generated due to the complete dissolution of feldspar surrounded by calcite cement. These pores would have been infilled by the calcite cement if the dissolution of the feldspar occurred before the precipitation of calcite. According to (Surdam et al., 1984), in buried sandstones, dissolution of only aluminosilicate minerals (commonly feldspar) in the presence of carbonate cement (commonly calcite) is possible; this may occur by the influx of acidic fluids containing carboxylic acids with high partial pressures of CO_2. In this case, the carboxylic acids may work as a buffer and preserve a constant PH; the increase in the partial pressures of CO_2 may suppress or decrease the solubility of carbonate, while feldspar and other aluminosilicate minerals will remain liable to dissolution. Therefore, in such conditions, it is possible for dissolution of feldspar with preservation and/or precipitation of calcite at the same time to occur in buried sandstones.

Similar phenomena have been reported by many authors, confirming that selective feldspar dissolution occurred in sandstone in the presence of carbonate cement and that dissolution of carbonate was suppressed (Yuan et al., 2015). Furthermore, (Macquaker et al., 2014) reported the presence of authigenic kaolin in Kimmeridge Clay Formation without any dissolution of the associated carbonate minerals. In a calcium isotope study

in organic-rich sediments, (Turchyn and Depaolo, 2011) also mentioned the suppression of carbonate dissolution in the presence of authigenic clay minerals. Therefore, in the presence of carbonate, dissolution of feldspar and enhancement of secondary porosity by organic CO_2 produced from the thermal maturation of organic matter in buried sandstones is possible.

This, along with the presence of evidence for dissolution of minerals and generation of secondary porosity observed in the studied samples of the overlying Heather formation, indicates that these diagenetic effects in both formations are most likely to have been formed as a result of deep diagenetic processes and are, therefore, not related to the unconformity surface.

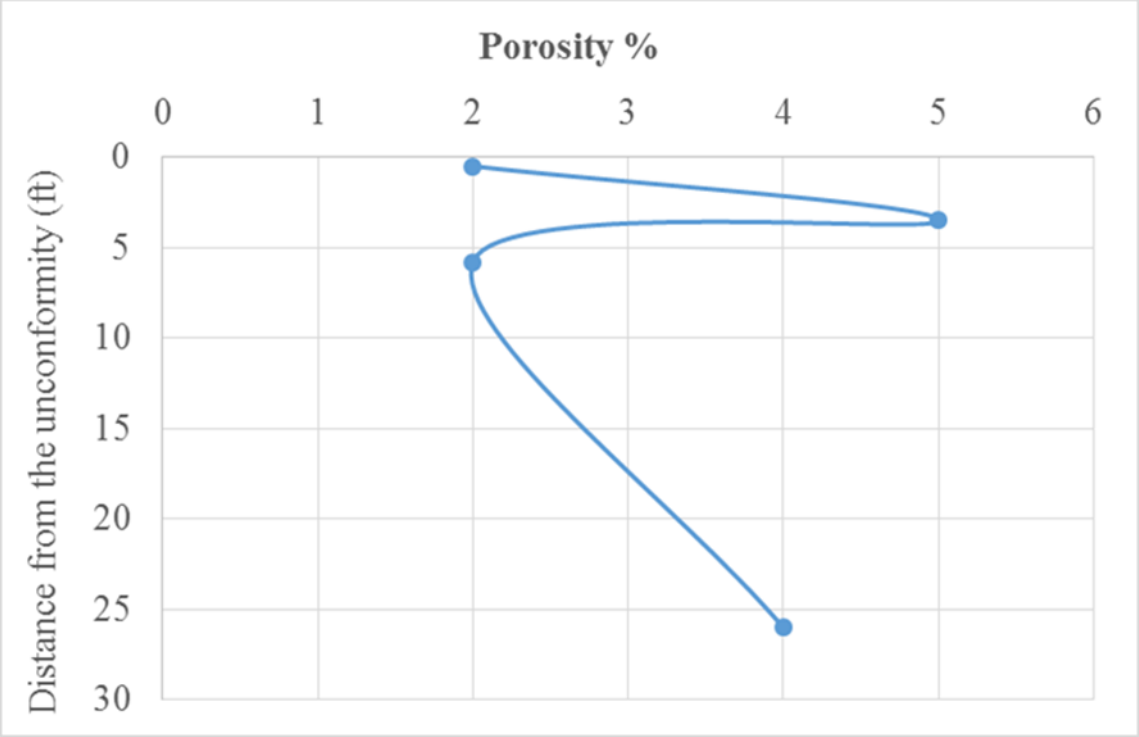

Figure 6-8. Vertical variation in the content of porosity toward the unconformity surface.

6.3.4 Conclusion

Variation in the distribution and content of feldspar, calcite and porosity of the Tarbert Formation lying below the Base Humber Unconformity was observed. This study is not concerned in interpreting the reason for this distribution and variation, the main target is to study and examine whether this distribution was formed as a result of diagenetic change related to the unconformity surface on the top of this formation or not.

Petrographic analysis showed that there are several lines of evidence for the post-depositional diagenetic changes within the Tarbert Formation. These include dissolution of some feldspar grains and enhancement of porosity and cementation of carbonate cements. The dissolution of some framework grains is interpreted to be the main source of the observed secondary porosity in the Tarbert Formation. However, most evidence indicates that there is no relationship between the observed distribution of minerals and porosity and the unconformity surface lying above the top of the Tarbert Formation. The evidence includes:

1. The absence of vertical systematic variation in the content and distribution of feldspar, kaolinite, calcite and porosity toward the unconformity surface. If the Base Humber Unconformity was the main cause of this variation, the content of feldspar grains and calcite cement should decrease systematically toward the unconformity surface and the content of kaolinite and porosity would be expected to increase systematically toward the unconformity surface.

2. Similar diagenetic processes have been observed in both formations below and above the unconformity surface. If the dissolution of feldspar and enhancement of secondary porosity is related to the unconformity surface located at the top of Tarbert Formation, it is difficult to explain the existence of similar diagenetic processes in the samples of the Heather Formation overlying the unconformity surface. This may indicate that the observed diagenetic effects are most likely to be related other diagenetic processes rather than the meteoric waters that are supposed to penetrate through the unconformity surface.

3. Dissolution of feldspar grains has been interpreted to post-date the majority of compaction processes despite the depth of burial, which exceeds 10670 ft.

4. Dissolution of feldspar grains has been interpreted to have been generated post-dating the precipitation of calcite and most likely to be due to the influx of acidic fluids containing carboxylic acids with high partial pressures of CO_2.

5. The presence of fresh and unaltered kaolinite with no signs of compaction, despite the depth of burial, which exceeds 10670 ft.

6.4 Well 15/17-B2 in Piper Field

This well was drilled in the Piper Field to examine the Upper Jurassic sandstones. The Piper Field is situated in Block 15/17 and located in the Northern margin of the Witch Ground Graben (WGG) in the Outer Moray Firth. The field contains four tilted fault blocks, dipping toward the northeast away from the graben. The reservoir of Piper Field comprises of two sandstone formations within the Upper Jurassic Humber Group, the Piper and Sgiath Formations (For more details about the geography and geology of the area please see (Schmitt and Gordon, 1991). In this section only the Piper Formation will be studied, as it is the only observed sandstone formation in the studied well.

In the studied Well 15/17-B2 the Piper Formation is the main reservoir unit and the Piper Formation is overlain unconformably by the Upper Jurassic Kimmeridge Clay Formation (Figure 6-9). The unconformity surface separating the Piper formation from the Kimmeridge Clay formation has been observed at a depth of 9656.3ft and is named the Base Kimmeridgian Unconformity (BKU). All samples were taken from this formation at vertical intervals with proximity to the unconformity surface, to study the possible diagenetic effect of this unconformity on the sediment underneath.

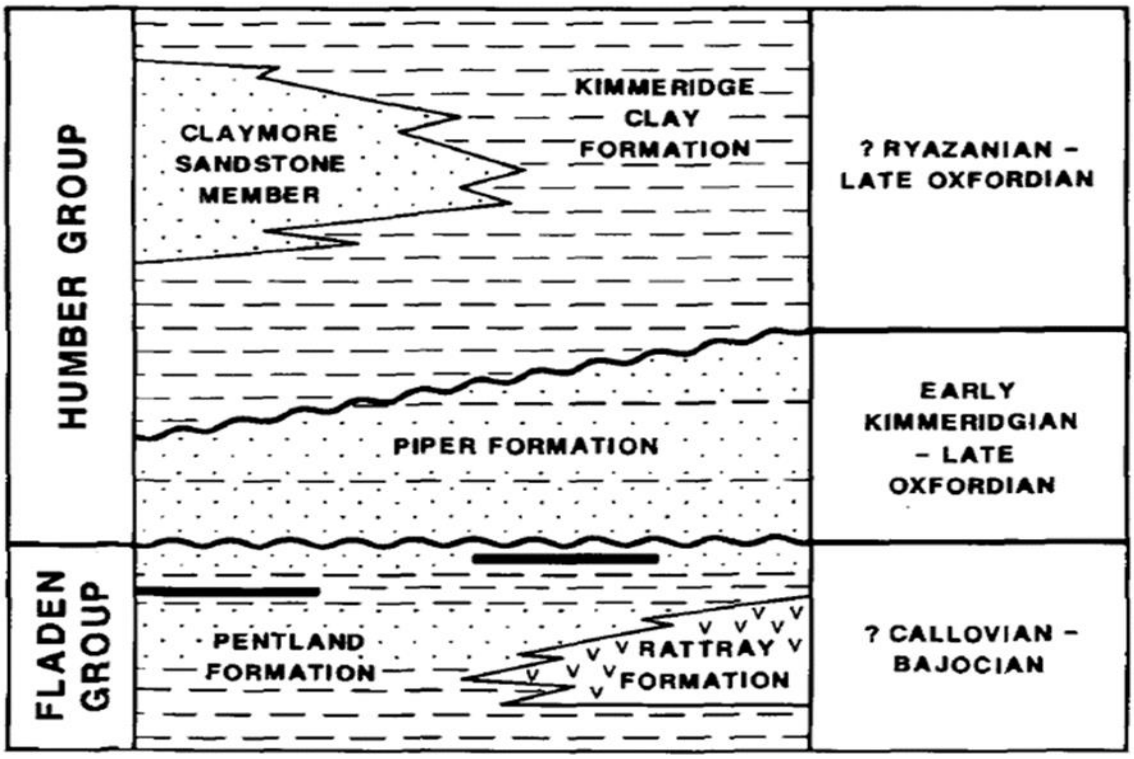

Figure 6-9. Stratigraphic relationships for the formation of the Upper Jurassic sediments in the Piper Field (from (Burley, 1986)).

6.4.1 Sedimentological analysis

This section will present the results of sedimentological descriptions which have been conducted for the available core from the studied well, allowing the observation of sediment details and interpretation of facies. Sedimentological description (core logging) was performed for more than 150 feet of the observed core.

6.4.1.1 Sedimentological analysis results

Figure *6-10* illustrates the stratigraphic core descriptions of well 15/17-B2 located in the Piper Field). The coring interval started from the Upper Jurassic Kimmeridge Clay Formation, just a few feet above the Base Kimmeridgian Unconformity which lies on the top of Piper Formation. In general, the Piper Formation is interpreted to be shallow marine sandstones composed of three sandstones facies interrupted by mud laminae (Burley, 1986).

6.4.2 Petrographic analysis

The main target of this study is the Piper Formation, which lies directly below the detected Base Kimmeridgian Unconformity, All the samples were taken from this formation at vertical intervals, with proximity to the unconformity surface, for further investigation and petrographic analysis, which included texture, minerology and porosity of the sandstone.

6.4.2.1 Lithological texture

Based on the grain size, three sandstone facieses were identified within the described core interval of Well 15/17-B2, these facies represent the Piper Formation in this well. Grain size ranged from fine to very coarse-grained sand in the upper facies, fine-grained sand in the middle facies but this was very occasionally associated with some coarse grains and fine to medium grains in the lower facies. The sandstone was medium to dark brown grey, non-calcareous, laminated mud with traces of fossils, and contained variably cemented sandstones with silica and calcite cement; sorting varied from poorly to moderately sorted sandstones, which consisted of subangular to subrounded sand grains (Table 6-3).

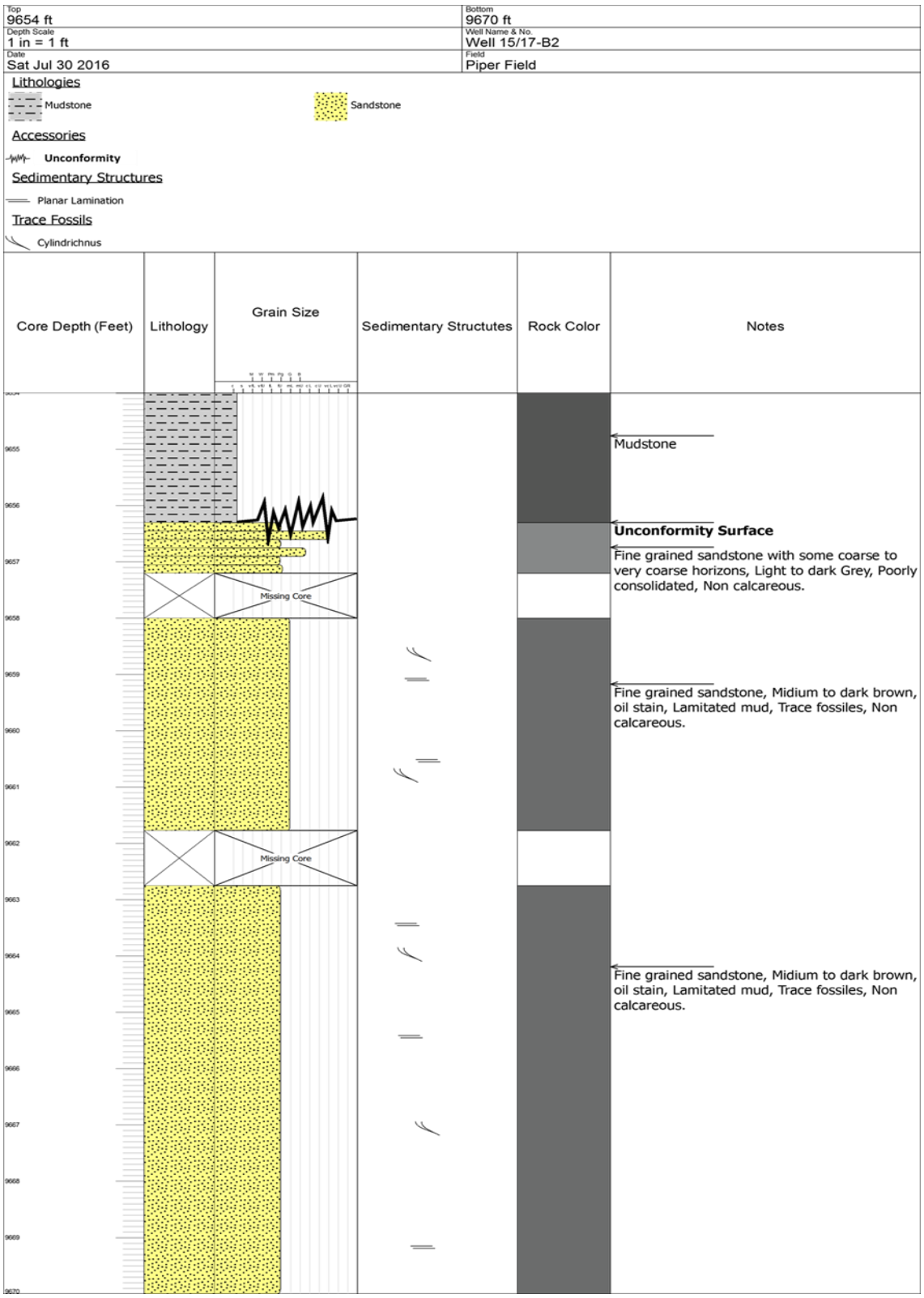

Figure 6-10. Lithological stratigraphy and core descriptions of the Piper Formation in Well 15/17-B2 in the Piper Field. The Base Kimmeridgian Unconformity is recognised at depth 9656.3 ft, just above the top of Piper Formation and separating Piper Formation from the Upper Kimmeridge Clay Formation.

Table 6-3. Showing the lithological texture of the studied piper formation in Well 15/17-B2. F-VCS = fine to very coarse sand, FS= fine sand and F-MS= fine to medium sand. P-M = poor to medium sorting, M= Medium sorting. SA-SR= subangular to subrounded sand.

Facies Code	Grain Size	Sorting	Roundness
3-8	F-VCS	P	SA-SR
3	FS	P-M	SA-SR
4	F-MS	P-M	SA-SR

6.4.2.2 Quantitative analysis

The main petrographic analysis data of the studied samples of Well 15/17-B2 is summarized in Table *6-4*.

Table 6-4. Petrographic analysis data for well 15/17-B2

Sample no.	Core Depth (ft)	Facies	CONSTITUENT (%)								Total %
			Porosity %	Framework Minerals %			Accessory Minerals %	Cements %		Others %	
				Quartz	Feldspar	Rock Fragment	Mica	Calcite	Clay	Iron Oxide and pyrite	
33	9657	3-8	12	61	1	0	0	23	1	2	100
34	9658	3-8	20	60	7	0	1	2	8	2	100
35	9659.3	3	12	64	10	1	2	0	7	4	100
36	9660	3-8	25	46	12	1	3	0	10	3	100
37	9664	4	22	47	13	1	2	0	13	2	100
43/B2	9669	4	5	50	9	10	1	10	13	2	100
44/B2	9677	4	11	56	7	6	2	3	14	1	100
45/B2	9700	4	23	44	7	9	1	0	14	2	100

6.4.2.2.1 Minerology

This section will describe in detail the main composition of the studied samples.

6.4.2.2.1.1 Framework Minerals

The principal detrital components, quartz, feldspar and rock fragments represented more than 60% of the composition of the Piper Sandstones. Monocrystalline quartz was the

main component and ranged between 45 -63%; some of these quartz grains were cracked and corroded. Furthermore, some samples showed grain-to-grain contacts (sutured grain contact), which may result from compaction processes: this was supported by the presence of fractured grains, particularly in the poorly sorted sand (Figure 6-11 A). The feldspar content varied from facies to facies, ranging from 1 up to 13%, and it is likely that the majority of this was potassium feldspar. Variable degrees of alteration, replacement and partial or complete dissolution of feldspar were observed in almost all samples (Figure 6-11 B). Rock fragments represented a small proportion of the total components, ranging from 0-3%, with the exception of one sample which reached 9%. There is a variety of mica and heavy minerals that occur locally and do not exceed 2%.

6.4.2.2.1.2 Authigenic minerals

Petrographic analysis of the studied samples indicated that the sandstones of the Piper Formation were friable to poorly cemented sandstones. Two main cement types were observed within the studied samples, clay and calcite cements (Figure 6-11 C). The dominant cement type in most samples was clay, with the exception of one sample which contained tightly cemented calcite. The clay cement content ranged from 7-19% and calcite cement occurred sporadically. Some pyrite was observed, as nodules in most samples, and ranged from 1 to 4% in content.

6.4.2.2.2 Porosity

The total observed porosity from the petrographic analysis samples within the studied samples of the Piper Formation ranged from 5-25%. This included the two different types of porosity, primary (intergranular porosity) and secondary porosity, which includes intragranular porosity and microporosity. The secondary porosity was interpreted to have been formed as a result of partial or complete dissolution of detrital grains (commonly feldspar) and/ or early calcite cement filling the pore spaces; microporosity refers to the tiny pores that may be preserved within plates of clay (Figure 6-11 D). Another type of secondary porosity was also observed, but did not contribute significantly to the total counted porosity. This is fractured porosity, which was observed in some samples surrounding the grain. The dissolution of some detrital grains and/or cements was the main cause for the generation of secondary porosity in the Piper Formation. However, in

most samples the generation of secondary porosity was followed by precipitation of either calcite or clay cements, reducing the total porosity of the sandstone.

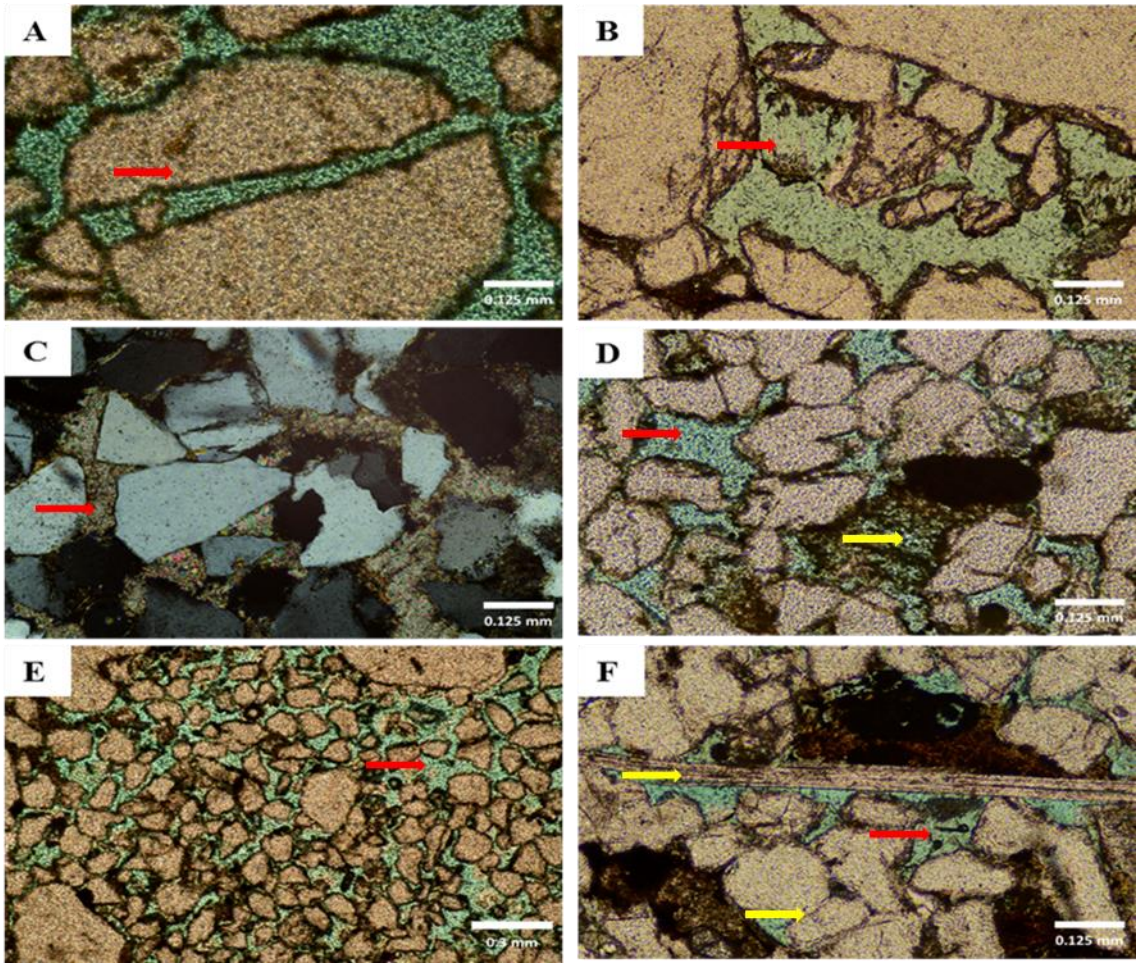

Figure 6-11. Thin-section photomicrographs showing **A**. Quartz grains that have been cracked and fractured due to compaction: Well 15/17-B2, 9657 ft. **B**. Generation of secondary porosity due to partial to complete dissolution of feldspar grains: Well 15/17-B2, 9658 ft. **C**. Early calcite cement filling the intergranular pore space and supporting the framework grains: well 15/17-B2, 9669 ft. **D**. Showing secondary porosity formed as a result of partial or complete dissolution of detrital grains and/ or early calcite cement filling the pore spaces (red arrow) and preservation of microporosity within plates of clay (yellow arrow) , well 15/17-B2, 9660 ft. **E**. Intergranular porosity which is interpreted to be secondary in origin and generated due to the dissolution of cement which was filling the pore spaces: Well 15/17-B2, 9657 ft. **F**. Showing the presence of uncompacted secondary pores (red arrow) within compacted sandstone sample, indicated by bending flake of mica and quartz grain contact (yellow arrows): Well 15/17-B2, 9659.3 ft.

6.4.3 Spatial distribution of feldspar and porosity below the Base Kimmeridgian Unconformity

This section will illustrate the point counted data obtained from the petrographic analysis of the Piper sandstone samples, to examine whether there is any relationship between the Base Kimmeridgian Unconformity which lies above the Piper Formation and the spatial distribution of minerals and porosity below this unconformity. This will be by examined by studying the vertical distribution pattern of feldspar and porosity of sandstone under the unconformity surface within this formation.

6.4.3.1 Feldspar

The content of feldspar grains in the Piper Formation ranged from 1 to 13%. The results from the point counted samples indicate that feldspar is occurring in varying proportions within the Piper sandstone units. The variation of feldspar content is most likely to be related to the variation in the facies of the Piper Formation and the provenance of the composition of each facies, and also because feldspar tends to be concentrated in the finer sand units. Most of the studied samples showed variable degrees of alteration, replacement and partial or complete dissolution of feldspar grains and generation and enhancement of porosity. Evidence for this alteration and dissolution of feldspar grains was observed in almost all the studied samples from the Piper Formation. Several lines of evidence indicate that this alteration and dissolution of feldspar is formed by post-depositional diagenetic processes. However, in relationship to the unconformity surface, no systematic variation in the content of feldspar was recognised below the Base Kimmeridgian Unconformity (Figure 6-12). If the dissolution of feldspar grains was caused by the penetration of meteoric water through the Base Kimmeridgian Unconformity, systematic vertical change of the feldspar volume would be expected and the degree of alteration and dissolution of the feldspar grains should be increasing toward the unconformity surface.

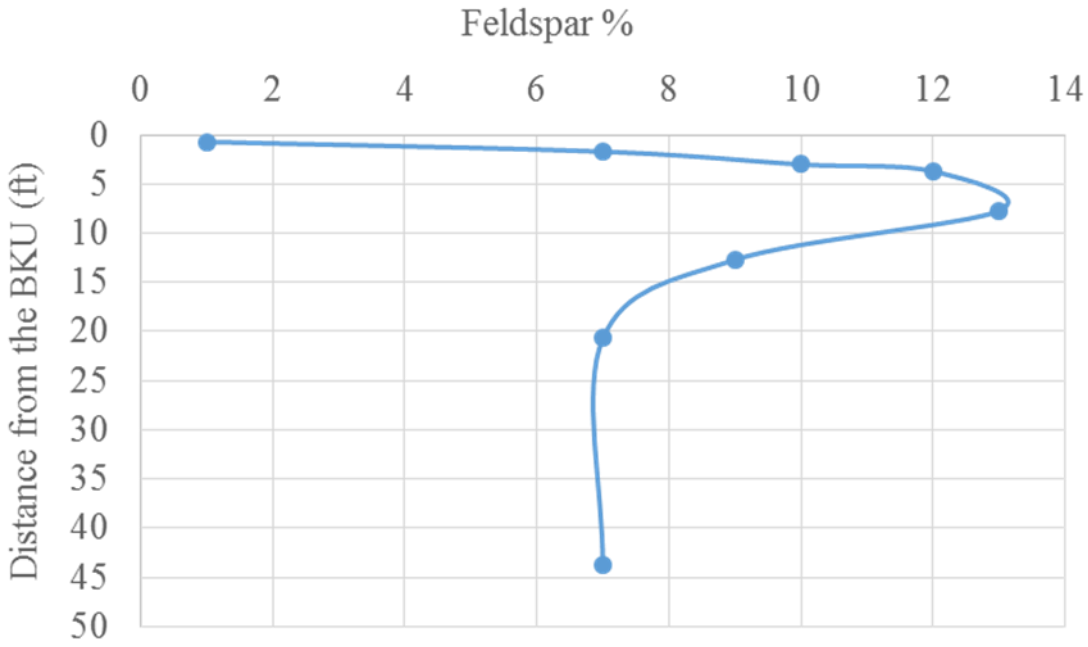

Figure 6-12. Distribution of feldspar grains below the Base Kimmeridgian Unconformity in the studied well.

6.4.3.2 Porosity

In general, the point counted porosity values determined from petrographic analysis was usually lower than the measured core analysis porosities. Two different types of porosity were recognised within the studied Piper Formation samples, primary and secondary porosity. Primary porosity was found to be variable in the studied samples and controlled mainly by the texture and cementation of each sample. However, the textures and heterogeneity of some of the analysed samples suggest that it is possibly for some of the observed intergranular porosity to be secondary in origin and generated due to the dissolution of cement, which was filling the pore spaces (Figure 6-11 E). Because no high content of cement was observed within the Piper sandstone, it is difficult to know what type of cement/s had been dissolved and produced this intergranular porosity. However, some sporadic patches of calcite cement were observed in some of the analysed samples. Therefore, it is possible that some of the observed intergranular porosity within the Piper sandstones was formed as a result of dissolution of early calcite cement that was supporting the framework grains, thus enhancing the total sandstones porosity.

The observed secondary porosity in the Piper Formation was divided into three types of secondary porosity: grain dissolution porosity, produced mainly by the dissolution of unstable framework grains (particularly feldspar), microporosity that formed within authigenic clays, filling the pore spaces, and fractured porosity generated due to the fracturing of some brittle grains or the fractured porosity surrounding some grains which represented only a minor percentage of the point counted porosity. The petrographic study indicated that most of the recognised porosity was primary intergranular porosity, but grain dissolution porosity represented a significant percentage as well. Most of the petrographic evidence indicated that the main diagenetic factor controlling the secondary porosity in the Piper Formation was the dissolution of feldspar grains and clay or calcite cements. However, no correlation between the volume of porosity and content of feldspar and clay or calcite cements was observed (Figure 6-13 and Figure 6-14). This lack of correlation may be interpreted to be due to the variation of the original amounts of both feldspar and clay in each sample. As mentioned above, the Piper Formation is subdivided into many sandstone units and each unit has its own composition and textural characteristics. Furthermore, the increase in porosity volume due to the dissolution of some detrital grains will be balanced by the generation and precipitation of a similar volume of diagenetic minerals that have been formed as products of the dissolved minerals.

In relationship to the unconformity surface, the total amount of recognised porosity did not change systematically toward the unconformity surface (Figure 6-15), whereas, if the dissolution of feldspar grains and the generation of secondary porosity was related to the location of the Base Kimmeridgian Unconformity lying on the top of the Piper Formation, the degree of porosity should increase upward toward the unconformity surface.

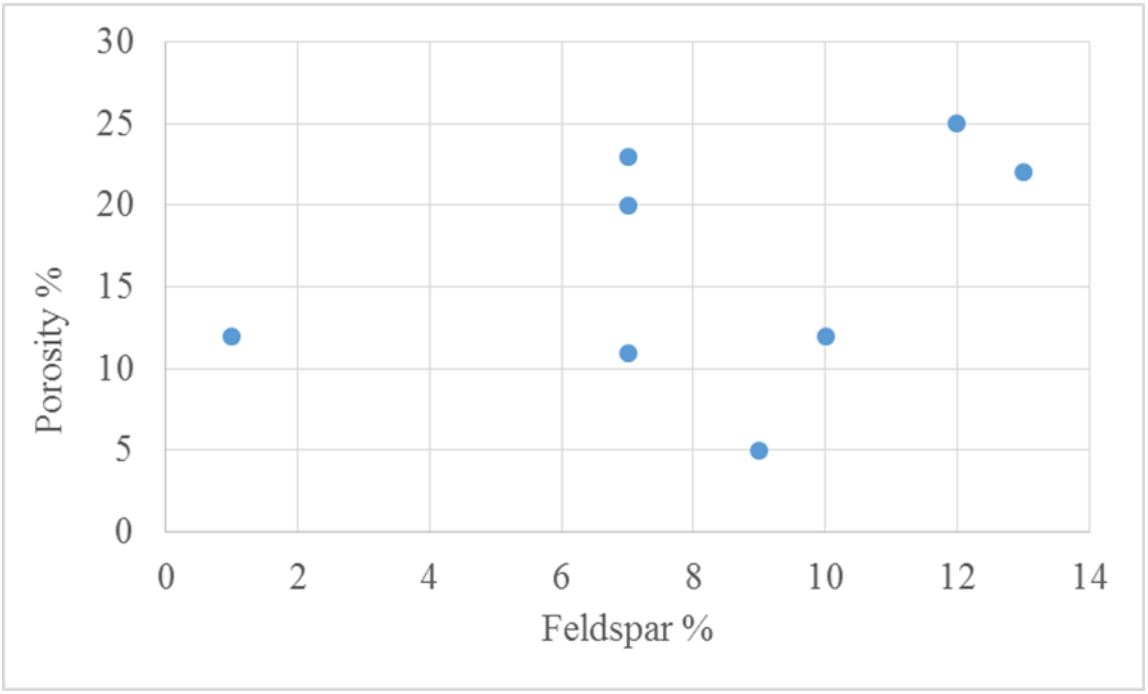

Figure 6-13. Lack of correlation between the porosity and the feldspar content below the Base Kimmeridgian Unconformity in the Piper Formation.

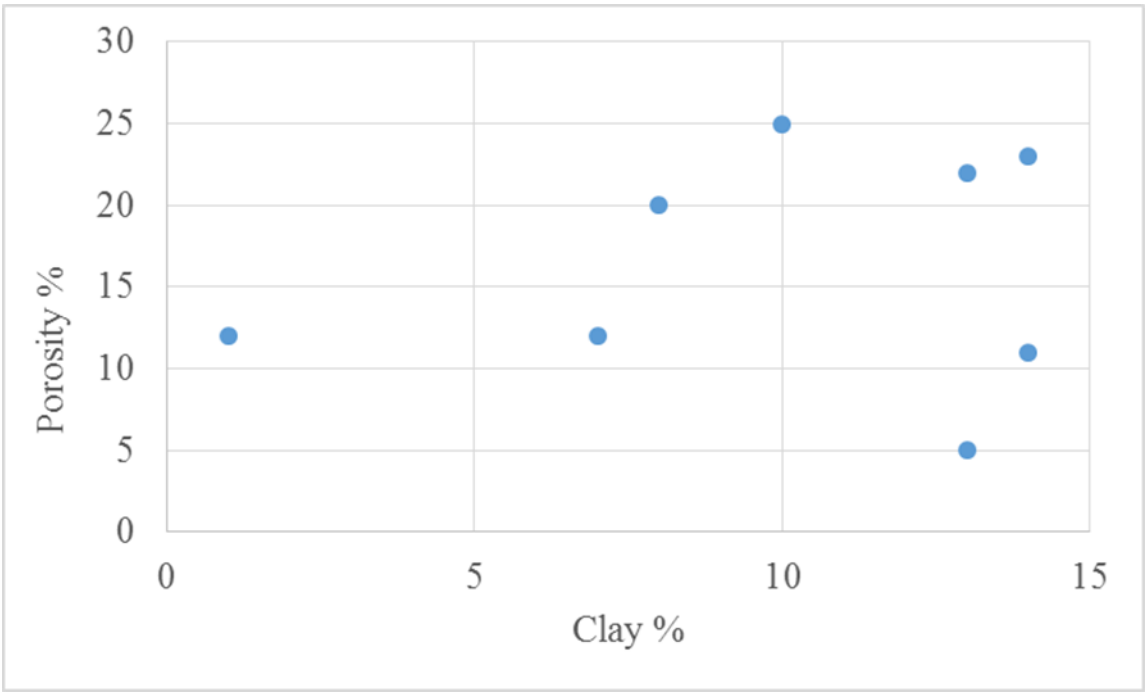

Figure 6-14. Lack of correlation between the porosity and clay content below the Base Kimmeridgian Unconformity in the Piper Formation

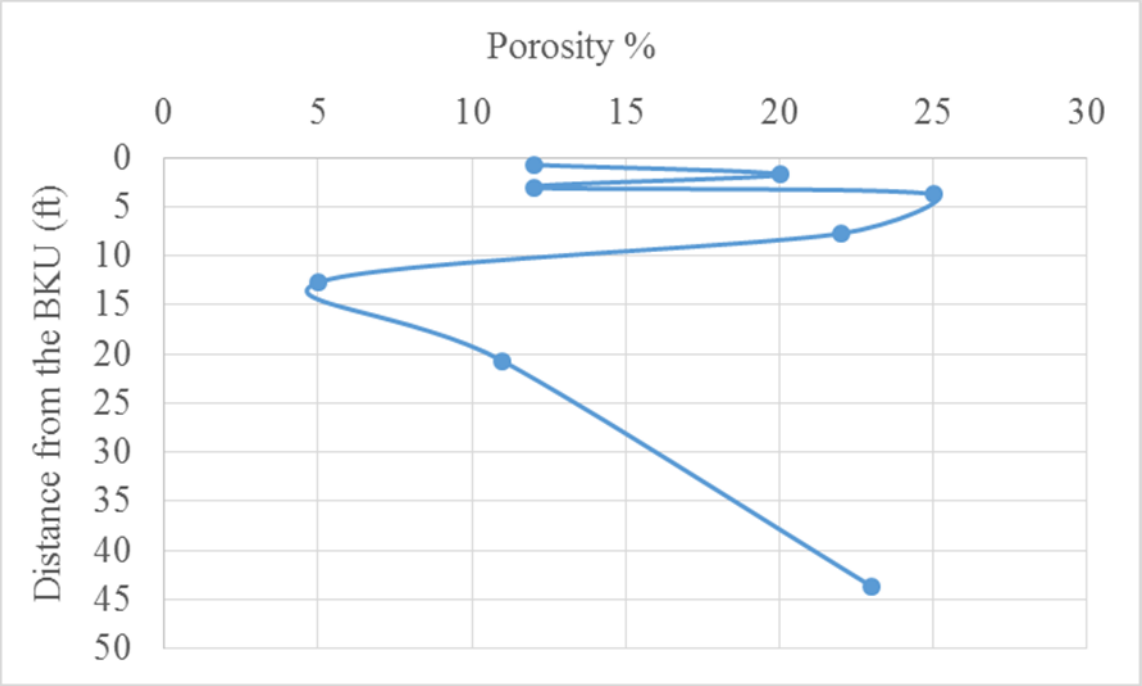

Figure 6-15. Distribution of porosity below the Base Kimmeridgian Unconformity in the studied well.

6.4.4 Discussion and Conclusion

The main diagenetic changes recognised within the Piper sandstones were dissolution of some framework grains (commonly feldspar) and enhancement of porosity. The dissolution of unstable minerals due to the influx of meteoric water through unconformity surfaces was the main hypothesis on which this study was based. Diagenetic changes are expected to occur if sedimentary rocks are subjected to the effect of meteoric water. In the area of interest, the Base Kimmeridgian Unconformity lies directly above the top of Piper formation; to examine whether there is any diagenetic changes within the Piper Formation or not, and if they exist, are they related to the influx of meteoric waters through the Base Kimmeridgian Unconformity or not, all the analysed samples were taken at regular intervals at depths starting directly below the unconformity surface and going deeper. Therefore, any possible diagenetic changes related to the unconformity surface would be expected to be seen in a vertical trend and increase with proximity to this unconformity surface.

The petrographic analysis results showed that there were several lines of evidence for the post-depositional diagenetic changes within the Piper Formation. These included the

dissolution of some framework grains, cements and enhancement of porosity. The dissolution of some framework grains and/or cements seems to be the main source of the observed secondary porosity in the Piper Formation. However, after a deep analysis of the collected samples, several items of petrographic evidence indicate that the dissolution and creation of secondary porosity in Piper Formation were not created by an influx of meteoric waters through the Base Kimmeridgian Unconformity, for instance, the following observations:

1. The absence of any decrease in feldspar content toward the unconformity surface; if the dissolution of minerals was related to the unconformity surface a systematic vertical decrease in the content of feldspar would be expected.
2. The absence of a vertical increase in the generated secondary porosity toward the unconformity surface; if the secondary porosity in Piper sandstones was created due to the influx of meteoric waters through the unconformity surface, the content of the generated porosity would be expected to increase in proximity to the unconformity surface.
3. The presence of uncompacted, oversized secondary pores and signs of compaction, which included fractured grains, quartz-grain to-grain contact and bending of mica grains) (as shown in Figure 6-11 E and F) within the same field of view of some samples. This indicates that the observed dissolution and generation of secondary porosity is most likely to post-date most of the mechanical compaction.
4. The presence of some petrographic evidence for the late dissolution and enhancement of porosity.
5. The difficulty of interpreting how such secondary porosity that may have formed near to the unconformity surface could be preserved in this depth of burial, which exceeds 3000 m.

Therefore, based on these results it is clear that the aggressive fluids responsible for the dissolution of some of the framework grains and cements and for the creation of secondary porosity in the Piper Formation are most likely to be highly acidic fluids capable of dissolving large amounts of unstable minerals that may have migrated into the Piper sandstones in deep burial after the majority of mechanical compaction processes. During the deep burial it is widely believed that generation of CO_2 or organic acids due

to thermal degradation of organic matter is the most common source of acidity (Surdam et al., 1984).

In the area of study, the Piper Formation is unconformably overlain by the Kimmeridgian clay Formation and underlain by the Bathonian mud rocks, both of which are considered to contain large amounts of organic matter. The Kimmeridge Clay Formation is widely considered as a highly mature source rock and the main hydrocarbon source for most of the reservoirs in the Outer Moray Firth area. According to (Burley, 1986), it is possible for this source rock, which is highly impregnated with organic matter, to produce a large component of the acidity that may be capable of dissolving calcite cement and framework grains. These possible acidic fluids that were generated may have been expelled from the Kimmeridge Clay Formation into the adjacent sandstones via permeable flow paths and may have created extensive secondary porosity by dissolving carbonate cement and some framework grains. Burley, (1986) suggests that the fault activity during the late Upper Jurassic and early Cretaceous juxtaposed the Kimmeridge Clay Formation against the sandstones of the Piper Formation. By the late Cretaceous, when burial depth of the Piper Formation was less than 500 m, the Kimmeridge Clay Formation in the adjacent Witch Ground Graben was already buried at a depth exceeding 2 km. Therefore, aggressive acidic fluids created due to thermal degradation of organic matter within the Kimmeridge Clay Formation in the Witch Ground Graben may have migrated along the bounding faults of the Witch Ground Graben into the Piper sandstones and created the observed secondary porosity (Figure 6-16 A). This creation of secondary porosity was shortly followed by the migration of hydrocarbons from the same source rock into the Piper Formation, filling the generated pore space and preserving the previously generated secondary porosity (Figure 6-16 B). This assumption was also supported by conclusions of (Burley et al., 1989), who interpreted the diagenesis in the Tartan Reservoir to be related to migration of a significant amount of hot fluids from the adjacent Witch Ground Graben to the Tartan reservoir along the bounding faults.

Based on these explanations, and since all the signs indicate that the dissolutions and the enhancement of porosity were occurring in a late stage and post-dated the majority of the mechanical compaction processes, the evidence clearly suggests that there is no relationship between the observed diagenetic changes, including the generated secondary porosity within the Piper Formation in the Piper Field, and the presence of the Base

Kimmeridge Unconformity which lies above the formation. Therefore, it seems that the late dissolution of the framework grains and/or cements and the generation of secondary porosity in the Piper Formation are most likely to be related to highly acidic fluids that may have been expelled from the nearby Kimmeridge Clay Formation and migrated to the studied Piper sandstones, rapidly followed by migration of oil, which has preserved the generated secondary porosity and prevented further compaction and diagenesis processes from taking place.

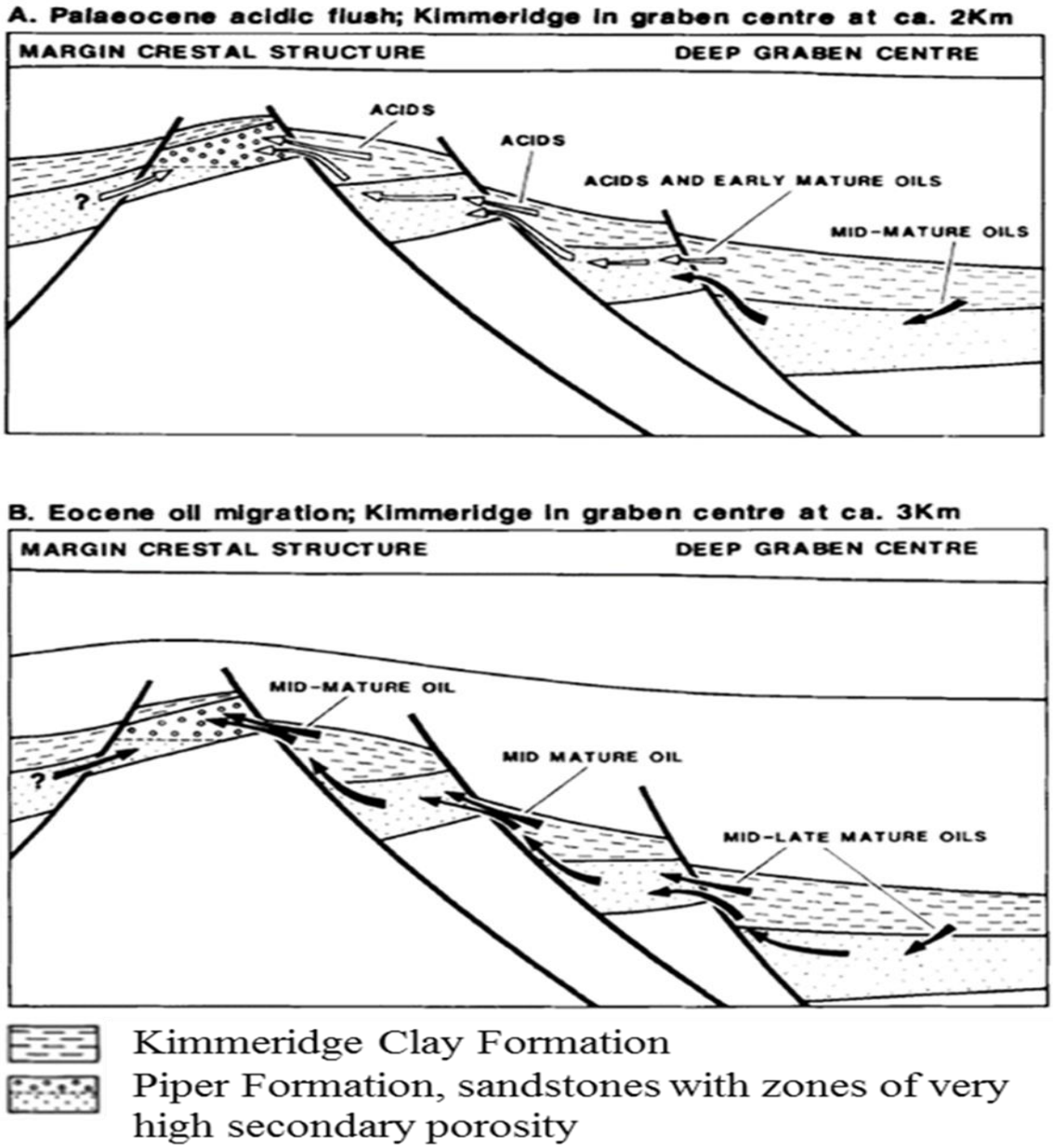

Figure 6-16. Schematic diagram showing a possible migration path for the acidic fluids and hydrocarbon from the graben to margin crestal structure (from (Burley, 1986)).

Chapter 7 **Summary and Conclusion**

Several studies have proposed that improved reservoir quality is due to enhanced secondary porosity formation and supported a profound relationship between the presence of an unconformity surface and the enhanced reservoir quality underneath (e.g. (Ketzer et al., 2009, Shanmugam, 1990). By contrary, other studies have indicated that there is no evidence for the existence of such a relationship (e.g. (Ehrenberg and Jakobsen, 2001).

In this study, both hypotheses were examined by evaluating the role of the unconformity in the distribution of porosity and clay minerals in selected North Sea Clastic reservoirs, particularly the Late Triassic Skagerrak Formation in the Kittiwake Field (underlying the Mid-Cimmerian Unconformity) in the Central North Sea and the Middle Jurassic Brent Group sandstones (underlying the Base-Cretaceous Unconformity) in the Tampen Spur area, in the Northern North Sea.

Detailed sedimentological and petrographic analyses, using both optical microscopy and Scanning Electron Microscopy, were undertaken on 212 core samples from the selected 32 wells in the area of study. This work documented lithology, texture, mineralogy and diagenetic characteristics, in order to understand the origin and timing of grain and/or cement dissolution and the formation of authigenic kaolinite, and the effect of these processes on the reservoir properties.

7.1 Principal findings

The results of the study show that there are several main post-depositional diagenetic changes within the studied sandstones samples, which include:

1. The dissolution of some framework grains (commonly feldspar) and cements (commonly calcite) in both studied areas.
2. The presence of authigenic kaolinite in both studied areas. However, the amount of the authigenic kaolinite was greater in the Tampen Spur area than in the Kittiwake Field.

Both of these diagenetic processes are well recognised in both studied areas and have had a significant effect on the reservoir properties. The dissolution of framework grains and/or cements was the main cause of the generated secondary porosity, and the main source of

mineral-rich fluids for the precipitation of authigenic kaolinite in the reservoir sandstones. Petrographic observations showed several lines of evidence for this dissolution of minerals, including the development of oversized pores and the partial and complete dissolution of detrital grains and carbonate cements. Different factors may have caused these diagenetic changes, which affected the reservoir quality. One of the potential factors is the effect of the unconformity surfaces, which overlie the reservoir sandstones. Examining evidence for and against this unconformity control has been the main target of this study.

From the results of the petrographic analyses, it is clear that the observed diagenetic changes in all the studied wells show no clear link to the presence of the unconformity surfaces at the top of the studied sandstones. Several lines of evidence support this conclusion, including:

1. A number of observations, which indicate that the observed dissolution of detrital grains (commonly feldspar) and/or carbonate cements (commonly calcite) and the formation of authigenic kaolinite post-date the majority of mechanical compaction processes. These observations include:
    a) Preservation of uncompacted delicate crystal remnants of feldspar lining the secondary pores formed by dissolution of feldspar grains.
    b) Preservation of delicate euhedral booklets of authigenic kaolinite and its association with high microporosity at burial depths exceeding 2000 m.
    c) Preservation of oversized secondary pores; these pores would have been destroyed if they had formed before most of the compaction processes occurred and would not resist the expected vertical stress formed due the continued deposition above.
    d) The presence of compaction signs in the main texture of the sands (including fractured grains, quartz grain-to-grain contacts and bending of mica plates) associated with uncompacted, oversized pores, delicate crystal remnants of dissolved feldspar grain and highly microporous kaolinite within the same sample.

    This evidence supports the interpretation that the dissolution of minerals, which enhanced the reservoir porosity and enabled the precipitation of authigenic

kaolinite, occurred at very late stages of diagenesis, and post-dates the majority of mechanical compaction processes associated with deep burial. It is clear, therefore, that the diagenetic changes observed in the reservoir sandstones studied were not caused by the influx of meteoric fluids during or shortly after uplift, exposure and creation of the unconformity surface.

However, it could be argued that the preservation of delicate euhedral booklets of authigenic kaolinite, the delicate crystal remnants lining the secondary pores from dissolved feldspar grains and the oversized secondary pores in the studied sandstones, has occurred because the late dissolution associated with meteoric waters percolating through the unconformity surface took place in already compacted sandstones. In order for the observed degree of compaction to occur, the reservoir units would need to have been buried to considerable depths (e.g. 1-2 km). However, this hypothesis can be disproved by noting that the maximum thickness of the sediments deposited above the studied sandstones prior to the uplift and partial or complete erosion, which led to development of the unconformity, is recorded as being only between a few metres and a few hundreds of metres, in all the studied wells and across the region as a whole. This thickness of sediments would have resulted in only the very initial phases of compaction before the development of the unconformity, and would not have caused the observed signs of compaction.

Another argument is that the compaction may have been arrested by an abundance of quartz cementation, and hence allowed preservation of the observed features. However, this hypothesis does not seem to be applicable in the study area, because there is no evidence for the presence of an abundance of quartz cement. Furthermore, quartz cement rarely forms at depths less than 1.5-2 km (Wilkinson et al., 2014) and commonly occur in deep burial and in temperatures above 70–80° C (Aplin and Warren, 1994), whereas the sediments exposed during unconformity development were at much shallower depths. Therefore, it seems that the secondary porosity formed due to dissolution of some minerals, which are, in many cases, associated with the precipitation of euhedral booklets of highly microporous authigenic kaolinite, is unlikely to have been formed as a result of influx of meteoric waters through the unconformity surfaces, which lie at the top of the studied sandstones and are most likely to have been formed in a late stage

and post-date the majority of the mechanical compaction processes. Otherwise, it is very difficult to explain how secondary porosity formed due to dissolution of some minerals could resist the effects of expected effective stress at depths exceeding 2000 m.

2. The absence of any obvious systematic distribution of framework grains and/or carbonate cements relative to the unconformity surface in any of the studied formations, regardless of how close the samples were to the unconformity surface. For instance, in the Tarbert reservoirs sandstones of Wells 34/10-1 and 34/10-8, where the Base-Cretaceous Unconformity is located directly at the top of Tarbert Formation, the amount of dissolution and the volume of dissolved feldspar and carbonate cement was not higher than in Wells 34/10-34 and 34/7-19, where the Base-Cretaceous Unconformity is located 4.5 m and 14.4 m respectively above the top of the Tarbert Formation. Furthermore, in both cases, the distribution of feldspar grains and carbonate cements was not vary systematically toward the unconformity surface. However, if the dissolution of feldspar and carbonate cements was related to the presence of the unconformity surface at the top of the studied sandstones, the degree of feldspar dissolution would be expected to increase with proximity to the unconformity surface.

   Another supporting example is that petrographic analysis and comparison between two of the studied wells within the Rannoch Formations (Brent Group) in Gulfaks Field showed a variation in the amount and distribution of plagioclase at each of the two locations. Petrographic analysis of Rannoch sandstone samples showed the presence of plagioclase within the upper part of Rannoch Formation in Well 34/10-4 which lies directly below the Base-Cretaceous Unconformity, whereas, in Well 34/10-1, the Rannoch Formation, which lies more than 90 m below the unconformity surface, was plagioclase free. If the dissolution of feldspar including plagioclase grains is related to the diagenetic effect of the unconformity surface, it is difficult to explain why plagioclase grains occur in Well 34/10-4 and particularly in samples closest to the unconformity surface and do not occur in Well 34/10-1, which is more than 90 m below the surface. The opposite trend would be expected and the volume of dissolved plagioclase should be higher in the well where the formation is closer to the unconformity than the other.

3. The absence of systematic vertical variation in the volume and distribution of secondary porosity upwards toward the unconformity surface. For instance, comparison between the well where the unconformity surface was located directly at the top of the Rannoch Formation and the well where the unconformity was located 94 m above the top of Rannoch Formation showed that, although secondary porosity formed by dissolution of some minerals was observed in both studied wells, this porosity was not higher in the well where the Rannoch Formation was lying directly below the unconformity surface than in the well where the unconformity surface was located more than 90 m above the top of Rannoch Formation.

4. The absence of any systematic increase in the content of kaolinite toward the unconformity surface in any of the studied formations regardless of how close these formations occur relative to the unconformity surface. The result indicate that most of the observed kaolinite was formed in situ and is related to a late diagenetic process. These observations include the presence of delicate euhedral booklets in most samples and the high microporosity within the kaolinite crystals. Moreover, no obvious vertical distribution trend of kaolinite content toward the unconformity surface was observed. If the creation of the kaolinite was related to influx of meteoric waters through the unconformity surface, a systematic vertical increase toward the unconformity surface would be expected. Furthermore, the volume of the generated authigenic kaolinite does not seems to be higher in the formations close to the unconformity surface than in the formations far away. In many cases the opposite result was determined: for example, the petrographic analysis results showed that in Well 21/18-4 in the Kittiwake Field, the amount of authigenic kaolinite was higher in sandstone samples that lie about 15 ft below the unconformity surface than in samples lying immediately below the unconformity surface, and again, if the formation of kaolinite was related to the creation of the unconformity surface, the opposite pattern would be expected.

Therefore, based on these results, it is clear that there is no evidence for the existence of a relationship between either the dissolution of feldspar grains and/or carbonate cements leading to the creation of secondary porosity or the precipitation of authigenic kaolinite and the presence of unconformity surfaces at the top of any of the studied sandstones in the North Sea.

In fact, the more likely cause of secondary porosity development and the other diagenetic changes observed is the subsurface influx of acidic fluid into the reservoir formations at depth. Two alternative mechanisms may be considered this process occurring in the studied area: (1) the influx of acidic fluids produced by thermal maturation of organic matter; and (2) the release and influx of organic acids and CO_2 that may have formed as a result of the biodegradation of oil. The results show that there is a possibility for the observed dissolution of some framework grains and cements and for the creation of secondary porosity and precipitation of authigenic kaolinite to be related to highly acidic fluids that migrated into the studied sandstones after they had become deeply buried and hence after the majority of the mechanical compaction processes had occurred. These acidic fluids would have been capable of dissolving large amounts of unstable minerals. During the deep burial it is widely believed that generation of CO_2 and organic acids due to thermal degradation of organic matter or as a result of biodegradation of oil are the most common sources of acidic fluids in the subsurface (Surdam et al., 1984).

In the areas of study, one of these mechanisms is most likely to be the main cause of the observed post-depositional diagenetic changes in the reservoir sections from the two main case studies, because both sections occur in close proximity to mature source rocks. The studied Middle Jurassic Brent Group formations lie above the Lower Jurassic shales of the Dunlin Group and below the Upper Jurassic marine shales of the Viking Group (Heather Formation and Draupne Formation). The Upper Jurassic Draupne Formation, which is equivalent to the Kimmeridge Clay Formation, is the main hydrocarbon source rock in the Tampen Spur area. The studied Skagerrak sandstone in the Kittiwake field is also close to the highly mature Kimmeridge Clay Formation. Furthermore, there is a marked correlation between the observed diagenetic changes and the degree of biodegradation of oil, particularly in the Gullfaks Field. This suggests that the release of organic acid and CO_2, formed as a result of oil biodegradation, is the preferred explanation for the observed post-depositional diagenetic changes. However, more studies are required to confirm the importance of the effects of organic acids and CO_2 on the studied North Sea sandstones.

In summary, this study has demonstrated no marked effect of the studied unconformity surfaces (both local and regional) on the underlying reservoir rocks in the studied area of the North Sea. This, of course, does not completely exclude the possibility that other long

exposed surfaces may have a demonstrable effect associated with them, but no evidence for these effects was found for any of the unconformities studied here. Therefore, it is suggested that any such effects that may be noted elsewhere are most likely to be a localised phenomenon and cannot be extended as a general rule to all unconformities.

7.2 Suggestions for future study

The research conducted here has opened the door for further studies, which are envisaged to further aid understanding of the origin of the observed late-stage diagenetic changes in subsurface reservoirs:

1. Difficulties were faced in accurately quantifying kaolinite from the other clay types and in distinguishing authigenic (in situ) kaolinite from the detrital kaolinite within the total clay fraction. In this study, it was found that kaolinite represents a large percentage of the clay fraction in each sample. Therefore, the counted percentage of clay was assumed to represents the percentage of kaolinite. It would be beneficial and more accurate if we can differentiate between the detrital and authigenic kaolinite. Two possible methods are recommended for further study in order to better recognise the distribution and quantify the amount of authigenic kaolinite:
    a. Raman Spectra microscopy analysis.
    b. QEMSCAN analysis (Quantitative Evaluation of Minerals by scanning electron microscopy).

2. In many cases the increase of porosity due to feldspar grain dissolution was not associated with precipitation of reaction products (such as kaolinite, illite …etc.). This may indicate that the reaction products resulting from the dissolution of grains have been removed from the sandstones and transported to other places by pore fluid flow in an open system where pore fluids can migrate easily and hence remove any products generated. Therefore, it would be beneficial to investigate where these products have been precipitated and how.

3. The study shows that different mechanisms may be considered regarding the possible origin and timing of the observed post-depositional diagenetic changes in the studied area. For instance, the late influx of acidic fluids produced by thermal maturation of organic matter or by release of organic acids and CO_2 that may form as a result of

biodegradation of oil. Future work on these particular mechanisms using geochemical analysis, for example, is recommended.

4. The study showed that any previous publications supporting unconformity impact on reservoir rock are most likely to be a localised phenomenon. Hence, it would be beneficial to study other petroleum basins than the North Sea.

5. This study, as well as previous studies, focus on clastic reservoirs, therefore, studding the impact of unconformities on other sediment facies e.g. carbonates rather than clastic is recommended.

6. In this study, an attempt was made to perform statistical analysis between the facies above and below the unconformity surfaces. However, there were no two similar facies found above and below an unconformity surface. In the area studied, the unconformities mostly separate formations from different depositional environments. For future work, identifying cases where same facies exist above and below the unconformity surface would be identical for statistical analysis which is considered to be useful for detailed comparative analysis between facies above and below the unconformity surfaces.

7. Instead of point counting, it is recommended that future work apply analysis of Backscattered electron Images collected through Scanning Electron Microscopy (SEM) in order to generate more precise quantitative results on porosity (primary and secondary), porosity distribution and mineralogical composition (quartz, feldspar, clay minerals, carbonate minerals and pyrite).

Appendices

Appendix A: Methodology

A. l Core description

A. 1.1 Procedure

Offshore data sources were used in order to understand and draw a general picture of the area of study prior to a detailed analysis. Using the British Geological Survey (BGS) data base, UK offshore data, the common data access (CDA) data base (also known as UKOilandGasData) and the Norwegian Petroleum Directorate (NPD) data base, 32 wells from the area of interest which were found to cross one or more unconformity surface were selected for further analysis. Representative intervals of each identified well were selected for further detailed sedimentological analysis and samples collection. After the identification of the appropriate intervals the proper intervals of cores were reviewed. The data of the chosen intervals were then integrated with core samples from the UK Northern North Sea, which were held at the British Geological Survey Keyworth Core Store, and from the Norwegian North Sea, which were available at the Norwegian Petroleum Directorate's core store, Stavanger.

In the core store, description started with determination of grainsize by visual comparison of small sandstone samples using Wentworth size classification scale, followed by the description of lithology and sedimentary structures of each well. Determination of grain size has been done by visual comparison of small sandstone samples using Wentworth size classification scale. After the determination of the grain sizes, description of lithology and sedimentary structures were made using the symbols listed in Section A. 1.2. Appropriate scale has been used for each studied core based on the length of the described interval. Attempt was made to draw a realistic rather than stylized sedimentary structures.

A.1.2 Symbols Used

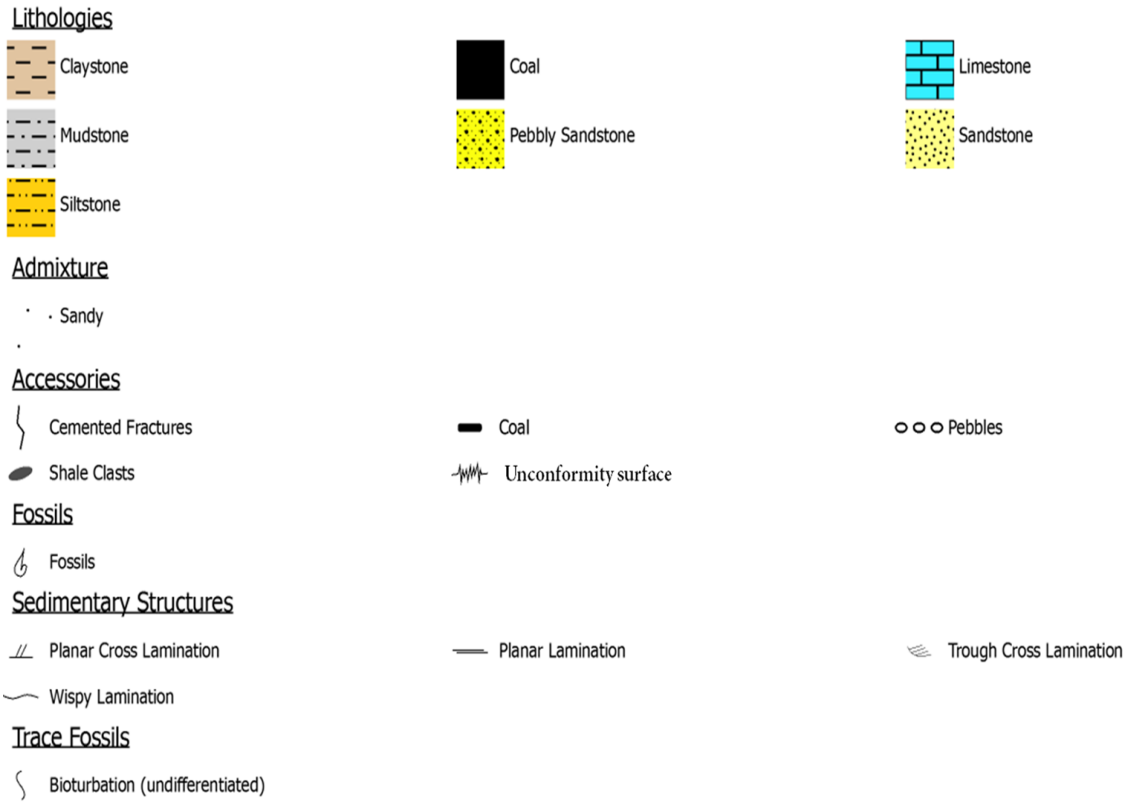

A.2 Thin-section Petrography

A.2.1 Sample Preparations

After the selection of samples from the appropriate core intervals, all samples were sent to specialist laboratory for thin-section preparation. Prior to the preparation of the thin-section, all samples were impregnated with blue coloured epoxy resin to be able to identify porosity. Each thin-section was then prepared with standard dimensions of 24X46mm and thickness of 30 microns.

A.2.2 Point Counting Procedure

A petrographic microscope with a circular rotating stage and an automated point counter has been used to point count the thin sections.

Point counting was made for all thin-section samples in order to estimate the main composition and porosity of these samples, using the automated point counter and a

mechanical stage attached to the used microscope. From literature, a range of 300-500 points is required to produce an accurate statistical data. For point counting validation, in this study 1000, 500 and 300 points were counted and compared for a number of thin-sections. A similar results were obtained for each thin-section with the studied points counting frequencies (1000, 500 and 300). Therefore it was decided to go for 300 points per thin-section.

Each thin-section was placed on the mechanical stage with mm graduated x-y stage translation controls to move the sample. Each thin-section sample was placed on the stage holder parallel to the x translation, the stage set to move the thin-section slide at regular intervals through the field of vision in straight line. In the end of each traverse over the sample the stage will move up toward the y axis by regular steps (generally 1 mm) and the second traverse is starts. In this way the traverse of each sample will be consistent.

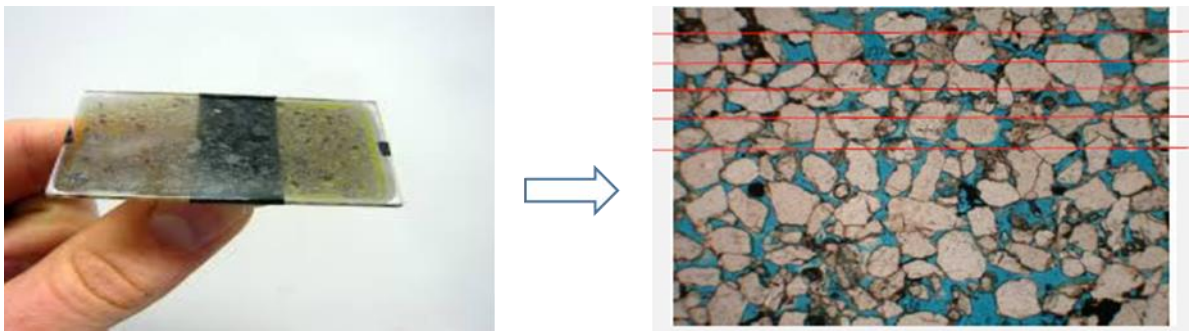

300-500 or more points

A.3 Scanning Electron Microscopy

All Samples used for the SEM analysis were uncovered polished thin-sections. Prior to the preparation of these thin-section, all samples were impregnated with clear epoxy resin. Each thin-section was then prepared with standard dimensions of 24X46mm.

For imaging of the samples Quanta FEG 650 SEM equipped with Oxford Instruments X-MaxN 150 mm EDX detector has been used (depicted below). The system is also equipped with a range of secondary (SE, GSE) and backscattered (BSE) detectors, a cathodoluminescence (CL) detector, an electron back scattered diffraction (EBSD) detector, and a wet scanning transmission electron microscopy (STEM) detector.

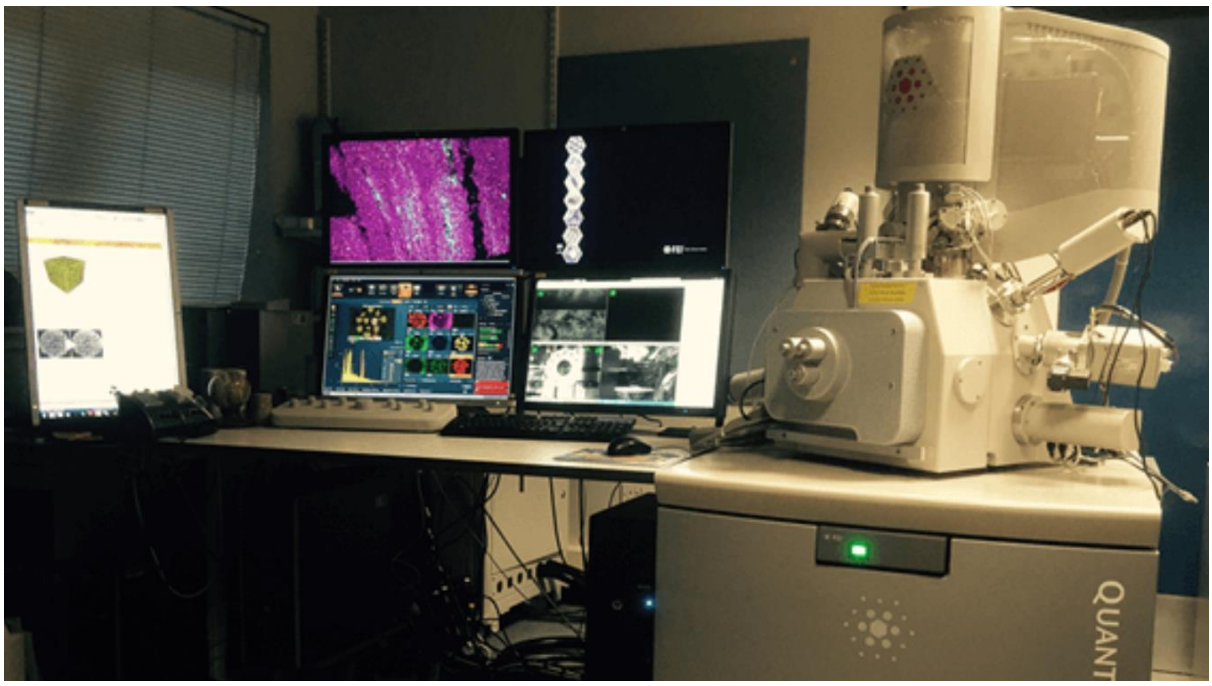

A beam of electrons is rastered over the sample which generates various types of radiations, which are used to infer sample characteristics such as composition and topography. The system operates with different modes; our samples were examined using low vacuum mode of operation, and were therefore uncoated, at 0.83 Torr. The microscope was used with an operating voltage of 20 kV, spot size of 4.5, working distance of 10 mm.

Many thousands of tiles can be constructed and joint together. The thin-sections were imaged with a BSE detector using the software Maps 2.1. This automatically collects a series of image tiles, that are then automatically stitched together to form large area – high-resolution image montages, these can be used to analyse grain composition, size, degree of weathering presence and characteristics of Kaolinite and abundance of porosity.

A.4 stratigraphy chart legend for (Figure 3-1)

Northern North Sea		Central North Sea		Southern North Sea	
1	Heimdal Sandstone member	1	Golspie Fm	1	Phillips member
2	Dornoch Fm	2	Mains Fm	2	Lambeth Fm
3	Teal Sandstone member	3	Ladys walk Fm	3	Prestwich Fm
4	Hermad Sandstone member	4	Orrin Fm	A	Silverpite evaporate member
5	Flugga Sandstone member	5	Rattrag volcanic member	B	Hewett Sandstone
6	Skadan Sandstone member	6	Ron volcanic member	C	Brockelschiefer member
7	Beauly member	7	Brora coal Fm	D	Amethyst member
8	Beauly member	8	Carr member	E	Bunther shale Fm
9	Mouse Fm	9	Fulmar Fm	F	Rot Halite member
10	Grid Sandstone member	10	Heather Fm	G	Muschelkalk halite member
11	Frigg Sandstone member	11	Ribber Sandstone member	H	Rogenstein member
12	Horda Fm	12	Burns Sandstone member	I	Keuper member
13	Skroo Sandstone member	13	Stroma member	J	Philips member
14	Rattrag volcanic member	14	Piper Fm		
A	Halibut carbonate	15	Flounder Fm		
B	Irish anhydrite member	16	Mey Sandstone member		
C	Inner carbonate member	17	Beauly member		
		18	Dornoch Fm		
		19	Cromarly Sandstone member		
		20	Forties Sandstone member		
		21	Grid Sandstone member		
		22	Tay Sandstone member		
		A	Inge volcanic member		
		B	Halibut carbonate		
		C	Gosephine Sandstone member		

A.5 Statistical analysis

All the data obtained from the studied wells has been investigated in detail in terms of the core characteristics (e.g. porosity and permeability) and description, followed by simple statistical analysis to compare the characteristics of the sediments lying above and below the unconformity surfaces. The full data, analysis, and initial results are provided in the attached CD. The CD contains specifically (1) wells screening database, (2) List of the selected North Sea wells, and (3) core description and initial statistical results for each studied well.

A.6 Raman spectroscopy

A.6.1 Procedure and Technique

Using Raman spectroscopy which was available at University of the West of Scotland, all samples were used measured using a Thermo DXR Raman microscope. This model had a selection of objectives ranging from 10X, 50X and 100X. For a majority of these samples, the 780nm laser was selected and used with a 10X objective at 5mW. Higher laser powers were known to affect the results so was cautious not to go too high in power. OMNIC software was used to collect and process the data, OMNIC spectra was used to identify phases based on the available mineral database.

The working principle of the Raman microscope is that a laser is focused onto the sample and the backscatter is collected. This backscattered light is then passed through a Rayleigh rejection filter and then into a full-range diffraction grating. This grating separates the light into different wavelengths for the charged couple device to detect signals. Raman intensity is mainly based on amount of current produced within a set amount of time. Smart background was selected, as in the spectrometer passively collects background data to improve measurements**.**

A.6.2 Difficulties encountered

These Raman measurements presented significant challenges. One major issue is that the samples themselves were not very Raman active, thus collection times took significant amounts of time. Thus, making a Raman map of high pixel density impractical for the number of samples to study. Another issue that presented itself was the fact that certain analysis of interest were not included with the available mineral library, without an analytical standard to measure; the spectral library could not be updated to be included in the spectral search.

Other challenges with the analysis included the spectral analysis with the OMNIC spectra software. Where outputs from the data showed species succession as quartz to be dominant in the spectra. Different wavelengths were tried to see if better quality spectra could be obtained but showed nothing significant.

Appendix B: Petrographic Data Tables

B .l Textures

Well 21/18-6

Sample N	Depth (ft)	Facies Code	Grain Size	Sorting	Roundness
24	10414.7	1	VFS	P	SA-SR
25	10415.7	1	VFS	P-M	SA-SR
26	10415.8	1	VFS	M	SA-SR
27	10417	1	VFS	P-M	SA-SR
28	10418.75	1	VFS	P-M	SA-SR
29	10420.2	1	VFS	P-M	SA-SR
30	10424	1	VFS	P-M	SA-SR
1/B1	10431.2	1	VFS	P-M	SA-SR
2/B2	10437.3	1	VFS	P-M	SA-SR
3/B2	10449.4	2	VF-FS	P-M	SA-SR
4/B2	10459.5	1	VFS	P-M	SA-SR
5/B2	10468	1	VFS	P-M	SA-SR

Well 21/18-2A

Sample N	Depth (ft)	Facies Code	Grain Size	Sorting	Roundness
50	10014.8	1	VFS	P	SA-SR
51	10016.8	1	VFS	P-M	SA-SR
53	10017.1	2	VF-FS	P	SA-SR
54	10017.5	1	VFS	M	SA-SR
55	10021	1	VFS	P	SA-SR
56	10023	1	VFS	P	SA-SR
23/B2	10026.5	2	VF-FS	P-M	SA-SR
24/B2	10033.8	2	VF-FS	P	SA-SR
25/B2	10053.9	1	VFS	P	SA-SR
26/B2	10076.9	2	VF-FS	P	SA-SR
27/B2	10111	1	VFS	P	SA-SR

Well 21/18-3

Sample N	Depth (ft)	Facies Code	Grain Size	Sorting	Roundness
6/B2	10332	1	VFS	P	SA-SR
7/B2	10332.5	1	VFS	P	SA-SR
8/B2	10333.5	2	VF-FS	P	SA-SR
9/B2	10336.5	1	VFS	P	SA-SR
10/B2	10343.8	2	VF-FS	P-M	SA-SR
11/B2	10352.8	2	VF-FS	P	SA-SR
12/B2	10361	2	VF-FS	P-M	SA-SR
13/B2	10377.8	2	VF-FS	P	SA-SR

Well 21/18-4

Sample N	Depth (ft)	Facies Code	Grain Size	Sorting	Roundness
14/B2	10698.5	1	VFS	P	SA-SR
15/B2	10698.75	2	VF-FS	P-M	SA-SR
16/B2	10700.5	3	FS	P	SA-SR
17/B2	10701.8	2	VF-FS	P	SA-SR
18/B2	10708.5	3	FS	P	SA-SR
19/B2	10714.5	2	VF-FS	P-M	SA-SR
20/B2	10724.5	2	VF-FS	P	SA-SR
21/B2	10734.15	2	VF-FS	P	SA-SR
22/B2	10746.5	2	VF-FS	P-M	SA-SR

Well 34/10-1

Sample N	Depth (ft)	Facies Code	Grain Size	Sorting	Roundness
1	1783.1	6T	M-CS	W	SA-SR
2	1784	4T	F-MS	M-W	SA-SR
3	1785.1	4T	F-MS	M-W	SA-SR
4	1840.2	6E	M-CS	W	SA-SR
5	1867.7	6E	M-CS	W	SA-SR
6	1877.65	2R	VF-FS	P	SA-SR
7	1880.3	2R	VF-FS	M-W	SA-SR
8	1916.3	2R	VF-FS	M-W	SA-SR

Well 34/10-4

Sample N	Depth (ft)	Facies Code	Grain Size	Sorting	Roundness
1	1826.5	2R	VF-FS	M-W	SA-SR
2	1835	2R	VF-FS	M-W	SA-SR
3	1841.8	2R	VF-FS	P-M	SA-SR
4	1843.1	2R	VF-FS	M-W	SA-SR
5	1848.4	2R	VF-FS	M-W	SA-SR
6	1868.1	2R	VF-FS	P-M	SA-SR
7	1898	2R	VF-FS	M	SA-SR

Well 34/10-8

Sample N	Depth (ft)	Facies Code	Grain Size	Sorting	Roundness
1	1823.3	4T	F-MS	W	SA-SR
2	1824.5	1-5T	VF-MS	P	SA-SR
3	1846.4	2T	VF-FS	W	SA-SR

Well 34/10-34

Sample N	Depth (ft)	Facies Code	Grain Size	Sorting	Roundness
1	1995	4T	F-MS	W	SA-SR
2	2000	4T	F-MS	W	SA-SR
3	2009	3-7T	F-CS	W	SA-SR

Well 33/9-13

Sample N	Depth (ft)	Facies Code	Grain Size	Sorting	Roundness
1	2732	2R	VF-FS	M-W	SA-SR
2	2733.5	2R	VF-FS	M-W	SA-SR
3	2738	2R	VF-FS	M-W	SA-SR
4	2743.9	2R	VF-FS	M-W	SA-SR
5	2750	2R	VF-FS	M-W	SA-SR
6	2767.9	2R	VF-FS	M-W	SA-SR

Well 34/7-16

Sample N	Depth (ft)	Facies Code	Grain Size	Sorting	Roundness
1	2390.07	6E	M-CS	W	SA-SR
2	2390.65	6E	M-CS	W	SA-SR
3	2393.8	6E	M-CS	W	SA-SR
4	2409.1	3-7E	F-CS	M	SA-SR
5	2410.8	6E	M-CS	W	SA-SR
6	2416.7	6E	M-CS	W	SA-SR
7	2429.8	6E	M-CS	W	SA-SR

Well 34/7-19

Sample N	Depth (ft)	Facies Code	Grain Size	Sorting	Roundness
1	2453.92	8T	VCS	M-W	SA-SR
2	2455.6	8T	VCS	P-M	SA-SR
3	2465.5	2T	VF-FS	M-W	SA-SR

Well 34/7-20

Sample N	Depth (ft)	Facies Code	Grain Size	Sorting	Roundness
1	2612.8	2T	VF-FG	M	SA
2	2615.5	2T	VF-FG	M	SA
3	2620.5	2T	VF-FS	M	SA

Well 30/6-10A

Sample N	Depth (ft)	Facies Code	Grain Size	Sorting	Roundness
1	2480	5T	MS	W	SA-SR
2	2483.5	5T	MS	W	SA-SR

Well 2/5-17

Sample N	Depth (ft)	Facies Code	Grain Size	Sorting	Roundness
19	10672.7	3-7	F-CS	P-M	SA-SR
20	10673.3	3-7	F-CS	P-M	SA-SR
21	10674	3-7	F-CS	P	SA-SR
22	10678	4	F-MS	M-W	SA-SR
40/B2	10678.5	4	F-MS	M	SA-SR
23	10681.5	4	F-MS	M-W	SA-SR
41/B2	10683.8	4	F-MS	M	SA-SR
42/B2	10704	4	F-MS	M	SA-SR

Well 15/17-B2

Sample N	Depth (ft)	Facies Code	Grain Size	Sorting	Roundness
33	9657	3-8	F-VCS	P	SA-SR
34	9658	3-8	F-VCS	P	SA-SR
35	9659.3	3	FS	P-M	SA-SR
36	9660	3-8	F-VCS	P	SA-SR
37	9664	4	F-MS	P-M	SA-SR
43/B2	9669	4	F-MS	P-M	SA-SR
44/B2	9677	4	F-MS	P-M	SA-SR
45/B2	9700	4	F-MS	P-M	SA-SR

B.2 Sandstone Classifications

Pettijohn et al (1972) and Pettijohn (1975) suggested a flexible approach on how to classify sandstones, and proposed that polycrystalline quartz grains should be considered as rock fragments (Figure B2.1).

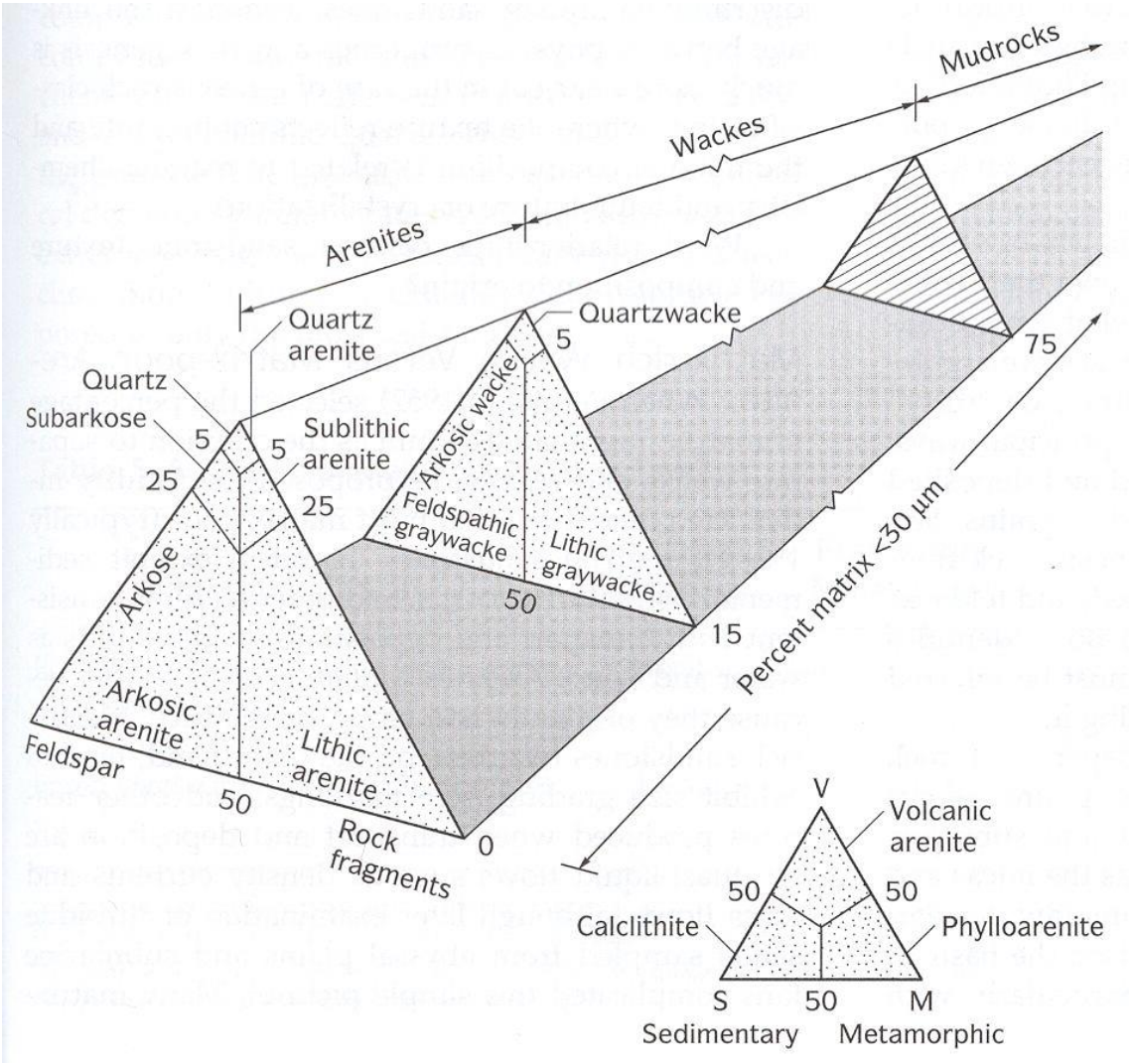

Figure B2.1. The classification scheme of Pettijohn et al (1972).

B.3 Mineralogical Composition and Porosity Data

Well 3/03-N14

Sample n.	Depth (m)	Facies	CONSTITUENT (%)								Total (%)
			Porosity %	Framework minerals %			Accessory minerals %	Cements %		Others %	
				Quartz	Feldspar	Rock Fragment	Mica	Calcite	Clay	Iron oxide and Pyrite	
1	10743.75	2	3	54	3	0	8	28	4	0	100
2	10743.9	2	5	55	2	0	10	22	6	0	100
3	10745.25	2	3	60	4	5	3	23	0	2	100

Well 211/12a-14

Sample no.	Core Depth (ft)	Facies	CONSTITUENT (%)								Total %
			Porosity %	Framework Minerals %			Accessory Minerals %	Cements %		Others %	
				Quartz	Feldspar	Rock Fragment	Mica	Calcite	Clay	Iron Oxide and pyrite	
34/B2	8241	2	2	48	12	0	2	0	28	8	100
35/B2	8241.5	2	2	45	12	1	5	28	2	5	100
36/B2	8243.75	2	16	48	11	1	0	0	20	4	100
37/B2	8250	2	2	57	11	0	4	1	23	2	100
39/B2	8250.5	2	11	55	9	0	7	0	16	2	100

WELL 211/23-A21

Sample no.	Core Depth (ft)	Facies	CONSTITUENT (%)								Total %
			Porosity %	Framework Minerals %			Accessory Minerals %	Cements %		Others %	
				Quartz	Feldspar	Rock Fragment	Mica	Calcite	Clay	Iron Oxide and pyrite	
6	8241	5	18	50	17	3	0	0	10	2	100
7	8241.5	5	22	40	20	2	1	12	0	3	100
8	8243.75	5	22	45	17	3	1	12	0	0	100
9	8250	5	18	35	17	3	7	0	17	3	100

Well 9/28-10A

Sample no.	Core Depth (ft)	Facies	CONSTITUENT (%)								Total %
			Porosity %	Framework Minerals %			Accessory Minerals %	Cements %		Others %	
				Quartz	Feldspar	Rock Fragment	Mica	Calcite	Clay	Iron Oxide and pyrite	
46	8664.6	4	15	60	4	0	1	20	0	0	100
47	8667.3	4	22	50	12	1	1	0	12	2	100
48	8678.5	4	24	50	17	0	1	0	7	1	100

Well 3/3-N15

Sample no.	Core Depth (ft)	Facies	CONSTITUENT (%)								Total %
			Porosity %	Framework Minerals %			Accessory Minerals %	Cements %		Others %	
				Quartz	Feldspar	Rock Fragment	Mica	Calcite	Clay	Iron Oxide and pyrite	
13	11425.7	4	20	55	13	0	1	10	0	1	100
14	11426.6	4	18	50	10	1	2	0	15	4	100
15	11427.2	4	15	60	7	0	2	0	14	2	100
16	11428.8	4	23	50	10	0	1	0	14	2	100
17	11433.8	3-7	23	50	10	3	1	0	12	1	100
18	11434.6	3-7	20	55	7	0	1	0	15	2	100

Well 14/19-3

Sample no.	Core Depth (ft)	Facies	CONSTITUENT (%)								Total %
			Porosity %	Framework Minerals %			Accessory Minerals %	Cements %		Others %	
				Quartz	Feldspar	Rock Fragment	Mica	Calcite	Clay	Iron Oxide and pyrite	
6	8241	3-8	5	58	2	0	0	35	0	0	100
7	8241.5	3-8	20	64	2	1	1	12	0	0	100
8	8243.75	3	18	60	7	0	1	0	12	2	100
9	8250	3-8	5	70	3	0	7	0	12	3	100
10	8250.5	4	1	42	5	0	5	0	46	1	100
11	8252.75	4	1	60	2	0	10	0	27	0	100
12	8259.1	4	17	58	5	6	2	0	12	0	100

References

Al-Gailani, M. B. 1981. Authigenic Mineralizations at Unconformities: Implication for Reservoir Characteristics. Sedimentary Geology, 29**,** 89-115.

Aplin, A. C. & Warren, E. A. 1994. Oxygen Isotopic Indications of the Mechanisms of Silica Transport and Quartz Cementation in Deeply Buried Sandstones. Geology, 22**,** 847-850.

Aplin, A. C., Warren, E. A., Grant, S. M. & Robinson, A. G. 1993. Mechanisms of Quartz Cementation in North Sea Reservoir Sandstones: Constraints from Fluid Compositions. Diagenesis and Basin Development. American Association of Petroleum Geologists Studies in Geology, 36**,** 7-22.

Bates, R. L. & Jackson, J. A. 1970. 1980. Glossary of geology (second edition): Falls Church, Virginia, American Geological Institute.

Besly, B. 1998. Carboniferous. Petroleum Geology of the North Sea: Basic Concepts and Recent Advances, Fourth Edition**,** 104-136.

Biddle, K. T. & Wielchowsky, C. C. 1994. Hydrocarbon Traps. Memoirs-American Association of Petroleum Geologists**,** 219-219.

Bjorkum, P. A., Mjos, R., Walderhaug, O. & Hurst, A. 1990. The Role of the Late Cimmerian Unconformity for the Distribution of Kaolinite in the Gullfaks Field, Northern North Sea. Sedimentology, 37**,** 395-406.

Bjorlykke, K. 1984. Formation of Secondary Porosity: How Important Is It? Clastic diagenesis**,** 277-286.

Bjorlykke, K. & Aagaard, P. 1992. Clay Minerals in North Sea Sandstones.

Bloch, S. 1994. Secondary Porosity in Sandstones: Significance, Origin, Relationship to Subaerial Unconformities, and Effect on Predrill Reservoir Quality Prediction.

Bowman, M. 2009. Cenozoic. Petroleum Geology of the North Sea: Basic Concepts and Recent Advances, Fourth Edition**,** 350-375.

Buckman, J. 2014. Use of Automated Image Acquisition and Stitching in Scanning Electron Microscopy: Imaging of Large Scale Areas of Materials at High Resolution. Microsc. Anal, 28**,** 13-15.

Burgess, P. M., Gurnis, M. & Moresi, L. 1997. Formation of Sequences in the Cratonic Interior of North America by Interaction between Mantle, Eustatic, and Stratigraphic Processes. Geological Society of America Bulletin, 109**,** 1515-1535.

Burley, S. 1986. The Development and Destruction of Porosity within Upper Jurassic Reservoir Sandstones of the Piper and Tartan Fields, Outer Moray Firth, North Sea. Clay Minerals, 21**,** 649-694.

Burley, S., Mullis, J. T. & Matter, A. 1989. Timing Diagenesis in the Tartan Reservoir (Uk North Sea): Constraints from Combined Cathodoluminescence Microscopy and Fluid Inclusion Studies. Marine and Petroleum Geology, 6**,** 98IN1105-104IN4120.

Cameron, T. 1992. The Geology of the Southern North Sea, Balogh Scientific Books.

Catuneanu, O. 2006. Principles of Sequence Stratigraphy, Elsevier.

Christie-Blick, N. 1991. Onlap, Offlap, and the Origin of Unconformity-Bounded Depositional Sequences. Marine Geology, 97**,** 35-56.

Cordey, W., Richards, P. & Association, U. O. O. 1993. Jurassic of the Central and Northern North Sea, British Geological Survey.

Davies, R., O'donnell, D., Bentham, P., Gibson, J., Curry, M., Dunay, R. & Maynard, J. The Origin and Genesis of Major Jurassic Unconformities within the Triple Junction Area of the North Sea, Uk. Geological Society, London, Petroleum Geology Conference series, 1999. Geological Society of London, 117-131.

Deegan, C. T. & Scull, B. J. 1977. A Standard Lithostratigraphic Nomenclature for the Central and Northern North Sea, HMSO.

Dillon, C. G., Worden, R. H. & Barclay, S. A. 2004. Simulations of the Effects of Diagenesis on the Evolution of Sandstone Porosity. Journal of Sedimentary Research, 74**,** 877-888.

Downie, R. 1998. Devonian. Petroleum Geology of the North Sea: Basic Concepts and Recent Advances, Fourth Edition**,** 85-103.

Ehrenberg, S. 1991. Kaolinized, Potassium-Leached Zones at the Contacts of the Garn Formation, Haltenbanken, Mid-Norwegian Continental Shelf. Marine and Petroleum Geology, 8**,** 250-269.

Ehrenberg, S. & Jakobsen, K. 2001. Plagioclase Dissolution Related to Biodegradation of Oil in Brent Group Sandstones (Middle Jurassic) of Gullfaks Field, Northern North Sea. Sedimentology, 48**,** 703-721.

Emery, D., Myers, K. & Young, R. 1990. Ancient Subaerial Exposure and Freshwater Leaching in Sandstones. Geology, 18**,** 1178-1181.

Erratt, D., Thomas, G. & Wall, G. The Evolution of the Central North Sea Rift. Geological Society, London, Petroleum Geology Conference series, 1999. Geological Society of London, 63-82.

Eschard, R., Tveiten, B., Desaubliaux, G., Lecomte, J. & Van Buchem, F. High Resolution Sequence Stratigraphy and Reservoir Prediction of the Brent Group (Tampen Spur Area) Using an Outcrop Analogue. Subsurface Reservoir Characterization from Outcrop Observations: Proceedings of the 7th IFP Exploration and Production Research Conference Held in Scarborough, April 12-17, 1992, 1993. Editions TECHNIP, 35.

Fraser, A. The Jurassic: From Regional Models to Field Development; the Impact of Sequence Stratigraphy on Hydrocarbon Geology, Introduction and Review. Petroleum Geology of Northwest Europe: Proceedings of the Fourth Conference (Ed. by JR Parker), Geol. Soc. Lond, 1993. 191-194.

Gao, X., Liu, L., Jiang, Z., Shang, X. & Liu, G. 2013a. A Pre-Paleogene Unconformity Surface of the Sikeshu Sag, Junggar Basin: Lithological, Geophysical and Geochemical Implications for the Transportation Of hydrocarbons. Geoscience Frontiers, 4**,** 779-786.

Gao, X., Liu, L., Wang, Y., Jiang, Z., Liu, G. & Shang, X. 2013b. The Characteristics of Unconformity Surface at the Bottom of the Paleogene and Its Significance in

Hydrocarbon Migration in the Sikeshu Sag of the Junggar Basin, Northwest China. Chinese Journal of Geochemistry, 32**,** 181-190.

Giles, M., De Boer, R. & Marshall, J. 1994. How Important Are Organic Acids in Generating Secondary Porosity in the Subsurface? Organic Acids in Geological Processes. Springer.

Giles, M. R. & Marshall, J. D. 1986. Constraints on the Development of Secondary Porosity in the Subsurface: Re-Evaluation of Processes. Marine and Petroleum Geology, 3**,** 243-255.

Glasmann, J. R. 1992. The Fate of Feldspar in Brent Group Reservoirs, North Sea: A Regional Synthesis of Diagenesis in Shallow, Intermediate, and Deep Burial Environments. Geological Society, London, Special Publications, 61**,** 329-350.

Glennie, K. 1986. Development of Nw Europe's Southern Permian Gas Basin. Geological Society, London, Special Publications, 23**,** 3-22.

Glennie, K. 2009. Petroleum Geology of the North Sea: Basic Concepts and Recent Advances, John Wiley & Sons.

Glennie, K. & Armstrong, L. 1991. The Kittiwake Field, Block 21/18, Uk North Sea. Geological Society, London, Memoirs, 14**,** 339-345.

Glennie, K. & Boegner, P. 1981. Sole Pit Inversion Tectonics. Petroleum geology of the continental shelf of northwest Europe. Institute of Petroleum, London**,** 110-120.

Glennie, K. W. 1998. Petroleum Geology of the North Sea: Basic Concepts and Recent Advances, Blackwell Publishing.

Glennie, K. W. & Underhill, J. R. 2009. Origin, Development and Evolution of Structural Styles. Petroleum Geology of the North Sea. Blackwell Science Ltd.

Goldsmith, P., Rich, B. & Standring, J. 1995. Triassic Correlation and Stratigraphy in the South Central Graben, Uk North Sea. Geological Society, London, Special Publications, 91**,** 123-143.

Graham, C., Armour, A., Bathurst, P., Evans, D. & Petroleumsforening, N. The Millennium Atlas: Petroleum Geology of the Central and Northern North Sea. 2003. Geological Society of London.

Habermehl, M. 2006. The Great Artesian Basin, Australia. Into the well from which you drink do not throw stones, 82.

Harwood, J., Aplin, A. C., Fialips, C. I., Iliffe, J. E., Kozdon, R., Ushikubo, T. & Valley, J. W. 2013. Quartz Cementation History of Sandstones Revealed by High-Resolution Sims Oxygen Isotope Analysis. Journal of Sedimentary Research, 83**,** 522-530.

Head, I. M., Jones, D. M. & Larter, S. R. 2003. Biological Activity in the Deep Subsurface and the Origin of Heavy Oil. Nature, 426**,** 344.

Helgeson, D. Structural Development and Trap Formation in the Central North Sea Hp/Ht Play. Geological Society, London, Petroleum Geology Conference series, 1999. Geological Society of London, 1029-1034.

Hillis, R., Thomson, K. & Underhill, J. 1994. Quantification of Tertiary Erosion in the Inner Moray Firth Using Sonic Velocity Data from the Chalk and the Kimmeridge Clay. Marine and Petroleum Geology, 11**,** 283-293.

Horstad, I., Larter, S. & Mills, N. 1995. Migration of Hydrocarbons in the Tampen Spur Area, Norwegian North Sea: A Reservoir Geochemical Evaluation. Geological Society, London, Special Publications, 86**,** 159-183.

Jian-Ping, C., Ming, Z. & Guang-Di, L. 2000. Importance of Unconformity in Oil and Gas Accumulation in the North-Western Slope of Junggar Basin. JOURNAL-UNIVERSITY OF PETROLEUM CHINA NATURAL SCIENCE EDITION, 24**,** 75-78.

Johnson, H., Leslie, A. B., Wilson, C. K., Andrews, I. & Cooper, R. M. 2005. Middle Jurassic, Upper Jurassic and Lower Cretaceous of the Uk Central and Northern North Sea, British Geological Survey.

Kay, S. 2003. The Heather Field, Block 2/5, Uk North Sea. Geological Society, London, Memoirs, 20**,** 291-304.

Kent, P. Outline Geology of the Southern North Sea Basin. Proceedings of the Yorkshire Geological and Polytechnic Society, 1967. Geological Society of London, 1-22.

Ketzer, J., Morad, S., Nystuen, J. & De Ros, L. 2009. The Role of the Cimmerian Unconformity (Early Cretaceous) in the Kaolinitization and Related Reservoir-Quality Evolution in Triassic Sandstones of the Snorre Field, North Sea. Clay Mineral Cements in Sandstones (Special Publication 34 of the IAS), 19**,** 361-382.

Krumbein, W. C. 1942. Criteria for Subsurface Recognition of Unconformities. AAPG Bulletin, 26**,** 36-62.

Kyrkjebø, R., Gabrielsen, R. & Faleide, J. 2004. Unconformities Related to the Jurassic–Cretaceous Synrift–Post-Rift Transition of the Northern North Sea. Journal of the Geological Society, 161**,** 1-17.

Lane, B. 1991. United Kingdom Oil and Gas Fields, 25 Years Commemorative Volume.

Larter, S., Wilhelms, A., Head, I., Koopmans, M., Aplin, A., Di Primio, R., Zwach, C., Erdmann, M. & Telnaes, N. 2003. The Controls on the Composition of Biodegraded Oils in the Deep Subsurface—Part 1: Biodegradation Rates in Petroleum Reservoirs. Organic Geochemistry, 34**,** 601-613.

Leckie, G. 1982. Lithology and Subsidence in the North Sea. Philosophical Transactions of the Royal Society of London. Series A, Mathematical and Physical Sciences, 305**,** 85-99.

Liu, B., Wang, Y.-H. & Qian, X.-L. 1997. Two Ordovician Unconformities in North China: Their Origins and Relationships to Regional Carbonate-Reservoir Characteristics. Carbonates and Evaporites, 12**,** 177-184.

Lundegard, P. D., Land, L. S. & Galloway, W. E. 1984. Problem of Secondary Porosity: Frio Formation (Oligocene), Texas Gulf Coast. Geology, 12**,** 399-402.

Macquaker, J. H., Taylor, K. G., Keller, M. & Polya, D. 2014. Compositional Controls on Early Diagenetic Pathways in Fine-Grained Sedimentary Rocks: Implications for Predicting Unconventional Reservoir Attributes of Mudstones. AAPG bulletin, 98**,** 587-603.

Miller, E. 1972. Parkman Field, Williston Basin, Saskatchewan. Mem.-Am. Assoc. Pet. Geol.;(United States), 16.

Mitchum Jr, R., Vail, P. & Sangree, J. 1977. Seismic Stratigraphy and Global Changes of Sea Level: Part 6. Stratigraphic Interpretation of Seismic Reflection Patterns in Depositional Sequences: Section 2. Application of Seismic Reflection Configuration to Stratigraphic Interpretation.

Morad, S., Ketzer, J. & De Ros, L. F. 2000. Spatial and Temporal Distribution of Diagenetic Alterations in Siliciclastic Rocks: Implications for Mass Transfer in Sedimentary Basins. Sedimentology, 47**,** 95-120.

Nguyen, B. T., Jones, S. J., Goulty, N. R., Middleton, A. J., Grant, N., Ferguson, A. & Bowen, L. 2013. The Role of Fluid Pressure and Diagenetic Cements for Porosity Preservation in Triassic Fluvial Reservoirs of the Central Graben, North Sea. AAPG bulletin, 97**,** 1273-1302.

Nielsen, O. B., Sorensen, S., Thiede, J. & Skarbo, O. 1986. Cenozoic Differential Subsidence of North Sea. AAPG Bulletin, 70**,** 276-298.

Oakman, C. & Partington, M. 1998. Cretaceous. Petroleum Geology of the North Sea: Basic Concepts and Recent Advances, Fourth Edition**,** 294-349.

Odin, G. 1985. Significance of Green Particles (Glaucony, Berthierine, Chlorite) in Arenites. Provenance of Arenites. Springer.

Penny, B. 1991. The Heather Field, Block 2/5, Uk North Sea. Geological Society, London, Memoirs, 14**,** 127-134.

Peters, K. E., Walters, C. C. & Moldowan, J. M. 2005. The Biomarker Guide, Cambridge University Press.

Pettijohn, F. J., Potter, P. & Siever, R. 1972. Sand Andsandstone. Bedin: Springer-Verlag, 62.

Rittenhouse, G. 1972. Stratigraphic-Trap Classification: Geologic Exploration Methods.

Saigal, G. C., Bjorlykke, K. & Larter, S. 1992. The Effects of Oil Emplacement on Diagenetic Processes: Examples from the Fulmar Reservoir Sandstones, Central North Sea: Geologic Note (1). AAPG Bulletin, 76**,** 1024-1033.

Schmitt, H. & Gordon, A. 1991. The Piper Field, Block 15/17, Uk North Sea. United Kingdom Oil and Gas Fields, 25**,** 361-368.

Scotchman, I., Johnes, L. & Miller, R. 1989. Clay Diagenesis and Oil Migration in Brent Group Sandstones of Nw Hutton Field, Uk North Sea. Clay Minerals, 24**,** 339-374.

Shanmugam, G. 1988. Origin, Recognition, and Importance of Erosional Unconformities in Sedimentary Basins. In: Kleinspehn, K. & Paola, C. (eds.) New Perspectives in Basin Analysis. Springer New York.

Shanmugam, G. 1990. Porosity Prediction in Sandstones Using Erosional Unconformities.

Shanmugam, G. & Higgins, J. 1988. Porosity Enhancement from Chert Dissolution beneath Neocomian Unconformity: Ivishak Formation, North Slope, Alaska. AAPG Bulletin, 72**,** 523-535.

Sloss, L. 1963. Sequences in the Cratonic Interior of North America. Geological Society of America Bulletin, 74**,** 93-114.

Spencer, A., Holter, E., Campbell, C., Hanslien, S., Nelson, P., Nysæther, E. & Ormaasen, E. 1987. Geology of the Norwegian Oil and Gas Fields. Graham and Trotman, London**,** 1-485.

Stoessell, R. K. & Pittman, E. D. 1990. Secondary Porosity Revisited: The Chemistry of Feldspar Dissolution by Carboxylic Acids and Anions (1). AAPG Bulletin, 74**,** 1795-1805.

Stricker, S. & Jones, S. J. 2016. Enhanced Porosity Preservation by Pore Fluid Overpressure and Chlorite Grain Coatings in the Triassic Skagerrak, Central Graben, North Sea, Uk. Geological Society, London, Special Publications, 435**,** SP435. 4.

Surdam, R. C., Boese, S. W. & Crossey, L. J. 1984. The Chemistry of Secondary Porosity: Part 2. Aspects of Porosity Modification.

Surdam, R. C., Crossey, L. J., Hagen, E. S. & Heasler, H. P. 1989. Organic-Inorganic Interactions and Sandstone Diagenesis. AAPG Bulletin, 73**,** 1-23.

Talukdar, S. 1985. Generation and Migration of Hydrocarbons in the Maracaibo Basin, Venezuela.

Taylor, J. 1990. Upper Permian—Zechstein. Petroleum Geology of the North Sea: Basic Concepts and Recent Advances, Fourth Edition**,** 174-211.

Taylor, P., Bennett, B., Jones, M. & Larter, S. 2001. The Effect of Biodegradation and Water Washing on the Occurrence of Alkylphenols in Crude Oils. Organic Geochemistry, 32**,** 341-358.

Thomson, K. & Underhill, J. Controls on the Development and Evolution of Structural Styles in the Inner Moray Firth Basin. Geological Society, London, Petroleum Geology Conference series, 1993. Geological Society of London, 1167-1178.

Turchyn, A. V. & Depaolo, D. J. 2011. Calcium Isotope Evidence for Suppression of Carbonate Dissolution in Carbonate-Bearing Organic-Rich Sediments. Geochimica et Cosmochimica Acta, 75**,** 7081-7098.

Ulmer-Scholle, D. S., Scholle, P. A., Schieber, J. & Raine, R. J. 2014. A Color Guide to the Petrography of Sandstones, Siltstones, Shales and Associated Rocks, American Association of Petroleum Geologists.

Underhill, J. 1998. Jurassic. Petroleum Geology of the North Sea: Basic Concepts and Recent Advances, Fourth Edition**,** 245-293.

Underhill, J. & Partington, M. 1994. Use of Maximum Flooding Surfaces in Determining a Regional Control on the Intra-Aalenian (Mid-Cimmerian) Sequence Boundary: Implications for North Sea Basin Development and Exxon S Sea-Level Chart. Recent advances in siliciclastic sequence stratigraphy, 58**,** 449-484.

Underhill, J. R. 1991. Controls on Late Jurassic Seismic Sequences, Inner Moray Firth, Uk North Sea: A Critical Test of a Key Segment of Exxon's Original Global Cycle Chart. Basin Research, 3**,** 79-98.

Underhill, J. T. & Partington, M. Jurassic Thermal Doming and Deflation in the North Sea: Implications of the Sequence Stratigraphic Evidence. Geological Society, London, Petroleum Geology Conference series, 1993. Geological Society of London, 337-345.

Vail, P. R., Mitchum Jr, R. & Thompson Iii, S. 1977. Seismic Stratigraphy and Global Changes of Sea Level: Part 3. Relative Changes of Sea Level from Coastal Onlap: Section 2. Application of Seismic Reflection Configuration to Stratigrapic Interpretation.

Wakefield, L., Droste, H., Giles, M. & Janssen, R. Late Jurassic Plays Along the Western Margin of the Central Graben. Geological Society, London, Petroleum Geology Conference series, 1993. Geological Society of London, 459-468.

Watson, R. S., Trewin, N. H. & Fallick, A. E. 1995. The Formation of Carbonate Cements in the Forth and Balmoral Fields, Northern North Sea: A Case for Biodegradation, Carbonate Cementation and Oil Leakage During Early Burial. Geological Society, London, Special Publications, 94**,** 177-200.

Wenger, L. M., Davis, C. L. & Isaksen, G. H. 2002. Multiple Controls on Petroleum Biodegradation and Impact on Oil Quality. SPE Reservoir Evaluation & Engineering, 5**,** 375-383.

Wilhelms, A., Larter, S., Head, I. & Farrimond, P. 2001. Biodegradation of Oil in Uplifted Basins Prevented by Deep-Burial Sterilization. Nature, 411**,** 1034.

Wilkinson, M. & Haszeldine, R. S. 2011. Oil Charge Preserves Exceptional Porosity in Deeply Buried, Overpressured, Sandstones: Central North Sea, Uk. Journal of the Geological Society, 168**,** 1285-1295.

Wilkinson, M., Haszeldine, R. S., Morton, A. & Fallick, A. E. 2014. Deep Burial Dissolution of K-Feldspars in a Fluvial Sandstone, Pentland Formation, Uk Central North Sea. Journal of the Geological Society, 171**,** 635-647.

Wolicka, D. & Borkowski, A. 2012. Microorganisms and Crude Oil. Introduction to Enhanced Oil Recovery (Eor) Processes and Bioremediation of Oil-Contaminated Sites. InTech.

Wu, K., Paton, D. & Zha, M. 2012. Unconformity Structures Controlling Stratigraphic Reservoirs in the North-West Margin of Junggar Basin, North-West China. Frontiers of Earth Science, 7**,** 55-64.

Yuan, G., Cao, Y., Jia, Z., Gluyas, J., Yang, T., Wang, Y. & Xi, K. 2015. Selective Dissolution of Feldspars in the Presence of Carbonates: The Way to Generate Secondary Pores in Buried Sandstones by Organic Co 2. Marine and Petroleum Geology, 60**,** 105-119.

Ziegler, P. 1977. Geology and Hydrocarbon Provinces of the North Sea. GeoJournal, 1**,** 7-32.

Ziegler, P. 1994. Cenozoic Rift System of Western and Central-Europe-an Overview. Geologie en Mijnbouw, 73**,** 99-127.